Predicting self-oxidation of coals and coal/biomass blends using thermal and optical methods

Claudio R. Avila, BSc.

Thesis submitted to The University of Nottingham

for the degree of Doctor of Philosophy

May 2012

Abstract

Self-oxidation and spontaneous combustion of coals is a problem of global concern. There are social, economic and environmental costs associated with this phenomenon and major incidents can, in extreme cases, lead to human casualties. More often however, damage is made to commercial facilities, the calorific value of the fuel is reduced and substantial release of noxious gases, particulate matter and CO_2 may contribute to local and international pollution levels.

This problem is not only restricted to coals, it also affects other carbonaceous materials such as biomass and potentially coal-biomass blends. A considerable amount of literature has been published, and whilst the causes are relatively well understood, the existing methods for predicting spontaneous combustion are not reliable enough for scientists or the coal industry. This research focuses on understanding the oxidation characteristics of coal, biomass and coal-biomass blends at low temperatures, with the aim of defining a set of experimental test procedures to identify coal and biomass propensity to spontaneously combust.

Based on a comprehensive literature survey, two main research areas were identified as feasible sources of information to detect prone coals: microscopy and thermal analysis. Considering these, an extensive experimental program was carried out using 42 coals (including at least three well known samples prone to spontaneous combustion), 10 different biomass types, and a number of coal-biomass blends, including diverse particle and sample sizes, at different stages of the oxidation process. Initially, pulverized coal samples (size <106μm) were subjected to thermogravimetric and calorimetric tests (small sample size), and differential thermal analysis (large sample size) using a large scale reactor. From these tests, the link between the weight loss/gain of the samples and the reactivity at low temperature

was confirmed, developing successfully two thermogravimetric tests to identify high risk samples. Afterwards, textural features of thermally altered coal samples (light reflectance and particle morphology) were studied by means of combined petrographic and image analysis techniques. Results showed that particle reflectance and textural changes depend on oxidation temperature, which are linked to the spontaneous combustion potential. Based on these results, two tests were proposed by comparing light reflectance before and after a slow oxidation, quantifying the formation of morphotypes associated with highly reactive samples.

A similar approach was used to study biomass and coal-biomass blends, focusing on the quantification of intrinsic reactivity and particle morphology by TGA and optical microscopy. For raw and char biomass particles, results showed a significant correlation between the optical and reactivity properties. Additionally, several new morphotypes were identified from biomass char samples. These characteristics were associated with the thermal behaviour of large samples, although these results did not suggest any distinctive indicator to identify samples prone to self-heat, concluding that the low temperature oxidation of biomass is a completely different phenomenon to that experienced by coals.

In the case of coal-biomass blends, the most relevant finding was a synergetic effect observed for the ignition temperature, which was always lower than the ignition temperature of the individual components. This finding has not been described in literature before, and further work is necessary in order to investigate this interaction in greater depth. Finally, a set of standardised procedures to assess the reactive properties of these materials has also been proposed.

Acknowledgements

First of all, I would like to acknowledge the Ministry of Planning of the Chilean Government for the economic support during the three years of this project. I would also like to acknowledge E.On for its generous financial contribution to support this research.

I am especially grateful to my supervisor Dr. Ed Lester who gave me the opportunity to develop part of my research career in UK. I would like to thank Dr. Will Quick (E.ON) for contributing with time and resources to this investigation. I would also like to express my deepest gratitude to Dr. Dave Clift, Dr. John Patrick, Ms. Marion Brice, Dr. Aled Jones, Mr. Michael Fletcher and Mr. James Oswin (SCHEE) for their professional contribution to this research. I am really thankful to Dr. Martin Schmidt (BAM) who contributed with a relevant number of samples that made this work possible. I would like to thank Dr. Rich Barranco (Imperial College), Dr. Mark Kennedy (Johnson Matthey), and Maria Mediero (University of Cambridge) for all their support, advice and help during these three years.

Lastly, I would like to thank my family and friends for all their love and encouragement. Thanks to my parents, brothers and little sister for their unconditional support. And thanks to my loving, encouraging, and patient wife. Thank you.

List of contents

Chapter 1. General overview

1.1 Introduction

1.1.1 The influence of coal in our society

Coal has been present in the world before the beginning of human history. This rock is the remaining of organic life over the last 360 million years. It is a petrified matrix of carbon formed during the primary age of the Earth through the deposition and compaction of organic matter from prehistoric animals, forest and soils [1] (Figure 1). In this period of time, this material has been exposed to extreme physical processes including high pressures and elevated temperatures through compaction, resulting in significant changes in its chemical structure. Then, the material has been concentrated in deep layers underground to remain as the mineral that is today known as coal [2,3].

| Original Organic material | Increase in heat and pressure | Increase in heat and pressure | Increase in heat and pressure |

| Peat | Brown Coal | Sub-bituminous | Bituminous | Anthracite |

Maturation degree (increase in coal rank)

Carbon content	60%	60 to 70%	71 to 77%	78 to 87%	> 88%
Volatile content	>53%	53 to 49%	48 to 40%	40 to 20%	< 20%
Water content	>75%	35 to 10%	25 to 10%	10 to 3%	< 5%
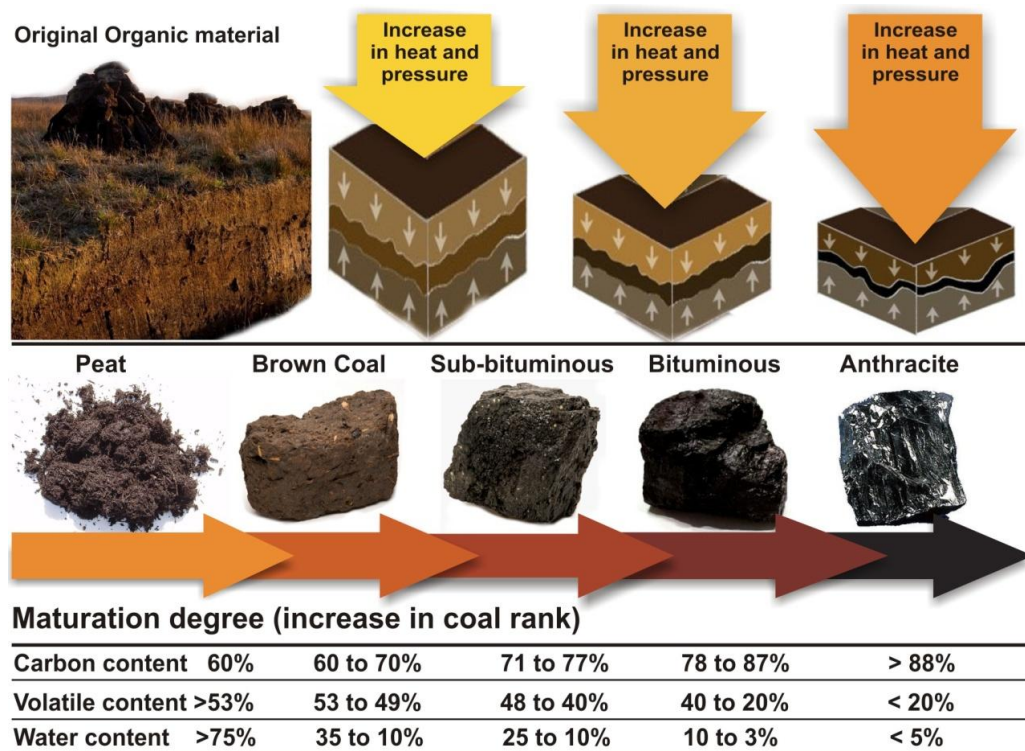
Figure 1: Coal formation process, with additional information from [2,1,3].

The impact of coal in our civilization is significant. Archaeological reports attribute the first uses of coal by human tribes with the discovery of fire (the exothermic reaction of coal oxidation). In this case, coal was used as an alternative to wood for cooking food and provide heat [4,5,6]. Later on, in the Iron and Bronze Age, it was used for melting and deformation of metals, which requires high temperatures that were only possible to be obtained by coal combustion. In addition, coal was used as an additive to change the strength properties of metals through the creation of the first metal alloys. Archaeological investigations have revealed that these materials contain a high concentration of carbon (examined by advanced metallographic analysis), which can only be explained by the use of coal as an additive [7].

By the end of the Middle ages, it was used to heat big castles and cities, as well as to obtain some early primary supplies such as methane gas. It was at this point in history that the first complaint arose about contamination produced by the smoke from coal fires. It was subsequently banned in London by King Edward I in 1276, because the local air quality had become so poor [8]. However, it was also a vital ingredient in some early discoveries, such as the gunpowder in China (around 10 AD), which was later introduced to Europe (around 13 AD) [9,10].

However, it was at the end of 17th century when coal use became central to the development of our civilization. Alongside iron, steam and railways, coal is the symbol of the industrial age. It was the primary matter that provided the energy needed for steam machines, transport, agriculture, and the power to sustain the new chain production lines being implemented during the industrial revolution. At this point, coal has revolutionized society, which had previously relied on manual labour towards a machine based manufacturing economy. At the same time, other discoveries such as electricity and artificial lighting increase the need for coal [11].

Spontaneous combustion of coal and natural coal fires have been documented during the whole history. The oldest record of a coal fire was found in China, specifically in the Xinjiang region, which started in the year of 1560. This fire has been active for at least 400 years, and just has been recently extinguished [12]. Nowadays, active coal fires can be found across the entire world as a problem of global proportions, with vast areas being affected in China, Australia, India, South Africa and North America.

1.1.2 The increasing coal consumption to cover the energy demand

Nowadays, coal is one of the most important globally traded fuels meeting growing energy requirements. 26% of primary energy needs in the world is produced from coal, providing 41% of worldwide electricity production (Figure 2) [13]. Coal has a high energy density (approximately 8000 to 15000 BTU or 13 to 24MJ kg^{-1} [14]); it also has a low production cost, for example coal for steam generation cost around U$47 to U$70 per short Ton (unit of mass equal to 2000 pounds, used by the coal industry), depending of the calorific value and the sulphur content; the metallurgical coal cost approximately U$150 per short Ton [13]. Finally, coal can be easily stored and transported, and it is available across the whole world [3].
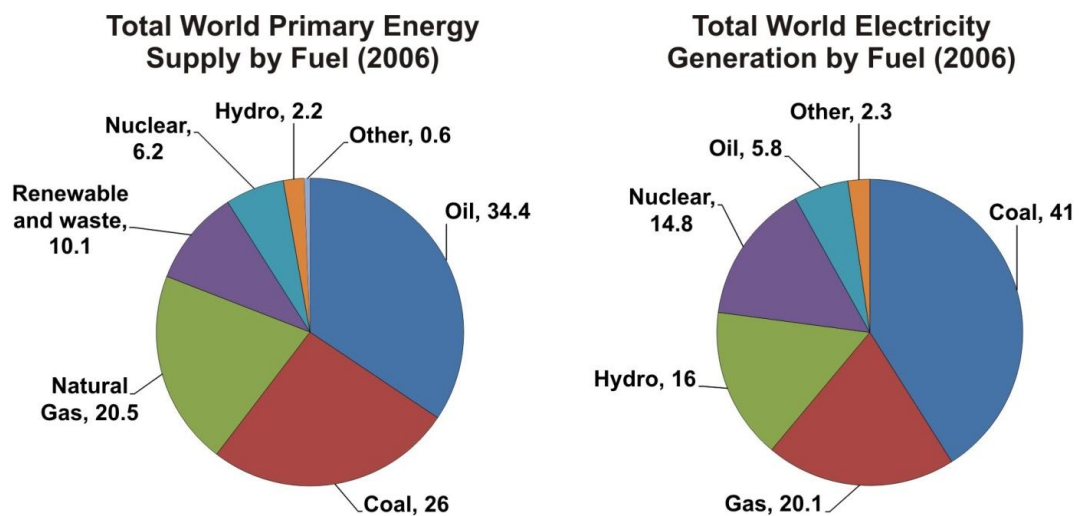
Figure 2: World energy outlook 2006, adapted from [14].

Despite all the problems and the negative image of coal, its use is expected to steadily increase. In 2009, 5990 million of tons (Mt) of coal were produced, from which 5210Mt was used for steam and electricity production directly, and 780Mt was used for coke making. It has been estimated that the reserves are in the order of 984 billions of tons (Bt), which could cover the demand for next 120 years (based on coal consumption of 2006) [14]. The largest worldwide reserves are located in United States (250Bt), Russia (150Bt), China (120Bt), India (85Bt) and Australia (80Bt). Nevertheless, the main producer is China with 2970Mt per year, followed by United States with just 920Mt per year. The main consumer of coal is Asia with a 54% of the global demand, in which China is one of the main contributors. The second largest consumer is the United States, which consumes approximately 20% of the worldwide production [13].

1.1.3 The impacts and hazards of coal use

Regardless of all its benefits, at the end of 20th century coal use became an active focus of debate due to its link with human health effects and climate change. With regard to the effects in human health, these are significant at early stages of production, specifically during the mining and extraction process. Among these, the main hazards are poisoning due to breathing of CO and methane; inhalation of heavy metals such as mercury, selenium, and arsenic; and casualties produced by gas explosions inside pits and coal fires (in the surface or inside pits) [15,16]. In the last decades, there has been an improvement in working conditions that has helped considerably to reduce and avoid these risks [17].

Regarding to the effects on the environment, the first place where these are seen is close to the mining sites, where millions of tons of waste dumps are generated. Also, when coal has high sulphur content, extraction generates gaseous aerosols to produce

acid rain, as well as contamination of natural water resources with heavy metals, affecting the flora and fauna that depend directly on this. Finally, it also contributes to release of particulate matter to the air; all of these factors leads to high levels of environmental pollution disturbing wildlife and human population in areas adjacent to the mining sites [18].

In addition to these, one of the main impacts of coal has been on climate change, which may prove to change the course of human history. It has been demonstrated that the natural CO_2 and methane concentration in the atmosphere produces a global warming effect, which helps to maintain the temperature at a stable value (~-10 to 40^oC, depending on the place). This natural phenomenon has relevance crucial for all the geological and biological cycles, as well as temperature and wind conditions necessaries to sustain the life in the earth [19]. However, it also has been revealed that there has been an increase in the CO_2 concentration due to human activities within the last 100 years [20,21,13]. Every day, millions of tons of coal are burned through the combustion process to obtain energy [14]. When added to the other emissions of CO_2 from fossil fuels, these emissions have led to an increase of the global concentration of CO_2 in the atmosphere, which is starting to modify all natural cycles. This had produced some negative effects such as increase of temperature in the ocean (reducing the solubility of O_2 and CO_2), helping to melt the ice in the poles, influencing changes in the wind directions, and then it is producing an unknown effect in the whole world life [20].

At the same time, the natural combustion of coal has received much less attention from the media, despite being a major source of CO_2 and CH_4 emissions [21]. The natural self-oxidation of coal has created several uncontrolled coal fires around the world, which are responsible for diseases and fatalities in humans around these sites.

These fires are also responsible for an uncalculated amount of noxious gases, particulate matter and CO_2 released into the atmosphere producing an unknown impact [22]. Lamentably, there are just a few active initiatives that trying to study the effects and the possible solutions to this underestimated problem.

1.2 Natural coal fires in the world: an underestimated problem

Figure 3 presents an overview of coal fires around the world. In these places, fires have been initiated by natural causes or by human activity, and some of these have been burning for hundreds of years. However, what is less clear is the magnitude of the area affected, the total gaseous emissions, and the potential impacts produced [22]. In addition to scientific studies by academics, there are also some intergovernmental initiatives such as the Sino-German initiative [23], and the American Government initiative [24], which have provided funding and support for research groups in order to clarify how some of these issues are linked to a global scenario.
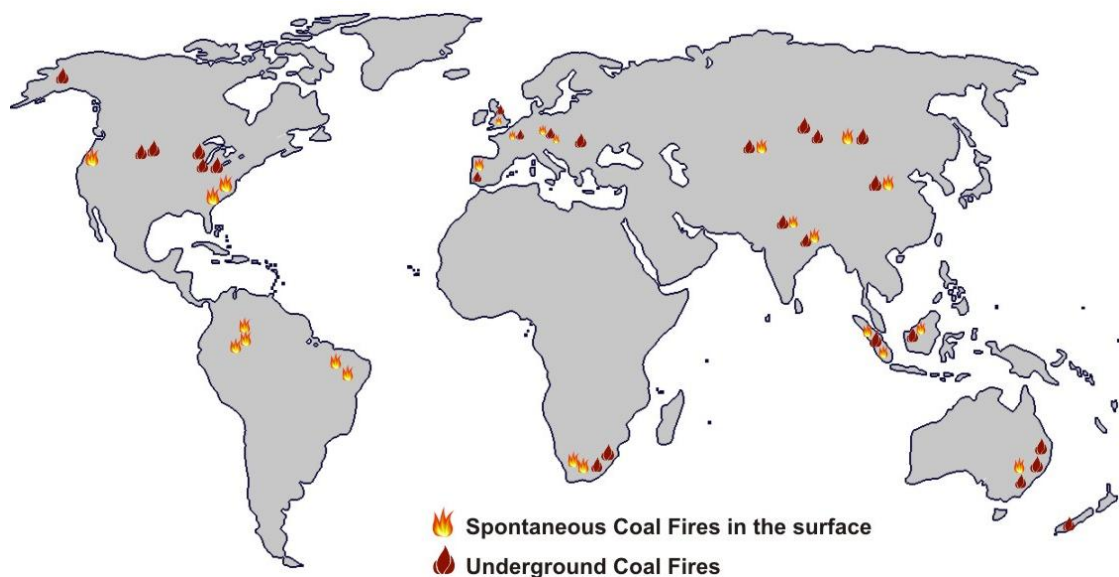
Figure 3: Overview of the coal fires events in the world.

1.2.1 Coal fires and spontaneous coal fires

In order to understand the consequences of a coal fire, it is prior necessary to understand its origins. Natural coal combustion can be triggered by different factors that have been classified in two main groups: fires produced by an external ignition source, or fires started spontaneously due to a self oxidation reactions that can occur in coal [25,26]. The first and the most common group of fires are produced by external sources of ignition. In these cases, the combustion reaction can be triggered by an external event such as a forest fire, lightning (which produce a fire directly or indirectly in the coal deposit), but the most frequent cause is through human-induced ignition [21,22,26]. Normally, the reaction starts from a highly exothermic stage releasing an elevated amount of heat, which increases the temperature of the coal deposit accelerating the oxidation into a self sustainable reaction. In this case the temperature of the reaction is close to $400^{\circ}C$ depending of the coal type [2].

The second case is not as frequent as the first, and it arises from a self-oxidation reaction. This reaction is a slow process that can take from several hours to days or weeks; passing through thermal decomposition and oxidation steps when the material is exposed to the oxygen present in the air [27,28]. At ambient temperature this reaction is thermodynamically spontaneous, which means that it does not need an external source of energy to progress. Compared with a conventional combustion, this is a series of parallel endothermic and exothermic reactions developed between 20 to $100^{\circ}C$, releasing some heavy volatiles as well as H_2O, CH_4 and CO, without the presence of a visible flame [29]. However, if the exothermic reactions outweigh the endothermic reactions, the rate of heating can increase considerably and release higher amounts of CO_2 and water, which added to a poor ventilation (reduced cooling not allowing the heat dissipation), it can be out of control and reach a

complete combustion stage [21,22,28]. This process is known in popular terms as "spontaneous combustion of coal", and its characteristics and identification are the main focus of this research.

It is important to clarify the differences between these two types of fire, because both evolve in a completely different way. It is a common error to confuse underground coal fires with spontaneous coal fires [25,26]. The first case requires an external source of energy to induce the fire, because the surface area exposed to the oxygen is not large enough to generate and accumulate the heat needed for a self-sustainable thermal run-away [30]. Also, these fires are characterized by high temperatures and once it starts, the chances to stop it without any external intervention are reduced [31,32]. The spontaneous combustion of coal could never reach the exothermic stage if the amount of heat produced is readily dissipated to the environment. However, if the heat is concentrated in the deposit, the possibilities to become a self-sustainable fire are high. The last point is important because an early detection of the self-oxidation reaction can translate to an action, which could considerably reduce the chances of reaching the high exothermally point resulting in an uncontrolled fire [33]. Perhaps a clear differentiation can be established by understanding the difference between ignition phenomena (the first case), with a self-heating phenomenon such as the spontaneous combustion of coal (second case).

1.2.2 Underground coal fires and surface coal fires

Natural coal fires can also be classified depending on the location in which it takes place: underground coal fires and fires in the surface [34]. Considering the underground coal fires, these are produced in the interior of seams and pits, due to gas explosions or induced by human activities such as welding works, electrical short circuits and smoking. Also, these can be produced by natural events such as

lightning, or ignition from forest fires close to the mining site. Underground coal fires can remain active for hundreds of years, consuming oxygen through the ventilation systems, burning at a very slow rate [32]. Surface coal fires could share the same origin as underground fires, there is the additional possibility of a spontaneous ignition [26,28,29]. This new classification, added to the explanation given in the previous section, is useful in understanding the characteristics of a coal fire. Figure 4 shows the different ways to classify a coal fire.
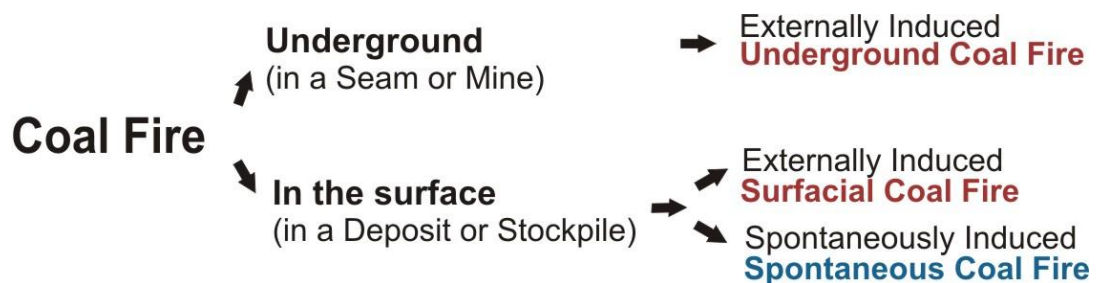
Figure 4: Classification of coal fires.

1.2.3 Historical reports of spontaneous coal fires around the world

In order to get an historical perspective, the information documented and available in the web can be organized in a histogram relating the numbers of references for the term "Spontaneous Coal Fire" with the time associated to these events. By using the time line tool provided by Google, it is possible to present the results as a graph (Figure 5). This gives an idea about the period of most activity, with most documents being generated around 1900, in the boom of coal industry.

Recently, there has been an increase in spontaneous coal fire accidents reported in mining sites, coal deposits and power stations. Among these, there have been reports of spontaneous coal fires with the Kleinkopje coal seam in South Africa since 1900 [35]; and in the El Cerrejon mine in Colombia [36] being amongst the most recurrent. In these cases, the frequency has been in order of days. There have also been several

accidents during the coal transport in marine vessels, extensively reviewed at the beginning of 20th century [37]; and accidents in storage sites at power plants, such as an incident reported recently in Spain, in which a spontaneous coal fire started in a coal deposit property of Union Fenosa in November 2007, which took a week to control the fire [38]; as well as in some mining sites in China [39], Australia [40], India [41], South Africa [42], and several more around the world [21,26,22,43].
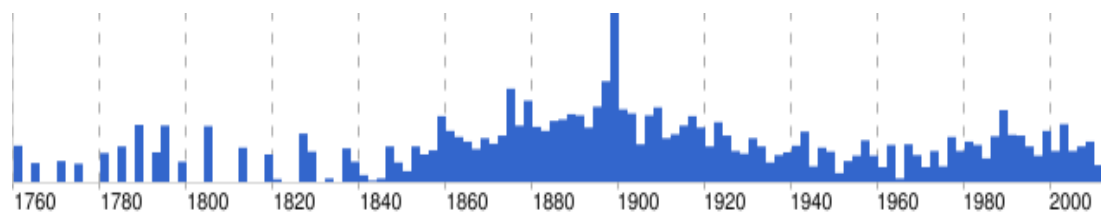
Figure 5: Histogram of number of references per year associated to the term "Spontaneous coal fire" displayed by Google.

From these experiences, it is noted that extinguishing a coal fire in a deposit (e.g. inside a power plant) can be an extremely complicated task due to the amount of coal involved, usually with stockpiles of up to Millions of tons [35]. These circumstances also brings severe economic losses due to the loss of calorific value, the need for extra labour to combat the fire, and in the most dramatic cases human casualties and damage to the main facilities associated to the coal deposit [39]. Clearly, there is an imperative to avoid these events throughout technical mechanisms and systems for early detection [44].

1.2.4 Effects of coal fires in the environment and human populations

The consequences of natural coal fires are vast and serious, and they affect the environment, the economy, social aspects and human health. On a global scale, the main concern is related to the emission of large amounts of greenhouse gases, which

has become the central focus of attention as a result of global warming issues [21,45]. However, the local and regional scale effects have immediate consequences that are far more evident in terms of impact on natural resources and human lives [46,45,22]. Also, coal fires are particularly severe in developing countries such as China, India and South Africa, where policies and available resources to mitigate the problem are scarce or have a low priority [35,39,41].

In addition, natural resources can suffer significant alterations. The first impact is a change in the geological environment, generating extensive zones of burned rocks and leaving large empty areas below the surface (in the case of an underground fire), with high potential risks of floodings and landslides. Also, burned rocks increases permeability and water retention that can produce changes in the physico-chemical conditions around the place, such as contamination of remote areas with heavy metals through water leaching [43,47]. At the same time, soil surfaces become more complex, which can accelerate processes such as soil desertification, wind and water erosion, and acid rainfall [43,47].

The emission of noxious gases emitted from coal fires, and the high temperatures reached produce significant alterations in the local flora and fauna. High temperatures at the surface around a coal fire can reach more than $100^{o}C$ destroying the vegetation, resulting in the death of microorganisms, insects and grass, which also reduces the biodiversity of these areas [43]. Those problems are enlarged when heavy rain fall and strong winds transmit pollutants to natural places adjacent to the affected sites, affecting the local human population [46].

Greenhouse gas emissions from natural coal fires are relevant but at the same time unquantified. A research group has estimated that coal fires in northern China produces each year around 0.49Mt of CO, 0.51Mt of SO_2, 0.3Mt of NO_2, 0.11Mt of

dust. This smoke and particulate matter are spread over vast areas that include some big cities, which presents a pollution index five times higher than the national standard [26]. In other estimations, natural coal fires in China burn 200Mt of coal per year, equivalent to about 20 per cent of the total amount of coal used by the United States for power generation [22]. The amount of coal involved in natural coal fires burning in India and France was partially estimated, unfortunately it does not represent the complete local landscape [41,43]. Therefore, with an uncertain numbers of active coal fires, it is even more difficult to obtain a global estimation of emissions across the world.

Coal fires also produce a high impact on human health, especially for local residents close to the burning sites. The long term exposure to the emission of noxious gases such as H_2S and SO_2 has direct relation to lung cancer and damage to the respiratory system [43]. Also, the prolonged exposure to a range of volatile organic species emitted from these fires, including xylene, toluene and benzene, could be another cause of respiratory diseases [42]. Recently, nanomaterials released from fires have been identified, which could be potentially hazardous; however, the impact of these substances on human health is currently unknown.

Finally, spontaneous coal fires are just a fraction of the natural coal fires; however these can damage the extractive and productive capacity of industries as well as reducing resources for mining resulting in economic losses. As mentioned earlier, there are some direct problems created by these such as the loss of material in deposits or in the mining site, redirection of the working force for extinguishing fires [41]. Alongside these, there is a reduction of the economic income for companies and governments, which also affects other businesses related directly or indirectly to the coal industry [43,47]. The cost of treatment of diseases produced in the

population due to poisoning and chronic intoxication, the recovery and decontamination of soils affected, the cost to reintroduce natural species in affected places, and the loss of environmental value of these sites and others indirect problems are even more difficult to quantify [43].

1.3 A new player: biomass used as a fuel to combat climate change

Considering the current living standards of our society, the impact of coal consumption has increased, and it is necessary to find clean and sustainable alternatives to replace it. As a result, the use of fresh biomass (energy crops & forestry waste) and the use of the organic fraction of municipal wastes are now considered clean sources of renewable energy. Both have a potential role to play in combustion and gasification processes [48,49] because they can reduce overall CO_2 and NO_x emissions [50], with a lower cost energy source [51], whilst reducing waste residues from other processes and the reliance on imported fuels. For these reasons the drivers over the last decade have been towards the greater use of biomass in energy production through environmental and economic policy targets established for the EU [52]. This area is still an active focus of policy debate. In the UK, the targets for CO_2 emission reductions from coal based electricity production by 2020 are currently set at 32% of 1990 emissions [53], thus creating several scenarios in which biomass has a key role [54]. Each scenario highlights the need to understand how biomass differs from coal during combustion or gasification.

Biomass combustion will be different from coal combustion, not least because of the huge differences in composition. The calorific value (cv) for biomass material can range from 4-19GJ ton[-1], with moisture contents of 2% to 60%, carbon contents of 20% to 80wt%, and volatile contents of ~10 to 70% [55]. A standard bituminous coal might have values of 36Gj ton[-1] for CV, 1% of moisture, 90% of carbon content and

22% of volatiles, although they can vary depending on the age of the coal [3,2]. Nevertheless, these differences are negative when coal is replaced directly by biomass, because the efficiency of the whole process is reduced considerably [71]. However, in the last ten years co-firing of coal-biomass blends has seen an increased interest in partial replacement of coal with biomass in power stations. Blending has been the route to minimizing the negative impacts. The advantages include the direct reduction of CO_2 with approximately 10% now being produced by the closed carbon cycle of biomass; the use of residues and organic wastes from other process, which reduce landfill disposal; a reduction in the ash waste generated due to its low ash content; and the diversification of the energy matrix [56]. Nevertheless, the negative impacts include the increase in NO_X emissions [56]; the synergistic effects produced by coal-biomass blends on ash deposition, which affects the heat recovery systems and reduce the efficiency of the whole process [56]; there is an increase in the energy needed for milling due to the fibrous nature of biomass [56]; and problems related to the seasonal fluctuations of the supply [54].

1.4 Potential risks of biomass and coal-biomass blends

Biomass under certain conditions also has the potential to suffer a thermal runaway. There have been incidents reported in the literature [57], but less scientific attention has been placed on this problem, probably due to its low incidence rate. However, some biomasses have a particularly high chance of spontaneous fires [58]. In these cases, the causes of the self-heating are different than those presented by coal, and bacterial activity is usually one of the main contributors through the heat released from the aerobic respiration process [59].

Also, the spontaneous combustion of coal-biomass blends is a potential problem that has not received any consideration. As co-firing initiatives are increasing, large

quantities of coal and biomass used for electricity generation are being stockpiled in power stations. These deposits share the same environmental conditions as coal, such as open stockpiling in the contact with rain, wind and sun radiation. Under these circumstances, there is insufficient information about the potential risks of thermal runaways produced by self-oxidation processes; about how a blend of these materials behave when stored for short or long periods of time; and also about any possible synergistic effects produced by biomass/coal blends [60]. As it will be shown later that environmental moisture and water content are critical parameters that link to the thermal runaway of coal. At the same time, fresh biomass and organic wastes are characterized by their high water content. The association of these two factors can have dramatic consequences with regard to a self-heating phenomenon.

1.5 Thesis overview

The aim of this research is the prediction of spontaneous combustion. After the review of the current global scenarios given in this Chapter, the scientific understanding of the spontaneous combustion phenomenon is reviewed in Chapter 2. Then, a methodological research proposal and the materials used to address these questions are presented in Chapter 3. The basic results of the investigation are presented in Chapters 4, 5 and 6; with an integrated view of all the results in Chapter 7. Finally, Chapter 8 presents the main conclusions and findings of the whole project, as well as some recommendations for further work.

Chapter 2. Understanding the self-heating process

2.1 Introduction

The first attempts to understand the spontaneous combustion of coal appear around the beginning of twentieth century. In 1908, Parr [27] was one of the earliest researchers to study the initial stages of coal oxidation, particularly around weathering phenomena. He quantified the effect of volatile release and the adsorption of oxygen by measuring the partial pressure and the combustibility of the gas generated in a sealed sample jar after being stored for 10 months. This study also reported the loss of calorific value during weathering with similar values to those reported in current literature (~1.5 to 3%). From this early work he concluded that the aerial oxidation of the sample at low temperature was responsible for the changes. However, in 1911 Parr went even further [28] by describing the "avidity of freshly-mined coal for oxygen" and the loss of hydrocarbons, including accurate details of the amount of CO, CO_2, CH_4 and O_2 involved in the reaction. Oxygen was found to "absorb very rapidly in a manner which does not result in the formation of carbon dioxide, but by direct incorporation into the molecular structure to satisfy certain of the unsaturated compounds". It was a relevant conclusion, and it is still part of the current understanding for the mechanism of the reaction. In 1926 [61,62], he went on to point to the effect of pyrite content as a factor for spontaneous combustion, but verifying that sulphur was not always the source [63]. Finally in 1929 [64], during a work related to low-temperature carbonization of coal, a coal sample was heated in a constant heating rate under an oxidative atmosphere (Figure 6), recording temperature profiles similar to these obtained using the crossing point temperature method, which was developed several years later (used nowadays for propensity

assessment). At this stage, this was one of the first graphic visualisation of the phenomenon.
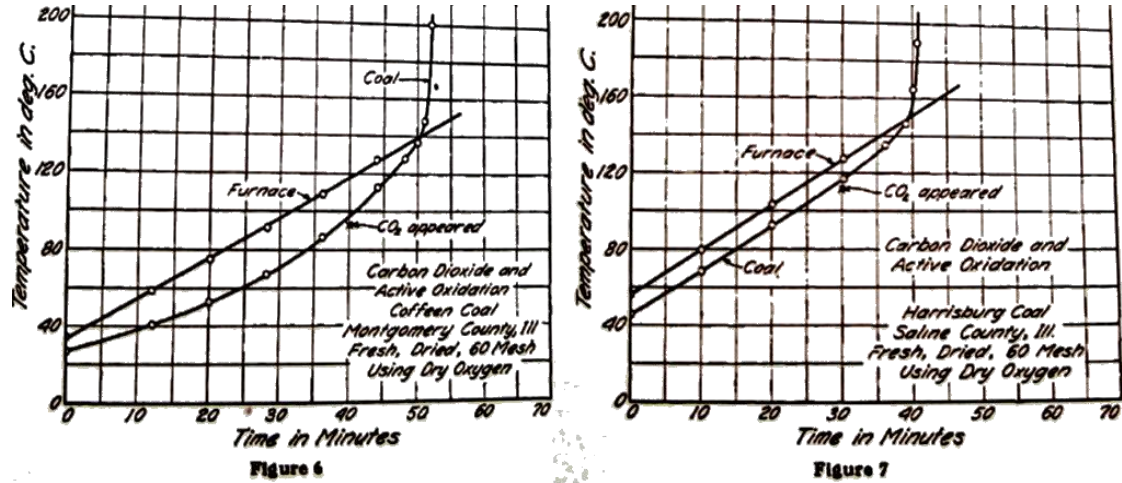
Figure 6: Experimental results obtained for Parr in 1926 [64].

In parallel to the work of Parr, in 1925 J. Davis developed an experimental method to quantify the loss of heating value, using a calorimetric device, indicating that coals stored at temperatures higher than 125°C would be extremely dangerous [65]. This was the first attempt to measure spontaneous propensity using the heat evolution rather than the rate of adsorption of oxygen [66]. This work identified some key parameters that influence the process including coal rank, particle size and surface area. Finally, Davis introduced the idea of the influence of moisture on the spontaneous heating of coal [67]. It was shown that "in dried coals spontaneous heating proceeds slowly from 70°C tending to stop around 97°C, indicating that the presence of moisture is required by the spontaneous heating reactions". Finally, it was concluded that coals with moisture content have pores filled with water that cannot absorb oxygen; and dried coals will extract moisture from the environment creating a heat of condensation, which increase its critical temperature [67].

However, later it was demonstrated that water content in some cases produce the opposite effect encouraging the reaction [68].

Over time, different scientific disciplines have tried to understand the phenomenon, using the tools available within their own field. Geologists introduced the use of microscopes to quantify mineral content and crystal structure of the coal matrix [69]; Engineers introduced measurements of bed temperature, calorific values, and fluid dynamics of the systems [70]; Chemists introduced the kinetics and mechanisms, identifying also the organic components involved in the reactions [29]. Recently, the integration of the results from these different areas has brought a clearer understanding of the process. However, although the causes are well known, there is still a need to develop safe and reliable methods for an early detection of the reaction. Spontaneous combustion incidents still happen that could probably be avoided.

2.2 The spontaneous heating reactions of coal

There are different oxidation reactions that coal can undergo depending on the magnitude of the variables involved in the process. In all cases, these reactions have an exothermic characteristic that contributes in a single or parallel way to the global phenomena of self-heating. The development of a mechanism to explain the phenomenon depends directly on the variables present and the specific chemical reactions involved. From literature, three main reactions appear to be possible [29]:

- The exothermic reaction of coal oxidation by oxygen directly.

- The exothermic adsorption of water molecules in the coal surface.

- The exothermic reaction of pyrite oxidation in the coal matrix.

A biochemical reaction of bacteria on the coal surface has been identified that produces heat [71,72]. However, this mechanism will be omitted from this research because the heat contribution has proven to be insignificant.

For all the three reaction mechanisms, the concentration of oxygen is essential, but also the presence of pyrite and water is a key factor to develop the global phenomena in some specific coals. These reactions are schematized in Figure 7.
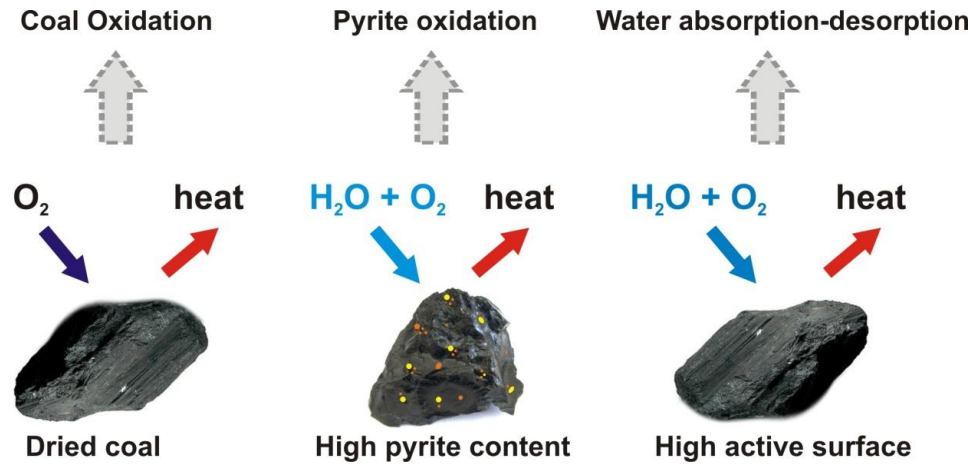
Figure 7: Different reactions that release heat, which contribute to the global self-heating process.

The contact of coal with molecular oxygen present in the air is the main cause of self-heating and spontaneous combustion. This oxidation phenomenon takes place immediately when coal is extracted from seams and comes into contact with air. Oxidation is a complex process that involves several steps and in some cases different reaction pathways depending on the chemical characteristics of the coal [73]. However, it also depends on the amount of coal since heat accumulation is critical in various exothermic reactions. In this case, technological variables such as height of deposit, degree of compaction, wind speed over the deposit, length in time of storage, and the lateral angles of the piles also play an important role in facilitating the heat accumulation [74]. All these factors combined are present during the transport and processing of the material, and they can encourage the development of the reaction.

2.2.1 Variables involved in the self-heating of coal

Several variables have been identified to be related to the self-heating of coal [29,73]. The most important ones are the dependency on the oxygen concentration and the temperature. The reaction is also significantly affected by the presence of water, particular minerals, and the particle surface area. All these variables have a strong influence on both the intrinsic reactivity and the global rate of the reaction. Most of these are considered in the different proposed mechanisms and in subsequent kinetics parameters associated with the self-heating phenomena. However, there is also a set of secondary variables from which the reaction has some dependency, but these are considered to be less significant. The variables identified in the literature are discussed below.

2.2.1.1 Temperature

Work on coal self-oxidation [75,76,77] has identified temperature as one of the most relevant parameters with a direct impact on the rate of reaction. For all chemical reactions involved in the self-heating process (exothermic and endothermic), it is common to use the Arrhenius equation to describe the dependency of the rate of the reaction with the temperature, which depends exponentially on this parameter [76]. This variable also has an effect on some secondary processes such as rate of oxygen diffusion through the coal matrix [78]; the adsorption of oxygen and water; and desorption and diffusion of products from the coal surface [75,77].

The temperature profiles in a coal pile are established by internal and external changes. First, it is affected mainly by internal conditions, such as the heat released by exothermic chemical reactions; and by physical phenomenon such as adsorption of vapours in the coal surface [79]. Also, there are some external parameters that affect the coal bed temperature such as the incidence of solar radiation [80]. Solar

radiation has not being studied deeply; however theoretical calculations have shown that this factor depends on the time of year but can be relevant [80].

2.2.1.2 Concentration of oxygen in the surface of coal particles

The concentration of oxygen is a critical factor and the main cause of spontaneous combustion, as some researchers have demonstrated [81,82]. The rate of the coal oxidation is directly proportional to the partial pressure of the oxygen in the surface of particles [83]. However, at the same time as oxygen is adsorbed in the coal, the active sites available for the adsorption are gradually reduced leading to saturation, which shifts the ignition point towards higher temperatures [84]. Oxygen concentration is also important for the secondary reactions that can lead to an indirect self-heating process, such as pyrite oxidation [61,62] and water adsorption (reviewed in Figure 7) [85]. For these reasons, the experimental measurement of oxygen consumption has been used as one of the early variables to estimate the propensity of a coal to spontaneous combust [28]. This parameter is still used to measure the oxidation ability of coals [86].

2.2.1.3 Moisture content in the coal sample

As a hygroscopic material, coal has a natural affinity to absorb water. For freshly mined coal, the inherent water content is proportional to the coal maturation reached during its geological formation (Figure 1) [2]. Depending on this, water can be found in three different phases: free moisture, loosely bound moisture, and tightly bound moisture (chemically bound moisture is not included), requiring different amounts of energy to be removed from the coal surface [87]. The original inherent water content can produce a dual effect in the coal oxidation: A) inhibition by the obstruction of pores and active sites available for the oxidation reaction [88], resulting in a cooling effect from the water desorption [68,85]; or B) enhancing the oxidation process by

acting as a catalyst [89]. The competition between these phenomena will determine the net amount of heat released. The different mechanisms in which inherent water plays a role are explained in Section 2.3.2.

2.2.1.4 Atmospheric moisture

When coal interacts with the atmosphere, water can be adsorbed or desorbed to reach equilibrium with environmental conditions. The physical adsorption of water in the coal particles is an exothermic process that releases heat in the order of 44.4kJ mol^{-1} (described in Section 2.3.2) [90]. The ability for coal to absorb moisture depends on the porosity and internal surface area, which also depends on coal rank i.e. higher surface areas for low rank coals [88]. When this phenomenon takes place and the evolved heat is not released, the temperature of the coal bed can rise and lead to a chain oxidation reaction [90]. For this reason, the relative humidity of the air is a significant variable in the process [79].

2.2.1.5 Mineral content of coal

Mineral content can have a dual effect in the self-heating phenomenon. With regard to self-oxidation, it has been found that some mineral can act as a catalyst enhancing the reaction [91,92]. It is not just pyrites that can releases heat during oxidation, but also some minerals such as calcium carbonate, NaAc, KAc [92], and $Cu(Ac)_2$ [93]. This can reduce considerably the barrier imposed by the activation energy, even if their concentration is small (usually in the range of 1 to 5%) [92]. Conversely, when the concentration of minerals in the coal matrix is higher, they can act as an inhibitor in the reaction, blocking the active sites and acting as a heat sink. This phenomenon usually occurs when the mineral content is above 5%wt [94], with the exception of some minerals that directly inhibit the reaction, such as KCl, NaCl [92], $CaCl_2$, and $Mg(Ac)_2$ [93]. The total mineral concentration is normally calculated as the residue

remaining after burn out, and the inhibitor effect is independent on the chemical composition of the minerals when their concentration is higher than 10% wt [94].

2.2.1.6 Size of coal particles

The effect of particle size has been studied by several researchers [95,96,97]. These studies have taken a range of sizes from pulverized coal particles (where 75% is less than 75μm), to lumps of several centimetres. The smallest particle sizes produce the maximum external surface area producing an increase in the rate of oxygen consumption [97], as shown in Figure 8. This increase in the external surface accompanying the reduction of particle size is of minor significance, compared to the increase in accessible internal surface, which is related directly to the self-oxidation reaction [98]. A maximum point is reached when kinetic control is achieved, particularly for particle sizes in the range below 500 to 100μm [99].
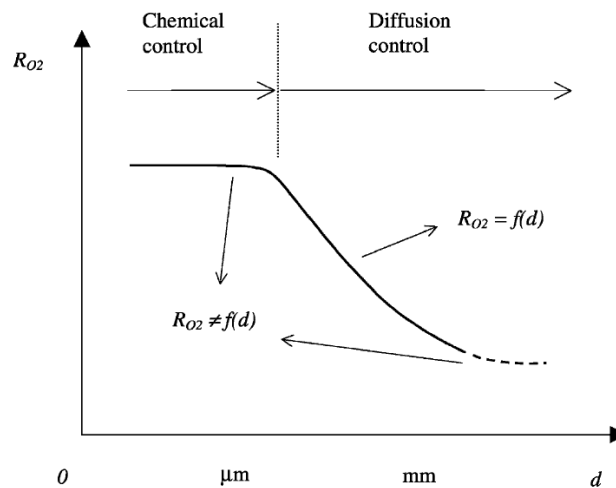
Figure 8: Typical trend used to exemplify the role of particle size in the different stages of the reaction rate of coal oxidation [100].

2.2.1.7 Porosity and internal surface area of coal particles

Surface area is relevant to the progress of the reaction, as explained in the previous section [97,78]. The main contribution to this comes from the internal porosity

structure of the coal, specifically from the microporous region (pore diameter less than 2nm), which for coals provides a considerably larger area than the macro porous structure (pore diameter greater than 50nm) [2]. This porosity is usually a consequence of an uncompleted geological process. For instance, it is understood that brown coals (lignite, low rank) have higher propensity for spontaneous combustion [101,89]. This is explained mainly through the high surface area available in this kind of coal, which provides a large number of active sites which can react with oxygen, and also because these sites are able to absorb moisture [102]. Other contributory factors include higher initial volatile and water content, compared to other types of coal (Figure 1).

2.2.1.8 Proportion of maceral components presented in coal

Maceral composition is analogous to the term "mineral composition". However, these are carbon structures formed by the original plant material during carbonization [1]. There are several maceral groups, but commonly the most frequent are three:

a) **Vitrinite**: formed by cellular walls or woody tissue of plant material. It has high calorific value and high volatile content, and normally it is the most abundant component of coal (50-90%) [1,2];

b) **Liptinite**: it is produced from spores, pollen, waxy and resinous parts of the plants. It has a lower calorific value but a high volatile content, being fluorescent under ultraviolet light. Normally, it is around 1-15% of the coal matrix – depending on origin and rank [1,2];

c) **Inertinite**: comes from material strongly altered and degraded during the coal formation. It has low volatile content and high calorific value, varying from 5 to 40% [1,2].

24

The influence of maceral composition in the spontaneous combustion phenomena is not well understood, since most techniques focused on thermal analysis instead of microscopy, but there are some reports that investigate this to some extent [69]. Petrography is a very common variable used to quantify the reactivity of coals by power stations, because it has been demonstrated that each singular maceral group has a particular combustion characteristic, and degree of reactivity [103,104].

2.2.1.9 Coal rank or vitrinite light reflectance

Coal rank can be defined as the degree of coalification reached by the carbonaceous material through the metamorphism [2,3]. This property can be measured through the reflection of the light, usually focussing on the light of the vitrinite maceral to suggest the maturity and the crystal structure of the coal matrix [105]. For instance, low coal rank such as peat and brown coal has a low rank value due to its high porosity and structural isotropy, which means that most of the light directed to the sample is captured by the porous structure. High rank coals such as anthracites and coke have high reflectance values, since most of the light is reflected because of highly developed anisotropy and a well ordered aromatic carbon structure. At the same time, the crystal structure has a direct relationship with reactivity. Low rank coals are more reactive than higher rank coals, which have a lower porosity, a lower adsorption capacity and reduced water content [2].

This parameter also has been substantially used by the coal industry as one of the main indicators of propensity to spontaneous combustion [75]. In this case, low rank coals share some critical variables such as high porosity and surface area; it has an affinity to absorb water; a high volatile content; and a high vitrinite and liptinite content [101]. However, there are cases where rank is high and the reactivity (or propensity) remains high as well [106]. A low rank coal with a high water content

and porous structure can be completely saturated making the coal relatively unreactive [88].

2.2.1.10 Density of the sample (weight change)

This variable is generally used by the coal industry to estimate the rate of the combustion reaction, reactivity, and the distributions of compounds such as moisture, volatiles, fixed carbon and ash content [107]. However, this has not been used to estimate the coals propensity to spontaneously combust. Just a few researchers have tried to link this parameter to the spontaneous combustion behaviour [108,109]. From these works, there is evidence that weight loss is directly connected to the volatile release when oxidation occurs at low temperatures [108]. However, their results are inaccurate, not showing a conclusive trend. Preliminary research has shown that it is possible to implement a thermogravimetric program to quantify the rate of the oxidation reaction and the oxygen adsorption in coals [109].

2.2.1.11 Volatile content and chemical composition of coal

Each coal is unique in terms of its chemical composition. The difference in their chemical attributes can provide valuable information about the potential reactions that a coal sample can undergo. These differences act as a 'fingerprint' of coals before, during and after the oxidation. In coal fire research, there are several experimental procedures that can quantify chemical composition such as: Gas Chromatography, used to calculate the composition of the gases released from seams [110] to monitor the rate of the reaction and the environmental impact associated [111]; Mass Spectrometry, used to identify compound and molecules present in coals prone to spontaneous combustion before and after the reaction [112]; Fourier Transform Infrared Spectroscopy (FTIR), used to characterize samples by detecting molecular groups associated to the self-oxidation reaction [113], as well as to

identify chemical alterations produced by weathering [114]; Ultimate Analysis (or Elemental Analysis), used to quantify elemental composition in terms of C, H, O, N, and S which form the majority of the weight of coal [115]; Proximate Analysis, used to quantify moisture, fixed carbon, ash and volatile content, which are usually estimated by thermogravimetric methods [107]. With regard to the self-oxidation process, the results of these experimental tests have been used successfully to identify the chemical reactions, to postulate mechanisms and calculate the rate of the reactions involved [29].

2.3 Mechanisms, kinetics and thermodynamics of self-oxidation reactions

In this section, the three main chemical interactions identified as the precursors of the spontaneous combustion of coal (Figure 7) are described. Understanding the mechanism and the kinetics of these reactions is fundamentally important when seeking to understand the spontaneous combustion process. Particularly, several mechanisms have been postulated to describe the different stages of the oxidation reaction, including the intermediate species and free radicals from which the main chemical changes occur. The details of these steps have been useful in suggesting the kinetics models that can be applied to theoretical scenarios, allowing the conversion and the rate of the reaction to be calculated [100]. Understanding the mechanism and kinetics is crucial to predict bigger systems in a variety of environmental conditions. These models provide useful tools in the design of transport and storage facilities, as well as providing information to calculate the real impact of each variable in the whole process (through a sensitivity analysis) [116]. However, due to the heterogeneous and complex chemistry of coal, the mechanisms for self-oxidation are still only partially understood.

2.3.1 Low temperature oxidation of coal by O_2

Coal oxidation at low temperatures will follow a completely different series of reactions from those at high temperature [2,3]. In this case the reaction takes place between 25 to $150^{\circ}C$ without flame, in a very slow process with a slight output of heat. When the amounts of coal are small (in the order of grams to a couple of tons), the exothermic reaction produces an insignificant effect over the rate of the reaction, mainly because the temperature is regulated by the heat transfer to the surroundings, which is maximized when the reaction area is reduced [117]. However, for a large amount of coal (in the order of hundreds to thousands of tons), the heat transfer to the surroundings is reduced compared with the amount of heat produced, which combined with the low thermal conductivity of coal generates a significant enthalpic effect. This heat accumulation accelerates the rate of the reaction, finally triggering the thermal runaway and the high temperature combustion [118,119]. add

The first attempts to characterize the reaction only estimated reaction rate, trying to establish theoretical mechanisms of oxygen absorption by coals. Parr and Kressman 1911 [28] were the first to maintain that freshly-mined coal absorbs oxygen in a manner which does not result in the formation of carbon dioxide, but by direct incorporation into the molecular structure, particularly around unsaturated compounds. They observed this by analysing the gas released after an incubation period for a number of coal samples. In 1908 Parr & Wheeler [27] concluded that the absorption of oxygen by bituminous coal was initially very rapid, even at ordinary atmospheric temperatures. They also noticed that it was not accompanied by the formation of water or oxides of carbon. The rapid sorption soon gave way to slow but extensive absorption, in which water and the oxides of carbon appear, accompanied by an increase in the coal bed temperature. However, these facts did

not explain the reaction mechanism that leads to spontaneous combustion, and they gave no indication of the reason why one coal is more liable to self-heat than another. Porter and Ralston in 1914 [120] also observed that the reactions were primarily oxidation reactions, in which the oxygen first combines with the coal to form an "unstable solid", which gradually breaks down with increasing temperature, forming the normal gaseous oxidation products. In 1925 Davis & Byrne [66] tried to estimate the rate of the reaction by measuring the heat released. Schmidt and Elder [121] demonstrated in 1936 that the total weight of a coal sample increases when the adsorption of oxygen takes place, indicating that the weight of the oxygen remaining on the coal was greater than the weight of carbon and hydrogen that was lost as gaseous products. Later, the same researchers measured the characteristic oxidation rates of coals [121] and concluded that the speed of oxidation increased with increasing volatile matter content.

After this successful development, the focus centred on improving the experimental techniques to calculate the rate of the reaction. Carpenter in 1964 [75,122,97,78] studied the effect of coal rank, temperature and the time on the rate of the oxygen consumption. Some of these results added to the findings of previous researchers [123] showing that the activation energy remained approximately constant for the low temperature oxidation, and confirmed that the reaction was dependent on temperature, in line with the Arrhenius equation. Based on the profiles of oxygen consumption obtained during the same work, a global mechanism was proposed that included three stages:

A) The external and macro porous surface controls the rate of oxygen consumption. At this stage, there are combined effects: the adsorption of oxygen, which blocks active sites; and the creation of new actives sites due to the

desorption of unstable solid-solid bonds. This will produce a linear rate of oxygen consumption [75].

B) By the second stage there is a large surface available, but now it is less accessible. Through combined effect of adsorption and desorption, an abrupt decrease in the oxygen consumption occurs [75].

C) At this stage, there is an even less accessible surface, in which the rate of adsorption of the oxygen controls the rate of the reaction. However, the increase in temperature could allow greater quantities of oxygen to be consumed before the change in the reaction rate [75].

This explanation was supported by calculations of the order of the reaction for the different stages [122], which was in the range of 0.01 to 2 for six samples studied, depending on the concentration of the oxygen on the coal surface. However these conclusions were not enough to formulate a definitive mechanism. Then, in a further study [97] the effect of particle size was introduced (previously studied by Schmidt [123]) and the accessibility of the internal surface to oxygen [78]. From these results it was concluded that the previous reaction regimes were influenced by particle size through an increase in the available reactive area, when there is a reduction of this parameter. For particles below the range of 2000µm to 36µm they found that the increase in the reactive surface area had a negligible effect on the rate of the reaction, being chemically controlled below these limits.

Despite all these efforts, the mechanism of the reaction is still unclear. In this context, one of the first to propose a molecular mechanism for the coal oxidation at low temperature was Marinov in 1977, who studied the changes in weight [108], elementary composition [124], and oxygen functional groups [82] produced by non-isothermal exposure of coals to oxygen. These studies combined IR-spectrometry,

gas chromatography, microscopy and thermogravimetry, which gave a wider vision of the phenomenon. Two reactive regions were identified: one where the hydrogen content remained invariable or increased, which means a possible interaction of coal with water in oxygen presence [108]; and a second region, where gases are produced in a higher rate producing self-ignition due to exothermic decomposition. From these observations it was deduced that the oxidation reaction could be considered as a redox process, in which the aromatic part of coal acts as an oxidizing agent, specifically where attached hydrogen is not affected by molecular oxygen [108,82]. The generation and elimination of hydrogen peroxide is assumed to be a reason for the endothermicity at some stages of the reaction. Then, the self-ignition is due to the combustion of low molecular weight products initiated by aldehyde oxidation [82]. These two conclusions have been used as a base for the proposed theoretical mechanisms. In parallel to these studies, there was also an interest in the specific factors that influence the global process, such as the role of water molecules and the heat released by its adsorption [85,79] (studied in Section 2.3.2); and the changes in coal structure due to oxidation [125,126].

The work of three specific research groups has been widely accepted by the scientific community. Each developed their own theories which have been used by others and thus they represent the current state of the art and they are described as follow:

J. Gethner, (1980-1987) [127,128,129,130,131,132].

Work on FTIR analysis of coal samples [127] showed that vacuum drying methods, used in previous work to study isolated coal-oxygen interactions, also induced complex changes in the coal matrix. These changes were indicative of variations in internal hydrogen-bonded interactions and in the number and types of cross linked

bonds [129]. In the same study, there were observed reactions involving carbon-oxygen groups, such as carboxylic acid groups changes in functionality, which meant an important perturbation of the organic coal reactive area after a drying process. From both findings, it was inferred that previous mechanistic implications about the low temperature oxidation reaction may not be correct, due to the alteration of the thermal history of the samples [128,129].

After these important points, the focus was to examine the mechanism. Coal samples were exposed to a mild thermal oxidation and subjected to FTIR analysis, which indicates the presence of at least three reactions, from which two are competitive taking place at low temperatures (Equation 1 & Equation 3, ~ 25°C), and one taking place at higher temperatures (Equation 2, ~ 100°C). Two of these reactions involve oxygen directly (Equation 2 & Equation 3), and the third is a decarbonylation that proceeds in the absence of oxygen (Equation 1). The steps are described as follows [131]:

Thermal pathway

$$\text{Equation 1} \qquad \textbf{(Coal)-OOH} \rightarrow \textbf{Coal} + \textbf{H}_2\textbf{O} + \textbf{CO}_2 + \textbf{CO}$$

Oxidation pathways

$$\text{Equation 2} \qquad \textbf{[Coal-C=O]} \bullet + \textbf{O}_2 \ \rightarrow \ \textbf{Coal} + \textbf{H}_2\textbf{O} + \textbf{CO}_2 + \textbf{CO}$$

$$\text{Equation 3} \qquad \textbf{Coal} + \textbf{O}_2 \rightarrow \textbf{[Coal-OOH]} \rightarrow \textbf{[Coal-C=O]}$$
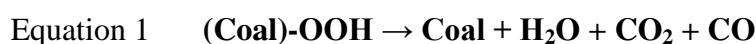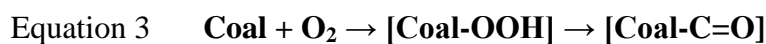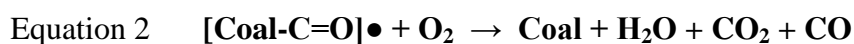
First, a variety of oxygenated carbonyl species are formed by the coal oxidation (Equation 3). At the same time, there is a loss of carbonyl species (Equation 1), which are different from those formed during reaction III (Equation 3). However, if they proceed during an extended period, the net change is approximately zero. Then, an oxidation reaction takes place due to the increase in temperature produced by

32

reaction I (Equation 1), which also interferes with reaction II (Equation 2), releasing CO, CO_2 and water. In addition, the reactions appeared to be sensitive to the presence of water molecules, similar to the findings of Marinov [108,132]. Finally, it was concluded that the overall effect of oxidation was dependent on time, temperature, history and pre-treatment of the sample [131]. These developments complemented the work of both Marinov and Carpenter. However, there were some complex interrelations that still require explanation and the mechanism remains unclear.

H. Wang et al (1999-2005) [99,133,134,29,100].

Based on previous research [29,100], theoretical analysis [99,133] and experimental work [134], Wang et al. proposed a multi-step mechanism which considered gas adsorption, formation of gaseous and solids products, and thermal decomposition steps. The detail of the mechanism proposed starts with the chemisorption of oxygen molecules in the pores of the coal surface, forming a group of carbon-oxygen complex at temperatures between ~20 to 70$^{\mathrm{o}}$C. These carbon-oxygen complex were classified in three groups: unstable (peroxygen, hydroperoxide and hydroxyl species); stable (carbonyl or carboxyl-containing species); and unreactives (humic acids) [29]. Then, when a slightly higher temperature is reached (~50 to 70$^{\mathrm{o}}$C), these oxygenated complexes undergo a thermal decomposition. The last reaction evolves in parallel to a direct reaction of coal oxidation, which also contributes to the emission of carbon oxides [100]. The reaction of the solid carbon-oxygen complex also could create new stable solid products, which can be decomposed at temperatures higher than 70$^{\mathrm{o}}$C, leaving available new active sites to be used by the reaction as shown in Figure 9 [100].

$$coal + O_2 \xrightarrow{\text{Burnoff}} CO_2, CO \text{ and } H_2O$$

$$coal + O_2 \xrightarrow{\text{Sorption}} \text{Unstable solid intermediate carbon-oxygen complexes}$$

$CO_2, CO \text{ and } H_2O$

Stable solid products, which tend to decompose at temperatures above 70°C
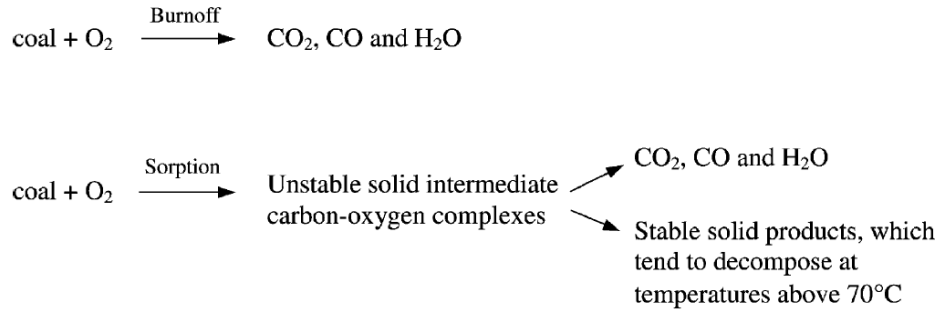
Figure 9: Potential pathways followed by the coal oxidation reaction. Proposed by Wang et al. 2003 [100].

The mechanism proposed by Wang is similar to that proposed by Gethner in 1984 [132]. However, from previous work a more detailed approach to the chemisorption sequence was introduced, which could explain the role of water molecules. This sequence also explains why other species are detected, and how the reaction regenerates the active sites, liberating carbon oxides. This process may also be catalysed by water molecules. The whole sequence is presented in Figure 10, in which **R•** represent the radical that starts the chain reaction [100].
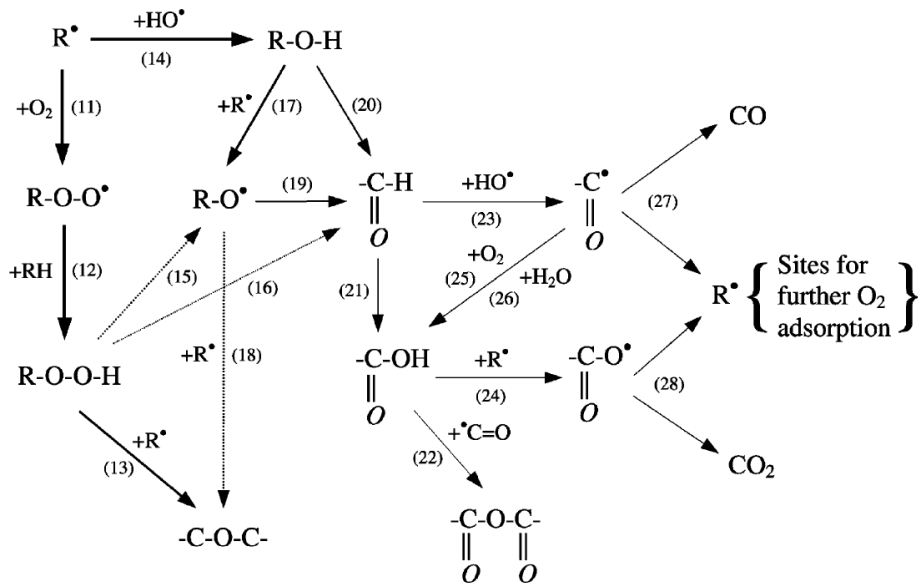
Figure 10: Mechanism of the chemisorption sequence proposed by Wang [100].

Finally, Wang suggested that two parallel reactions sequences contributed to the emission of carbon oxides during oxidation (as shown in Figure 11); however, depending on the particle size and the porosity of the coal, the reaction is controlled by continuing diffusion for reactive coal, or kinetically controlled for less reactive coal [29].
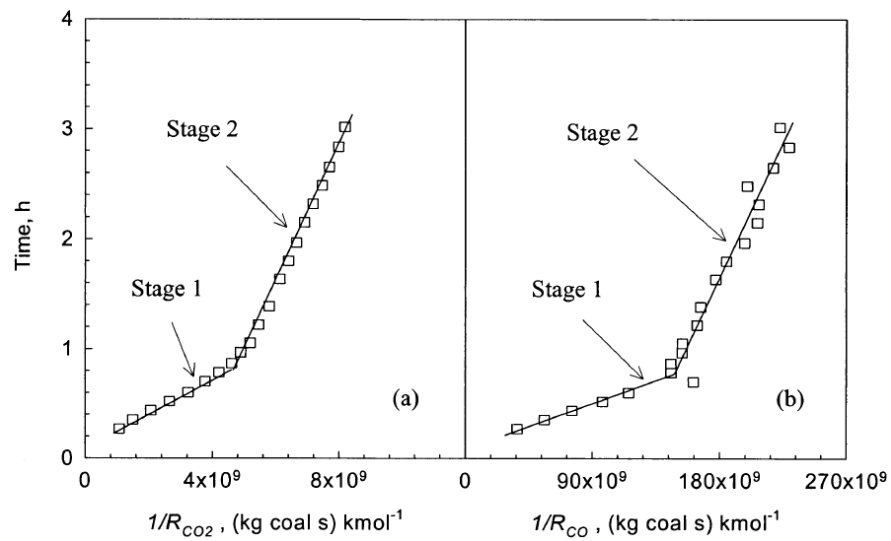
Figure 11: Different stages for the emission of CO_2 and CO during the coal oxidation at low temperature. Wang et al. 2003 [29].

After the contribution of Wang and co-workers, no further experimental advances have been reported about the mechanism. However, some theoretical work has been produced in which algorithms of Molecular Dynamics were used to demonstrate previous findings and explore potential unknown pathways. One of these is described as follows:
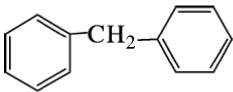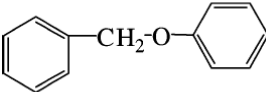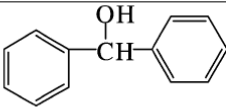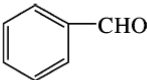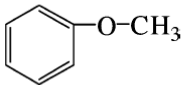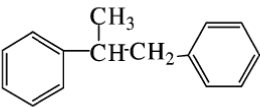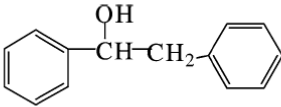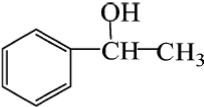
T. Shi et al (2005) [135]

Shi et al. recently investigated the mechanism of oxidation at room temperature using quantum chemical methods. A model of coal surface in which the reactions take place was proposed, simulating eight types of active groups connected to one or

two aromatic rings linked to the surface. Afterwards, the mechanism of oxidation of all these components was simulated by density functional theory (DFT) and ONIOM methods (stands for our own n-layered integrated molecular orbital and molecular mechanics); both programmed using numerical software. The simulation provided useful information about the activation energy of each component selected and the potential oxidation reactions that it could suffer. It also provided information about coal structure and thermodynamic data associated with these reactions. For theoretical applications, coal was replaced by a single aromatic ring, considered stable and unreactive during the oxidation. It was also considered that the oxidation reaction takes place between actives groups and oxygen. The active groups used in this research are presented in Table 1.

Table 1: Model of coal molecules used in the simulation [135]

R1	R2	R3	R4
$-CH_2-$	$-CH_2-O-$	$-CHOH-$	$-CHO$
ΔH=-18.65 kJ/mol	ΔH=21.3 kJ/mol	ΔH=-31.35 kJ/mol	ΔH=66.2 kJ/mol

R5	R6	R7	R8
$-OCH_3$	$-CH_3CH-CH_2-$	$-CHOH-CH_2-$	$-CHOH-CH_3$
ΔH=-14.94kJ/mol	ΔH=-125.55kJ/mol	ΔH=-30.20kJ/mol	ΔH=-17.77kJ/mol

From the results obtained, it was demonstrated that the assumption of replacing the coal matrix by phenyl groups did not have any influence on the oxidation of active groups. Then, based on the activation energies and the Gibbs free energy calculated, six of the eight compounds were found to react spontaneously with the atmospheric oxygen at room temperature. In addition, the opposite scenario where the reverse

reaction is prohibited at room temperature was assumed. Finally, the six spontaneous reactions were found to be exothermic. According to these results, it was possible to establish an order of reactivity between active groups (Table 1) as follows: (R7)> (R3)> (R8)> (R6)> (R1)> (R2)> (R4)> (R5), in which reaction 2 and 4 are endothermic.

However, there was some criticism about this work. First, none of the reactions studied produces carbon monoxide, a product found in previous experimental research. Secondly, reactions 2 and 4 were not found to be spontaneous at room temperature and endothermic; however, these are the main reactions proposed by Wang [100], Clemens [89] and Petit [136], as responsible for the self-heating. The mechanisms reviewed are summarized in Table 2.

Table 2: Summary of mechanisms proposed for coal self-oxidation.

Research group	Mechanism	Technique used	Range T
Carpenter et al (1964) [75,122,97,78]	multi-step (3 steps)	Gas chromatography, FT-IR, reactor designed to measure oxygen consumption	25-150°C
J. Gethner, (1982-1987) [127,128,129,130,131,132].	multi-step (3 reactions, in 2 series)	FT-IR	25-100°C
H. Wang et al (1999-2005) [99,133,134,29,100]	multi-step (2 parallel reactions sequences)	Gas chromatography & FT-IR (gas emission of coal bed, isothermal reactor)	25-100°C
T. Shi et al (2005) [135]	multi-step (eight reactions)	Computational chemistry	Start at room temperature

2.3.2 Physical and chemical interactions between coal and water

Water can interact with coal in several ways [98,88], but none of these includes a direct chemical reaction. These interactions are linked to the self-heating process in three different ways: A) by the heat produced from the physical processes of sorption and desorption in the coal surface; B) by a catalytic function in the low temperature oxidation reaction of coal by oxygen; and C) by blocking porous and actives sites available for the main oxidation reaction, producing an inhibitory effect in the thermal runaway.

2.3.2.1 Heat produced by adsorption and desorption of water

A) Moisture adsorption (enhancing self-heating)

The adsorption of moisture in coal has been identified as a major source of the heat that is responsible for the thermal runaway [79]. It is a physical phenomenon produced when water molecules in a liquid or vapour phase are deposited in the pores of the coal matrix by electrostatic forces. This is a spontaneous and exothermic process, with a net enthalpy of adsorption of 44.35kJ mol^{-1} [90], when considering just the adsorption phenomenon itself. Regarding the global self-heating process, there is a difference in the total heat contribution depending on whether the adsorption of water takes place in a liquid or in vapour phase. When liquid water is absorbed, the heat released is in part captured by the water, which has a high calorific capacity producing just a slight rise in temperature in the coal bed, because heat is accumulated in part by the fluid.

However, the thermal behaviour of the global process differs considerably when water molecules are adsorbed in a vapour phase [79]. In this case, it is added to the heat of adsorption (44.35kJ mol^{-1}) the latent heat of condensation of water (40.65kJ mol^{-1}), resulting in a total contribution of 85kJ mol^{-1}, twice as high as with liquid

adsorption. It was found that this phenomenon is much more significant with low rank coals due to their higher internal surface area [89]. Additionally, this heat is released directly to the coal because the mass of water vapour available to capture the heat is negligible compared to the adsorption process with liquid water. Vapour adsorption produces a considerable increase in the coal bed temperature, which is enough to start the chain of the spontaneous combustion reaction [79]. The heat released in this case is even higher than the net heat contribution produced by the direct coal oxidation reaction. It means that the coals capacity to adsorb water or moisture, and the heat released in this process are key variables when assessing a coal ability to self-heat.

B) Moisture desorption (inhibiting self-heating)

In contrast to the adsorption of water, an opposite thermal effect is produced when moisture is desorbed from the coal matrix [85]. In this case, the process needs an energy input since this phenomenon is endothermic, which is different to the adsorption value due to the hysteresis of the process. In this case, the energy requirement is in the order of 11.9 to 14 mol^{-1} [137], when the moisture is released as vapour. If the water in the coal matrix is liquid, then the total heat requirement is even higher because the heat of vaporisation must be included. Overall, this process produces a cooling of the coal bed, which also acts as a heat sink from the parallel reaction of coal oxidation by molecular oxygen, allowing natural weathering but inhibiting the thermal runaway [68].

2.3.2.2 Catalytic effects produced by water in the chemical interaction between coal and oxygen

Besides the direct enthalpic contribution produced by adsorption and desorption, water molecules also catalyse the direct oxidation of coal by air. This idea is derived

from the coal-oxygen complex theory from which water affects the nature of the radical sites where oxidation occurs [29]. This contributes to the generation of peroxi-radicals and the generation of oxygenated solid complex, which are later desorbed from the coal surface and decomposed by aerial oxidation releasing a large amount of heat [89].

This mechanism is complex and still creates disagreements between scientists. Some researchers maintain that the catalytic action is carried out by physically and chemically adsorbed water (surface wetting) instead of water vapour present in the gas phase [138]. Others have shown experimentally that some coals show a large increase in temperature when exposed to moist oxygen instead of dry oxygen, attributing this effect to the moisture present in the gas; however, for this process it is not clear if the vapour is adsorbed on the coal surface first [139]. Finally, it also has been agreed that water affects the nature of the radical sites in which the oxidation takes place [138], which also produces an alteration of the normal thermal behaviour of the direct coal oxidation by molecular oxygen [88].

2.3.2.3 Inhibitory effects produced by water saturation of the active sites

It is possible to identify two inhibitory effects produced by water. The first relates to the residual liquid water deposited in capillary cavities into the coal matrix. This water inhibits the oxidation process by hindering access to reactive sites, and then delaying the contact between molecular oxygen and coal. The oxygen needs to be dissolved first and then transported through the water, presenting a low mass diffusion in this liquid [88]. Considering the case that oxygen finally reacts with the coal surface, water also dissipates the heat produced by the oxidation reaction [89], when moisture content in coal is extremely high (above 20%). The second case is produced when coal has been extensively exposed to air and water, reaching

saturation on the surface reducing the natural oxidation process to a minimum. Since there are not enough active sites to react, the coal cannot produce a significant thermal response that could lead to a thermal runaway [140]. Table 3 presents a summary of all the interactions studied.

Table 3: Summary of water-coal interactions effecting thermal runaway

Reference	Interaction	Effect in the self-heating	Description
[79,88,141,142]	Adsorption of water in the coal surface	enhancing	Net heat release, increasing temperature of coal bed
[89,138]	Catalytic effect in oxidation reaction	enhancing	Reducing activation energy and acting as intermediary
[89,88]	Saturation of coal porous with water molecules	inhibiting	Blocking porous and access to active sites for oxygen molecules
[68,85,89,140]	Desorption of water in the coal surface	inhibiting	Net heat absorption producing a cooling effect in the coal bed

2.3.3 Reaction of pyrite oxidation

A secondary reaction produced by the oxidation of pyrites by oxygen has also been suggested as one contributor to the self-heating of coal [143,61,63]. Pyrites (FeS_2) are present in coals in different mineral formations such as cubic yellow pyrites and rhombic marcasite, in different morphologic forms [144]. In some extreme cases pyrite content can exceed 12%wt; however, in most cases where coal is utilized it range from 0.1 to 5%. Chemically, these minerals are oxidized by oxygen and water through an exothermic reaction that releases 661.07kJ mol^{-1} for mol of FeS_2, or 16.74 Joules per ml of oxygen consumed [25].

It has been found that the global rate of the reaction is similar for both types of minerals; however, there are discrepancies among researchers about the reaction mechanism. In general terms, the chemical reaction of pyrite oxidation can be described as:

$$\text{Equation 4} \qquad 2\,FeS_2 + 7O_2 + 16\,H_2O \rightarrow 2H_2SO_4 + 2FeSO_4 \cdot 7H_2O$$
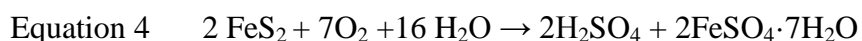
This reaction produces a set of products with a higher volume than the initial reactants, which contribute to the fragmentation of coal, exposing a greater surface area to the air thus accelerating the reaction [25]. The self-heating process is maximized through pyrite oxidation when found in a concentration between 5 to 10%. Concentration greater than 10% or lower than 5% produces a negligible effect in coal self-heating [145]. Nowadays, this problem has been minimized at power stations and in the coal industry through the targeting of coal with low pyrite concentrations, mainly due to the strict environmental regulations for the abatement of SO_2 emissions. For this reason, scientific efforts have mainly concentrated on the interactions of coal-water and coal-air.

2.4 Methods developed for detection and quantification of spontaneous combustion of coal

After the study of the variables and reactions involved, a considerable number of methods have been created to detect or estimate the degree of oxidation that a coal can suffer. From these, the most common approaches are using thermal analysis, considering micro and macro scale experiments. These tests are based on the net amount of heat released by the sample, and the dependence of specific parameters to the temperature. Later, other methods have been introduced considering optical parameters (e.g. microscopy and rank analysis [105]) which provide an idea of the crystal structure of the carbon matrix that is associated directly to the reactivity of

the fuel. Finally, there are some miscellaneous methods that consider a set of less conventional parameters such as gas concentration.

2.4.1 Thermal methods to estimate self-oxidation potential of coals

The common approaches used to predict the spontaneous combustion phenomena are based on thermal analysis [146]. In this case, the main laboratory techniques based on the direct temperature measurement to estimate reactive properties include Differential Thermal Analysis (DTA), Calorimetry, Differential Scanner Calorimeter (DSC), isothermal reactors, and adiabatic reactors. In addition, gas composition analyses are used to obtain information about gaseous reactants, intermediaries and products present before, during and after the oxidation reaction. From these, the most important laboratory techniques are Fourier-transform infrared spectroscopy (FTIR), Gas chromatography (GC) and Mass spectrometry (MS).

2.4.1.1 Methods for testing intrinsic properties of coals

In this section, a number of thermal tests used to measure the intrinsic properties of coals are described. The main characteristic of these tests is the analysis of a small sample mass (in the order of milligrams to grams).

A) Differential Thermal Analysis (DTA): This technique has been used extensively to characterize thermal changes in coal samples. However, there are just a few reports in which it is used directly to assess low temperature oxidation. The usual experimental procedure of DTA exposes coals to a steady heating rate, measuring the temperature difference between the sample and a reference material heated under same conditions. Then, the difference is used to observe the heat evolution of the sample, which relate to the potential chemical reactions that are occurring. This method have been used by Banerjee et al. 1967 [147], Marinov 1977 [108,82], Gouws et al. 1989 [148,149], Pis et al. 1996 [150], and in all cases only

using a small amount of sample (≤20mg). Some of the results obtained from these researchers showed that the thermogram can be divided into three different stages during the heating process [147]. The first stage has been associated to the endothermic releases of moisture from the coal sample. Then, the second stage is slightly exothermic relating to the beginning of the oxidation process. From this stage, it has been concluded that the slope is lower for coals with lower propensity to spontaneous combustion [148]. The third stage is highly exothermic and it has been linked to the main combustion phenomena that coal can undergo. The last stage has not been used to infer properties relating to the self-heating process. In Figure 12, a typical thermogram obtained by DTA is presented.
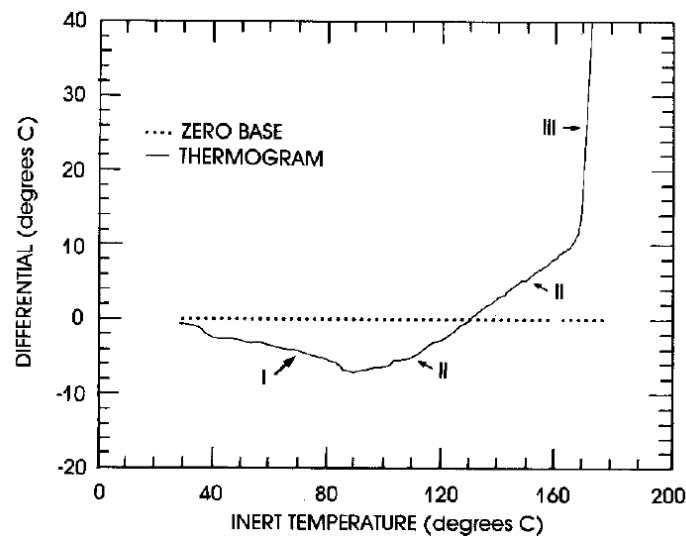
Figure 12: A typical thermogram from a DTA showing the three main regions present during the low temperature oxidation of coal. Extracted from [148].

A standard procedure has been proposed to identify coals prone to spontaneous combustion using this technique [149]. From the characteristics of the thermogram it is possible to calculate the slopes of each segment. These slopes can be considered as a simple index of propensity, but also useful to introduce a mathematical correction

to the crossing point method (reviewed in Section 2.4.1.2) creating a composite index. However, both indices obtained from this technique have been severely criticized, since they produced contradictory predictions of coal self-heating potential [149].

B) Differential Scanner Calorimetry (DSC): The coal sample and a reference material are heated under the same thermal conditions for the same period of time, allowing the difference in energy emitted from each crucible. In this case, the difference between the amount of heat needed to increase the temperature of the sample, and the amount of heat necessary to raise the temperature of a reference material is measured as a function of temperature [151]. Consequently, any difference is therefore directly as a result of physical or chemical transformations taking place.

Reports in the literature about this technique are scarce (Garcia et al. [152], Sahu [153], Mohalik et al. [154,155]). In these, a clear experimental procedure for coal assessment is not defined. Also, the reliability of these are questionable for several reasons: the range of temperature in which the experiments have been carried out (20 to 1000°C) [152] (Figure 13); and the use of raw curves without the subtraction of the environmental noise [154,155]. These issues introduce problems in the analysis and in the sensitivity of the results. Despite all these criticisms, it could be feasible to establish a systematic way to predict propensity using this instrument, which is an important issue for future research.
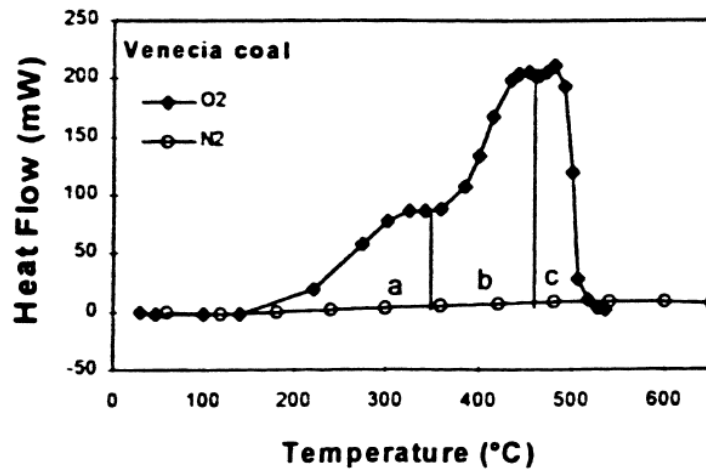
Figure 13: A typical DSC profile obtained for coal [152]. As can be seen, the areas a, b and c are discussed by the author as stages of the self-oxidation phenomena, which contradicts the temperature range proposed by previous researchers [100].

C) **Thermogravimetric Analysis (TGA):** This technique is widely used to characterize coal samples by the coal industry, especially when obtaining reactivity data and compositional characteristics [107]. For fire research, this instrument has allowed the measurement of parameters such as reactivity of coal in air at low temperature, under different heating and atmospheric conditions [156,108,82], as well as some basic properties such as volatile content, mineral and moisture content, and fixed carbon [107]. However, this technique has not been used to quantify the propensity of coals to spontaneous combustion directly, since it is argued that the reaction is too slight to be detected by the instrument [29].

Some TGA experiments have shown a link between weight loss and the self heating behaviour of coal [108,82,157,156]. Researchers reported the increase of weight of the sample between 20 to 300°C when it is exposed to a heating ramp [108]. However, this approach has some issues relating sampling scale, which was in the order of grams. When an attempt was made to reduce the sample weight to micrograms, the accuracy of the results was dramatically reduced by the sampling

46

noise generated by the instrument. The findings reported in this work were confirmed by other techniques (e.g. FT-IR, GC-MS), but not yet confirmed using a TGA with a higher sensitivity.

Another thermogravimetric analysis reported was exposing coals to a constant heating rate (5°C min^{-1}) under different oxygen concentrations (Figure 14) [158]. As can be seen from the graph, the temperature range has no relation to the ranges proposed by previous researchers [100]. Also, the resolution of the curves between 20 to 300°C is reduced, making it impossible to detect any anomalous behaviour during the low temperature process.
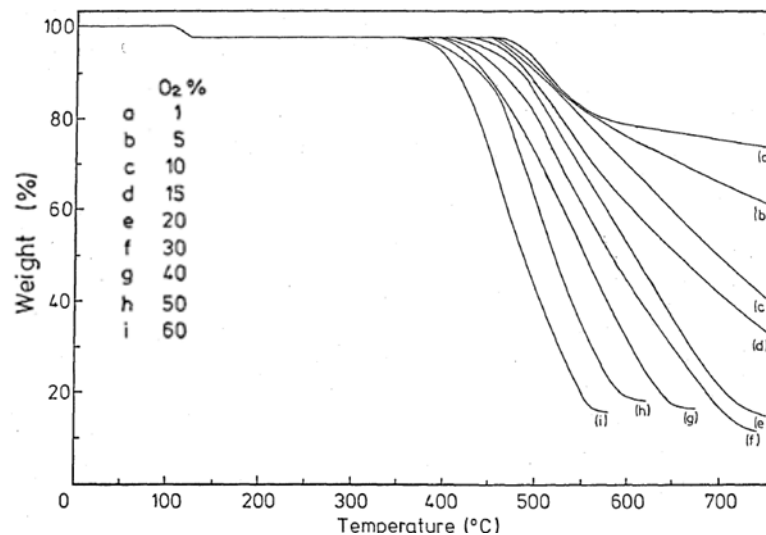
Figure 14: TGA profiles obtained for a coal sample exposed to a constant heating rate under different oxygen concentrations [158].

2.4.1.2 Large sample size experiments to evaluate self-heating potential of coals

These tests have been designed to measure properties exhibited in large systems, which have a relationship to the global process of thermal runaway. In these cases, the phenomenon is controlled by heat and mass transfer interactions present in a large scale deposits. The most frequent parameters measured are temperature, the

heat released, and the gas emissions accompanying a natural or induced oxidation process.

A) Adiabatic Oxidation test: This was one of the first methods reported in literature to assess spontaneous combustion liability [66]. This simulates the thermal runaway by eliminating the heat loss to the environment produced by the coal oxidation. Usually, the experimental procedure deposits a coal sample in a thermally isolated sample holder that is submerged in a thermal bath, in which the temperature is adjusted periodically to follow the temperature rise in the centre of the sample holder. The air flow passing through the sample is also adjusted to minimize the heat loss, and to provide enough fresh oxygen to react with the coal sample. Finally, the subsequent temperature response depends of the initial temperature of the sample [159]. The initial temperature is adjusted depending of the original conditions of coals studied (freshly mined or pre-oxidized samples), having in common a starting value of 40°C [159,160]. Figure 15 shows a typical result [161].
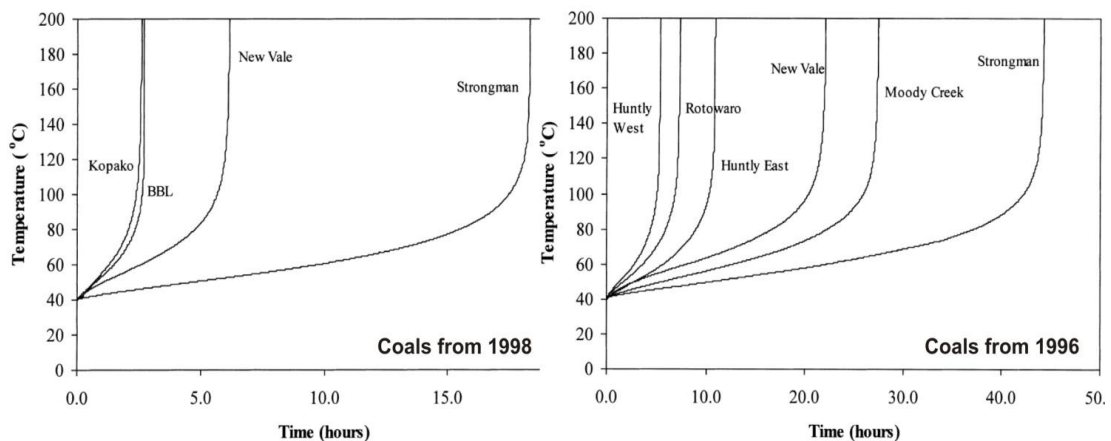
Figure 15: Self-heating curves obtained from adiabatic oxidation test for New Zealand coals. Adapted from Beamish [161].

There are technical issues regarding the implementation of this test. First, these tests can take several hours [159] or several days [160], depending on the reactivity and

the amount of sample used. Secondly, as the heat release is almost imperceptible, there are technical problems in the adjustment of temperature in the thermal bath and in the measurement of the heat loss. The standardization of the test is another problem because it has been implemented using considerably different parameters such as different reactor sizes, diverse particle sizes, and air flows, which have a major impact on the results obtained.

From this test, an experimental index called "*Self-heating rate test R_{70}*" was developed [160,161]. This index has been used mainly by the coal industry in Australia. It is defined as the reciprocal of the time taken for the sample to reach $70^{\circ}C$ in an adiabatic oven from a starting point of $40^{\circ}C$. In practical terms, it is the slope obtained from the graph "temperature vs time" between 40 to $70^{\circ}C$, representing a critical heating rate of the sample (Figure 16). Reference values of this index are: at $<0.5^{\circ}C$ h^{-1}, coals are considered as safe; between $0.5^{\circ}C$ h^{-1} to $0.8^{\circ}C$ h^{-1}, coals are considered of medium risk; and at $>0.8^{\circ}C$ h^{-1}, coals are considered prone to self-heating.
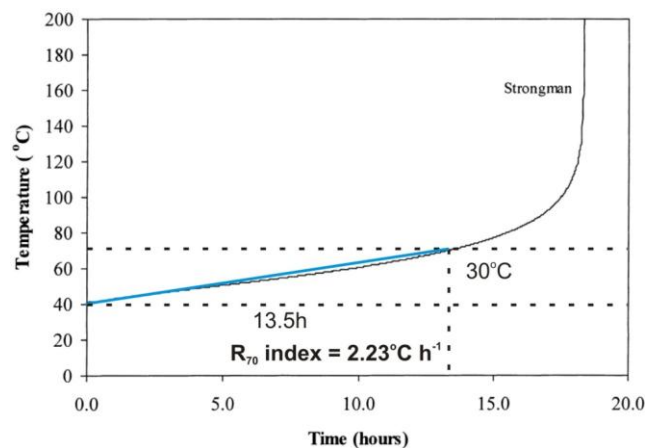
Figure 16: Self-heating rate R_{70} Index for a New Zealand coal sample [161].

The adiabatic oxidation test has been used by Davis 1925 [66], Shonhardt et al 1984 [162], Gouws et al. 1991 [163], Ren et al. 1999 [159], Beamish et al. [160,161,164],

Nordon 1985 [165], Humphreys 1981 [166], and Vance et al. 1996 [139]; in a mass range from 100g to 10kg.

B) Frank-Kamenetskii method: This method is an application derived from the Frank-Kamenetskii theory of self-heating of materials [30]. The general theory is a mathematical model deduced from a mass and energy balance applied to an idealized slab of coal. The differential equation obtained from the energy balance is:

$$\text{Equation 5} \qquad \rho \cdot Cp \cdot \frac{\partial T}{\partial t} = \lambda \frac{\partial^2 T}{\partial x^2} + \dot{q}'$$

In which ρ is the density of the material; Cp is the heat capacity; λ is the thermal conductivity, and $\dot{q}'$ is the heat generated by the reaction. A stationary solution of this equation provides the temperature profiles in the material:

$$\text{Equation 6} \qquad \lambda \frac{\partial^2 T}{\partial x^2} = -\dot{q}'$$

For this equation, Frank-Kamenetskii found a stationary solution when the balance is applied to a material prone to self-heating. In this case, Equation 6 can be expressed as:

$$\text{Equation 7} \qquad -\dot{q}' = -\Delta H_{Rx} \cdot \rho \cdot A \cdot e^{-E/RT}$$

In which ΔH_{rx} is the heat of the reaction and the group $A \cdot e^{-E/RT}$ is the dependency of the reaction with the temperature. Applying border conditions to a slab of size L, and some assumptions related to the self-ignition process, it has been defined the Frank-Kamenetskii parameter δ [30]:

$$\text{Equation 8} \qquad \delta = \frac{\Delta H_{Rx} \cdot \rho \cdot A}{\lambda} \cdot \frac{E \cdot L^2}{R \cdot T_0^2} e^{-E/R \cdot T_0^2}$$

In which T_o is the ambient temperature. As can be seen from (Equation 8), the parameter δ is a dimensionless number, which depends on the geometry of the

system and it represents the ratio between the heat generated by the reaction (numerator) and the heat diffusivity of the system (denominator). Depending of the system geometry, it is possible to calculate a critical value of this parameter (δc), causing three different situations: A) $\delta < \delta c$, in this case the reaction cannot reach the self-ignition temperature, and the heat dissipation is faster than the heat produced by the reaction; B) $\delta \approx \delta c$, this is the critical condition of equilibrium between the heat produced and the heat dissipated; and C) $\delta > \delta c$, in this case the heat produced by the reaction exceeds the rate of heat dissipation, and thermal runaway occurs. The Frank-Kamenetskii parameter (δ) has been used as a tool to predict self-ignition temperatures of different materials as reactive powders [167], waste and carbonaceous deposits [168], and coal [101,169].

C) The Heating Basket method (particular application of the Frank-Kamenetskii method in coals): The Frank-Kamenetskii model also has been applied for the coal self-heating phenomena. In this case, several reports exist [101,170,76], which have adapted the theoretical conditions to laboratory scale facilities in order to determine the coal propensity. This has been the base for the experimental "Heating Basket method" proposed in the work of Jones 1999 [170], from which the normal procedure can be described as follow:

- A specific volume for the coal sample is defined, which is a cube of 3m length per side. For this volume is considered $T_o = 50^o$C as a critical temperature.

- For this specific geometry, the δc parameter is calculated to be 2.57.

- Then, using the Equation 8, T_o and δc, the T_o^2 is calculated for a cube of 10cm to be 140^oC.

- Finally the cube is introduced in an oven at 140^oC for a period of time, and it is observed whether there is ignition.

The theoretical basis of this method has been applied to several engineering problems. However, it is not commonly used to predict the self oxidation of coal due to several technical issues. First, δ and δc are very sensitive to the activation energy and the pre-exponential kinetic factor, the heat diffusivity, the heat capacity, the sample density and the heat of the reaction, which are difficult to calculate or measure. Second, the value δc is often considered constant and independent of the coal sample, as can be seen from the work of Jones [101,170,169]. However, δc was originally obtained by using the kinetic and thermal parameters of an arbitrary coal sample. This means that the "tendency" to self-heating from this method is relative to a single and arbitrary coal sample.

A general criticism associated with this test and the Frank-Kamenetskii theory is around its theoretical basis. In relation to the prediction of coal self-heating, the model does not consider important factors such as the catalytic activity of species involved or generated during the process (water and pyrite for instance), the latent heat of vaporization or condensation generated by some components in the system, and the presence of complex reactions, which depend on the heat evolution of the whole process. In addition, the role of water in the coal oxidation process is not considered in the model, where the moisture is transported through the porous matrix of coal. This could have serious consequences on the predictions, because this dictates the adsorption and desorption rates and the subsequent heat release from these interactions. Finally, the implementation of this test also requires long experimental periods to find the critical temperatures in which the ignition takes place. All these factors made this test less desirable to the coal industry.

D) Isothermal oven or Isothermal reactor testing: In this test, a coal sample is placed in an oven at a certain constant temperature, and the time that it takes to reach

the thermal runaway is measured. If the experiment fails and there is not thermal runaway after a preset period of time, the temperature in the oven is increased to a predetermined value. Then, the experiment is repeated sequentially to find a temperature when the thermal runaway starts within the specific period of time [92,146,171]. This test could be considered as a practical modification of the Frank-Kamenetskii test method, since both share the same theoretical base; however, it was developed independently from this previous test. An example of this is presented in Figure 17.
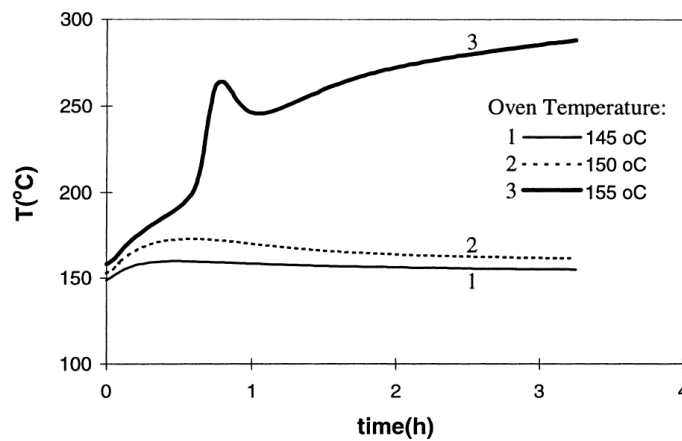
Figure 17: Experimental results from an isothermal reactor test. In this case, the critical temperature was 155°C [92].

Considering the scarce number of reports about this test, this can be considered as a non conventional testing procedure, probably due to the technical issues that arise during its application and interpretation. The first criticism is about the preset period of time to increase the oven temperature, which is in the order of days, considerably short compared to the natural time of the thermal runaway (weeks to months). Second, the size of the reactor and the size of the sample basket used are arbitrary, which explain the considerable differences between different experiments reported [92]. In addition, the critical temperatures from this test are very different from those

obtained by alternative methods, being closer to the self-ignition temperature rather than a critical self-heating temperature.

E) Crossing-point temperature method (CPT): This method shares several aspects with the Frank-Kamenetskii method, since this is based on the heat and mass balances applied to a reactive system, but considering the non-stationary solution of the mathematical problem. Two different experimental approaches have been reported:

E.1) Classic CPT method (early development ~1900): This method is a simplified experimental procedure to assess coal reactivity [25,172,173,174,175]. Experimentally, a coal sample is placed into a symmetric sample holder, which is introduced in an oven. Then, a constant and slow heating ramp is applied recording the temperature in the centre of the oven and the temperature in the centre of the sample. From this, the crossing-point value is considered to be when both thermocouples reach the same value. An example is shown in Figure 18.

The simplicity of this method introduces some errors such as overestimating the value of the critical temperature. This could happen when the heating ramp is not slow enough to provide a stationary temperature profile into the sample holder, and when a hotspot is produced far from the centre of the sample (where the thermocouple is located). As can be seen from Figure 18 (B), the crossing point is merely a 'snapshot' of the whole process, and it does not reflect the rate at which the sample temperature increases before and after the crossing point. These issues have been solved in part by the creation of several indices, calculated from the full temperature profile obtained during the experiment [148,149,146].
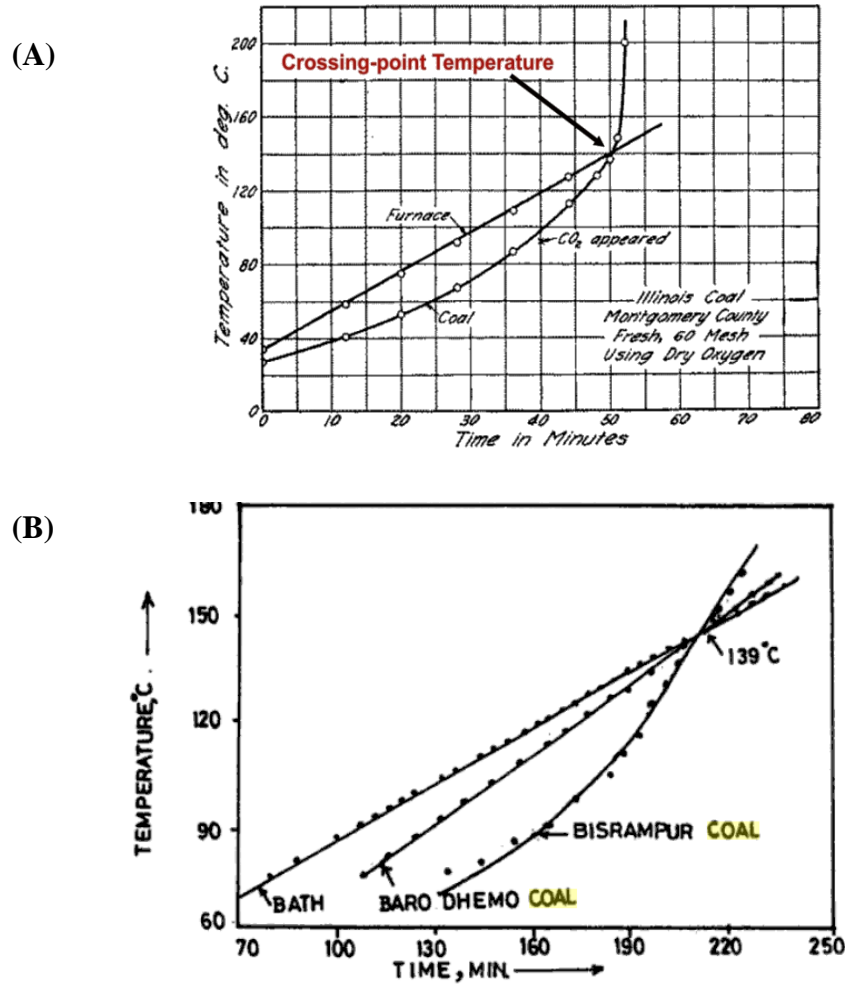
Figure 18: Crossing point temperature method. (A) Adapted from Parr et al. 1925 [172]; (B) Extracted from Nandy et al. 1972 [173].

E.2) The new CPT method (Chen method, 1990) [70]**:** Despite the title 'crossing-point temperature' as the original, this is a new method based on the transient solution of the heat and mass transfer problem proposed by Frank-Kamenetskii. In this case, Chen [70] applied the mass and energy balances over a similar differential element than this used in Equation 5. However, the resulting equation was replaced in Equation 7 to obtain:

$$\text{Equation 9} \qquad \rho \cdot Cp \cdot \frac{\partial T}{\partial t} = \lambda \frac{\partial^2 T}{\partial x^2} + \Delta H_{rx} \cdot \rho \cdot A \cdot e^{-E/RT}$$

Applying symmetry conditions, produced by an assumption of a symmetric profile of temperature developed when the temperature is close to the critical value, Equation 9 becomes:

$$\text{Equation 10} \qquad \frac{\partial T}{\partial t} = \frac{\Delta H_{rx}}{Cp} \cdot A \cdot e^{-E/RT}$$

From this equation, under a constant heating the critical temperature is found when the temperature profile is completely flat.

In order to use this theory experimentally, several attempts have been made [176,177,76,148,149,70,92]. In general, several thermocouples are used to measure the coal temperature in regions close to the centre of the sample whilst this is constantly heated. Then, when the temperature profile recorded is flat, the crossing temperature is produced (as can be seen in Figure 19). The limitations of this method are similar to those found for the Frank-Kamenetskii method. In this case, the simplifications assumed introduce a large variability of the results. For instance, some variables are difficult to standardize: the different packing conditions of the material into the sample holder, the air flow conditions applied, the oxygen concentration, the moisture in coals and in the gaseous environment, the particle size, and the effect introduced by reactor size.

Although this is one of the most cited techniques in literature, the use of this method by the coal industry is limited just to obtain the lower estimate of the ignition temperature. In addition, it is not popular when predicting propensy to spontaneous combustion due to its poor repeatability. From data in the literature, most of the results are based on different experimental conditions, which have produced different critical temperatures for same groups of coal tested. Finally, this method is a relative test for comparing samples, but not to be used as an absolute indicator.
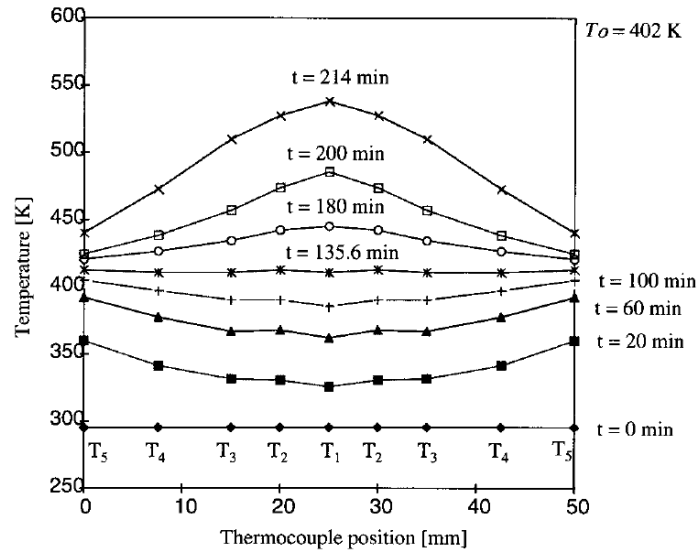
Figure 19: Experimental temperature profiles of a coal sample exposed to a heating ramp using Chen's approach. In this case, the critical temperature is 129°C [177].

F) Measurement of oxygen consumption and gas analysis: This technique is based on the evolution of the oxygen consumed and the gaseous products released when coal is subjected to thermal stress. This technique has been used to quantify propensity directly [178], as well as to understand reaction and kinetic mechanisms [179].There are two types of thermal conditions applied (isothermal and non-isothermal tests), which can be performed in batch or continuous system:

F.1) Isothermal oxygen consumption of coal: This procedure can be executed in a batch or in continuous flow reactor system. The isothermal batch system was developed during the early studies of spontaneous combustion testing [28,27]. In this case, the sample is introduced in a sealed container, and the partial pressure of oxygen in the system is measured after a preset period of time. After that, the mass of oxygen consumed is measured. This was also called the "oxygen avidity method" and "the static method", and its results were expressed as a volume of oxygen consumed in a specific segment of time per coal mass [29].

57

A continuous system uses a continuous gas flow through a reactor containing the coal sample. The inlet gas contains oxygen in a specified concentration, and a percentage of moisture can also be included. The temperature in the gas and in the coal bed is kept constant during the entire experiment [178]. In order to calculate the oxygen consumption, the partial pressure of oxygen in the inlet and in the output are measured by using a gas analyzer. The composition of the gaseous products can also be analysed by using Gas Chromatography [178], FTIR, Mass Spectrometry or a similar technique to identify the compounds generated, and calculate the complete mass balance of the system.

Comparing both techniques, the batch system is a time consuming method. This can take from weeks to several months. The continuous system is a faster technique, but requires instruments sensitive enough to measure the small concentration changes in the gas products generated [29]. In the same way for both, their results can be expressed as a volume of oxygen consumed per mass of coal.

F.2) Non-isothermal oxygen consumption of coal: In this case, the experimental work has been implemented only as a continuous system [64,179,180,162]. The laboratory procedure is similar to the isothermal experiment, but now the sample is exposed to a controlled heating ramp during the air oxidation. The heating rates reported for this test are slow (0.8°C min^{-1} [179] [86]; 0.4°C min^{-1} [162]). Figure 20 presents some results from this test. Particularly, for high rank coals results have shown that oxygen consumption decrease with an increase in the temperature (from 30 to 50°C) reaching a minimum. Then, above 50°C the consumption increases again, keeping a steady increasing rate [86].

The difficulty with using this test as an indicator of propensity is the complexity of generating a clear index. For both procedures (isothermal and non-isothermal), it is

difficult to obtain a temperature that could be considered as critical. Second, these tests depend on a large number of variables such as the gas flow; the volume of the reactor and the area of contact between coal and gas; the residence time of the gas in the reactor and the duration of the experiment; and the amount of sample used.
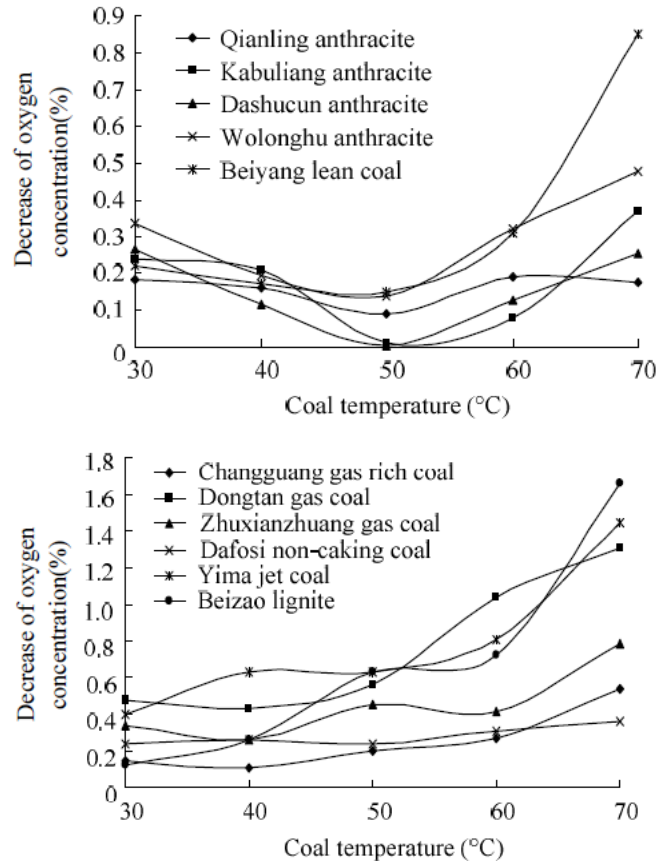
Figure 20: Oxygen consumption profiles obtained for A) high rank coals, and B) low rank coals. The heating rate applied was 0.8°C min^{-1} [86].

2.4.2 Reactive properties of coals estimated from textural characteristics

Since the beginning of coal mining, petrographic information has been a primary form for coal characterization. Coal petrology has relevance in technological applications as a tool to predict combustion performance, degree of coal oxidation, coal reactivity, and estimate the proportion of unreactive material [114]. In general, these parameters can be determined from two main variables:

a) Maceral composition: an optical classification of different organic components from their initial plant materials [1]. Maceral analysis refers to the systematic quantification of maceral components presents in a coal sample (defined in Section 2.2.1). It is possible to estimate the average reactivity of the whole sample, considering the concentration of higher reactive macerals such as vitrinite and liptinite. Also, the quantification of the sub-maceral fusinite combined with the degree of light reflectance allows an estimation of the unreactive content of the sample [181].

b) Rank value: a measure of light adsorption or reflection by the sample [1,2]. The rank value has been used by the coal industry as an index to identify coals prone to spontaneous combustion (Section 2.2.1.). A low rank value means a low degree of light reflection, produced by disorganized crystal structure and high porosity or isotropy. This is determined mainly by its maturity, and correlates well with volatile content and moisture content. On the other hand, coals with high rank values have a high degree of light reflectance, due to its well-organized crystal structure (or anisotropy) and low porosity, low volatile and low moisture content, which also means a lower degree of reactivity [1,3]. All these characteristics allow an association between coal rank and reactivity. In the case of low rank coals, the high surface area and heat released by water adsorption also increases its potential to react at low temperatures. For these reasons, coal rank is currently used as an index that is directly proportional to self-oxidation potential [69].

In addition, coal can suffer physical and chemical transformations due to physical phenomena such as temperature variation or natural oxidation, relating to changes in its petrographic properties [114,182]. Several researchers have shown that light reflectance of vitrinite particles increases with an increase in temperature in an

oxidative atmosphere. The rate of this change is related to maturity and maceral composition [114,182,183,77]. Petrographic analysis is considered to be the most suitable technique for detection of weathering and the early stages of oxidation as a result of natural exposure [115]. Nevertheless, studies are limited to a small number of coals and well-established trends relating to self oxidation are scarce. Finally, petrology has been used to identify particle morphology and detect textural alterations, which can be proven through the assessment of large numbers of particles [184].

2.4.3 Miscellaneous methods to estimate self-heating potential of coals

Some alternatives methods have been implemented to detect propensity to spontaneous combustion on-site. In this case, systems are large scale and commonly open to the atmosphere (in the order of a few tons to a millions of tons). The normal parameters measured are the temperature at specific points in a coal stockpile [185,186], the emission of specific gases products (CO and CO_2 for instance) [187], the wind speed around the pile [116,119], the slopes of the coal deposits [74], and the raining and environmental conditions of the sites. In general, these tests can confirm numerical models [118] and low scale experiments, which require extrapolation up to large coal stockpiles.

Figure 21 shows the thermal profile obtained from large scale stockpile tests, using a 15 ton coal facility ($16m^3$) stored for a period of two weeks [186]. The total research period took five months, and a maximum temperature of 140^oC was reported at the end of the experiment. The experimental results have shown that the hotspot formed within the first two weeks reached a maximum temperature of 100^oC, which was surprisingly close to the surface of the stockpile (Figure 21 B). This result not only contradicts their own model predictions, but also the models of others who suggested

that the hotspot must be located near the centre of the pile [118,119,117]. These tests can reproduce the origins of a spontaneous coal fire quite accurately, and this can be virtually impossible at laboratory scale. Also, important experimental data from these tests has been used to confirm previous results acquired at a lower scale.
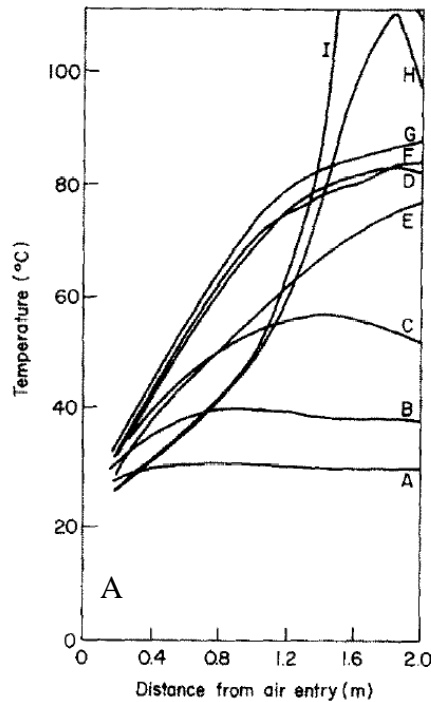
Figure 1 Temperature–distance profiles at different times: computed results. A, 20; B, 40; C, 60; D, 80; E, 100; F, 120; G, 200; H, 320; I, 340 h from start
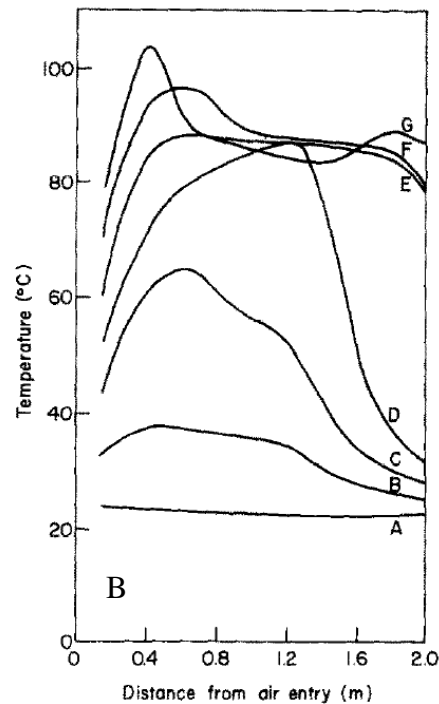
Figure 2 Temperature–distance profiles at different times: experimental results. A, 0; B, 20; C, 40; D, 60; E, 80; F, 100; G, 120 h from start

Figure 21: Thermal profiles for a 15 ton facility between 1 and 15 days of storage. A) Model results, B) experimental results [186].

However, there are major disadvantages associated with the practical application of these tests. The most relevant among these relates to the large scale of the system, which is an impediment for a rapid implementation. These also need extra resources such as machinery and a large land site available to perform the experiments. In addition, these tests are time consuming (from weeks to several months), which introduces problems in the repeatability of the results. These are also affected by

uncontrolled variables such as the weather conditions at the moment of the experiment (winter or summer; rainy, sunny or cloudy), the environmental temperature (high and low), and the wind speeds. Finally, there are some parameters such as particle size and compaction of the deposit [96], which are almost impossible to repeat. For these reasons, the coal industry has not adopted these tests on safety grounds. However, some of the experimental features such as the thermocouple locations and the methodology used for gas analysis have been implemented in industrial deposits, as a way of monitoring anomalous conditions in coal stockpiles.

2.5 Developing new methods for spontaneous combustion detection

The existing testing methods to identify coals prone to spontaneous combustion are not reliable enough to be used by the coal industry, despite the large number that has been proposed. This creates several doubts when safety procedures are implemented, exposing industries to an extra risk derived from a wrong analysis. The current methods in use are based on the assessment of variables such as coal rank, temperature of the coal deposit, the heat evolution of the stockpile, and the oxygen concentrations nearby, ignoring secondary parameters such as the mass loss of coals, changes in petrology and chemical composition as a result of weathering. Also, improvements in the data analysis could reveal new information, being able to characterize the phenomenon from a different perspective (e.g. thermogravimetric data and image analysis for instance).

2.5.1 Thermogravimetric analysis as a tool to identify prone coals

Thermogravimetric analysis (TGA) remains as a secondary tool to identify prone coals. Most of the standard thermal tests developed to quantify the spontaneous combustion behaviour focus on the direct reading of temperature profiles, excluding changes in the total weight of the sample. In this context, thermogravimetric analysis

provides the history of the sample mass associated to external changes in temperature.

From this instrument, it is possible to obtain precise values for degradation temperatures during the oxidation process; to quantify the adsorption and desorption of oxygen, moisture and volatiles; and quantify reactive or unreactive components of samples [151]. Thermogravimetric analysis is also frequently used by the power industry to assess coal reactivity, obtaining kinetics parameters of fuels such as reaction order, activation energy and pre-exponential factors [188,189,190]; to calculate reactivity under different atmosphere conditions [191]; and to quantify physical characteristics such as moisture, volatile, carbon and ash content [107,192]. In addition, different non-isothermal tests have been reported in the literature to calculate burning profiles of coal and char particles [193], which can be useful to predict the operating conditions of industrial reactors. Most of these tests were designed to provide information about the oxidation reaction at high temperatures [194,195]. Some researchers disagree about the use of TGA to obtain information of coal oxidation at low temperatures (below 150°C), because this is close to being within the margins of error for the instrument [196]. Nevertheless, technological advances in thermogravimetric analyzers have improved the accuracy of data collection, and significant improvements in the control of temperature and data analysis have been achieved, resulting in this tool being more suited to precise low temperature measurements [197].

Successful attempts using thermogravimetry to estimate propensity of coals to spontaneous combustion have not been reported. However, there are a number of potential techniques such as non-isothermal methods [193] that could reveal important information about the self-heating of coal [191]. Considering the

experience of previous researchers [108,198], there are two potential non-isothermal tests: First, different stages of the weight loss can be spotted through a single heating ramp in air. Depending on the specific heating rate applied, there are several measurable parameters such as percentage of oxygen absorption and water desorption [107], starting combustion temperature, and peak and burnout temperatures [191,193]. Second, by using an integrated approach it is possible to study the effect of temperature on sample weight, calculating an index independent of the heating rate applied. This is possible by carrying out parallel experiments at different heating rates, using a similar experimental approach to calculate kinetics parameters by TGA [199]. Additionally, the derivative of the weight loss can also be associated with each heating rate to determine how coal reactivity is affected by changes in temperature. Depending on the magnitude of these changes, coal samples could be classified in terms of its propensity to react with air. These potential uses of TGA to quantify coal oxidative behaviour represent a clear research opportunity.

2.5.2 Advanced image analysis techniques applied to coal science

Image Analysis (IA) is a relative recent technique that has gained momentum in many areas of scientific analysis. Its growth during the last decades has been dictated by the enhancement of computational systems, both software and hardware. This technique could be described as a series of steps from image acquisition and processing. Many different disciplines routinely use IA including biology, mineralogy, chemistry, engineering and manufacturing process [200]. The main sequence of steps starts with the image acquisition, by means of a digital camera or a similar device implemented alone or in conjunction with other equipment such as a microscope. After that, the image is stored. This has been enhanced in last few years due to advances in microchips and electronics, allowing bigger images to be stored

for processing, resulting in more information. Manipulation and enhancement of the image is the next step, and this has also been optimized in the last years due to improvements in software. In addition, images can be mathematically transformed, processing them in spatial or frequency domains, separating or reconstructing particles or objects to obtain more detailed information. Finally, the results can be represented as a new image or saved in a data base [200].

For coal science, there have been successful attempts to use image analysis. Initial work was based on recognizing maceral content and the calculation of rank using automated systems [201]. This basic research was carried out using systems attached to microscopes (without any computer processing), applying greyscale recognition under a fixed light exposure. The same concepts of processing are applied nowadays, using digital devices to obtain and process the information automatically [202,103,203]. Development increases in the Nineties, when the improvements of computer and digital cameras allowed image capture and post-processing easily. Some of this work was carried out at Nottingham University studying coal properties, performing automated maceral and rank measurements [104,204,205], and creating a coal char morphotype characterization [206].

For a normal image, a pixel is the minimum single piece of information available and it is represented by a specific colour level. Images can be defined as Colour (well known as RGB) and Grey Scale Images (GSI). A Grey Scale image is a representation in which the colour pixels range is defined in 256 different levels, starting from black (level 1) to white (level 256), passing through all the different tonalities produced by the combination of black and white, divided in 255 different levels. Then, the image contains a specific number of pixels that could be represented in a histogram. The image histogram is a plot of the total number of

pixels of each grey scale level, against the grey scale interval (from 1 to 256). As can be seen from Figure 22, the image histogram is a useful route to quantify overall optical properties and to determine material characteristics from a large number of particles. For instance, the background resin of a coal mounted sample appeared in the image as black, corresponding to a large peak around 0-70GSU in the image histogram. The vitrinite maceral is another major constituent presented in the sample showing a peak around 70-150GSU in the image histogram. Finally, the high light reflectance of fusinite makes that these particles appear in the region close to the white, which is around 150-255GSU.
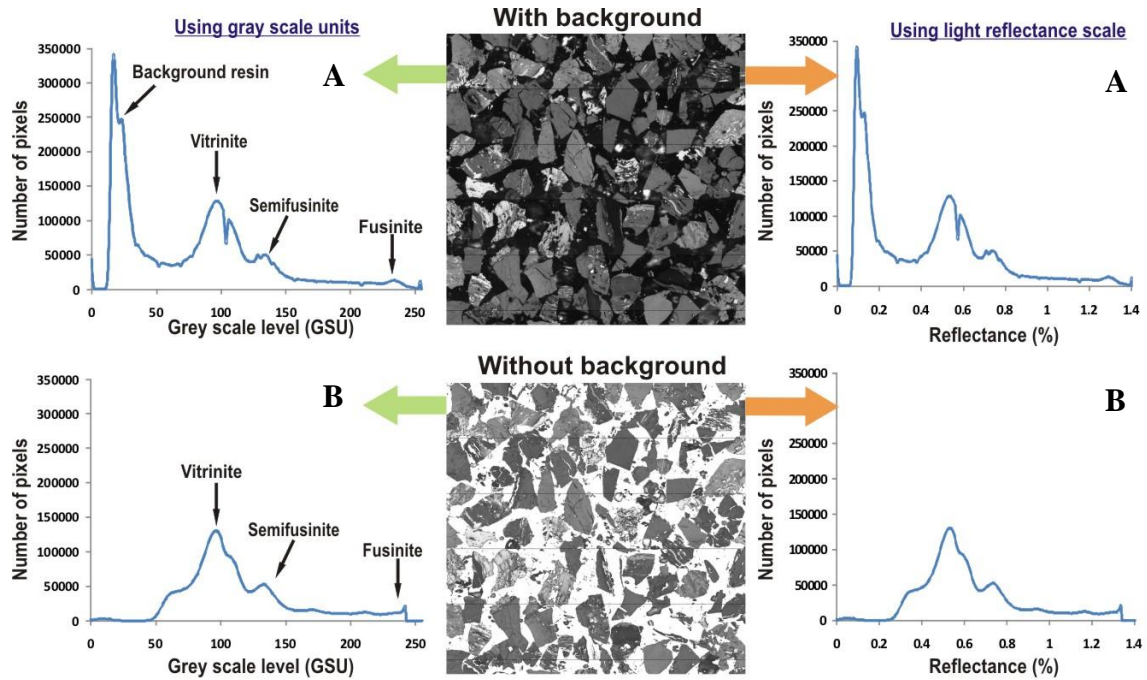
Figure 22: Histogram of images from a coal sample: A) Raw image including background resin; and B) processed image. Both cases are represented using grey scale units (left) and equivalent light reflectance scale (right).

Histograms obtained from grey scale images have been used to calculate the random reflectance of a coal samples, and linked successfully to the manual measurement of rank [201]. Also, these have been related to the maceral content

[201,202,104](schematized in Figure 22). For coal fire research, changes in maceral fractions under certain conditions such as weathering, natural or artificially created oxidation can be quantified using image analysis.

Besides, IA has been implemented for particle identification, morphological classification, and for characterization of coal and char particles [206]. In addition, measurement of particle size distribution, diameter, roundness, length and mineral content of coal particles have also been studied [200], defining standardized procedures for industrial applications [207]. Nowadays, algorithms of image processing of coal are focused in obtaining parameters such as random reflectance, particle size, and particle morphology. However, the use of these techniques to detect thermally altered coal particles has not been used, representing another clear research opportunity.

2.5.3 Spectroscopy, a less explored tool for coal characterization

Spectroscopy is the study of the interactions between energy and matter. In this case, an electromagnetic beam is directed to a sample surface and the absorbance or reflectance of energy is measured. Several techniques have been developed by altering the frequency of the beam such as ultra violet spectroscopy (UV region λ~10 to 400nm) and Infrared spectroscopy (IR region, λ~0.7 to 300μm) between the most common. In these cases, the changes in the different regions of the spectrum emitted and absorbed provide valuable information about molecular vibration, bond stretching and bending, useful to characterize molecular groups incorporated into the sample [208]. Fourier transformed infrared spectroscopy is a particularly attractive tool for coal research because most of the organic functional groups that are present in coals interact with infrared light [209]. This tool has been used to evaluate different chemical attributes of coals such as weathering and change of functional

groups by aerial oxidation [210]; characterization of macerals such as liptinite, vitrinite and sub-maceral groups [211,212,213]; analysis of specific organic structures such as aliphatic and aromatic groups [214]; and study of changes in technological characteristics of coals such as plastic properties, volatile matter and variations in mineral matter composition [114].

Some literature exists where this technique has been used to estimate the propensity of coal to spontaneously combust [106,215,132]. The most relevant study investigated the chemical changes during the natural oxidation of a set of high volatile bituminous coals and found that clear differences existed between fresh and oxidized samples [106]. Specifically, the study shows a marked loss of aliphatic groups with increasing oxidation, as well as an increase in carbonyl and carboxylate groups. This study also concluded that aromatic groups were less affected by the oxidation process. In a recent study [215], changes in active functional groups were observed during low temperature oxidation of coal, which confirmed the presence of specific components assumed during the mechanism formulation [132]. In this, aliphatic hydrocarbons such as methyl and methylene, react with oxygen atoms absorbed by pores on the coal surface generating unstable solid intermediate carbon-oxygen complexes, which then decompose into gaseous products (CO, CO_2) and stable solid complexes [128,131]. Consequently, the use of FTIR to identify a fingerprint of coals prone to spontaneous combustion, and the use of this tool to estimate the impact of the coal oxidation are attractive research opportunities. Finally, FTIR could also be combined with other techniques such as thermogravimetry (TG-FTIR), differential scanning calorimetry (DSC-FTIR) and mass spectrometry (MS-FTIR), to visualize the phenomenon in a more advanced way.

2.6 Spontaneous combustion potential of biomass and coal-biomass blends

The spontaneous combustion is a reaction that could affect other materials different from coal such as biomass, coal-biomass blends, organic and forestry wastes. For all these materials, the thermal runaway shares the same fundamentals: an imbalance favourable to heat production instead of heat release through the stockpile. However, in the case of hygroscopic biological materials such as biomass and waste, bacterial activity is a primary cause.

2.6.1 Incidence of self-heating in biomass materials

Several incidents of thermal runaway have been reported for different types of biomass: sawdust [216,217,218], wood chips [218,217,57], composting piles [58], hay piles [58], rapeseed and soybean piles [59], municipal waste [219,220], charcoal [220], eucalyptus leaves [216], yard trimmings [216], pistachio nuts and palm kernel among the most frequent [221]. In literature, a vast number of accidents are reported; however, information about the mechanism and the reactions that take place is further complicated by the complex biochemistry involved. A review of the global mechanism and the variables involved is given below.

2.6.2 Global mechanism

The precise mechanism in which these incidents took place remains unknown, but in all these cases the same steps have been reported: a) a rise in temperature due to fermentation; b) water vaporization; and c) a critical temperature is reached and thermal runaway takes place. These steps are described as follow:

a) An initial rise in temperature produced by the aerobic respiration of living plant cells and microbes incubated into the pile, which liberates heat by direct oxidation of plant chemicals [216]. The normal temperature range of the microorganism interacting into the pile can vary from 20-40°C (mesophiles) to 40-80°C (facultative

thermophiles) [222]. At this stage, the temperature in the pile does not rise above 70-90°C until all free water is removed [216].

b) Water vaporization produced by the previous temperature increase. From this, the pile can lose nearly all the free water reaching a temperature approximate to 100°C, where all the microorganisms are killed. At this stage, oxygen still flows into the pile, reacting with plant chemicals to produce even more heat, increasing pile temperature and acceleration the oxidative chemical reactions [216].

c) Once the pile has lost all its free water, the thermal runaway is produced. At this stage, the biomass pile is rich in carbonaceous material with ignition temperatures around 130-160°C [221]. Also, at this stage the rate of heat release by the chemical reactions is higher than the heat loss, and the thermal runaway will take place eventually reaching the ignition temperature [216,221].

2.6.3 Potential variables involved in the biomass self-heating

Several factors affect this process such as the oxygen concentration, temperature and moisture content, which play an important role facilitating the growth of microorganisms. Also, there are additional parameters such as the activation energy of the biochemical reactions, the catalytic activity of microbes (biocatalysis), the dependency of particle size and the pile compaction (porosity of the pile), which also influence the self-heating.

2.6.3.1 Oxygen, temperature and pile compaction

Oxygen is a fundamental reactant for both biotic (biochemical) and abiotic reactions. In the first case, oxygen is used for cellular breeding, reaching a maximum consumption when the temperature is close to the optimum growing temperature of each specific microorganism evolving. In the second case, oxygen acts as an oxidant of the carbon structures, showing an Arrhenius type dependency on temperature,

similar to that shown by coal [221]. The pile compaction is a technological factor that also has influence over these parameters. In the case of oxygen, a low compaction degree facilitates its diffusion through the pile allowing higher heat dissipation. Conversely, a high compaction degree obstructs the oxygen transport, but at the same time reduces heat dissipation. The intermediate state is the most hazardous situation because there is sufficient oxygen and the correct conditions for biological activity, accelerating the rise in temperature [221,216].

2.6.3.2 Moisture

Water content plays an important role in the process supporting several interactions that maintains microbial activity. In this case, water can be used by microbes as a substrate, a transport medium, and a thermo regulator [216]. The thermal properties of water also have major influence on the process, for instance a high water content pile can produce heat at a lower rate by obstructing oxygen diffusion. Elevated water content levels can also inhibit the growth of the microorganisms, and requires a higher energy input to be evaporated [222]. However, when water is totally eliminated the ignition temperature of the material is reduced considerably [218]

2.6.3.3 Activation energy

The number of chemical and biochemical reactions that take place in a biomass pile is uncertain. In the case of biochemical reactions, the activation energy is reduced considerably by biological activity, decomposing large hydrocarbon chains into simple compounds that are easy to oxidize. This action has a direct effect on the subsequent chemical reactions, which also are facilitated by a reduction of the activation barrier (biocatalytic effect) [221,216,222].

2.6.3.4 Particle size

For biomass materials, the reactivity not only depends on access of oxygen to the active sites at which reactions take place, but also it depends on the surface area in contact with the biological activity. At laboratory scale, with large particles the phenomenon is controlled by heat and mass transfer restrictions in a similar way to coal. When the particle size is reduced, a chemical control of the reaction is reached. However, a reduction in particle size also facilitates the compaction, which restricts the mass transfer and increase the heat conduction [220]. Some researchers maintain that the same rule as applied to coals can be applied to biomass [216].

2.6.3.5 Other factors

Other factors can also be named, which have been less studied:

- The influence of inorganic materials such as metals which can act as catalyst. For instance, the contamination by iron and aluminium is common in composting and landfills deposits [216].

- The influence of cellular wall thickness and the internal structure of biomass particles. As it will be demonstrated in this thesis, the morphology of the biomass has a direct relationship with intrinsic reactivity [223].

2.6.4 Testing procedures

Several experimental procedures have been used to estimate the spontaneous combustion of biomass materials. However, most of them only take into account the final oxidation stages (close to the ignition point), without giving relevance to the biological activity of the material. In those cases, the same standard testing procedures have been used as for coal assessment. These included the Frank-Kamenetskii and the heating basket method [218,217], Chen's method (modified crossing point temperature) [70], the classic crossing point temperature method

[220,58], the isothermal oven test (referred to as the constant temperature method) [220], and spontaneous ignition tests [57]. Biomass testing has not generated any new additional method other than those used for coal assessment.

2.6.5 Potential problems of coal-biomass blends.

Co-firing of coal-biomass blends is being implemented across Europe targeting the reduction in carbon dioxide emissions [54]. During the last decade, biomass has been adopted by power stations using three different approaches, on which the storage facilities associated depend directly [60]:

- Direct co-firing: In this case, biomass and coal are burned in the same boiler furnace. The milling and the subsequent injection depend on biomass type, and can be performed using combined or separate equipment. This is a straightforward technology and the cheapest [224].

- Indirect co-firing: In this case, biomass is gasified in a separate unit, and the fuel gas is burned in the coal boiler. This technology allows higher fuel flexibility and cleaning the gas before injection into the boiler, increasing the useful life of the unit. However, it requires a higher investment [224];

- Parallel co-firing: biomass is burned in a separate boiler and the steam produced is combined with that coming from the coal boiler. This is the most expensive alternative because it requires the construction of a new unit for biomass burning [224].

Information about synergetic interactions during storage and subsequent blending problems is scarce. Also, investigations have focused on high temperature combustion reactions that take place inside the reactors [225], and the slagging problems produced by the residual mineral matter when it reaches the heat recovery units [60]. However, information about potential interactions at low temperatures in

industrial reports is highlighted as a possible further concern [226]. In relation to technical and scientific papers, little information exists about spontaneous combustion of coal-biomass blends.

Currently, mixed coal-biomass storage facilities do not exist [60] because fuels are milled and blended in situ, seconds before injection in the boilers [56]. This situation does not represent a risk; however, if the use of organic material is finally adopted by the industry in a large scale, blending could have important advantages and disadvantages. In this context, the best scenario is given by negative synergetic interactions. The potential risk of spontaneous combustion of the single components (coal and biomass) will be higher than the blended material, which represents an exceptional opportunity to reduce the probability of incidents. Conversely, the worst scenario could be where mixed fuels are more likely to spontaneously combust than the separate individual components. Understanding this requires further study, representing a clear research opportunity.

2.7 Biomass and coal-biomass characterization

For biomass, it is necessary to study the thermal behaviour and the material morphology to generate predictive models. A number of techniques have been used to classify coal char morphology [206,227,228], and the same methods can be used for biomass particles. Some researchers have used scanning electron microscopy (SEM) analysis to observe char structures although this technique can be more qualitative than quantitative [229,230,231,232]. Optical microscopy using reflected light techniques (potentially coupled with automated image analysis) could also be used for biomass char characterization.

Thermogravimetric studies can also provide relevant information about chemical reactivity (intrinsic reactivity) of the feed material and subsequent char products

[233]. Previous investigations have focussed on coal char reactivity using TGA analysis [234,235]. In this case, it is possible to find studies which relate physical factors with reactivity behaviour, such as heating rate effects [236,232], influence of atmosphere used [234], relevance of different pressures [231], and the significance of particle size [231,232].

The existence of a link between shape and particle reactivity would be an interesting and important area for study, particularly since biomass particles are generally fired in much larger sizes (>500microns). Changes in reactivity and char morphology with increasing particle size, might also impact burnout performance.

2.8 Research opportunities and thesis scope

The thermal runaway of carbonaceous materials is a major problem not only for industry, but also for the wildlife and the population affected by these incidents. A key to prevent those events is performing a precise assessment of the variables involved, which will depend mainly of the consistency and accuracy of the testing methods used. At present, there are several experimental procedures that are used by the scientific community to predict the spontaneous combustion of materials; however, most of them are based on the measurement of a restricted number of variables, delivering in some cases contradictory results. In order to address the problem from a new point of view, it is necessary to increase the spectrum of variables used to quantify the phenomenon to a wider range. As the energy requirements and global warming concerns increase, the use of environment friendly materials such as biomass and organic wastes arises as attractive alternatives; however, there is little information about the application of coal tests to biomass. Finally, co-firing is also a feasible alternative to reduce carbon emissions, but there

is available little information about the possible synergetic effects produced in the reactive properties of coal-biomass blends at low temperatures.

2.8.1 Research questions

Considering the ideas recently exposed, a number of research questions will drive this research:

- Since it has been demonstrated that the spontaneous combustion phenomena is closely related to sample weight, would it be possible to differentiate materials prone to spontaneous combustion based in the information obtained from weight loss as a result of changes in thermal conditions?

- Can the optical information obtained from microscopy studies be used to predict the phenomenon of spontaneous combustion? If this is the case, how reliable this kind of testing would be?

- Could the same procedures be used for coal testing in the study of spontaneous combustion of biomass?

- Is there any synergetic effect in the thermal oxidation of coal-biomass blends, which increase or decrease the probability of a spontaneous fire?

2.8.2 Thesis scope

Finding adequate answers to all these research questions presents clear research opportunities, which is the main aim of this investigation. In general, a study of the phenomena of spontaneous combustion of coal will be carried out considering the work of previous researchers, the search of historic records of spontaneous coal fires, and also the introduction of new methods to identify propensity at laboratory scale. Alongside these, a parallel study of biomass self-oxidation will be carried out, based on past events and experimental work with the aim to understand the biomass self-heating phenomenon. In this case, the experimental investigations consider two

characteristic biologic materials: raw biomass and charcoal (biologic oxidised material). Ultimately, from the results obtained for coal and biomass independently, the study is extended to coal-biomass blends.

In particular, the experimental study will be conducted by two experimental techniques: a) thermo-chemical analysis, focused on thermogravimetric and calorimetric tests; and b) studies of the optical properties of materials involved by optical microscopy. In this context, thermal data have proven to be essential to obtain kinetics and thermodynamic parameters that allow measurements of the intrinsic rate of reactions and the global rates observed in restricted heat-mass transfer environments such as a stockpile. Then, the connection of the weight loss of the sample with the self-heating phenomena, and the heat released by this reaction will be quantified by thermogravimetric and calorimetric studies. Additionally, microscopy and image analysis tools will be used to study morphologic and structural changes produced by the oxidation reaction, linking these with the information obtained by thermal methods, with the aim of identifying possible optical characteristics of coals prone to spontaneous combustion. Finally, considering all the properties studied and the results obtained, a set of experimental procedures will be proposed to identify coals prone to spontaneous combustion, to identify the possible risks associated to the storage of biomass, and the potential hazards of coal-biomass blends.

Chapter 3. Experimental methods for spontaneous combustion research

3.1 Research plan

The main focus of this study is to develop new methods for identification and quantification of the potential of spontaneous combustion of coal, biomass and coal-biomass blends. In order to complete this task, the main variables associated to the self-heating phenomena were identified for measurement and experimental quantification by thermal analysis and optical microscopy. Thermal methods provide a unique source of information to assess the potential of a material to suffer a thermal runaway. These techniques are used to obtain information of "reactivity" and kinetics; to measure the specific degree of oxidation of samples; quantify composition including moisture, carbon content and volatile matter; and also to artificially create thermal alterations in the material. In addition, microscopy and advanced image analysis techniques were used to identify other characteristics including light reflectance; the mineral and maceral composition; the morphology of particles; and the degree of oxidation. All of these parameters are closely related to the phenomena studied, and can be measured directly for each sample.

In both cases, characteristics could be quantified at different stages of the self-oxidation process. Physical properties can be measured directly from the initial sample (original properties of the fresh material); during a specific treatment (e.g. temperature, pressure, concentration profiles on-line); and after the treatment (e.g. changes in chemical and optical properties as a result of the heating process). Finally, the combination of all these techniques will provide a new approach to the

understanding of the self-heating phenomena. Applied experimental techniques at different stages of this research are presented in Figure 23.
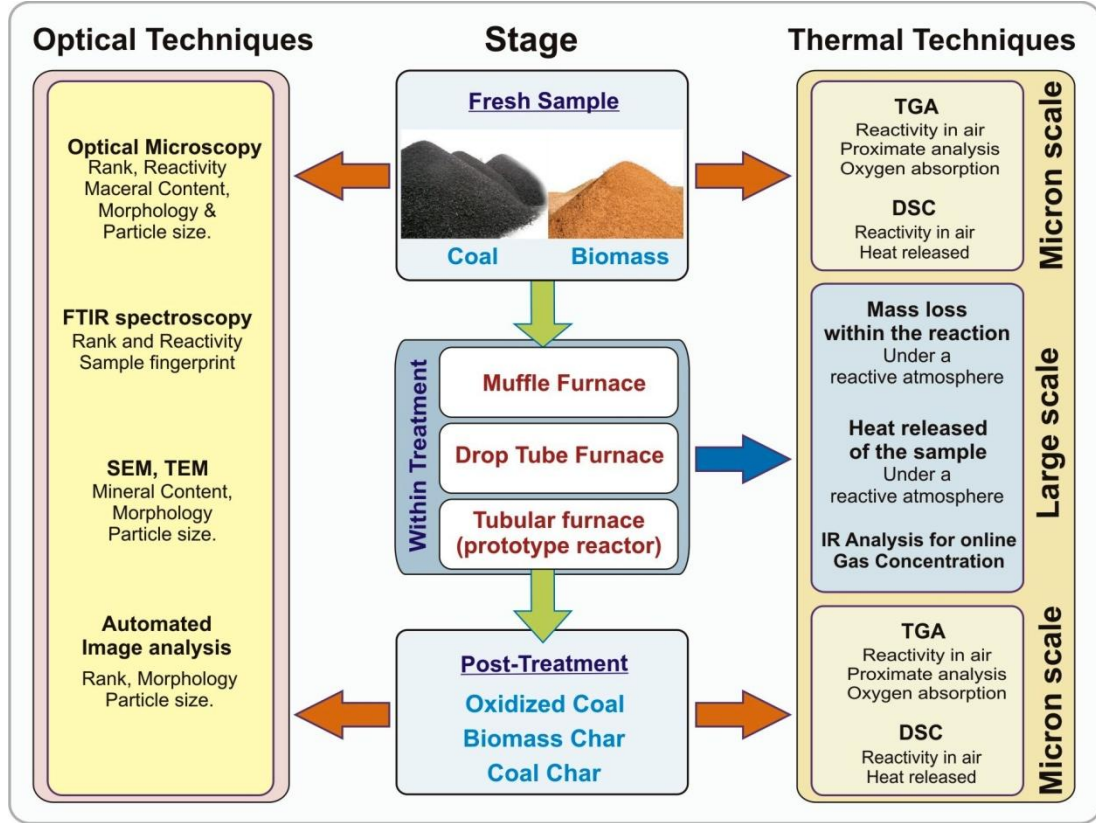
Figure 23: Diagram of processing and analysis of the sample. Two main techniques of analysis are applied at different stages of sample processing.

3.2 Sample collection and preparation

3.2.1 Coals selection

For this research, 42 coal samples from different parts of the world were used. From these, 29 samples were used directly in a main set of experiments designed to identify key features of the self heating process. Then, this information was used to develop a new set of methods for spontaneous combustion assessment. This coal selection included at least three samples well-known prone to spontaneous combustion, as well as three unreactive samples which were used as standards or

benchmarks for reactive or unreactive coals. There are also two samples with high sulphur concentration, and four samples with high water content. The samples covered a vast range of coal types such as lignite, bituminous and semi-anthracites. The selection of samples and their main characteristics are presented in Table 4. Additionally, 13 special samples were provided by the Federal Institute of Material Research of Berlin (BAM), to be used as a reference in the assessment of the testing procedures developed. These samples were collected from natural fires and coal deposits, and the information about their propensity is well known.

Between the samples used, Fenosa coal has recently suffered an incident of spontaneous combustion. This sample is a low rank Indonesian coal being used in a power station located in the north of Spain. The real name of this sample has not been provided. Instead, in this report this coal is identified by the name of the power station who suffered the incident (Union Fenosa). About the incident, there are several press releases which provide general details [38]. From these, it is possible to extract the following information: A considerable amount of smoke and steam started being released from a coal deposit located in A Coruna port on November 13th 2007, in which were stored 70.000 tons of coal arrived two weeks before. Then, in order to eliminate the hotspot heavy machinery was used to remove the coal from the deposit. This produced a higher steam release, but there was absence of a visible flame. The smoke produced was described by witness as strongly smelly, itchy and similar to the natural gas smell. A week of work was needed to remove all the material stored into the deposit and to extinguish the hot spot (17 November 2007).

Table 4: List of worldwide coals selected for the research project.

	Coal name	**Origin**	**Type of coal**	**Characteristics**
1	Fenosa	Indonesia	Lignite	Prone to spon. comb.
2	Orupka	Nigeria	Lignite	High reactive
3	North Dakota	USA	Lignite	Prone to spon. comb.
4	Hambach	Germany	Lignite	High water content
5	Illinois #6	USA	High volatile bituminous	High reactive
6	Pocahontas #3	USA	Low volatile bituminous	Coal blend
7	Indiana EDF	USA	Bituminous	1.8%S
8	La Jagua	Venezuela	Bituminous	
9	La Loma	Colombia	Bituminous	
10	El Cerrejon	Colombia	Bituminous	High reactive
11	Blue Creek	Australia	Bituminous	
12	Bulli	Australia	Bituminous	(old sample)
13	Hunter valley	Australia	Bituminous	
14	Kaltim prima	Indonesia	Bituminous	High reactive
15	Indo	Indonesia	Bituminous	(old sample)
16	Goedehoop	S. Africa	Bituminous	
17	Kleinkopje	S. Africa	Bituminous	(old sample)
18	Bulawayo	Zimbabwe	Bituminous	
19	Zondag 1	Russia	Bituminous	
20	Sines	Portugal	Bituminous	
21	Littleton	UK	Bituminous	
22	Daw Mill	UK	Bituminous	
23	Yanowice	Poland	Bituminous	
24	Asfordby	UK	Bituminous	
25	Lea Hall	UK	Bituminous	
26	Deep Navigation	UK	Bituminous	(old sample)
27	Bentinck	UK	Bituminous	
28	Nadins	UK	Bituminous	
29	Ironbridge	UK	Bituminous	(old sample)

The coal deposit in use was a closed dome, with ventilation in the top of the structure, and located besides a maritime port. Personnel working in the site also commented that ventilation inside was poor and there was high humidity in the area. Finally, a representative sample was collected from the site. Some images of the incident are shown in Figure 24.
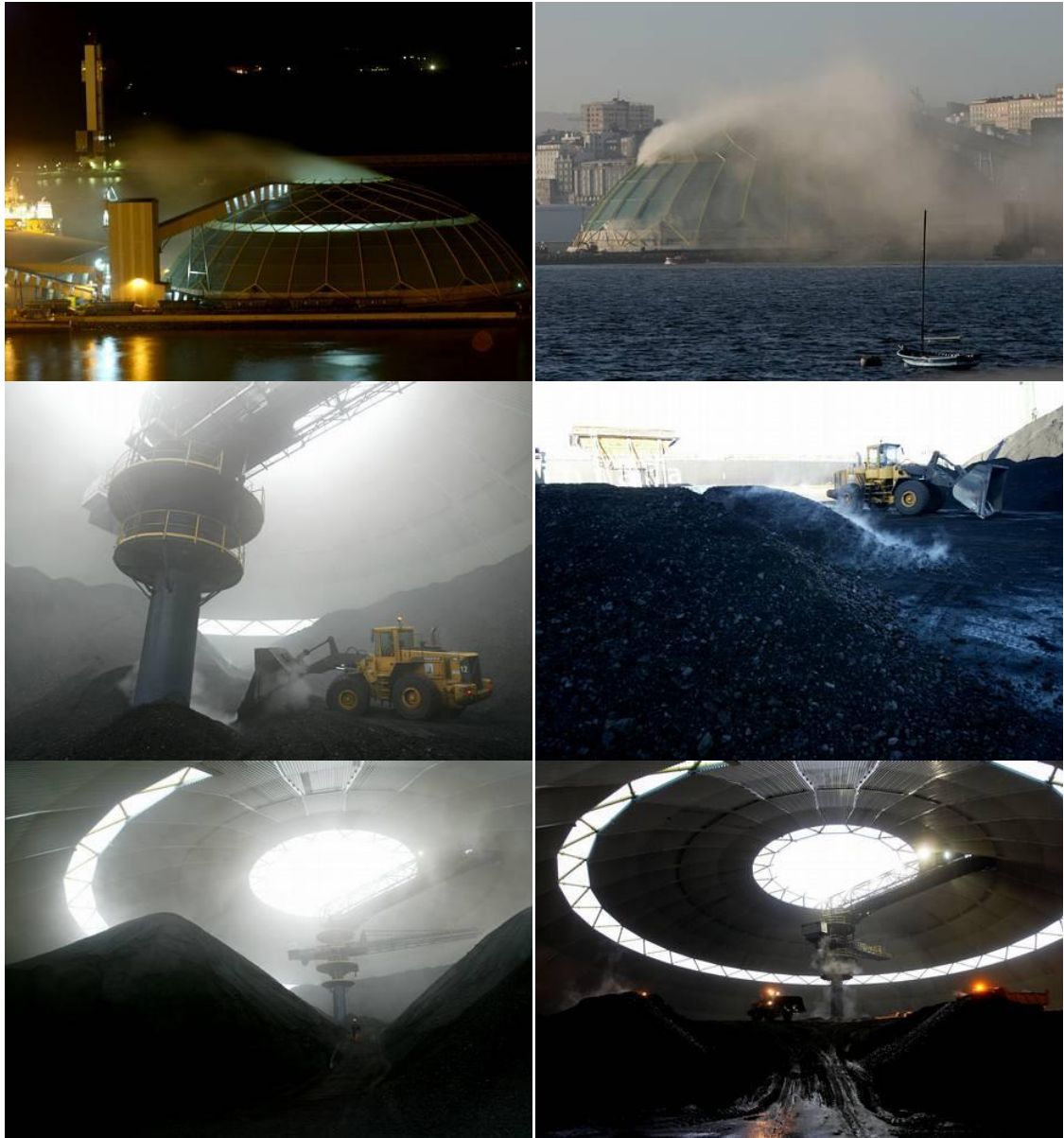
Figure 24: Images of the spontaneous coal fire produced in Spain 2007 [38].

3.2.2 Biomass selection

Biomass materials were also obtained from different sources. Most of them were a combination of energy crops and residues being tested currently in the UK as a potential substitute of coal in combustion processes for electricity generation.

Table 5: List of worldwide biomass selected for the research project

	Biomass name	Origin	Characteristics
1	Miscanthus	UK, Crop	Energy crops
2	Corn	UK, Animal feed	Energy crops
3	Wheat	UK, Flour production	Agricultural feedstock
4	Short cereal	Chinese, Cereal residue	Agricultural feedstock
5	Sunflower	UK, Oil production residues	Agricultural feedstock
6	Rapeseed	UK, Oil production residues	Agricultural feedstock
7	Dried distillation grain (DDG)	UK, Ethanol production residues	Corn processed
8	Dried distillation grain without soluble (DDGS)	UK, Ethanol production residues	Corn processed
9	Olive wood	Spain, Oil production residue	Forest wood
10	Swedish wood	UK, Sawdust residue	Forest wood

3.2.3 Sample preparation

3.2.3.1 Coal

Coal samples were prepared in a similar way for all the experiments. In some particular cases (it will be indicated), there was a special pre-treatment of the sample. First of all, particle size was standardized due to the different sample origins. The procedure is detailed as follows: fresh samples were pulverized and sieved in order to obtain a set of four different particle size fractions. Approximate 1kg of each sample was milled using a Laboratory disc mill (equipment described section 3.3). Subsequently, the sample was sieved capturing the fraction below 1180mm mesh. After a series of sieving, all particles above 1180mm were milled once more by hand with the aim to reduce the size of the whole sample. Then, particles were sieved using the British standard for coal sieving [237], collecting the following size ranges: fraction <106μm, 106-212μm, 212-500μm, and 500-1180μm. Finally, 10 gr. of each size fraction were kept in glass bottles to be used in the small sample size experiments. The remaining material was kept in sealed plastic bags, vacuum sealed

and stored in a dry place prior to be used in large scale experiments. Table 6 is a list of the material prepared and the corresponding experiment.

Table 6: Particle size distribution of coal fractions

Experiments	<106	106-212μm	212-500μm	500-1180μm
TGA, DSC, FT-IR Microscopy (small sample size)	10 g bottle	10 g bottle	10 g bottle	10 g bottle
Spon. comb. reactor, DTF, coal-biomass blends (macro scale)	600 g sealed bag	100 g sealed bag	100 g sealed bag	100 g sealed bag

3.2.3.2 Biomass

Fresh samples were crushed and sieved to obtain six different particle size fractions. Approximate 2 kg of each sample are milled using a cutting mill machine (equipment described section 3.3), and the fraction below 2130mm mesh was captured. After sieving, all particles above 2130mm were crushed. Then, particles were separated into six size fraction ranges: 53-75, 75-106, 106-212, 212-300, 300-600 and 600-1180μm. Finally, 15g of each size fraction were kept in glass bottles to be used in the small sample size experiments and 10g of each size fraction were kept in glass bottles to prepare char particles. The remaining material was kept in sealed plastic bags, vacuum sealed and stored in a dry place to be used in the large scale experiments (Table 7).

Table 7: List of biomass material prepared and their associated experiment

Experiments	53-75μm	75-106μm	106-212μm	212-300μm	300-600μm	600-1180μm
Raw material (TGA, FT-IR)	15g bottle	15g bottle	15g bottle	15g bottle	15g bottle	15g bottle
Char preparation (TGA and microscopy)	10g bottle	10g bottle	10g bottle	10g bottle	10g bottle	10g bottle
Spon. comb. reactor, coal-biomass blends	-	-	1200g bag	-	1200g bag	-

3.2.3.3 Coal-Biomass blends

Coal-biomass blends were prepared in situ, before each experiment, using four different ratios of coal:biomass 95:5, 90:10, 85:15 and 80:20 respectively. In these cases, blends were prepared using 500g of seven selected samples of pulverized coal (particle size <106μm), blended with four crushed samples of biomass in two particle sizes (106-212μm and 300-500μm). The blend was mixed manually in a Vickers jar with capacity of 500ml, using a spoon for 5 minutes to obtain a homogeneous blend. For each blend, 10g was kept in a glass bottle to be used in small sample size experiments. The remaining material was used directly in large scale experiments (Table 8).

Table 8: Coal-biomass blend material prepared for oxidation experiments

Experiments	106-212μm	300-600μm
TGA, FT-IR (7 coal samples blended with 4 biomass, in 4 proportions, total 112 samples)	15g bottle	15g bottle
Spontaneous Combustion reactor (7 coal samples blended with 4 biomass, in 4 proportions, total 112 samples)	100g bag	100g bag

3.3 Equipment and experimental procedure for sample preparation

3.3.1 Drop Tube Furnace

A drop tube furnace developed by E.On (formally known as Powergen UK) and situated at the Department of Chemical and Environmental Engineering at The University of Nottingham is used to produce biomass char samples under controlled conditions to reproduce combustion conditions (Figure 25). The furnace is pre-heated by three heating elements located in the top, centre and bottom of the reactor, each managed remotely from a main controller unit. The furnace operates in a temperature range from 300 to 1300°C, and three different resident times: 200ms,

400ms and 600ms. For each residence time there is a specific gas flow, which has been calibrated under standard conditions. The sample is fed at the top of the furnace automatically by a screw feeder in a rate of 1g min^{-1}, and collected in a water cooled probe at the bottom of the reactor. The outlet is connected to a cyclone which separates the solid char particles from the flue gas.

This equipment was used to study the structure of biomass particles and compare the effect of a high heating rate environment on the reactivity and morphology of particles. For this test, five biomass types in six different particle sizes were used. Samples were passed through the furnace, operating at 1000°C, 1% oxygen concentration and using a residence time of 600ms. The experiment required approximately 5g of fresh material to pass through the screw feeder system. Finally, the material is stored in glass bottles for microscopy and TGA analysis.
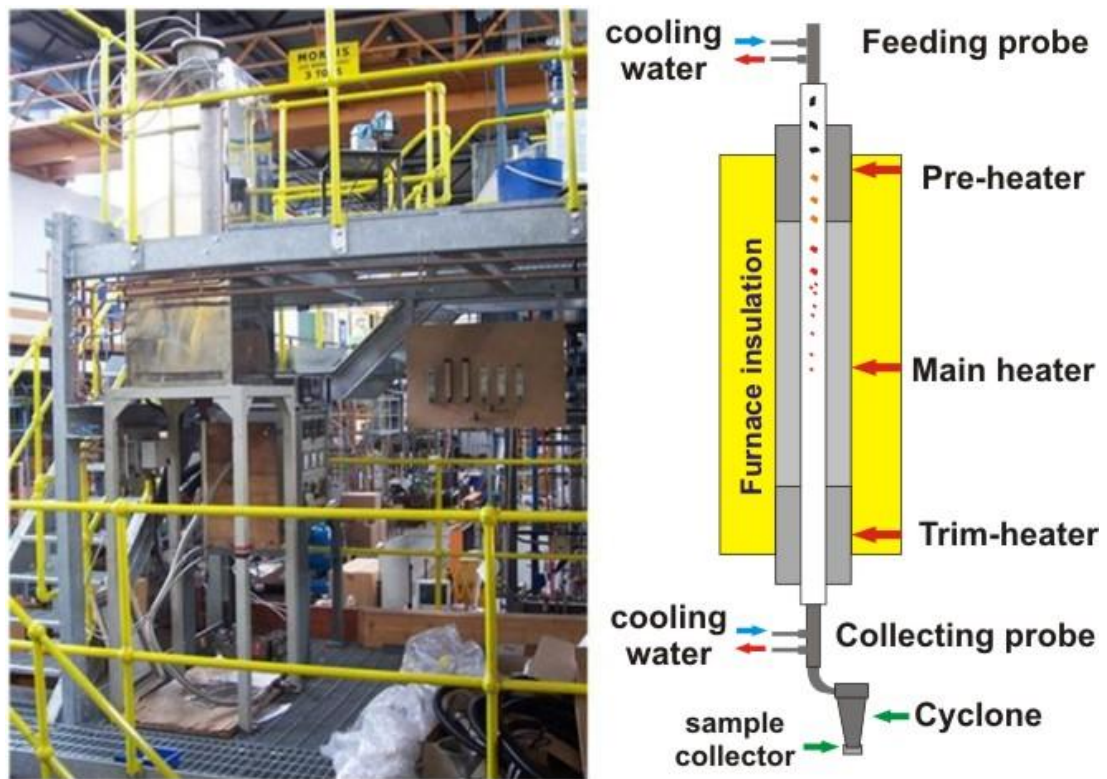
Figure 25: Drop tube furnace.

3.3.2 Muffle furnace

A Carbolite muffle furnace model OAF 10/1 was used to produce biomass char samples under fix bed conditions (Figure 26). The furnace is pre-heated by means of an electrical resistance at 1000°C connected to power supply on 220/230 volts A.C. The experimental is described as follows: Ceramic crucibles were filled with 10g of fresh biomass and a closed ceramic lid (to allow pyrolysis but with reduced air ingression in order to minimise combustion) and placed directly into a preheated Muffle furnace at 1000ºC. Samples were left for 3 minutes, to allow pyrolysis stage to be completed, after which the crucibles were removed and placed in a dessicator to avoid the re-introduction of moisture.

Figure 26: Carbolite muffle furnace (left) and cutting mill Pulverisette15 (right).

3.3.3 Cutting mill

A laboratory cutting mill model Pulverisette 15 (Fritsch) was used for grinding biomass particles (Figure 26). A rotor inside the mill revolves the material at high speed (3000rpm), fractioning by means of a cutting plate located in the inferior part

of the mill. The fine material is collected in the bottom of the equipment in a stainless steel basket attached.

3.3.4 Laboratory disc mill

A laboratory disc mill model Tema T 750 K (Figure 27), is used for grinding minerals and organic materials. The mill has a cylindrical chamber with two concentric cylinders that allow the milling of 100g of sample. The discs (Figure 27, right side) are agitated by horizontal vibrations, grounding the material by impact and friction. The time of milling is preset by an analogous timer, in a variable range from seconds to hours. All coal samples were pulverized using this device.
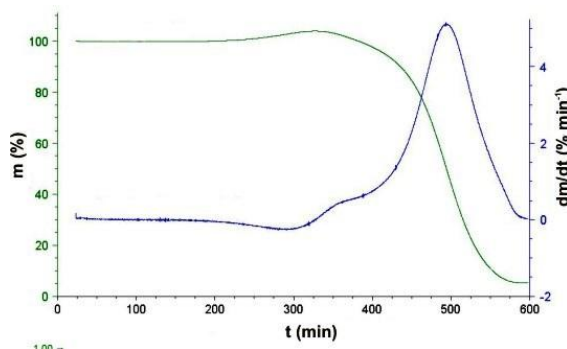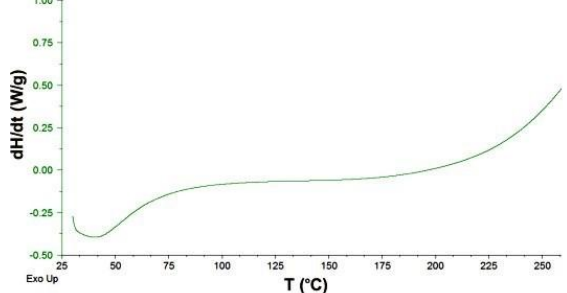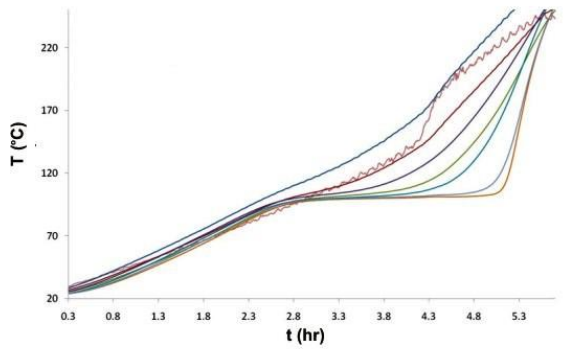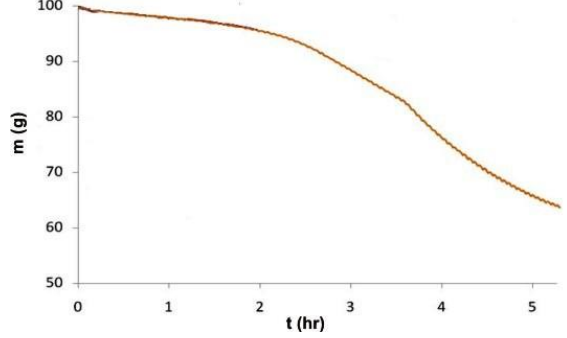
Figure 27: Laboratory disc mill, similar model to the actual used.

3.4 Equipments and methods used for thermal analysis

Three main thermal techniques were used: thermogravimetric analysis (TGA), differential scanner calorimeter (DSC), and differential thermal analysis (DTA). Each provides useful information about the response of coals in a heated environment that could be related to the issue of self-heating. Techniques and their characteristic profiles are summarized in Table 9.

Table 9: Thermal techniques used in this research. Adapted from [151]

Method	Parameter measured	Instrument employed	Typical curve
TGA	Weight (m) and weight loss (dm/dt)	Thermo balance	
DSC	Heat flow (dH/dt)	Calorimeter	
DTA	Temperature (T)	DTA apparatus designed	
DTA	Mass (m)	Balance attached to DTA apparatus designed	

3.4.1 Thermogravimetric analysis

Thermogravimetric analysis (TGA) is one of the most common tools used for thermal coal characterization. From this, it is possible to study mass change as a

function of temperature and time, providing information about thermal stability, composition, reactivity, kinetics and relevant physical properties of the samples.

3.4.1.1 Equipment used for sample analysis

Thermogravimetric analysis (TGA) was carried out using a TA Q500 (TA instruments Co.), with a gas flow of 100ml min^{-1} and a sample size of 4-20mg. This instrument has 16 platinum pans located in an auto sampler tray, which is controlled from a remote desktop that is also used to control the heating programs and record the weight of the sample as a function of time. Five main methods have been used: Proximate analysis, reactivity in air, slow pyrolysis, spontaneous combustion testing, and absorption of oxygen.

3.4.1.2 Sample preparation and analysis

The experimental procedure to load the sample pans is described as follow:

a) Platinum crucibles were clean and tared using the auto sampler tool.

b) Approximately 10mg of sample was placed in the platinum crucibles (sample preparation described in section 3.2.3).

c) Sample is run using a software controlled program.

3.4.1.3 Methods

i) Intrinsic Reactivity: The intrinsic reactivity test identifies the propensity of samples to lose weight whilst being heated at a fixed ramp rate in air (10^oC min^{-1}). There are key values that can be obtained from this test: a) initial temperature (the stage at which at 1%wt conversion is achieved); b) peak temperature (where combustion or devolatilisation rates reach a maximum); and c) burnout temperature (where 99% of the carbonaceous material has been combusted).

ii) Proximate analysis [107]: This test was used to measure volatile, fixed carbon, ash and moisture content. First, samples were heated from ambient to 105^oC under a

constant heating rate in nitrogen (10^oC min^{-1}). After reaching 105^oC the temperature was kept constant for 5 minutes; the weight loss to this point was attributed to the moisture content. Then the sample was heated from 105^oC to 920^oC under a constant ramp rate in nitrogen (10^oC min^{-1}), and held at the maximum temperature for 15 minutes; this weight loss was attributed to the volatile content. Finally, N_2 gas flow was switched to air at 920^oC for 15 minutes to calculate the fix carbon content. The remaining weight in the pan corresponds to the ash content.

iii) Slow pyrolysis test: This test identifies the behaviour of volatile matter in the sample whilst being heated at a slow ramp rate in nitrogen (5^oC min^{-1}). There are key values that can be obtained from this test: a) initial temperature (the stage at which at 1%wt volatilization is achieved); b) peak temperature (where devolatilisation rates reach a maximum); and c) final temperature (where 99% of the volatile material has been released from the sample).

iv) Spontaneous combustion testing: This test is used to identify samples which are highly reactive in air at low temperatures. The fundamentals of this test are explained carefully in Chapter 4. The test consists in a set of different heating ramp rates in air (experiment executed using heating rates of 3, 5, 7, 10, 20, 30, 40 and 50^oC min^{-1}). There are key values that can be obtained from this test: a) derivatives of weight against time; and b) the slope of the derivative plot in the linear segment of the curve, at low temperature.

This information can be plotted to form a profile of heating ramp rate vs slope obtained, which is unique for each sample and possibly relates to the self-heating phenomena.

v) Absorption of oxygen: This test identifies samples which absorb oxygen at low temperature whilst being heated at a slow ramp rate in air (executed twice using

heating rates of 3 and 5°C min^{-1} under an air atmosphere). There are key values that can be obtained from this test: a) initial temperature (the stage at which an increase in sample weight starts); b) peak temperature (where increased weight of the sample reach a maximum); and c) % of maximum oxygen absorption (% of weight reached in the peak temperature). This test considers just the net oxygen adsorption and its fundamentals are explained in Chapter 4.

3.4.2 Differential Scanning calorimeter

Differential scanner calorimeter (DSC) is used to study the heat released at low temperatures during volatilization and oxidation. In this case, a nitrogen atmosphere is used to study of the heat of volatilization of the sample; and an air atmosphere is used to measure the heat of O_2 adsorption.

3.4.2.1 Equipment used for sample analysis

A differential scanner calorimeter model Q2000 (TA instruments Co.), with auto sampler for 50 Tzero aluminium crucibles, and a temperature accuracy of ±0.01^{o}C was used. The sample size range was 4 to 20mg, and the gas flow was set at 100ml min^{-1} to have equivalence with the TGA analysis. In this instrument the atmosphere used is nitrogen. Alternatively, a differential scanner calorimeter model Q10 (TA instruments Co.), with a temperature accuracy of ±0.01^{o}C was also used. The sample range was 4 to 20mg, and the gas flow was set at 100ml min^{-1}. In this instrument the atmosphere used was air (21O_2-79 N_2).

3.4.2.2 Sample preparation and analysis

For both instruments, the procedure for loading the sample is similar and it is described as follows:

a) Aluminium crucibles were clean and tared manually in a precision balance.

b) Approximately 10mg of sample was placed in the aluminium crucibles (preparation of sample described in Section 3.2.3).

c) An aluminium lid was placed over the top of the pan, and then compressed by using a hand press (executed when N_2 atmosphere is used).

d) Crucibles were located in the auto-sample tray of the instrument.

e) The experiment is run using software control.

3.4.2.3 Methods

i) Heat of volatile and water release: For this procedure, 10mg of pulverized coal sample was placed into the sample pan and then exposed to a heating ramp under a Nitrogen atmosphere (experiment executed twice using 10 and 20°C min^{-1} heating ramps). The temperature range of these experiments varied from ambient temperature to 300°C. From this test heat evolution profiles were obtained, which related to the mass evolution profiles. Also, profiles were compared with the same procedure but executed in air to observe the net heat evolution produced by the oxygen adsorption.

ii) Heat of oxygen adsorption: For this test, 10mg of pulverized coal sample was placed into the sample pan and then exposed to a heating ramp under air atmosphere (experiment executed using 5, 10 and 20°C min^{-1} heating ramps). The temperature range of these experiments varied from ambient temperature to 300°C. From this test were obtained the heat evolution profiles under air, which were used to obtain the net heat evolution produced by the oxygen adsorption in coal particles.

3.4.3 Prototype reactor for thermal analysis of a large sample

A thermal reactor was designed at Nottingham to achieve two main objectives: Study the chemical behaviour of the sample at a slow ramp of temperature, measuring simultaneously the weight loss, the gas released and the temperature in real time at

different positions (crossing point temperature test, CPT); and produce sufficient material for studying the degree of oxidation using reflectance analysis.

3.4.3.1 Reactor design

i) Furnace reactor: This apparatus was a vertical tubular furnace, powered by three heating elements (top, centre and bottom), and managed by an external controller unit in a temperature range between room temperature to 1000°C. The furnace had a diameter of 0.06m and 0.75m of length, with a sealed connection for gas extraction at the top. Dry air was fed into the furnace by an air diffuser installed at the bottom of the unit. The diffuser was connected to a compressed air supply line and controlled by a flow meter in the range 1-6L min^{-1}, which was installed in the line before the diffuser. The entire installation is shown in Figure 28.
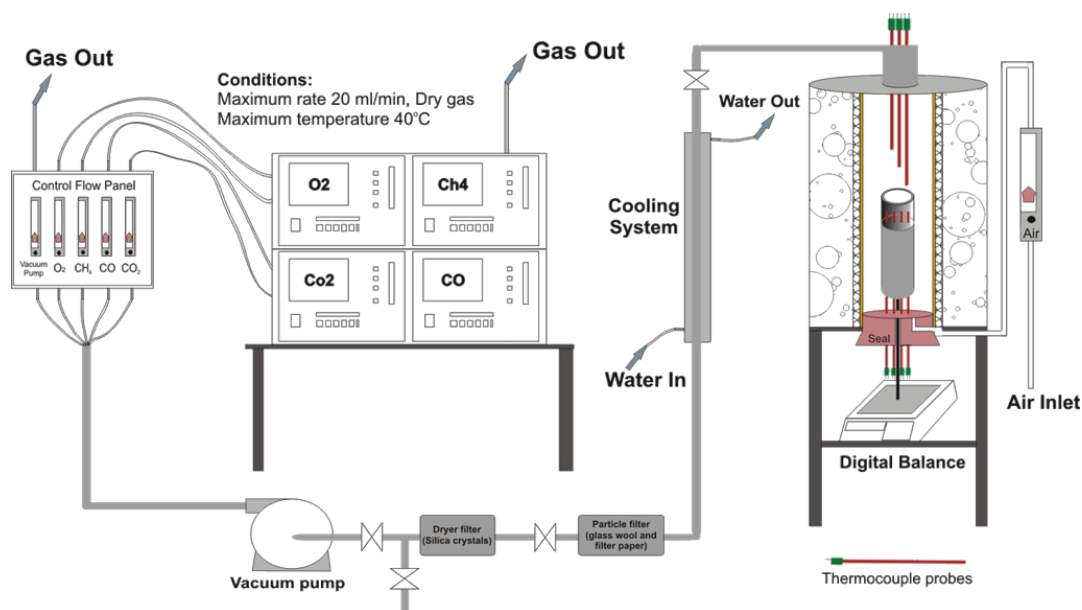
Figure 28: Diagram of experimental reactor.

ii) Sample holder and temperature reading system: The sample holder was a stainless steel cylinder of 100ml of capacity. The diameter of this was 0.05m; the length was 0.08m; and the net volume was 98.9ml. The metallic recipient had 7

holes, with 13 thermocouples set at different positions (Figure 29). Also, the sample

holder rest on a platform, which is connected by a rigid base to a balance, thermally

protected using high temperature ceramic insulation (Figure 30).
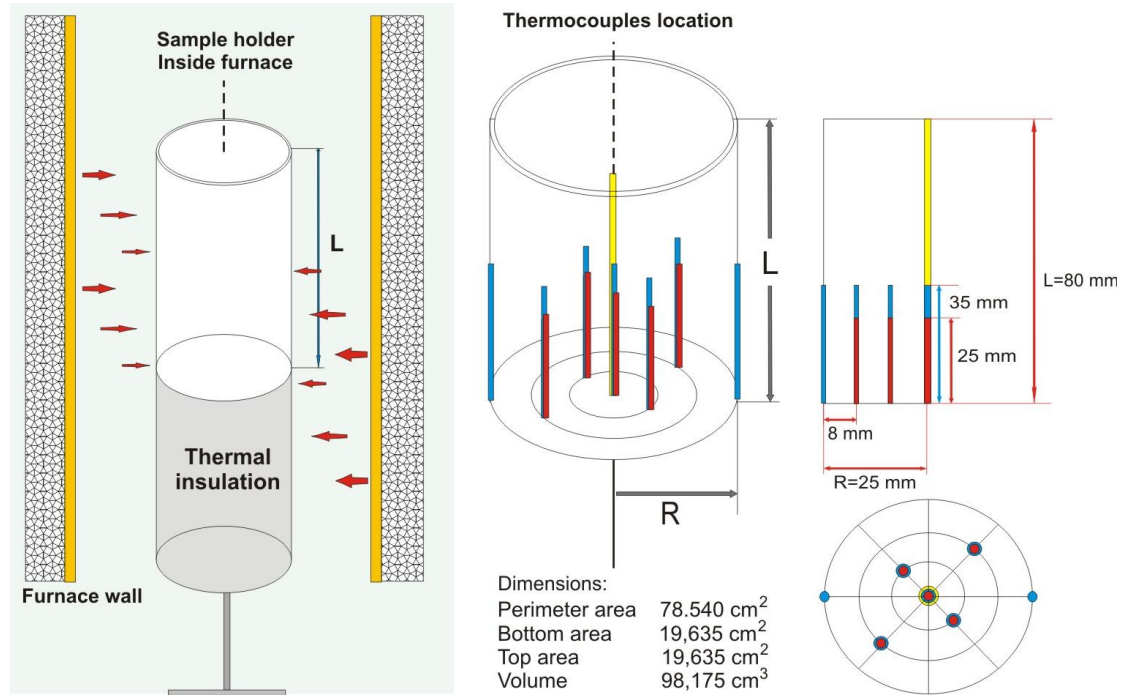
Figure 29: Diagram of sample holder designed. The heat transfer is restricted to the

axial edge and the mass transfer is restricted to the top of the sample holder.

All thermocouples were K type and 0.6m in length, model SuperOMEGACLAD XL

(sheathed-quick disconnect with miniature size plug; Chromel-Alumel type with an

insulated junction and minerally insulated body, Omega brand). Seven of these had a

diameter of 1mm, and were located 35mm from the bottom of the sample holder

(Figure 29, blue colour). Five thermocouples had a diameter of 0.5mm and were

located 25mm from the bottom of the sample holder (Figure 29, red colour). Finally,

a single thermocouple with a diameter of 1mm was located exactly in the centre top

of the sample holder (Figure 29, yellow colour).
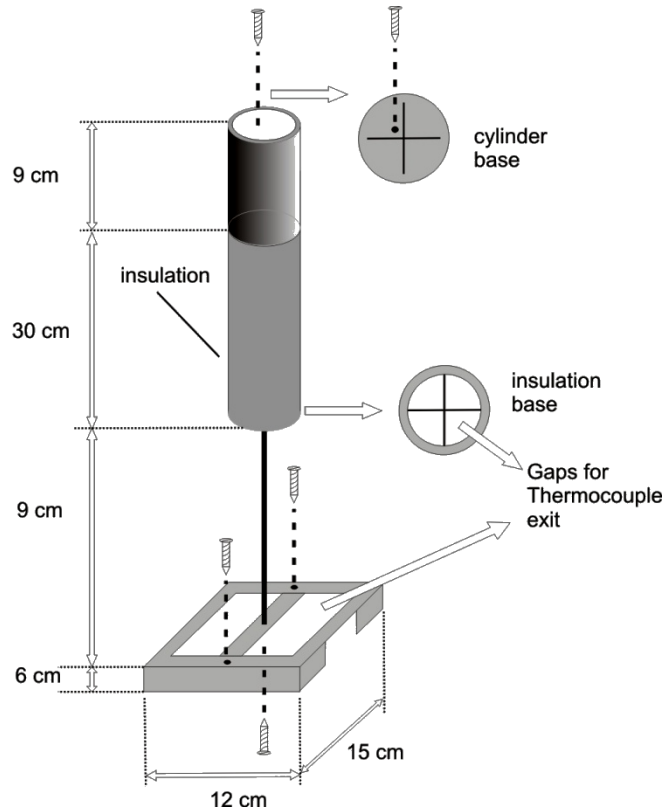
Figure 30: Sample holder structure, which was positioned on a balance.

All thermocouples were connected to two Picolog data acquisition system model TC-08, with an automatic cool junction adjustment for each thermocouple. The device allowed temperature readings in real time, with a maximum sample rate of 1 reading per millisecond. Both devices are controlled by a script executed in Labview (described in Section 3.6), which allows the user to set the sample rate.

iii) Gas analysis system: A vacuum pump collected the flue gas from the top of the furnace and pumping this through a heat exchanger to reduce its temperature from a maximum of $400^{\circ}C$ (maximum temperature of design) to $30^{\circ}C$, in order to achieve an appropriate temperature for the gas analyzer system (below $40^{\circ}C$). Two filters were installed to capture the particulate matter and moisture present in the gas. The first filter was a glass cylinder filled with glass wool; and the second, a drying filter made from glass and filled with silica gel particles; both located between the pump and the heat exchanger (as it is shown in Figure 28). After the pump, a fraction of the

flue gas was fed into the gas analyzers (designed capacity of 50-200ml min^{-1} per channel). The normal operational flow was 80ml min^{-1} per channel, and the remaining gas was sent to a fume extraction.

The gas analysis was carried out using a Servomex 1440D gas analyzer, with an analogue output in the range of 0-12V that was connected to the data acquisition system. The first analyzer was capable of measuring CO and CO_2 concentration in the range of 0.0 to 20.0%. The second analyzer measured O_2 and CH_4 concentrations in the range of 0.0 to 25.0% for O_2 and 0.0 to 5.0% for CH_4. In both cases, the reading was in real time, with a maximum sample rate of 1 reading per millisecond. It was also controlled by a script executed in Labview (described in Section 3.6), which allowed the user to control the sample rate.

iv) Mass analysis system: A balance model Explorer-Pro 6102 (Ohaus) was used to record the mass of the sample during the experiment. The balance provided an analogue output in the range of 0-12V, and it was connected directly to a computer thought a COMM port by means of a RS-232 cable. The balance was located below the centre of the furnace, to allow a reading of the weight in real time, with a maximum sample rate of 1 reading per second. Labview was used to control the instrument, allowing the user to set the sample rate.

v) Data acquisition system (DAQ): The circuit for data acquisition is shown in Figure 31. This circuit was used to drive all the analogue signals through a series of devices to a computer. Then, the signals were cleaned, processed and saved in real time using a program code wrote in Labview 9.0, which at the same time allowed the synchronization of all the instruments, standardising the sampling rate for all the signals. The default sampling rate was 5 readings per second (algorithm details are given in Section 3.6). Finally, a picture of the whole system is shown in Figure 32.
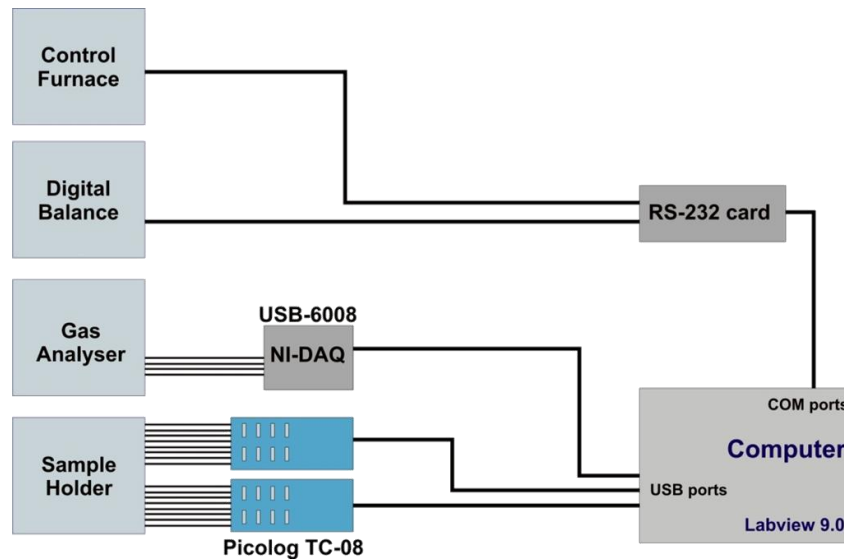
Figure 31: Diagram of the data acquisition system.
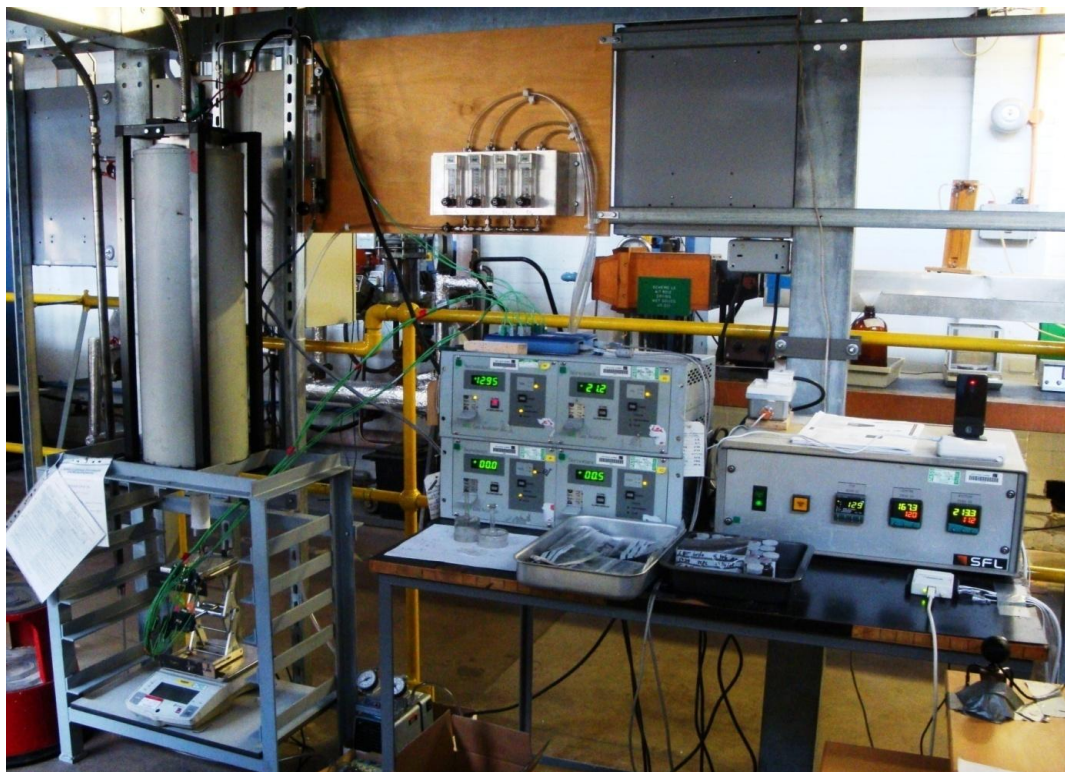
Figure 32: Photograph of the reactor system.

3.4.3.2 Sample preparation and analysis

i) **Preparation of coal samples:** For all coal samples, 100g were weighted and placed into the sample holder. Initially, half of the sample was introduced after

which it was ensured that all gaps between thermocouples were filled. Then, the sample holder is shaken followed by the introduction of the remaining material. In the case of low density samples, hand pressing was used to charge the material. Finally, the surface edge of the cylinder was left flat, 1mm below the level of the top thermocouple.

ii) Preparation of biomass samples: For this experiment, the amount of sample was relative to the type of biomass used, depending on their respective density. For all grain textured biomass, the procedure was similar to that these used for coal, but with approximately 60g (enough to fill the sample holder). In the case of fibre textured biomass, the amount of sample was reduced to approximately 35g.

iii) Preparation of coal-biomass blends samples: For this experiment, the amount of sample was set to 90g (enough to fill the sample holder). The blending process was implemented in situ, and the experimental procedure was similar to that used for coal samples.

3.4.3.3 Experimental procedure

i) Experiment (A): 100g of sample was placed in the sample holder and located in the experimental position over the balance and in the centre of the furnace. Then, thermocouples were connected to the interface data logger, which was already connected to the main PC unit. The pumping system was switched on, and a gas flow of 80ml min^{-1} was set up to feed the gas analyzers. After all these steps, the balance was tared. When all instruments were running, the mass, temperature and concentration readings were checked by the software (described in Section 3.6). Finally, the software starts recording all the variables measured, and the furnace controller simultaneously initiates the heating stage. A heating ramp of 0.5^{o}C min^{-1} was applied to the sample holder. When the oven temperature reaches 300°C, the

furnace is switched-off and the cooling stage starts. In this case, the sample was cooled down naturally inside the furnace and the profile of cooling was also recorded. Finally, when the temperature of all thermocouples reached 30°C, the data recording was stopped and sample was removed and disposed of.

ii) Experiment (B): Experiment B used the same initial conditions as experiment (A). The recording of all the variables starts simultaneously with the furnace heating. With experiment B a heating ramp of 0.5°C min^{-1} was used but as the oven temperature reached 250°C, all data recording was stopped and the sample was removed from the centre of the furnace. Afterwards, the sample holder was cooled down by a cotton sponge saturated in water. Approximately 5 minutes was needed to cool the temperature from 250 to 50°C. After that, the material was removed from the sample holder and spread in a metallic tray for two minutes to reach a temperature of ~30°C. Finally, 10g of the material is saved in a crystal bottle (to be used in the small sample size experiments), and the remaining is stored in a vacuum sealed plastic bag.

3.5 Microscopy and spectroscopy of coal and biomass

Microscopy was also used to characterize coal samples for two main studies: the characterization of the material structure; and the determination of optical properties of coal and biomass. In both cases, the observations were performed manually (classical approach) and using automated image analysis (using image processing algorithms developed specifically for this research).

3.5.1 Reflected Light Microscopy and Oil immersion techniques

For this study, Reflected Light Microscopy was used with an oil immersion objective lense, which increased the contrast between the sample and the mounting media. Standard analysis such as maceral content and rank analysis was carried out, as well

as classification of shape, measurement of particle size, area and porosity using image analysis.

3.5.1.1 Equipment used for sample analysis

A reflected light microscope model Leitz Orthoplan II POL-BK, with oil-immersion objectives was used. The microscope had a 10X eyepieces, and several objective lenses in a range of 10 to 50X magnification, which provide a total magnification range of 100 to 500X. The microscope also had a colour digital Zeiss AxioCam camera with a 2-axis automated stage control, to allow the synchronization between the stage and the digital camera in order to obtain mosaic images. The camera was connected to a computer using an optic fibre cable and operated with KS400 V3.1 software.

3.5.1.2 Sample preparation and analysis

i) Petrographic blocks preparation: There are two types of block mounting which are described as follows:

> **a) Cold mounting (for biomass and soft materials):** particles were placed in plastic moulds (3cm diameter), and embedded in Epoxy liquid resin in a proportion of 3:10 (% weight) respectively. Then, the material was placed in a vacuum impregnator for 15 minutes, and then left 24 hours for drying.

> **b) Hot mounting (coal and coke materials):** in this case, particles were homogeneously blended in a proportion of 3:2 (% weight) with Carnauba paraffin wax. Then, the material was placed in the metallic container of a pressure mounting machine model Labopress-3 (Struers), filling the top with 10g of pure Carnauba paraffin wax (to increase the thickness of the block). Then, the mixture was heated at 25KN of pressure to $150^{o}C$ for 10 minutes, and cooled by water for

10 minutes. Finally, the solid block was removed from the machine, ready for the polishing step.

ii) Block polishing: For cold and hot mounting, the polishing procedure was similar. An automatic metallographic polisher model Rotopol (Struers), with a range of speed of 150 to 300rpm is used. Firstly, blocks were polished at 150rpm for 2 minutes and 20N of pressure using a 600 grit grinding paper. Consecutively, the same procedure is repeated using a 1200 grit grinding paper. Then, the blocks were polished using 2400 grit grinding paper for 40 seconds under 15N of pressure and 150rpm. After this, the material was polished using a 4000 grit grinding paper for 20 seconds under 15N of pressure and 300rpm. Finally, the material was polished using a colloidal silica suspension of 0.04μm, for 2 minutes at 15N of pressure and 150rpm, to obtain a resolution of 0.04μm in the final stage of polishing.

3.5.1.3 Methods

i) Maceral analysis [181]: In this test, the maceral groups described in Chapter 2 (Section 2.2.1, H) were identified following the British Standard procedure for Maceral analysis [181]. The proportions of Maceral groups were determined by a manual or automated point count procedure, considering 250 points, and four maceral groups (vitrinite, semifusinite, fusinite and liptinite). Each point was positioned using a mechanical stage, capable of advancing the specimen laterally in equal steps, with a single count per particle. For this, the step length must be set as a half of the maximum particle diameter (for more details, refer to the standard [181]).

ii) Rank analysis [105]:

In this case, the British Standard procedure was used for coal rank analysis. Experimental conditions required a standard and stable source of light with a wavelength of 546nm, which was reflected at near normal incidence from a specified

area of a well-polished vitrinite particle, under an oil immersion objective. The reflected beam is measured using a photomultiplier (or similar device), and compared with the light reflected under identical conditions from a standard reference (sapphire and glass, in this case). The procedure required a minimum of 100 points to be measured, obtaining a maximum, minimum and average value from the reflectance histogram of the sample (for more details, refer to the standard [105]).

iii) Automated image acquisition and image analysis: Colour mosaic images of 15 by 15 were captured automatically for each sample using an automated system described in the previous section. The procedure to operate the microscope was similar to those described for Maceral and Rank analysis. In this case, the exposure time of the camera was adjusted automatically for the program KS-400, using a calibration procedure with a sapphire or glass standard. The mosaics were converted to a grey scale format to obtain a grey scale histogram (as described in Chapter 2) using a code developed in Labview (described Section 3.6). Images were used to obtain parameters such as particle size distribution, and area of the total number of particles per block, or for single particles as well.

3.5.2 Scanning electron Microscope

A Scanning Electron Microscope was used to study the surface of particles and changes in internal structure of both, biomass and coal samples. Two techniques were used: a) adhesive disks for surface analysis, and b) polished surfaces for internal structure analysis.

3.5.2.1. Equipment used for sample analysis

EDAX-SEM analysis was carried out using a Scanning Electron Microscope model Quanta 600 with energy dispersive X-ray. This SEM was also combined with a

mineral liberator analyzer software (MLA) that provides a tool to relate mineral content with surface area for biomass and coal particles analysis.

3.5.2.2 Sample preparation and analysis

i) Surface analysis (A): Adhesive disks samples are prepared using particles below 1mm of diameter, separated after a gently hand sieving. Then, these were spread manually over the surface of an aluminium carbon adhesive disk, removing all particles not attached to the surface by a manual blower. Finally, carbon disks were exposed directly to the electron beam.

This test allowed qualitative analysis of the characteristics of particles including macro porous structure, volumetric geometry and specific features presented such as ash deposition, identified using EDAX analysis. This test was used performed for fast visual analysis, prior to quantitative analysis.

ii) Cross section analysis (B): Polished blocks were prepared using the same procedure described previously (Section 3.5.1). Then, blocks were treated in a vacuum chamber to remove volatiles and moisture absorbed, prior carbon coating which increased the conductivity in the surface for higher magnification analysis.

From this test, it was possible to analyse and quantify the mineral content and crystal structure linked to the specific areas of particles. From this test was it also possible to calculate parameters associated with the particle morphology, especially for materials that could not be analyzed using Reflected or Transmitted light microscopes such as cross section of biomass particles. In the same way, stored image mosaic could also be quantified using image analysis algorithms.

3.6 Software designed for control, data acquisition and data analysis

A set of computational algorithms were written to facilitate the data acquisition and analysis of online instruments, as well as the analysis of images. All these codes

were developed in Labview 2009 (version 9.0) from National Instruments. The specific details of the software are shown in Appendix 1.

3.6.1 Software designed for data acquisition

The variables to be acquired in real time are mass, temperature and gas concentration. Each of these signals comes from a specific instrument using a single interface. Once the computer has established communication with the instrument, the reading process can be executed by a simple algorithm, which is shown in Figure 33. The main program synchronizes the execution of all these loops (one for each variable measured), delivering a single file with the information recorded at the end of each experiment. In all these cases, the default sampling rate was 1 reading every 5 seconds. The initial input of the program was the initial mass of the sample to be tested. The graphic interface developed for each loop is presented in Appendix 1.
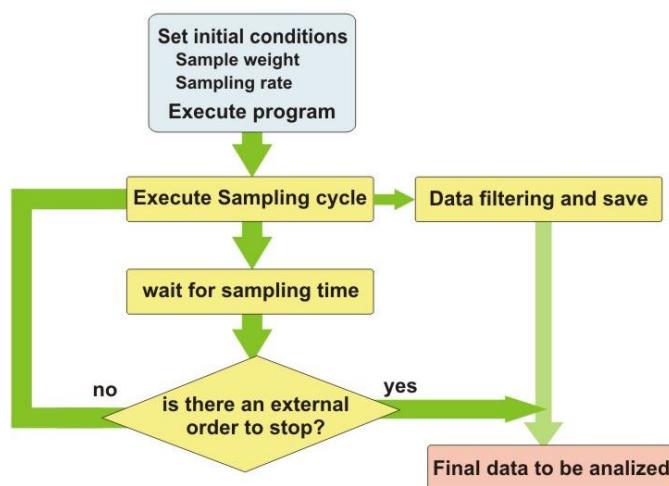
Figure 33: Loop sequence executed for data capture using the system described in Figure 31.

3.6.2 Algorithm used for data processing

An integrated algorithm is used for data processing of the signal obtained from the reactor described in Section 3.4.3. The aim of this program is to prepare the output

signal coming from the data acquisition system shown in Figure 141, before analysis. In this case, the signal is divided into different single channels, with applied filters for noise removal, as shown in the diagram in Figure 34 by the icon Time Averaging. Also, new output channels are created by the calculation of derivatives (e.g. mass to obtain mass loss rate); as well as the differential temperature profiles by subtracting a blank temperature profile. Finally, the voltage reading from the concentration analyzer is transformed and filtered into percentage units. This program has been written in Labview, and applied after the experimental testing.
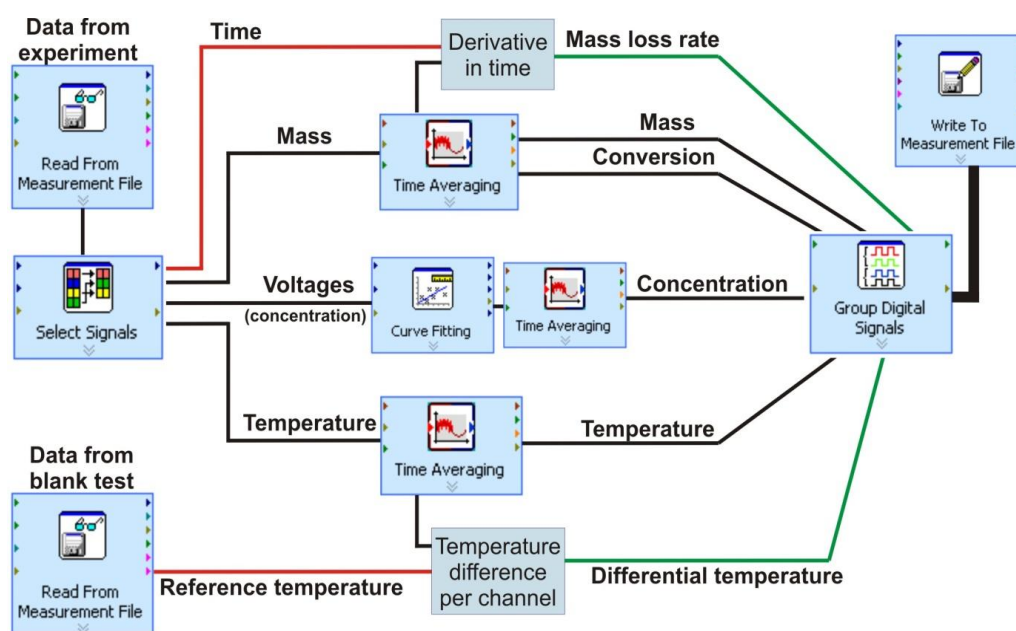
Figure 34: Algorithm used for data processing and filtering.

3.6.3 Program used for image analysis

A set of algorithms were developed for analysing mosaic images. All these algorithms follow a similar sequence: a) image acquisition; b) manipulation of the image (to obtain a grey scale image and to remove noise); and c) the application of sub-codes to obtain particular information from the image. The first algorithm was designed to obtain grey scale histogram (shown in Figure 35). These histograms

were compared in order to obtain difference between samples, as well as for comparison between fresh and oxidized samples.
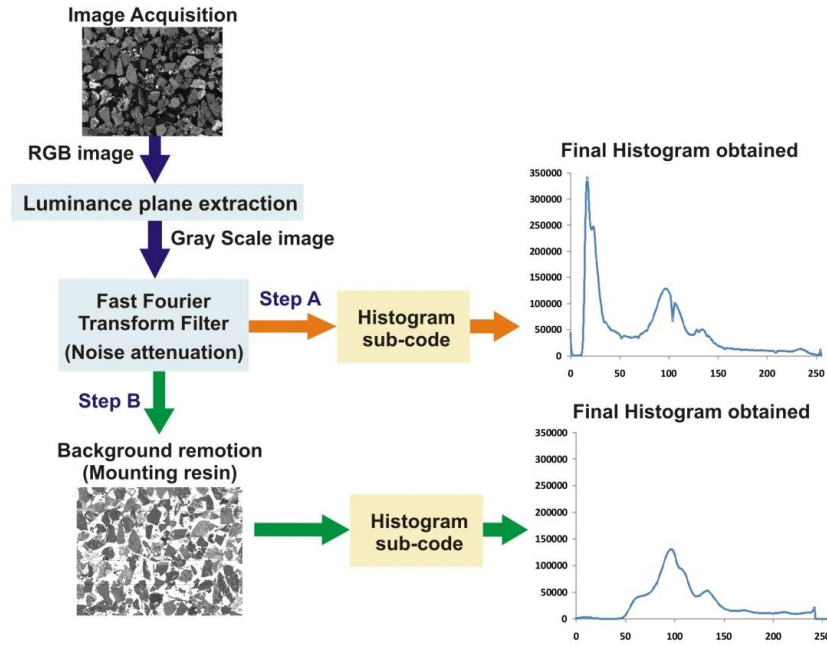
Figure 35: Algorithm developed for histogram acquisition.

The second algorithm was designed to perform a morphologic characterization of particles. In this case, the original image obtained using the automated microscope system was standardized at grey scale, and then cleaned by a Fourier transform filter. After this, the image is transformed to a binary mode by using a threshold histogram, removing all material between 0 to 50 grey scale units (GSU) and leaving the remaining in a unique colour tone. From this manipulated image, it is possible to perform a particle analysis test to calculate morphologic parameters [200]. The algorithm (shown in Figure 36) used the Vision Assistant of Labview, in order to process a large number of images. A database for each image was generated, containing the following parameters: diameter of particle (maximum and minimum); area of particle (with pores and without pores); roundness; percentage of pores per particle; maximum and minimum length per particle; and the total number of

particles analysed. These data were used to compare between samples and quantify the impact of the oxidation.

Finally, a third algorithm was partially developed to quantify the thermal alterations produced in treated coal samples. However, this test was performed manually due to the complex implementation of this in a computer code (the algorithm is shown in Appendix 1).
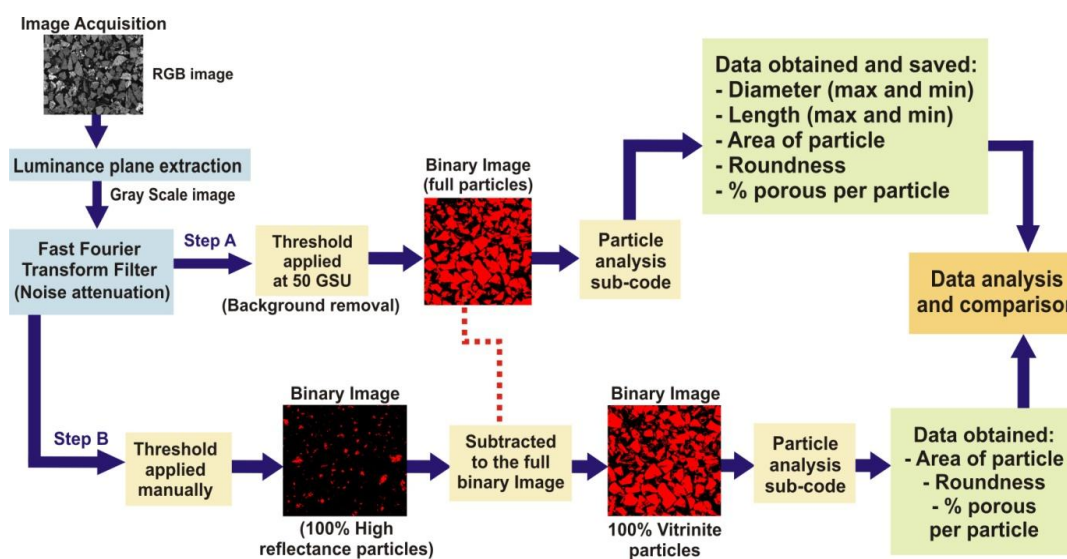
Figure 36: Algorithm developed for morphologic characterization of particles.

Chapter 4. Thermal analysis of coal at low temperature

4.1 Thermal characterization of fresh coals

4.1.1 Proximate analysis

Proximate analysis was carried out on fresh coal samples. The results are shown in Table 10, from which samples can be classified as standards sub-bituminous and bituminous coals, according to existing correlations used by the coal industry [238]. These correlations establish two specific relationships: A) water content is inversely proportional to the fixed carbon content, and at the same time, it is directly proportional to the volatile content; and B) water content is inversely proportional to the fuel ratio (volatile/carbon).

Table 10: Proximate analysis of coal samples used

Coal	As received				Dry, ash free basis		
	Moisture (wt.%)	Volatiles (wt.%)	Fixed Carbon (wt.%)	Ash (wt.%)	Volatiles (wt.%)	Fixed Carbon (wt.%)	Carbon/ Volatiles (wt.%)
Hambach	37.5	38.1	23.1	1.3	62.2	37.8	0.6
North Dakota	22.0	31.2	39.6	7.2	44.1	55.9	1.3
Fenosa	10.9	43.3	43.8	2.0	49.7	50.3	1.0
Nadins	7.4	35.6	50.4	6.7	41.4	58.6	1.4
Orupka	6.0	37.7	48.0	8.3	44.0	56.0	1.3
Asfordby	5.5	35.3	57.3	2.0	38.1	61.9	1.6
Lea Hall	5.5	35.2	57.4	2.0	38.0	62.0	1.6
Yanowice	5.1	26.9	60.8	7.3	30.7	69.3	2.3
Littleton	5.0	31.9	51.5	11.6	38.2	61.8	1.6
La Jagua	4.3	36.2	58.4	1.2	38.3	61.8	1.6
Ironbridge	4.1	34.9	52.4	8.6	40.0	60.0	1.5
Zondag 1	3.9	27.0	61.3	7.8	30.6	69.4	2.3
Indo	3.8	30.8	50.9	14.4	37.7	62.3	1.7
La Loma	3.8	45.1	39.3	11.9	53.5	46.5	0.9
Illinois #6	3.7	38.0	43.8	14.6	46.5	53.5	1.2
Bentinck	3.6	33.9	56.8	5.7	37.4	62.6	1.7
Kaltim prima	3.5	38.0	54.5	4.0	41.1	58.9	1.4
Blue Creek	3.5	28.9	59.7	7.9	32.7	67.3	2.1

Table 10, continuation

Coal	As received				Dry, ash free basis		
	Moisture (wt.%)	Volatiles (wt.%)	Fixed Carbon (wt.%)	Ash (wt.%)	Volatiles (wt.%)	Fixed Carbon (wt.%)	Carbon/ Volatiles (wt.%)
Kleinkopje	3.5	22.8	54.9	18.8	29.3	70.7	2.4
El Cerrejon	3.5	36.7	58.1	1.8	38.7	61.3	1.6
Daw Mill	3.3	34.9	56.3	5.5	38.3	61.7	1.6
Indiana EDF	2.8	33.2	53.1	10.9	38.5	61.5	1.6
Sines	2.7	27.8	56.2	13.4	33.1	66.9	2.0
Goedehoop	2.3	25.7	57.9	14.1	30.7	69.3	2.3
Hunter valley	2.2	27.3	52.3	18.2	34.3	65.7	1.9
Bulawayo	1.6	26.5	61.7	10.2	30.1	70.0	2.3
DeepNavigation	1.0	10.1	81.8	7.1	11.0	89.0	8.1
Bulli	0.9	22.3	67.5	9.4	24.8	75.2	3.0
Pocahontas #3	0.6	18.8	75.8	4.9	19.8	80.2	4.0

4.1.2 Intrinsic reactivity of coals

Intrinsic reactivity test was carried on all the samples (Table 11) to obtained peak and burnout temperatures, which are used to categorize 'reactivity'. Low values for peak temperature represent higher reactivity, which in this case were proportional to the burnout values. The relationship between these parameters which are generally used when investigating high temperature reactions is discussed later. Finally, the impact of physical parameters and the influence of intrinsic reactivity in the spontaneous combustion tendency have not been studied yet. The dependency of the low temperature oxidation with these properties will be discussed in the next sections.

Table 11: Intrinsic reactivity test (temperature values ±2°C)

Coal	Peak Temp. (^{o}C)	Burnout Temp. (^{o}C)
Hambach	338	519
North Dakota	354	500
Orupka	361	503
Fenosa	380	477
Nadins	418	557
Sines	456	
Illinois #6	460	560
Asfordby	464	554
La Loma	464	574
Goedehoop	480	567
Deep navigation	486	565
Bulawayo	487	571
Indo	489	574
Lea Hall	490	570
El Cerrejon	493	568
Ironbridge	502	579
Bentinck	507	
La Jagua	510	558
Kaltim prima	512	580
Hunter valley	513	
Pocahontas #3	520	
Zondag 1	526	590
Blue Creek	530	
Bulli	534	657
Daw Mill	535	583
Littleton	536	574
Yanowice	539	
Indiana EDF	541	
Kleinkopje	554	

4.2 Thermal analysis of coal using small sample size

This section reports the experimental results of thermogravimetric and differential scanning calorimetry tests carried out for the coal samples. The objective of these tests was to obtain information about the inherent reaction of coal oxidation at low

temperature, observing basic transformation that could be associated directly to the reaction mechanism, as well as to be comparing the results obtained from the large scale thermal tests.

4.2.1 Thermogravimetric analysis of coal at low temperature

Two experiments were carried out using this technique. The main objectives were: i) to study the weight evolution at low temperature and the impact of an induced temperature change (Section 4.2.1.1); and ii) to study and quantify the weight increase produced at low temperatures (Section 4.2.1.2).

4.2.1.1 Propensity of coal to react during a temperature change

The basis of this study has a theoretical formulation. The focus was quantifying the impact on mass loss rate produced by a change of temperature (at low temperatures), instead of using a classical kinetic approach. The change in the rate of the reaction during a temperature increase gives an indication of the propensity of the sample to react. For coal samples, weight is a variable that depends on time and temperature and can be experimentally recorded continuously using the TGA. It is therefore possible to produce derivatives curves in time and temperature, which are defined as:

$$\text{Equation 11} \qquad \dot{m} = \frac{\partial m}{\partial t} = f(T, t)$$

$$\text{Equation 12} \qquad \dot{\omega} = \frac{\partial m}{\partial T} = f(T, t)$$

These partial derivatives were obtained from a profile of mass as a function of time and temperature (Figure 37).

For this work, the two major experimental approaches were used: isothermal and non-isothermal methods. The first keeps the sample under a constant temperature, during a specific period of time (in Figure 37, curves parallel to the time axis). The second exposes samples to a constant heating rate (in Figure 37, coloured curves).

Then, different non-isothermal TGA tests reveal the full map of the sample weight as a function of these variables (T, t). In the same way, mass curves have continuous derivatives, which represent the weight loss rate. This information (obtained at low temperature) was the basis of the first test developed.
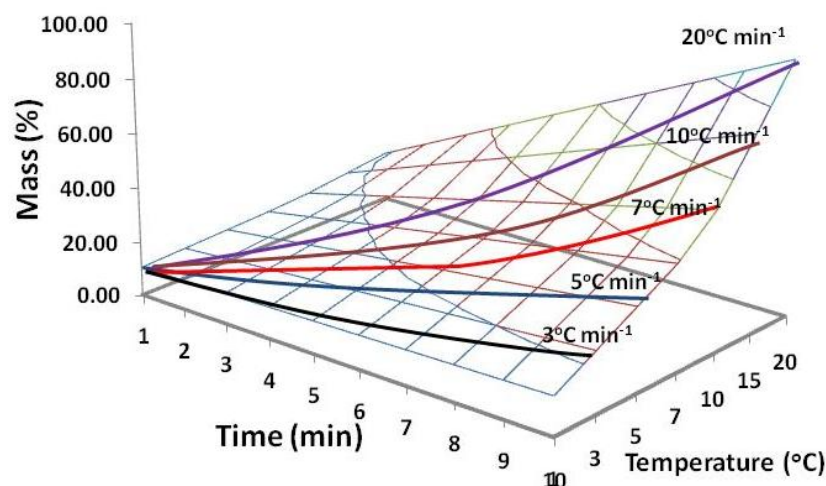
Figure 37: Mass profile as a function of time and temperature. Coloured lines represent different heating rates.

Experimentally, weight loss profiles were obtained for all coal samples using several heating ramps in the TGA (1, 3, 5, 7, 10, 20, 30, 40 and 50°C min^{-1}). From these, derivative curves in time were calculated for each coal sample and for each heating rate. For a standard coal sample at the initial stages of heating, the derivative curve exhibits a linear segment that was approximated by a linear trend, as can be seen from Figure 38. These results were found for all the samples without exception, as a characteristic response at low temperatures.

The linear stage of the derivative weight loss took place immediately after the main moisture release (90-120°C), finishing with an increasing devolatilisation rate that leads to the main combustion reaction (approximately at 300-350°C). The temperature range of this linear period was slightly higher than reported for the

mechanism of the spontaneous combustion reaction; however, this represents the early stages of oxidation, which could be related to the self-heating phenomenon. As can be seen from Figure 38, these linear trends also depend on the heating rate, and this specific characteristic produced a relationship between heating rate and mass loss for each sample.
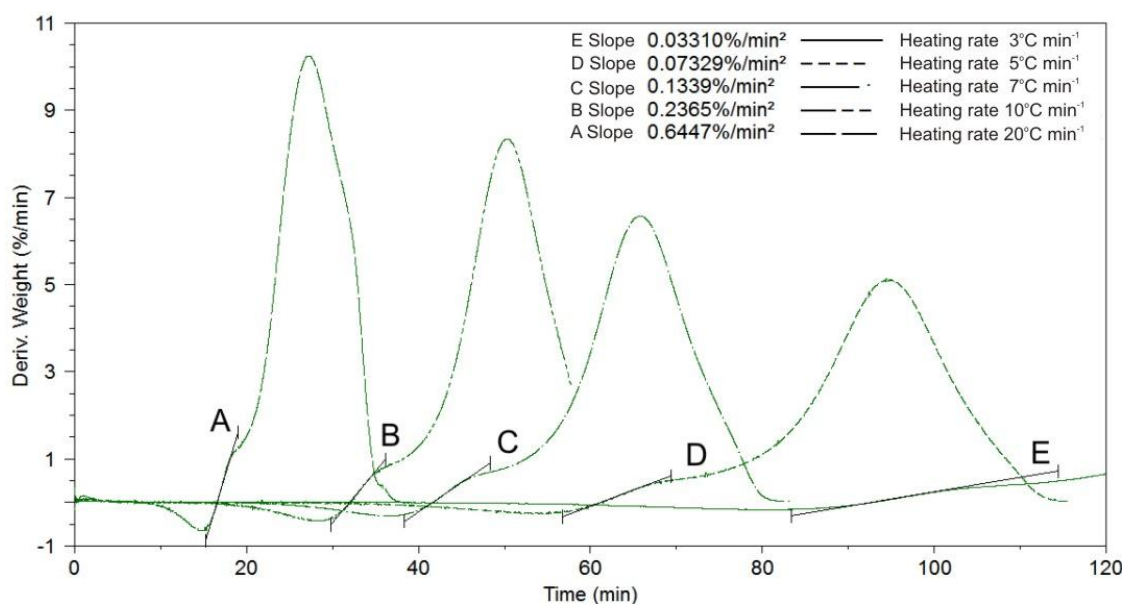
Figure 38: Derivative curves obtained for a standard coal sample under different heating ramps. At low temperature, all samples showed a linear segment.

At low heating rates (1 to 20°C min^{-1}) there was a direct relationship between the slope of the linear segment of the derivative curve, with the respective heating rate applied (Figure 39). Considering higher heating rates, it was observed that this actually corresponded to a sigmoid (higher order). However, the regression coefficient of the linear approximation was close to 1 for all the coal studied, and then it was considered as a linear tendency for this study. Subsequently, the slope of this profile was defined as the TG_{spc} index (thermogravimetric spontaneous combustion index), which was particular for each coal sample (slope of Figure 39).
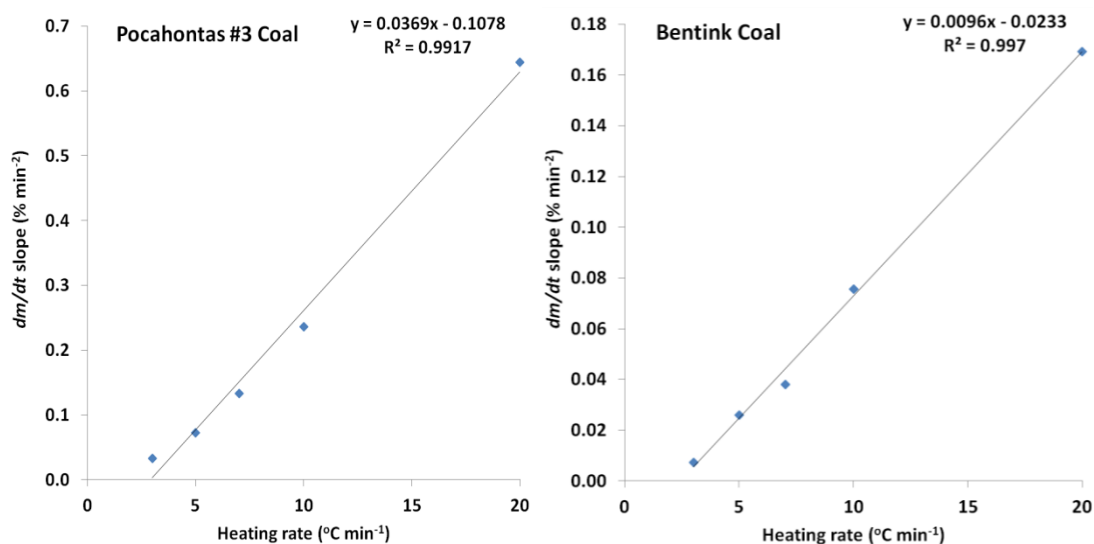
Figure 39: Heating ramp applied against slope of derivative curves (linear period) for two coals. These profiles are unique for each sample.

The TG_{spc} index can be expressed mathematically as the ratio between the weight loss rate variation and the temperature change due to an external source:

$$\text{Equation 13} \qquad TG_{spc} = \frac{\Delta weight\ loss\ rate}{\Delta Temperature}\ (wt\ \%\ °C^{-1}\ min^{-1})$$

The same procedure described was applied for all samples and the results are presented in Table 12 (Additional sample profiles are shown in Figure 40).
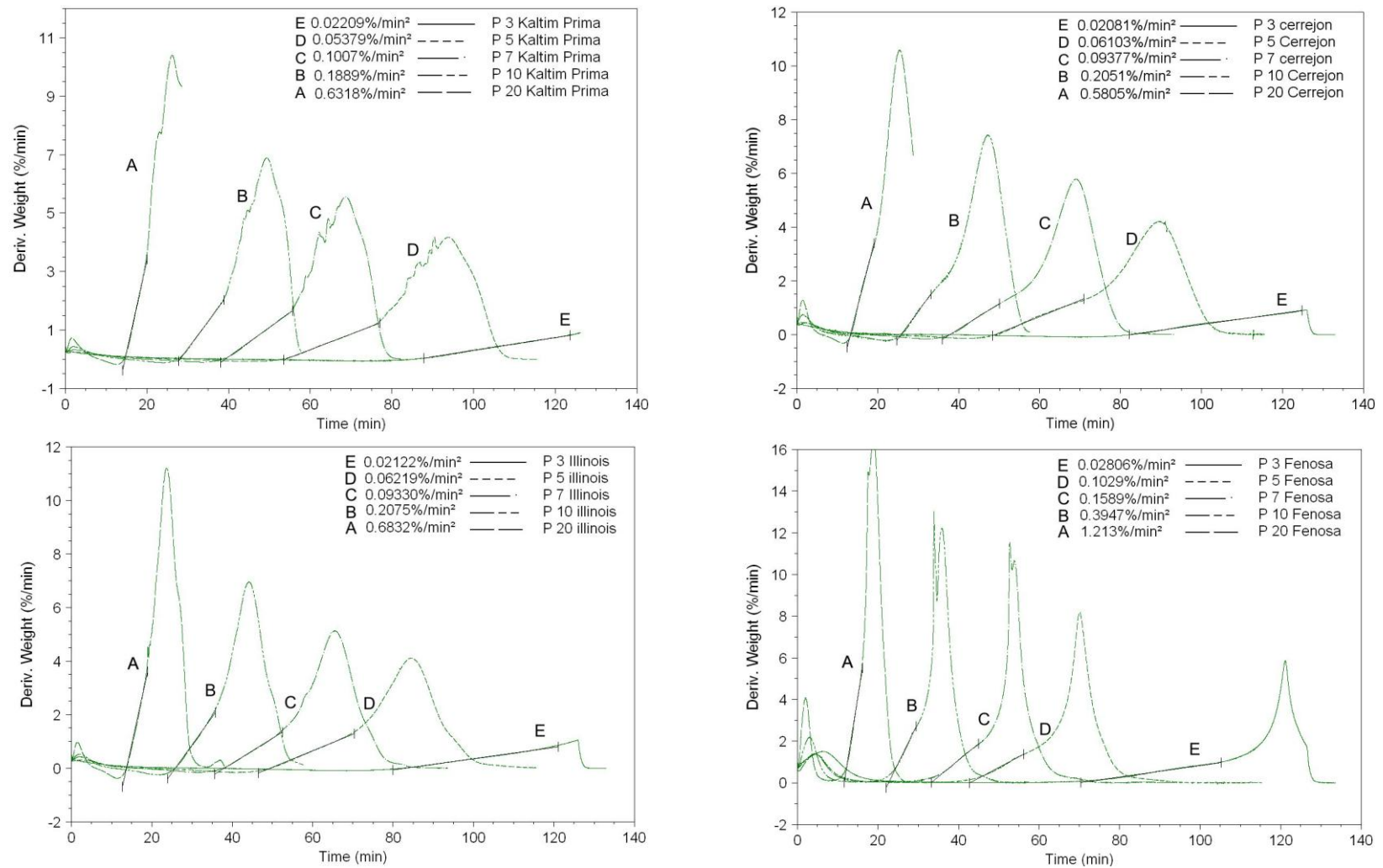
Figure 40: Derivative profiles obtained for selected coal samples (Kaltim Prima, El Cerrejon, Illinois #6, and Fenosa coals).

117

Table 12: Slopes obtained for different heating ramps applied (wt % $^{o}C^{-1}$ min^{-1})

Coal	Heating Ramp applied (^{o}C min^{-1})					
	3	5	7	10	20	30
Fenosa	0.0291	0.1047	0.1648	0.3727	1.3010	2.6500
Orupka	0.0410	0.0888	0.1949	0.3625	1.3150	2.6270
North Dakota	0.0384	0.1319	0.2032	0.4838	1.8310	3.9970
Hambach	0.0082	0.0275	0.0348	0.1282	0.3433	0.7042
Illinois #6	0.0209	0.0634	0.0950	0.2150	0.7096	1.2490
Pocahontas #3	0.0331	0.0733	0.1339	0.2365	0.6447	1.2520
Indiana EDF	0.0118	0.0332	0.0507	0.0934	0.2547	0.4441
La Jagua	0.0181	0.0419	0.0731	0.1300	0.4232	0.9041
La Loma	0.0179	0.0516	0.0821	0.1810	0.5566	1.1140
El Cerrejon	0.0208	0.0599	0.0923	0.1965	0.5823	1.1010
Blue Creek	0.0211	0.0531	0.0943	0.1692	0.5150	0.9314
Bulli	0.0321	0.0466	0.1381	0.1452	0.4329	0.7247
Hunter valley	0.0200	0.0500	0.0894	0.1788	0.5281	1.0210
Kaltim prima	0.0222	0.0540	0.1022	0.1906	0.6608	1.2660
Indo	0.0196	0.0435	0.0896	0.1494	0.4985	1.0690
Goedehoop	0.0203	0.0419	0.0912	0.1692	0.5596	1.1110
Kleinkopje	0.0121	0.0323	0.0495	0.0885	0.2882	0.5200
Bulawayo	0.0244	0.0608	0.1082	0.1976	0.5886	1.1150
Zondag 1	0.0207	0.0421	0.0871	0.1268	0.4043	0.7614
Sines	0.0224	0.0565	0.1042	0.1858	0.6146	1.1800
Littleton	0.0171	0.0415	0.0705	0.1198	0.3743	0.7262
Daw Mill	0.0140	0.0350	0.0601	0.1052	0.2792	0.7015
Yanowice	0.0126	0.0321	0.0527	0.0922	0.2611	0.5530
Asfordby	0.0233	0.0532	0.0931	0.1646	0.4169	0.9670
Lea Hall	0.0189	0.0457	0.0755	0.1368	0.4264	0.8155
Bentinck	0.0075	0.0261	0.0381	0.0757	0.1694	0.2931
Nadins	0.0160	0.0305	0.0669	0.1076	0.3269	0.6776
Ironbridge	0.0177	0.0477	0.0782	0.1247	0.4384	1.0210

The selection of the heating ramp applied and the comparison of the TG_{spc} index between samples are discussed as follows:

i) **Selection of heating ramps applied:** The TG_{spc} index calculated depends on the heating rate. When this index was calculated using a set of lower heating rates,

the TG_{spc} value changed considerably compared to the higher heating rates. Considering the actual rate observed during actual spontaneous combustion occurrences (a negligible rate increase), the use of slow heating rates allows a closer observation of the real phenomenon. However, at the same time there was a need to optimize between the experimental testing time required to generate a result and the reliability of the results themselves. For this reason, several values of the TG_{spc} were calculated using an increasing number of points for each coal sample (Table 13), with the aim to find the optimum set of heating rates.

As expected, when the TG_{spc} was calculated using slow heating rates $(3,5,7,10^{o}C$ $min^{-1})$, the value was lower than those obtained when using higher heating ramps $(3,5,7,10,20,30^{o}C$ $min^{-1})$. However, despite the difference in values, a comparative plot revealed that these differences were similar for all samples (Figure 41). Additionally, the associated deviation coefficient of the linear approximation for each set of experiments (r^2) was similar and close to 1 for all the tests.
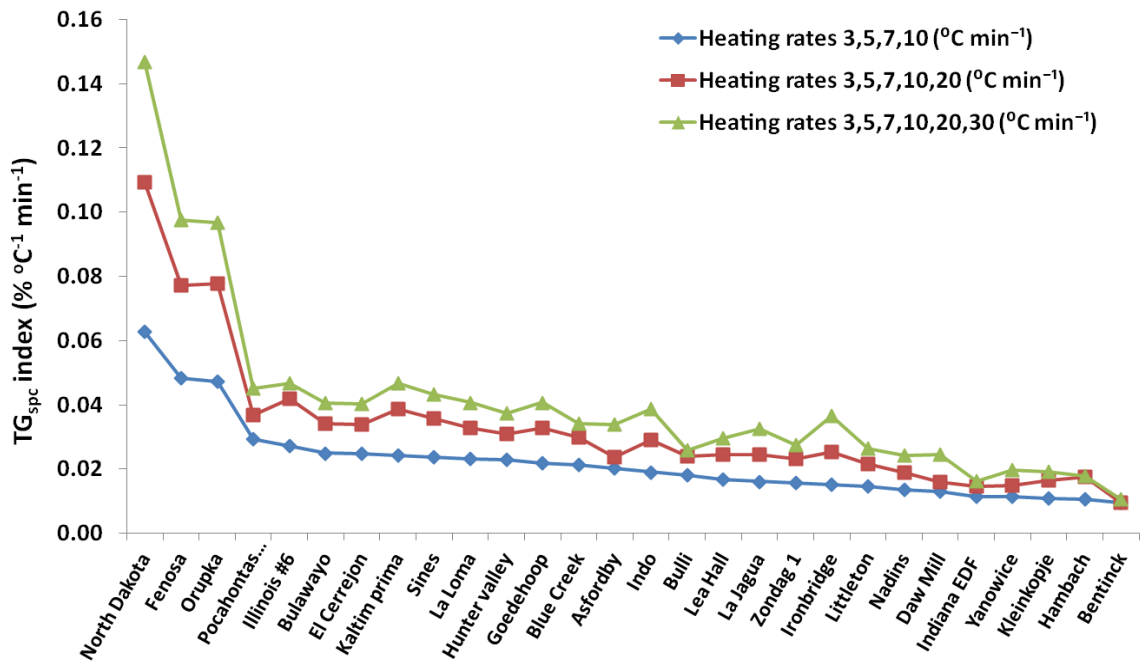
Figure 41: Graphic comparison of the TG_{spc} index, considering an increasing number of heating rate values used.

Table 13: TG$_{spc}$ index by using different number of heating rates (% ^{o}C^{-1} min^{-1})

Coal	Ramp used (^{o}C min^{-1})					
	3,5,7,10		3,5,7,10,20		3,5,7,10,20,30	
	TG$_{spc}$ index	r^2	TG$_{spc}$ index	r^2	TG$_{spc}$ index	r^2
Fenosa	0.048	0.96	0.077	0.97	0.098	0.97
Orukpa	0.047	0.98	0.078	0.97	0.097	0.98
North Dakota	0.063	0.95	0.109	0.97	0.147	0.96
Hambach	0.011	0.99	0.018	0.97	0.018	0.99
Illinois #6	0.027	0.96	0.042	0.98	0.047	0.99
Pocahontas #3	0.029	0.99	0.037	0.99	0.045	0.98
Indiana EDF	0.012	0.99	0.015	0.99	0.016	0.99
La Jagua	0.016	0.99	0.025	0.98	0.033	0.97
La Loma	0.023	0.96	0.033	0.98	0.041	0.98
El Cerrejon	0.025	0.97	0.034	0.99	0.040	0.99
Blue Creek	0.021	0.99	0.030	0.99	0.034	0.99
Bulli	0.018	0.83	0.024	0.97	0.026	0.99
Hunter valley	0.023	0.98	0.031	0.99	0.037	0.98
Kaltim prima	0.024	0.98	0.039	0.98	0.047	0.98
Indo	0.019	0.99	0.029	0.98	0.039	0.97
Goedehoop	0.022	0.98	0.033	0.98	0.041	0.98
Kleinkopje	0.011	0.99	0.017	0.98	0.019	0.99
Bulawayo	0.025	0.99	0.034	0.99	0.041	0.99
Zondag 1	0.016	0.99	0.023	0.98	0.028	0.98
Sines	0.024	0.99	0.036	0.98	0.043	0.98
Littleton	0.015	1.00	0.022	0.98	0.026	0.98
Daw Mill	0.013	0.99	0.016	0.99	0.025	0.94
Yanowice	0.011	0.99	0.015	0.99	0.020	0.97
Asfordby	0.020	0.99	0.024	1.00	0.034	0.96
Lea Hall	0.017	0.99	0.025	0.98	0.030	0.98
Bentinck	0.010	0.98	0.010	1.00	0.011	1.00
Nadins	0.014	0.98	0.019	0.99	0.024	0.97
Ironbridge	0.015	1.00	0.025	0.97	0.036	0.95

The set of heating rates 3,5,7,10,20^{o}C min^{-1} was selected based on the deviation coefficient and the time needed to perform the experimental testing. This selection allowed the index calculation of a single coal sample in a day of experimental work,

whilst using the slowest possible heating ramps. Lower heating ramps required a considerably longer experimental time, whilst producing a similar trend. Figure 41 shows that the significance of the TG_{spc} index is relative to other samples rather than an absolute value. Finally, it was concluded that the use of this indicator must be standardized by defining a sample as a standard case, which shows the limit between high risk for spontaneous combustion and safe.

ii) Comparison of TG_{spc} index between samples: Figure 42 shows the second order profiles for all the samples studied. It was observed that high reactive coals samples (e.g. N. Dakota & Fenosa) showed higher values for the TG_{spc} index. The lowest values resulted from known low 'reactive' coals. These results agreed with the available data about spontaneous coal fires suffered by these coals. It also agreed with parallel experimental tests carried out including the crossing point temperature test and rank analysis shown later.
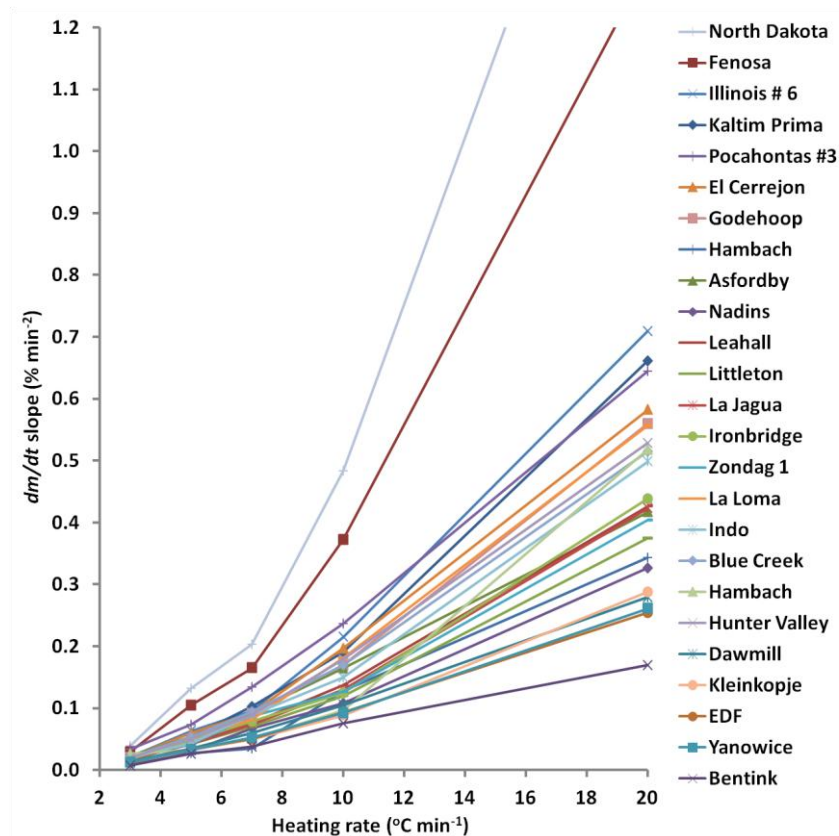
Figure 42: Comparison of the second order slopes with the heating ramp applied.

121

Considering the information showed in Figure 41 and Table 13, samples were classified in 5 groups by a decreasing order of the TG_{spc} index, which was associated with high to low reactivity (Table 14). From this, all samples included in group 1 are well known high risk coals. Group 2 included some reactive samples such as Kaltim Prima, El Cerrejon, and Illinois #6, which had presented incidents of spontaneous fires.

Table 14: Coal classification in decreasing order of TG_{spc} index

Group	Characteristic	Coal	Agreement with historic information
1	High reactive at low temperature	North Dakota Fenosa Orukpa	Excellent (clearly identified) Excellent (clearly identified) Excellent (clearly identified)
2	Reactive at low temperature	Illinois #6 Bulawayo El Cerrejón Kaltim prima Sines Pocahontas #3	Very good Good Very good Very good Poor (unreactive) Good
3	Less reactive at low temperature	La Loma Hunter valley Goedehoop Blue Creek Indo	Very good Poor (unreactive) Poor (unreactive) Poor (not reactive) Poor (not reactive)
4	Not reactive	Ironbridge Asfordby La Jagua Lea Hall Zondag 1 Littleton Bulli	Very good Poor (reactive) Poor (reactive) Poor (reactive) Very good Very good Very good
5	Unreactive at low temperature	Daw Mill Nadins Yanowice Kleinkopje Hambach Indiana EDF Bentinck	Poor (reactive) Poor (reactive) Very good Very good Very good Good Good

4.2.1.2 Weight increase at low temperature

When coal samples were exposed to air under a heating ramp in the TGA, oxygen adsorption took place across the temperature range of 100 to 300°C. This response was identified by a small weight increase, and corroborated by information obtained from previous research, which discussed the same phenomenon. This oxygen adsorption was the key argument to sustain the actual mechanism of the self-heating reaction, in which the formation of solid carbon-oxygen complexes on the coal surface identified as the first stage of this reaction, followed by exothermic desorption producing a temperature increase in the coal bed (reviewed in Chapter 2). Figure 43 shows the thermogravimetric profiles for different coal samples, organized by geographic origin and coal type. These profiles were obtained using a slow heating rate in air (3°C min^{-1}). The same phenomenon can be observed when using higher heating ramps; however, the absorption rate decreased when the contact time between the sample and air was reduced (higher heating rates meant reduced segments of contact time at low temperatures).

From this initial observation, two arbitrary heating rates were selected (3 and 5°C min^{-1}) to quantify the oxygen absorption among samples using the TGA. In both cases, it was possible to identify 3 main parameters: a) maximum weight increase; b) initial temperature (at the start of the weight increase); and c) peak temperature, which is the temperature at which the maximum weight increase is produced. The results are shown in Table 15. For both heating ramps the weight increase varies from 0.0% to a maximum of 4.37%. In all cases, it was higher for the slow heating ramp applied ("*% diff. Increase*" column in Table 15). As can be seen, the reduction in heating rate resulted in an increase of up to 80% oxygen adsorption.
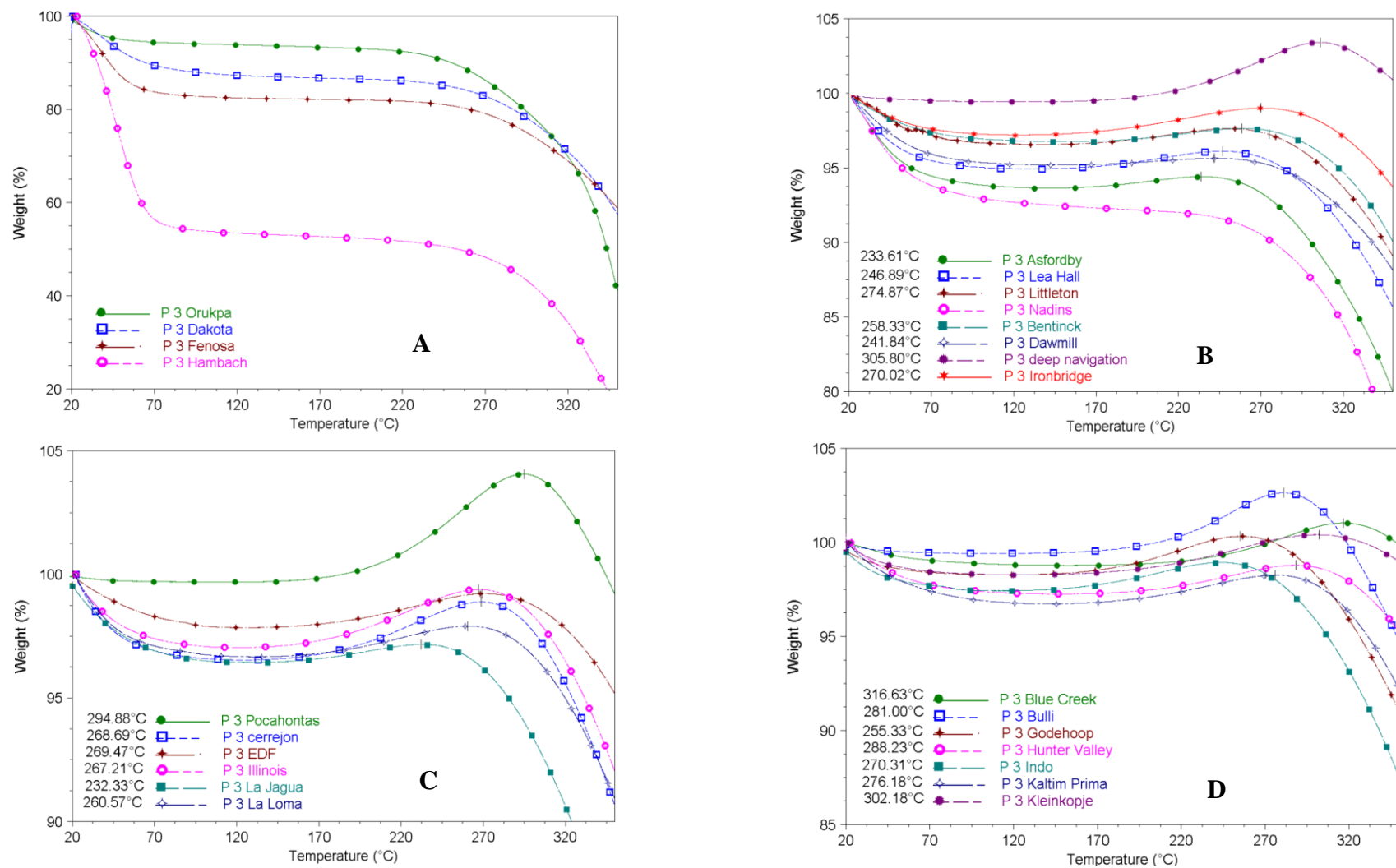
Figure 43: Low temperature weight increase for coal samples obtained by using a $3^{\circ}C$ min^{-1} heating ramp in air. Lignite samples (A); British coals (B); South and North America coals (C); and Australia, South Africa and Indonesian coals (D).

124

Considering the theoretical reaction mechanism, high reactive coals were expected to show the highest weight gain, due to a potential 'affinity' to absorb oxygen. However, five samples produced 'nil' weight increase (in both experiments), and three of these were well known high reactive coals prone to spontaneous combustion.

Table 15: Weight increase observed at low temperature under air atmosphere

Coal	Ramp applied 3°C min^{-1}			Ramp applied 5°C min^{-1}			% diff.
	% incr.	T_{min}	T_{peak}	% incr.	T_{min}	T_{peak}	increase
Fenosa	0.00			0.00			0.0
Orupka	0.00			0.00			0.0
North Dakota	0.00			0.00			0.0
Hambach	0.00			0.00			0.0
Nadins	0.00			0.00			0.0
Illinois #6	2.35	120	267	2.52	114	267	-7.2
Pocahontas #3	4.37	112	295	4.17	103	326	4.6
Indiana EDF	1.38	124	269	1.09	135	282	21.0
La Jagua	0.73	124	232	0.61	169	281	16.4
La Loma	1.24	131	261	1.14	122	256	8.1
El Cerrejon	2.35	121	269	2.20	124	266	6.4
Blue Creek	2.25	153	317	1.95	183	329	13.3
Bulli	3.22	105	281	1.91	138	318	40.7
Hunter valley	1.52	151	288	1.32	155	297	13.2
Kaltim prima	1.53	139	276	1.21	151	284	20.9
Indo	1.50	112	244	1.58	126	274	-5.3
Goedehoop	2.04	121	255	0.45	144	236	77.9
Kleinkopje	2.13	123	302	1.91	120	295	10.3
Bulawayo	2.61	134	276	2.21	148	284	15.3
Zondag 1	1.27	118	240	1.36	138	285	-7.1
Sines	1.73	119	249	1.48	123	258	14.5
Littleton	1.07	136	250	0.71	156	263	33.6
Daw Mill	0.44	147	242	0.08	117	248	81.8
Yanowice	0.93	131	257	0.65	145	266	30.1
Asfordby	0.77	142	234	0.56	152	242	27.3
Lea Hall	1.19	132	247	0.82	142	252	31.1
Deep Navigation	3.98	121	306	3.46	133	313	13.1
Bentinck	0.88	152	258	0.54	170	267	38.6
Ironbridge	1.81	121	270	1.50	122	265	17.1

In addition, the starting and peak temperatures observed were also lower for the lowest heating rate applied (with a few exceptions which were within experimental deviation). In those cases, the minimum starting temperature recorded was 104°C and the maximum was 180°C. The minimum peak temperature registered was 232°C and the maximum was 330°C for the set of coals studied. The overall temperature interval recorded during these experiments was higher than the temperature range described by the theoretical mechanism (estimated from ambient temperature to 150°C). This temperature interval corresponded to the net oxygen adsorption observed, which was the difference between the total oxygen adsorbed and desorbed during the whole process. The single contributions of these parameters cannot be identified in TGA by using this experimental procedure.

4.2.1.2.1 Coal classification regarding weight increase and temperature range

A classification of coals in terms of its weight increase and temperature range is shown in Table 16. For this classification, the temperature range was defined as the arithmetical difference between the peak temperature and the starting temperature, representing the temperature interval in which the oxygen adsorption was increasing. A combination of these two variables could be used to estimate the stability of the coal-oxygen complex formed for each coal.

Table 16: Coal classification regarding weight increase and temperature range

Group	Weight increase	Coal	Temperature range (^{o}C)
1	Weight increase not shown	North Dakota	0
		Fenosa	0
		Orukpa	0
		Nadins	0
		Hambach	0

Table 16, continuation

Group	Weight increase	Coal	Temperature range (^{o}C)
2	Slight weight increase (0.1 to 1.2%)	Asfordby	92
		Daw Mill	95
		Bentinck	106
		La Jagua	108
		Littleton	114
		Lea Hall	115
		Yanowice	126
3	Medium weight increase (1.2 to 1.8%)	Zondag 1	121
		La Loma	129
		Sines	130
		Indo	132
		Hunter valley	137
		Kaltim prima	138
		Indiana EDF	146
4	Important weight increase (1.8 to 2.5%)	Goedehoop	134
		Bulawayo	141
		Illinois #6	147
		El Cerrejón	147
		Ironbridge	149
		Blue Creek	164
		Kleinkopje	179
5	Major weight increase (2.5% and up)	Bulli	176
		Pocahontas #3	182
		Deep navigation	185

4.2.1.2.2 Relationship between weight increase and self-oxidation potential

Observed weight increase can be linked directly to the self-oxidation phenomenon.

From this observation, the potential of coals to suffer self-oxidation can be explained

as a result of two main reactions that compete:

1st reaction: oxygen adsorption phenomena forming coal-oxygen solid

complexes on the coal surface.

2nd reaction: desorption of coal-oxygen solid complexes and their exothermic degradation in the gas phase.

The first reaction corresponds to the initial step of the theoretical mechanism. This is considered an endothermic stage in which oxygen molecules are adsorbed on the coal surface forming coal-oxygen complexes. This was confirmed by the weight increase observed in the TGA. However, at early stages (below 100°C) this reaction is masked by water desorption. According to the mechanism, this reaction is also restricted by the temperature range and the availability of reactive sites. The last parameter is controlled by available free active sites, and those created by desorption of water molecules from the coal surface. This could explain (in part) the observed differences for different coals during the TGA experiments, and the observed weight increase above 100°C.

The second reaction corresponds to the final step of the theoretical mechanism (coal-oxygen complexes desorption). This is considered to be an exothermic reaction, which generate the majority of the heat responsible for the overall temperature rise in the coal bed (confirmed by DSC tests, Section 4.2.2). This reaction is also restricted by temperature range, depending on the stability of the complex solids formed. The stability of these complex solids was characteristic of each coal, explaining why differences in mass gain and peak temperature were observed. Based on these concepts and the results obtained, a complementary explanation to the mechanism of the self-heating reaction is proposed: ***the problem of coals prone to spontaneous combustion is produced when the desorption of coal-oxygen complexes governs the entire process***. Consequently, this characteristic could be observed and quantified directly by TGA analysis.

If the desorption reaction is the key, then the stability of the solids complex is also critical. Less stable complexes are desorbed at lowest temperatures, reacting exothermally with the oxygen gas to produce CO, H_2O and CO_2, which increase the temperature around the particles increasing the rate of the reaction [134]. Conversely, when the solids formed are stable, the temperature range is wider and the peak temperature is higher, producing a higher weight increase. This explanation was confirmed by additional research, which is described in Chapter 7.

4.2.1.2.3 Quantification of the self-oxidation potential by using TGA

The explanation to the phenomenon allows the use of TGA to quantify the self-oxidation potential of coals. TGA profiles identify 3 characteristic weight loss curves, which were explained considering the 2 step reaction mechanism and the chemical reactions that govern the process (Figure 44).

Prone coal	Reactive	Low reactive
Mass increase not seen	**Narrow temperature range**	**Wider temperature range**
Fenosa, North Dakota, and Orukpa shown same profile	(In this case 125°C)	(In this case 175°C)
	Slight mass increase	**High mass increase**
	(In this case 0.93%)	(In this case 4.28%)
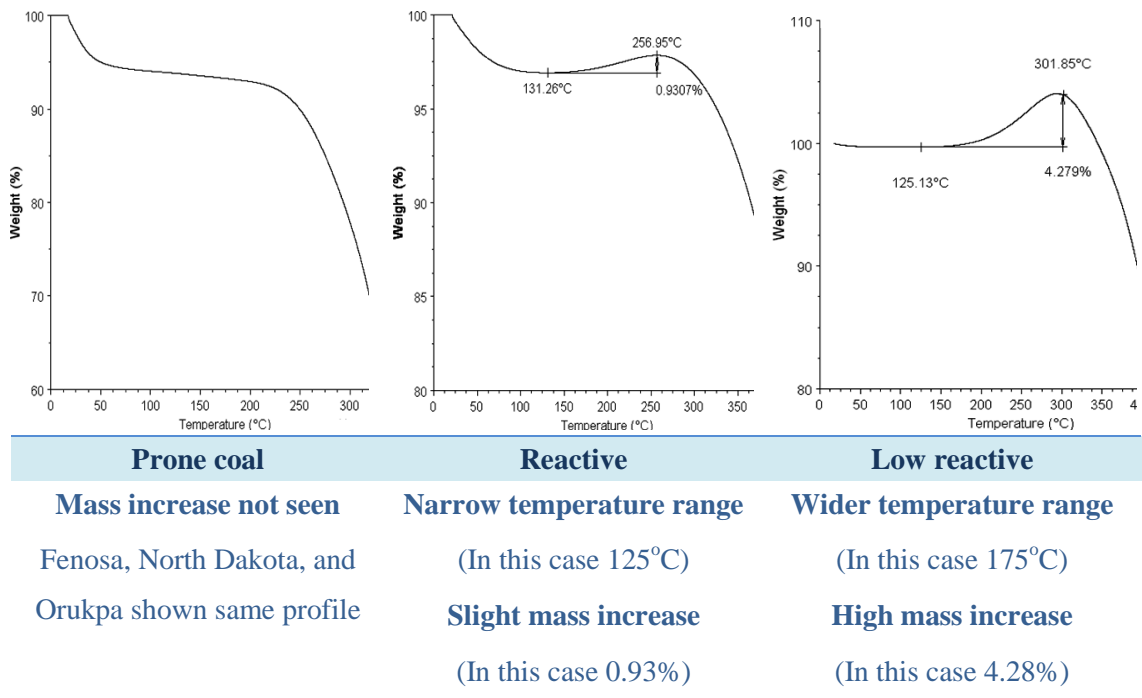
Figure 44: Weight loss profiles obtained by TGA for characteristics coal samples (net oxygen adsorption in air).

In the first case (Figure 44, left), it is possible to observe a nil weight increase. Experimentally, this profile was characteristic of coals prone to spontaneous combustion (Orukpa, Fenosa & North Dakota coals). Then, according to the previous explanation, the desorption stage governs the process. In the second case (Figure 44, centre), it is possible to observe a slight weight increase produced by oxygen adsorption. This profile was characteristic of reactive coals (El Cerrejon, Kaltim Prima & Illinois #6 coals). These coals were classified in an intermediate reactivity range because under specific conditions they can also suffer thermal runaway. In this situation, according to the mechanism explanation there is an equilibrium between the adsorption and desorption phenomenon. Finally, in the third profile (Figure 44, right), it is possible to observe an elevated weight increase produced by oxygen adsorption. This profile is considered to be characteristic of low reactive coals (Pocahontas#3, Deep Navigation & Bulli). In this case, the oxygen adsorption governs the process, reflecting a wider temperature range due to the stability of the solid complexes formed. This agrees with the previous explanation given.
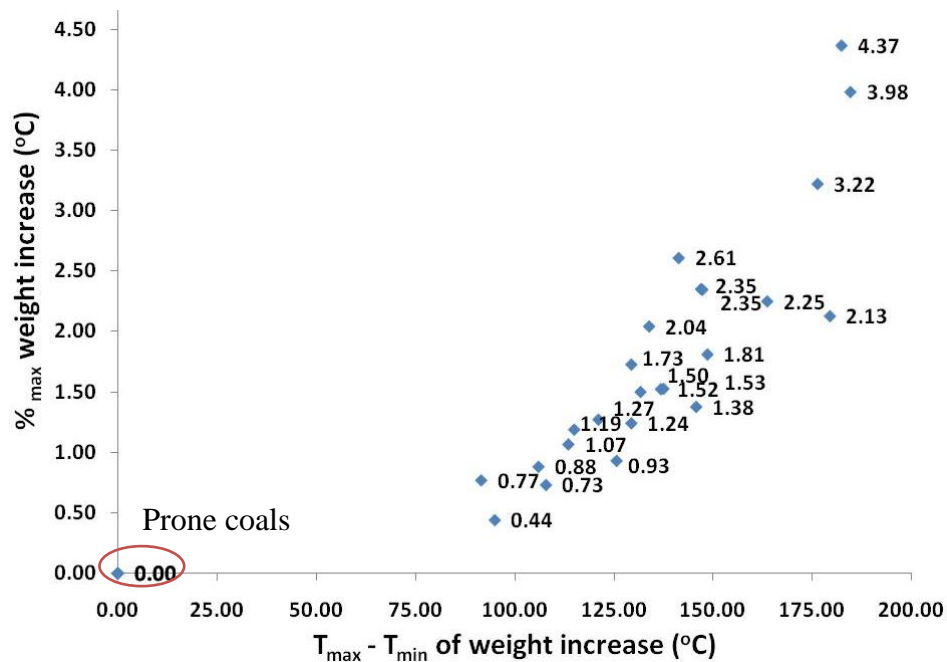
Figure 45: Relationship between weight increase and the temperature difference.

Consequently for the three cases explained, the comparison between historic data and the results obtained from the TGA test, there was a strong correlation between these two parameters. This means that depending on the type of TGA profile obtained, the total mass gain, and the starting and the peak temperatures of the process, coals can be classified by their potential to undergo self-oxidation. Figure 45 shows a relationship between the maximum weight increase and the temperature range in which this was observed, from which coals prone to spontaneous combustion can be clearly identified.

4.2.1.2.4 Influence of water content, coal ageing and exceptions to the rule

The water content of a low reactive coal sample can produce an effect in the TGA profile, which could be considered as highly 'prone'. This was the case for Hambach coal (Figure 43, A), with a profile characteristic of a prone coal. However, this is considered as unreactive by the coal industry due to the extreme water content (approximately 37.5%). From the TGA profile, this coal has lost 45% of the total mass before 100°C (produced by water evaporation), which means that the oxygen adsorption pattern was hidden by the high amount of water being released. A drying step for coals like this one (with water content higher than 25%) could reveal the real oxidative tendency. Nevertheless, coals with extremely high water contents are naturally less prone to spontaneous combustion due to the high energy requirements to vaporize all the water before the thermal runaway can begin. These kinds of coals are an exception, but can be identified based on the free moisture content from proximate analysis.

A second exceptional case can be identified in highly reactive coals, which have been exposed to the atmosphere for a long period of time losing their reactive potential (weathering). This was the case of Kleinkopje coal (Figure 43, D), which

produces a 'safe' TGA profile, with an elevated temperature range and slight weight increase. The coal sample used for the experiment was more than 3 years old, stored in a small particle size with some exposure to air. Consequently, active sites were saturated by oxygen and moisture showing a reduced reactive potential indeed. This confirms the predictions of the TGA test, but also stipulates the conditions of the coals needed for a successful test. From historic data, fresh Kleinkopje coal can be highly reactive, and there have been several incidents of spontaneous combustion in South Africa. Unfortunately attempts to access fresh supplies of Kleinkopje coal were unsuccessful.

4.2.1.3 Relationship between both thermogravimetric tests developed

Figure 46 shows a graphic comparison between the two main parameters for the two TGA tests (% of weight increase and TG_{spc} Index). In both cases, coals prone to spontaneous combustion were identified successfully. However, differences were detected within the intermediate coals. As can be seen from Figure 46, there is a linear relationship between the weight increase and the TG_{spc} Index for those coals identified as safe in both cases. This trend shows that coals with a high weight increase were identified by the TG_{spc} Index as 'medium reactive', and coals with a slight weight increase were identified as less reactive by the TG_{spc} Index. This trend is contradicted between both tests.

However, the temperature range for the TG_{spc} Index is higher than the temperature range used to obtain the maximum weight increase. This explains the differences and also suggests that the second TGA test can deliver more reliable results. In addition, the value of the TG_{spc} Index fluctuates between 0.01 and 0.03wt % $^{o}C^{-1}$ min^{-1} for all the safe coals, which correspond to a 30% of the total interval range (considering that prone coals are situated between 0.045 to 0.07wt % $^{o}C^{-1}$ min^{-1}). This means that

spontaneous combustion coals are clearly identified, but the difference between the safe samples is insignificant. Finally, the deviation coefficient of the linear approximation is poor (~0.6), which means that this relationship is not conclusive.
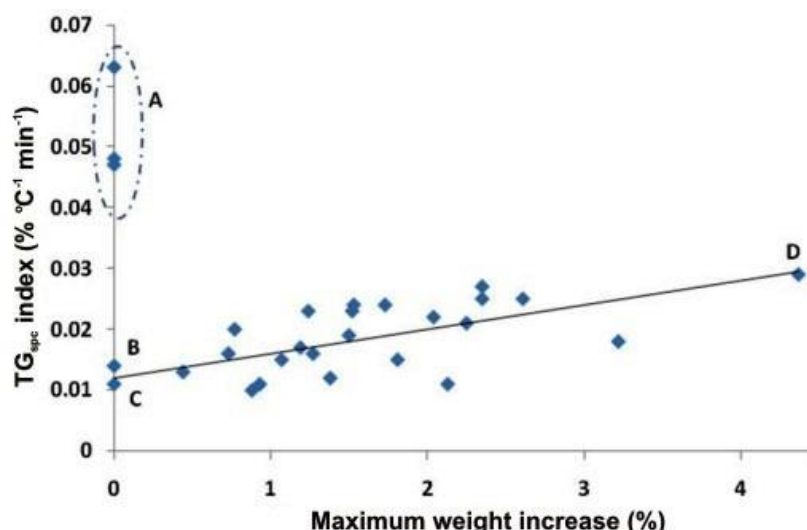
Figure 46: Relationship between TG_{spc} Index and the maximum weight increase registered (using a heating rate of 3^oC min^{-1}). In the top circle A: Fenosa, North Dakota and Orukpa coals; B: Hambach; C: Nadins; and D: Pocahontas #3.

4.2.2 Differential scanning calorimeter tests

Two experiments were carried out using this technique. The main objectives were: i) to study the heat evolution under a slow heating ramp in air (4.2.2.1); and ii) to study the link between heat release and weight evolution under similar conditions (4.2.2.2).

4.2.2.1 Heat evolution under air atmosphere

Heat evolution was measured for all the samples studied using a single thermal ramp of 5^oC min^{-1}, at ambient pressure in dry air. The heating rate was selected to study the samples under similar conditions than those used for the TGA experiments, allowing a comparison between both techniques. Higher heating rates would have increased the instrument sensitivity, but would also create conditions far remote from actual reaction conditions. On the other hand, lower heating rates reduced the

experimental sensitivity of the instrument whilst increasing the experimental time. Figure 47 shows DSC profiles for a representative number of samples.
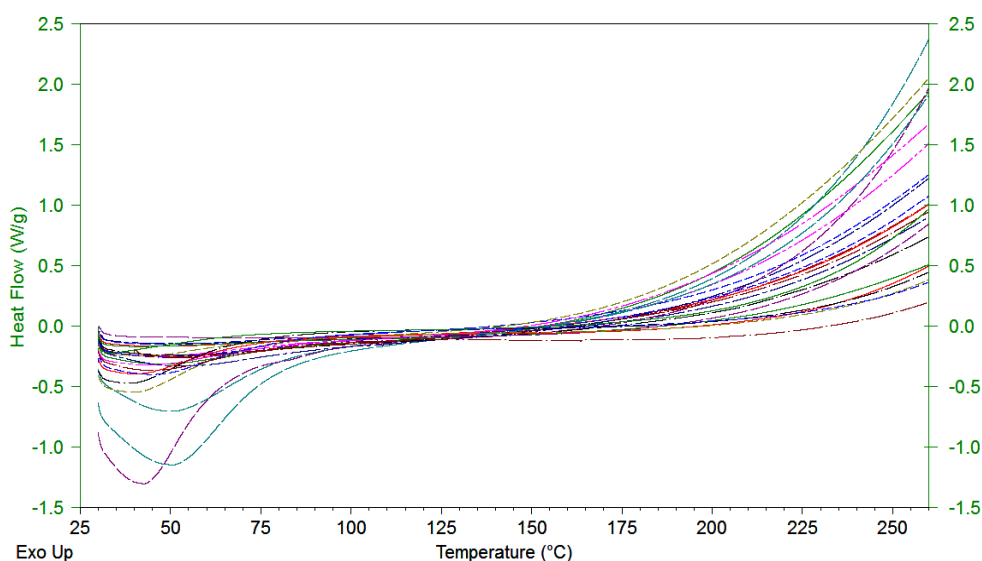
Figure 47: Heat evolution for all the samples studied using a DSC. The heating rate applied was 5°C min^{-1} in an air atmosphere.

The DSC data was analyzed after removal of a baseline recorded for an empty blank sample. The relative enthalpy associated to the specific stages of the reaction was then obtained by the integration of the heat flow, during the time in which exothermic and endothermic peaks were identified. As can be seen from Figure 47, the first peak was identified from ambient temperature to ~120°C (negative values produced by the heat absorbed when water was evaporated). The second peak took place approximately from 130°C and upwards (positive values generated by the oxygen adsorption and oxidation). This peak was hidden by a major peak produced by the complete oxidation reaction that took place at higher temperatures (started around 200-250°C). The full combustion peak was not recorded due to technical limitations of the instrument, ending the experiment at 300°C (this DSC was unable to carry out decomposition experiments).

From these results, the integration of the heat flow profiles was defined by two different cases, due to two possible interpretations (schematized in Figure 48). The first considers the initial heat absorbed calculated by integrating the curve from 35°C (arbitrarily selected due to stability of the DSC curve at this temperature), and the temperature at which the heat flow is zero ($Q=0$). The temperature of this point was particularly characteristic for each sample. Then, the heat generated was calculated by integrating from $Q=0$ to 250°C. The final temperature was also arbitrarily selected as a conservative limit of the low temperature oxidation reaction. The results for this case are shown in Table 17.
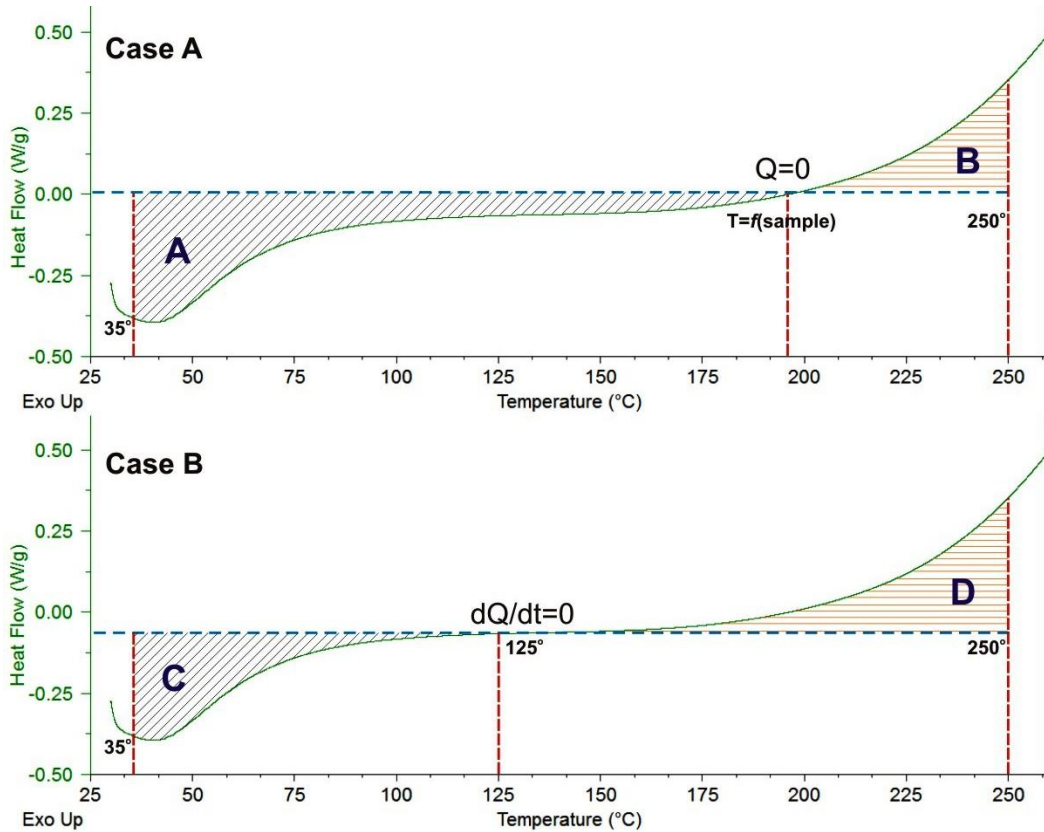
Figure 48: The two different cases used for the integration and calculation of the heat absorbed and released from coal samples.

The second considers the calculation of the heat adsorbed by integrating the heat flow curve from 35°C, to the point in which the heat flow rate was zero ($\frac{\partial Q}{\partial t} = 0$). As

can be seen from Figure 48, this took place approximately at 125°C for all the samples studied. Finally, the heat released was calculated by integrating the curve from 125°C to 250°C. The results for this case are shown in Table 18. In general, the heat value calculated using the second integration approach showed the lower estimates. For both integration methods, lower values of the endothermic heat calculated meant higher values for the estimated exothermic heat. Figure 49 compares both integration methods by plotting the relation between the endothermic and exothermic heat for each case. This comparison was approximately linear, confirming that there was no significant difference between both approaches.

Finally, the results obtained in case B were considered for subsequent analysis since these curves were relative, reflecting small changes before and after the inflection point observed during the heat evolution (as can be seen from Figure 48).

Table 17: Case A, integration considering Q=0 as transitional point

Sample	Time (min)	T (^{o}C)	Endothermic peak *A (J g^{-1})	Exothermic peak *B (J g^{-1})
N Dakota	21.7	137.8	519.8	663.2
Hambach	19.9	128.6	415.0	590.9
Fenosa	21.4	136.3	336.6	753.5
Nadins	22.3	140.9	188.5	485.5
Dawmill	22.1	139.6	150.3	417.3
Asfordby	20.2	130.1	147.2	785.5
La Jagua	20.6	132.6	128.7	441.5
K Prima	21.8	138.5	125.8	314.8
Lea Hall	18.0	119.4	123.9	769.0
El Cerrejon	19.9	128.8	115.6	622.1
La Loma	18.0	129.5	111.1	437.2
Kleinkopje	23.6	147.2	80.2	199.9
Illinois	15.3	105.6	73.7	907.8
Goedehoop	21.4	136.3	72.2	360.5
Hunter Valley	18.4	121.5	67.3	442.1
Bentinck	13.5	96.8	40.7	602.5
Pocahontas	13.4	96.2	6.1	315.6

Table 18: Case B, integration considering dQ/dt=0 as inflection point

	Sample	Time (min)	T (°C)	Endothermic peak *C (J g^{-1}) 35-125°C	Exothermic peak *D (J g^{-1})		
					125-200°C	200-250°C	Total 125-250°C
Group 1	Illinois	19.1	125	110.5	179.1	667.6	846.7
	Lea Hall	19.1	125	137.4	171.7	577.7	749.4
	Asfordby	19.1	125	133.0	170.8	633.4	804.2
	N Dakota	19.1	125	470.3	160.2	563.9	724.1
	Fenosa	19.1	125	298.5	159.0	641.7	800.8
	El Cerrejon	19.1	125	106.7	138.9	495.1	634.0
Group 2	Hambach	19.1	125	414.1	103.0	489.1	592.1
	Nadins	19.1	125	139.6	126.9	416.7	543.6
	Bentink	19.1	125	89.0	117.6	397.4	515.0
	La Loma	19.1	125	100.0	114.1	338.6	452.7
	Dawmill	19.1	125	110.9	111.7	352.9	464.6
	La Jagua	19.1	125	111.2	111.0	357.2	468.2
Group 3	Hunter Valley	19.1	125	73.4	101.1	332.3	433.4
	Kaltim Prima	19.1	125	94.4	86.9	266.1	353.0
	Goedehoop	19.1	125	52.0	86.1	299.4	385.4
	Kleinkopje	19.1	125	49.5	52.5	181.6	234.1
	Pocahontas	19.1	125	18.0	50.8	243.9	294.7
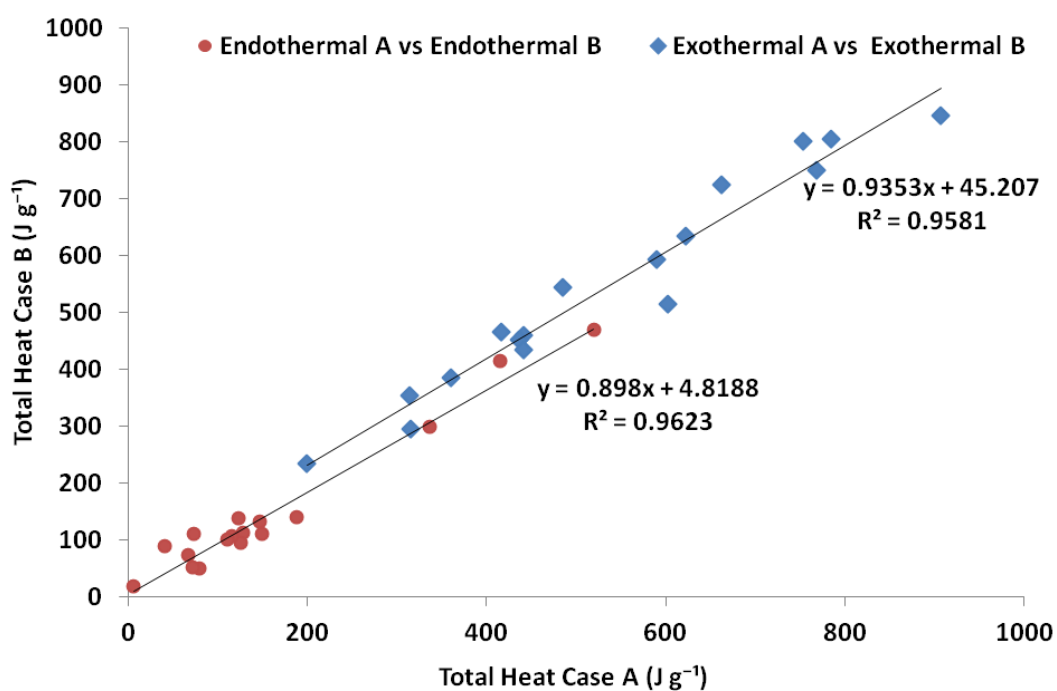
Figure 49: Comparison of integration cases A and B.

Afterwards, specific conclusions can be made about the integration results. First, in both cases the thermal response observed was similar and directly proportional to the moisture content (Figure 50, A). High water content coals reported the highest absorbed heat. Secondly, it was concluded that the net energy consumed related to the first peak was linked directly to the water release process (Figure 50, A).
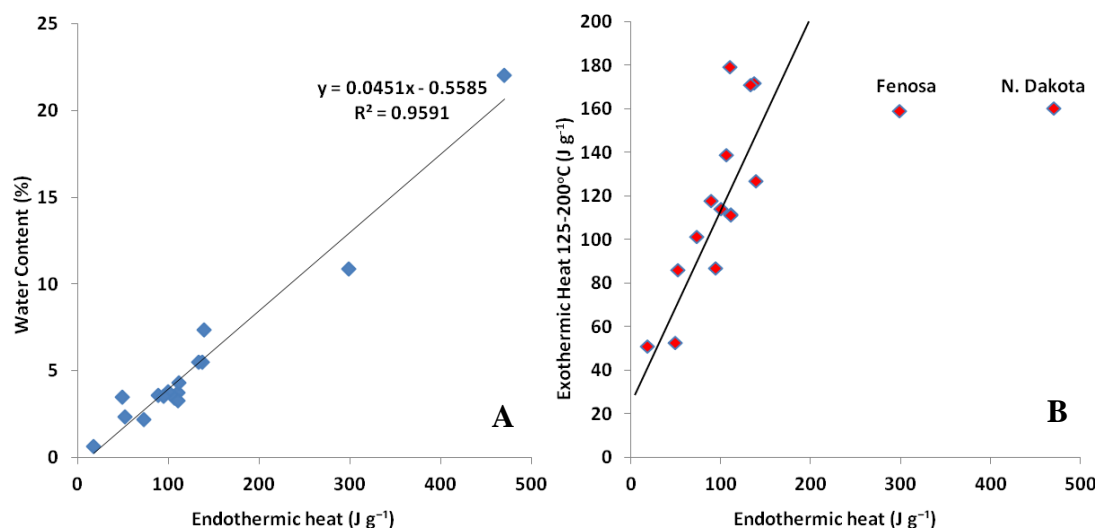
Figure 50: Relationship between water content and heat absorbed (A); and heat absorbed against initial heat released in the range 125-200°C (B).

However, the analysis of the heat released during the exothermic stage is complicated because during this stage there were several chemical reactions progressing in parallel making it impossible to identify individual enthalpic contributions directly from the DSC profile. For this reason, the exothermic integration area was sub-divided considering the two most important reactions described in the mechanism: firstly, an initial segment in which the oxygen adsorption presumably controls the reaction (considered from 125 to 200°C, similar interval than the TGA by the weight increase); and second, a segment in which the desorption of coal-oxygen complexes probably controls the reaction (from 200 to 250°C). These two segments were also reported in Table 18.

Regarding the first segment (125-200°C), all coals with water content below 10% showed a heat release that was directly proportional to the heat consumed during the endothermic stage, as can be seen in Figure 50 (B). This suggested a kind of compensation phenomenon produced during the initial moments of the exothermic stage, in which the heat released was equivalent to the heat required to evaporate the water content during the endothermic stage. Additionally, the origin of this heat release is unknown, and two alternatives were considered: firstly, it could be produced by the adsorption of oxygen over the coal particles (suggested by the slight weight increase detected in the TGA after 125°C); or secondly, it could be associated with the re-adsorption of water vapour molecules in the coal surface (the heat of water vapour adsorption in the surface of coal particles has similar magnitude than the water latent heat).

In addition, the heat needed to vaporize the water from coals with high water content was considerably higher than the heat finally released by the sample. This result seems to be inconsistent with the case of Fenosa and North Dakota (both well known prone to spontaneous combustion coals), from which a pronounced exothermic response was expected or a considerable difference with the others coal samples during this temperature segment.

Regarding the second segment (200-250°C), the heat evolution continued with the trend established during the first. In this occasion, coals with high reactivity towards self oxidation (Fenosa and N. Dakota) showed an increasing rate of heat release, detected only by the use of the derivative of the heat flow profile. Figure 51 compares the heat flow profiles and their corresponding derivatives for a selected number of coals, which identify this tendency. In this example, the heat flow of Fenosa coal was not the highest, but it shows a clear acceleration in the rate

compared with the other coal samples. The same phenomenon was observed for N. Dakota coal.
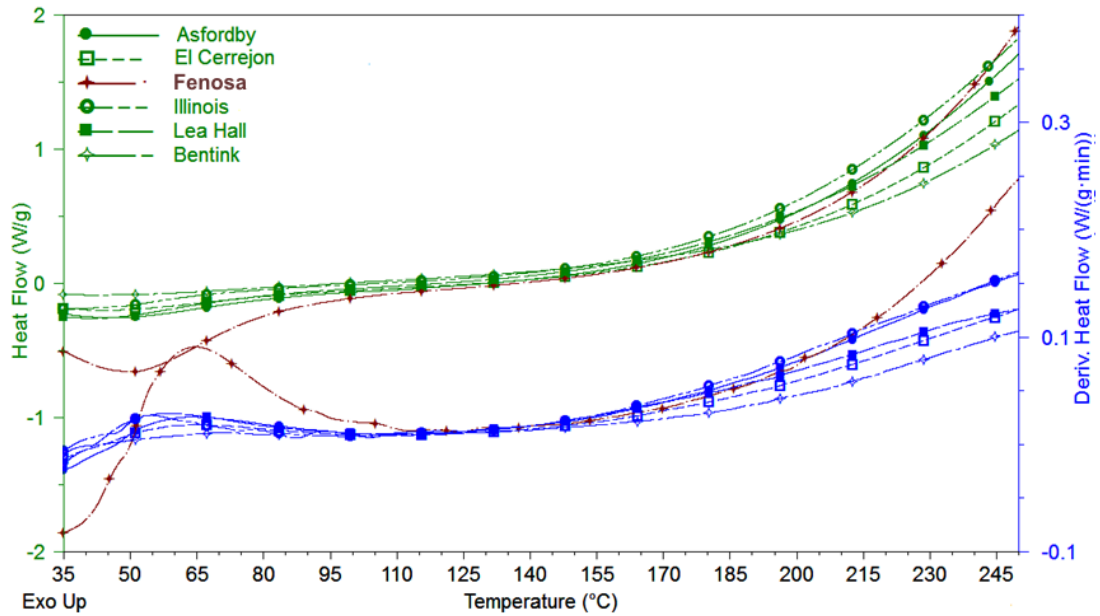
Figure 51: Fenosa coal showed an increasing heat releasing rate above 200°C (by using a high resolution DSC curve).

Considering the information reported by other researchers about the self-oxidation temperatures, the temperature range in which the derivative curve showed an increasing rate was elevated. Then, this change could also be related to the beginning of the complete oxidation reaction, characterized by an intense exothermic profile. Finally, coal samples were classified in three different groups, based on their thermal responses:

    i) Group 1: formed by coals characterized by a large endothermic heat peak and a large exothermic heat response.

    ii) Group 2: formed by coals characterized by a medium endothermic heat adsorption and a medium exothermic heat response.

    iii) Group 3: formed by coals with a small endothermic heat peak and a small exothermic response.

4.2.2.2 Link between heat released and weight evolution

The study of the link between the heat released and the weight evolution during the low temperature oxidation reaction was a fundamental part of this work. The temperature range in which this link could be established was narrowed to the temperature range 100-250°C. Nevertheless, as it was explained previously there were several different interactions taking place at the same time including water vaporisation, oxygen adsorption, volatile release, oxygen desorption and the volatile combustion, which affects both weight and heat flow. Subsequently, an initial representation is shown in Figure 52 comparing the DSC and TGA profiles for representative samples. In this comparison, all the samples were exposed to the same heating rate (5°C min^{-1}), under similar atmospheric conditions (1 bar, dry air).

Figure 52 shows the temperature segment between 125 to 200°C where most of the DSC curves maintain identical shape, and all the TGA plots remains unaltered during this segment (left side of vertical red line). Above 200°C the weight increase for particular samples becomes important, as well as the heat flow being released. Figure 53 (A) is a schematic of the relationship between maximum weight increase (Table 15) and the endothermic heat (Table 18). From this, an inversely proportional relationship was identified with some key points of agreement. Firstly, coals with the lowest heat requirement (during the endothermic stage) show the maximum weight increase. Secondly, coals with the highest heat requirement during the water release stage show nil weight increase. This tendency implies a 'compensation phenomenon' (described in the previous section), in which the water release is in part responsible for the heat response during the beginning of the exothermic stage. This observation would be valid if the endothermic stage is indeed linked to the exothermic stage. However, there are two strong counter arguments. Firstly, this tendency does not

relate directly to the weight increase with the exothermic response; and secondly, the temperature range in which both variables were measured is considerably different.
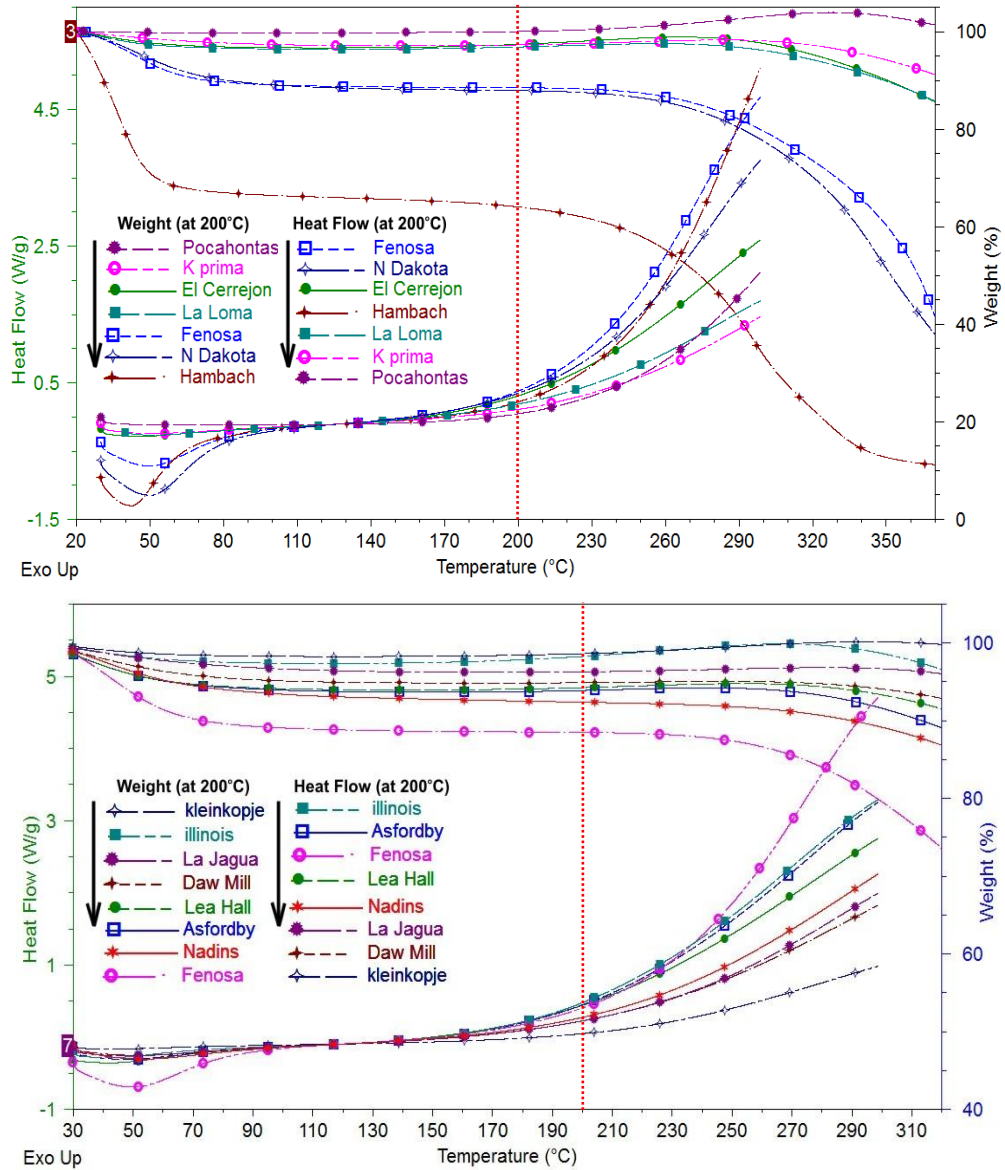
Figure 52: Graphical association between heat released (left axis) and sample weight (right axis), both under the same heating rate.

Figure 53 (B) presents the relationship between the maximum weight increase and the total exothermic heat calculated. In this case, there were key points of agreement, but no clear trend. In this correlation the highest weight increase (more than 4%) matches the lowest heat release during the exothermic stage. This supports the idea

about how this process depends of the stability of the coal-oxygen complexes formed over the coal surface (causing the weight increase). The other side of the curve shows the high water content and high reactivity coals, which registered important values for heat release during the exothermic stage. These coals were characterized by a nil weight increase produced by the fast decomposition of the coal-oxygen complexes that were 'potentially' formed above their surface, generating a strong exothermic response. This agreed with the hypothesis of two competing reactions taking place in parallel, and also with the hypothesis of the influence of the stability of these coal-oxygen complexes, which determine the reaction that governs the entire phenomenon and thermal response shown by the coal. If the last explanation is confirmed, the problem of identification of coals prone to spontaneous combustion could be solved.
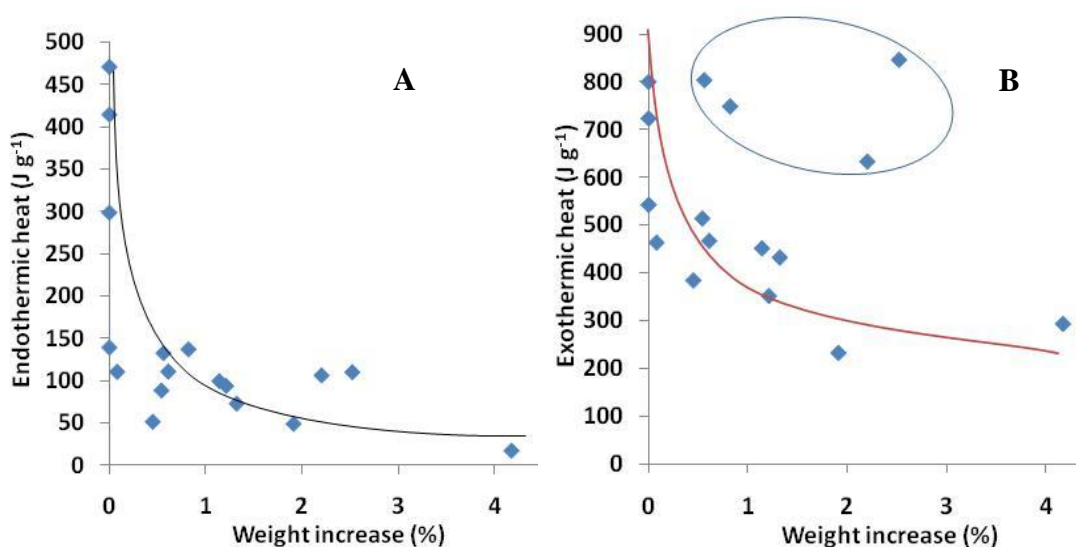
Figure 53: Total weight increase obtained from TGA and its relationship with endothermic (A) and exothermic heat (B) measured by DSC.

However, some coals did not follow these trends. On one side (supporting the hypothesis), Hambach with a high water content showed a low heat release during the exothermic stage, not suffering the compensation phenomenon expected. This

can be explained by the extremely high water content evaporated (~37%), which masks the weight increase. In this case, the stability of the oxygen complexes was high, confirmed by the poor thermal response exhibited above $100^{o}C$. On the other side (contradicting the hypothesis), some intermediate coals did not follow this trend (Figure 53, B, circle) such as Illinois#6, El Cerrejon, Lea Hall and Asfordby. All of these were classified as reactive (considering the intrinsic reactivity test), with low ash and high carbon content. This set of coals show heat release, but at the same time they register a medium weight increase, which contradicts the general explanation.

In conclusion, when considering all the information, evidence suggests a link between heat release and weight evolution of the sample at low temperature. However, this must be confirmed by further experimental work on more coals. In all cases studied, the sensitivity and the error associated to the instrument could produce important differences. Also, the conditions of the sample before the experiment are critical in obtaining reliable results. In addition, from DSC measurements no significant differences were found in the heat release by the normal coals and well-known spontaneous combustion coals. Subsequently, the net self-oxidation process cannot be differentiated by using differential scanning calorimetry as a single technique (specifically the use of a single thermal ramp of $5^{o}C$ min^{-1}). In this case, the use of a simultaneous TGA-DSC instrument could be a key area for further evaluation. Finally, despite the evidence about a possible thermal response, the implementation of an experimental method to identify prone coals by using DSC was found to be inaccurate. Also, a detailed study considering additional factors is needed. Further work would require a statistically relevant number of coals, and the implementation of rigorous sampling conditions on site, to preserve the original

properties of the samples. It was observed that a short period of contact between the samples and air changed the thermal response of the coals under study considerably.

4.3 Thermal analysis of coal using medium scale reactor

This section presents the experimental results obtained for the thermal testing of a large coal sample. This test was performed for all coals, and the main objective was to obtain information about the global thermo-chemical evolution of the system under restricted heat-mass transfer conditions. This information was vital in order to evaluate the effects of the mass and energy transport in a bulk environment, over the global rate of the reaction and its association with thermal runaway. In addition, global characteristics of the system were studied and its link with the intrinsic reactivity properties of coals obtained from TGA and DSC. Finally, results were used to calculate the crossing point temperature index (CPT) and estimate the ignition temperature; both currently used to predict coal propensity.

In general, a single experiment was performed for all samples using the reactor designed: a heating ramp in air at $0.5^{o}C$ min^{-1}, from ambient temperature to $250^{o}C$, which provided information about two different aspects:

     i) Thermal behaviour: In order to study the transient thermal profiles (4.3.1), and the effect of water content on these (4.3.2); to obtain the crossing point temperature (CPT) in all its different definitions (4.3.3) and to measure the ignition temperature of each coal (4.3.4).

     ii) Mass evolution: In order to study the weight evolution during a heating ramp and its relationship with temperature, as well as compare the mass change observed using TGA (4.3.5).

4.3.1 Transient temperature profiles

Transient temperature profiles were obtained for all coal samples (characteristic samples are presented in Figure 54, Figure 55 and Figure 56). These figures show different temperature profiles registered for diverse radial positions inside the sample holder, which were plotted in the time domain. The slope of each single thermocouple denotes the characteristic heating rate for the specific position recorded. For all the samples, the bulk system behaves similarly to a solid body under a constant temperature increase (0.5°C min^{-1} in air).
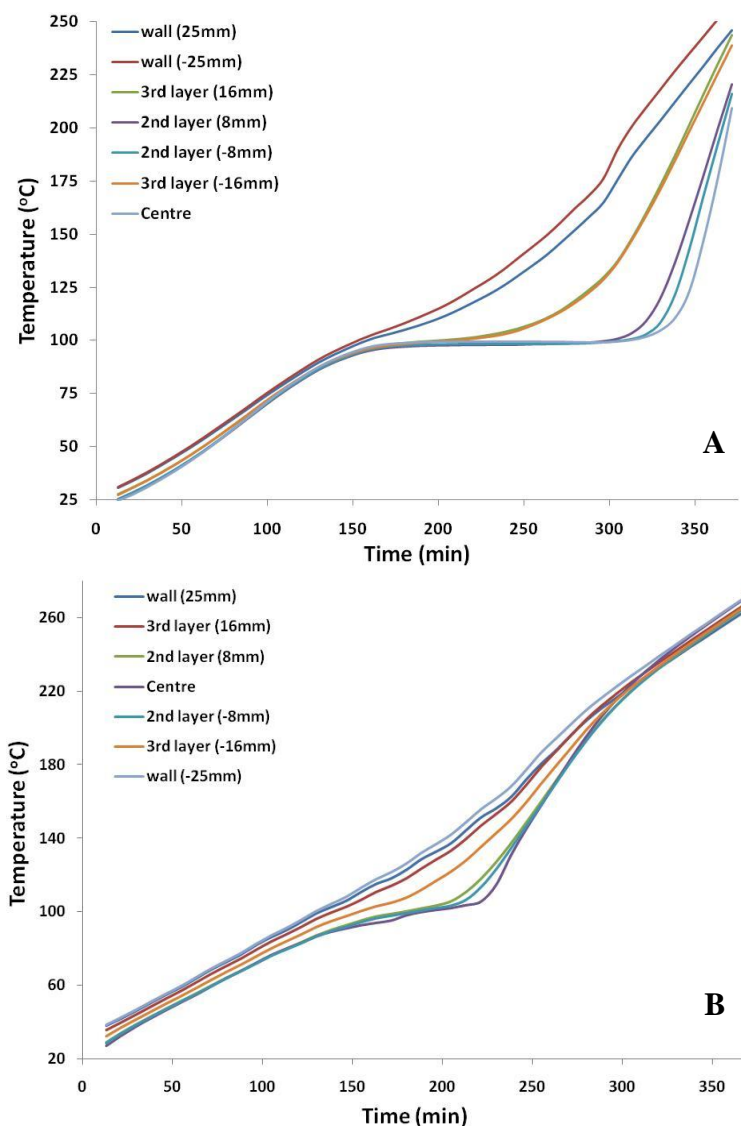
Figure 54: Thermal profiles for North Dakota (A) and El Cerrejon (B) coals. The heating rate used was 0.5°C min^{-1} in air.

The difference between the temperature in the centre and the temperature in the surface of the sample holder was influenced by the coal rank, water and volatile content. The differences between thermocouples readings were also an indication of the global thermal conductivity inside the sample container, which was formed by the contribution of the single components (moisture, mineral matter, volatiles and carbon content).
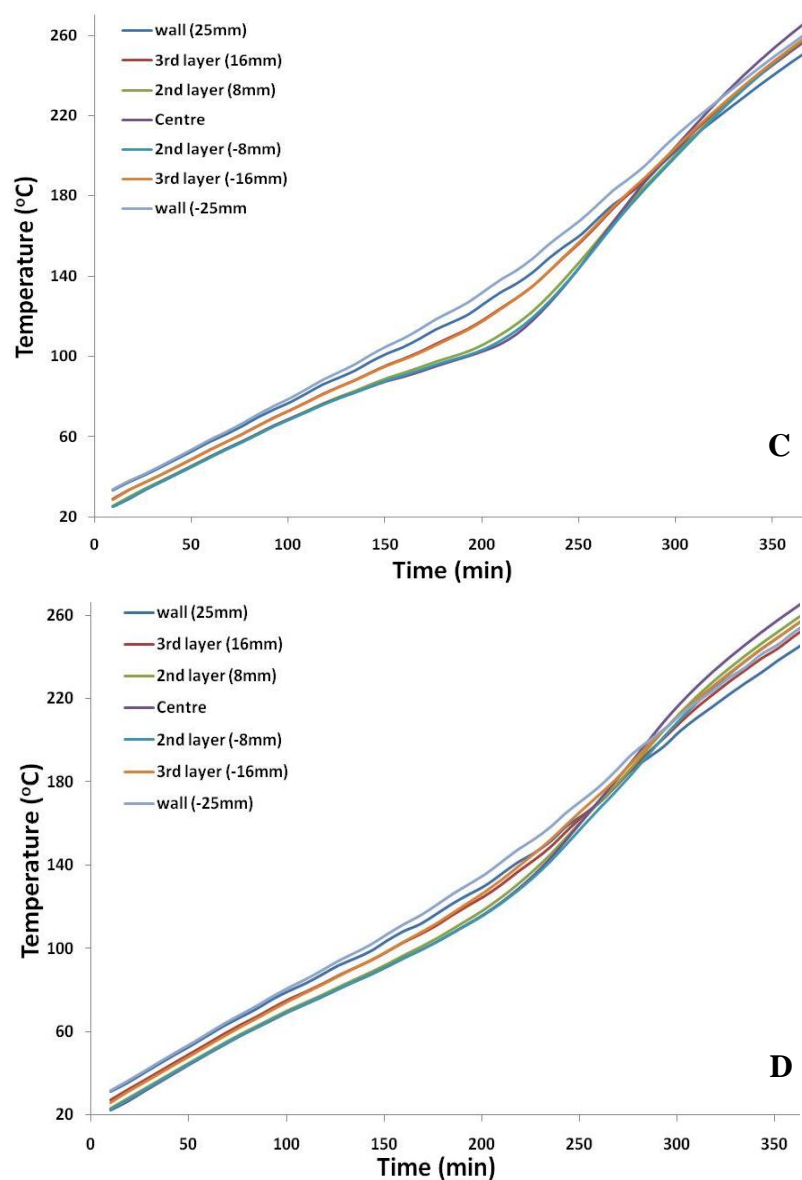
Figure 55: Thermal profiles for Kaltim Prima (C) and Zondag1 coals (D), both medium water content and 0.6 rank. The heating rate used was 0.5°C min^{-1} in air.

One of the first identifiable attributes in the system was an inflection point in the thermal profiles around 100°C, which was found for all samples. This corresponds to the effect of the water vaporization, recorded by all the thermocouples (analyzed in next section). When the water was completely eliminated, the region close to the centre of the sample showed an increase in the heating rate, which was higher than the rate recorded close to the surface. This produced a crossing temperature region that ended with the sample ignition (after the crossing).
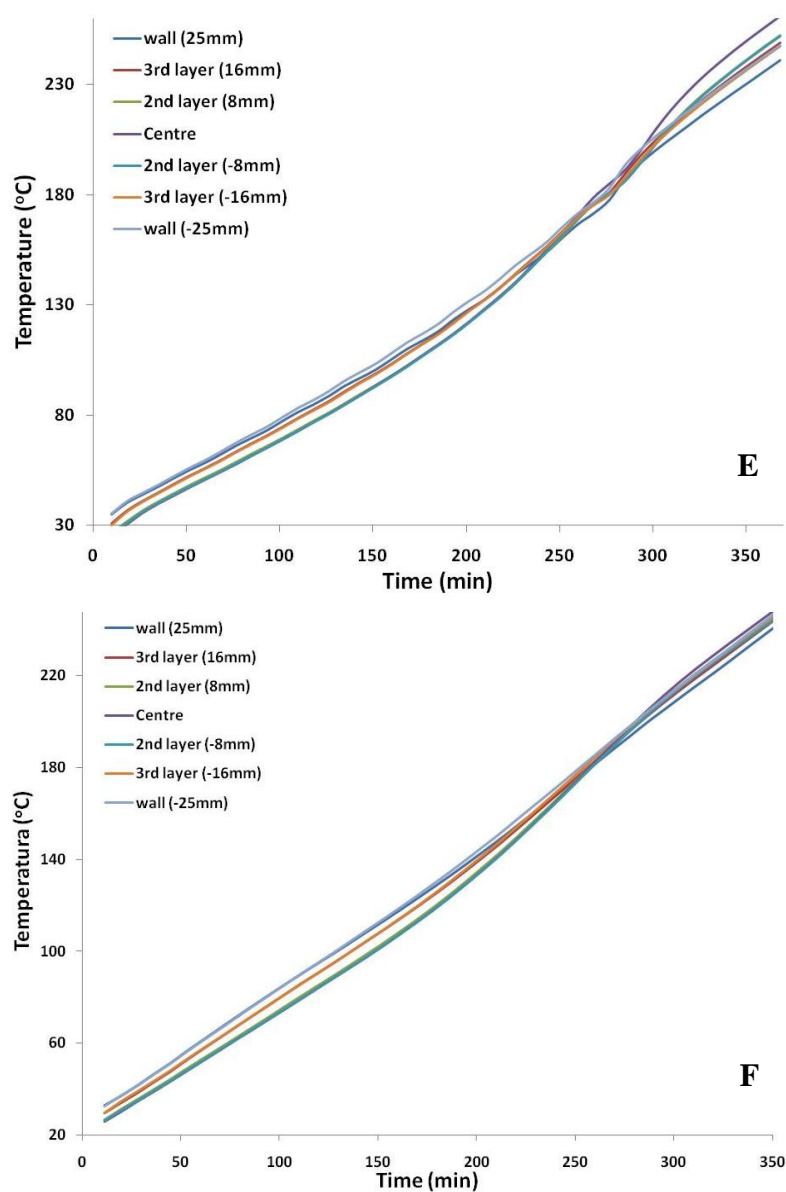
Figure 56: Thermal profiles of Pocahontas (E) and Deep navigation (F) coals; low water, high volatile and high rank coals. The heating rate used was 0.5°C min^{-1} in air.

As can be seen from profiles, the intensity of the oxidation before the crossing region increased with a decrease in water content. For dried and high rank coal samples, the slope change was smooth and the crossing zone took place at higher temperatures, compared to those samples with an elevated moisture content (Figure 56).

Figure 57 compares the thermal evolution for all the samples studied, considering the single thermocouple located in the centre of the sample holder. From this, it was possible to observe a 'buffer effect' produced by the water vaporization, particularly pronounced in the high water content samples (Fenosa, North Dakota and Hambach). This buffer effect delays the crossing temperature region, giving the impression of less reactive samples. However, Fenosa & North Dakota are both prone to spontaneous combustion, also showing an early crossing region around 80 to 100°C.
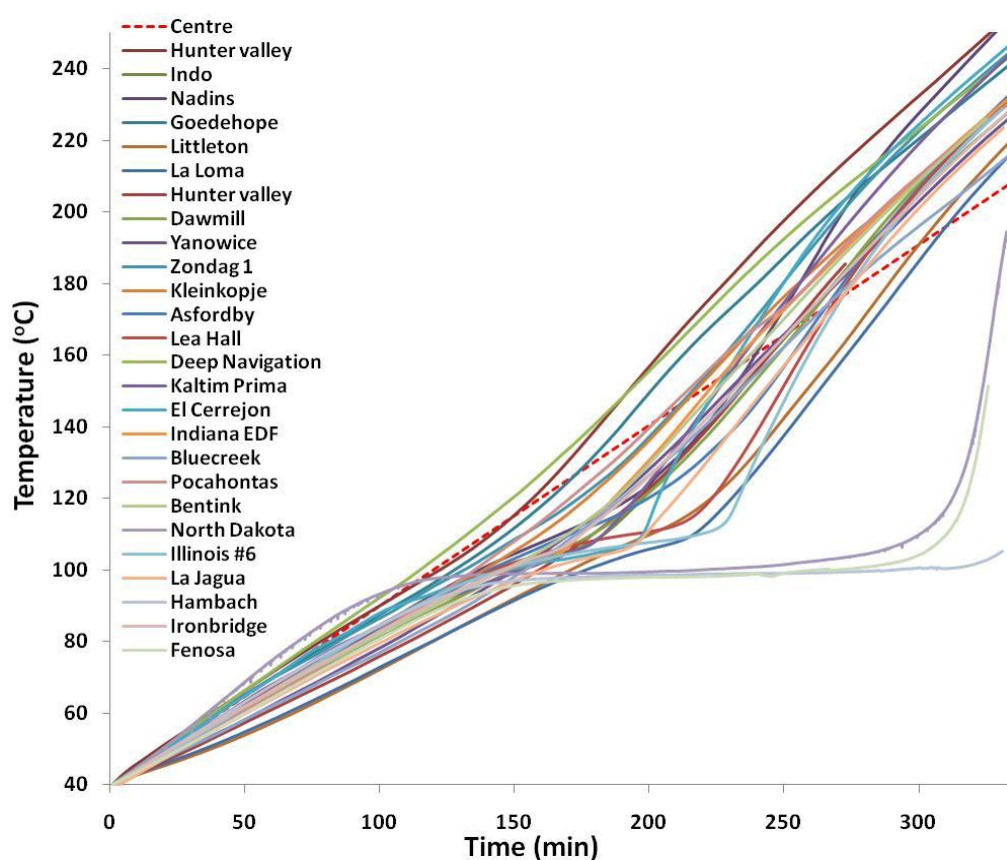
Figure 57: Comparison of central thermocouples for all coal studied. The red dots curve is the furnace heating rate recorded (0.5°C min^{-1}).

The heat transfer produced across the vertical axis can be estimated from the temperature recorded at two axial positions: z=25 mm and z=35mm (from the bottom of the sample holder). For all the samples, these temperatures showed a negligible difference (less than 2%, as can be seen in Table 19), which allowed the effects produced by the axial thermal conduction to be eliminated in further analysis. Finally, experimental results reported recently [239] showed similar thermal profiles obtained for bulk coal samples using an equivalent reactor. This confirms the validity and repeatability of the results obtained by using the thermal reactor.

4.3.2 Influence of water content in thermal profiles

The influence of water content has been studied by other research groups using analogous experiments to those previously shown [239]. These investigations suggested that water delays the coal-oxygen reaction, which also agreed with the results obtained in this work. The explanation provided in those investigations was based in the inhibition produced by a water layer around the coal surface, in which the oxygen is dissolved prior to reaction with the coal. Also, it was suggested that an increase in water content requires more energy to be removed, which lessens the heat accumulation [140]. However, the observations made from these experiments, the historic data available, and the conclusions from the small particle size tests (TGA, DSC) do not support this conclusion. To the contrary, several high water content coals used in this research suffer thermal runaway (confirmed by results obtained) rather than the dried samples, which were classified as safe for most of the experiments.

The difference between the previous explanation and the results observed during this work is produced by the confusion over the terms 'self-oxidation' reaction and subsequent 'thermal runaway' process, and the 'low temperature ignition

phenomenon' that a coal can suffer. This clarification (mentioned also in Chapters 1 and 2) helped to correctly interpret the evidence found during this work, focussing on the self-oxidation problem.

The experimental results were divided in different thermal segments considering the water evaporation temperature as a key point. Three zones were defined: an initial region from 40 to 90°C, recorded as an 'initial heating rate' (IHR, Figure 58 & Table 19); an intermediate region from 90 to 120°C, where the water vaporization controls the mass change and the thermal profiles; and a final region from 120 to 200°C, which was a 'final heating rate' (FHR) before sample ignition (Figure 59).

Figure 58 shows the thermal profiles for the IHR zone obtained for all coal samples. In this thermal segment, central thermocouples placed at different axial positions showed a lineal behaviour for all coals. These profiles were approximated by a linear trend, in which the slope corresponded to the initial heating rate (IHR, Table 19). For these linear approximations the lowest deviation coefficient obtained was 0.98. In this temperature range, most of the slopes were below the furnace rate with two exceptions: Deep Navigation and North Dakota coals. In the first case, the sample had high thermal conductivity and the water content effect was nearly undetectable. The thermal profile was linear and the difference with the furnace rate was lower than 2% average. North Dakota showed an important effect of water content in the whole profile. The difference with the furnace heating rate was also important; deviating by approximately 25% at certain points. This behaviour was explained by its high reactivity (determined by parallel experiments).
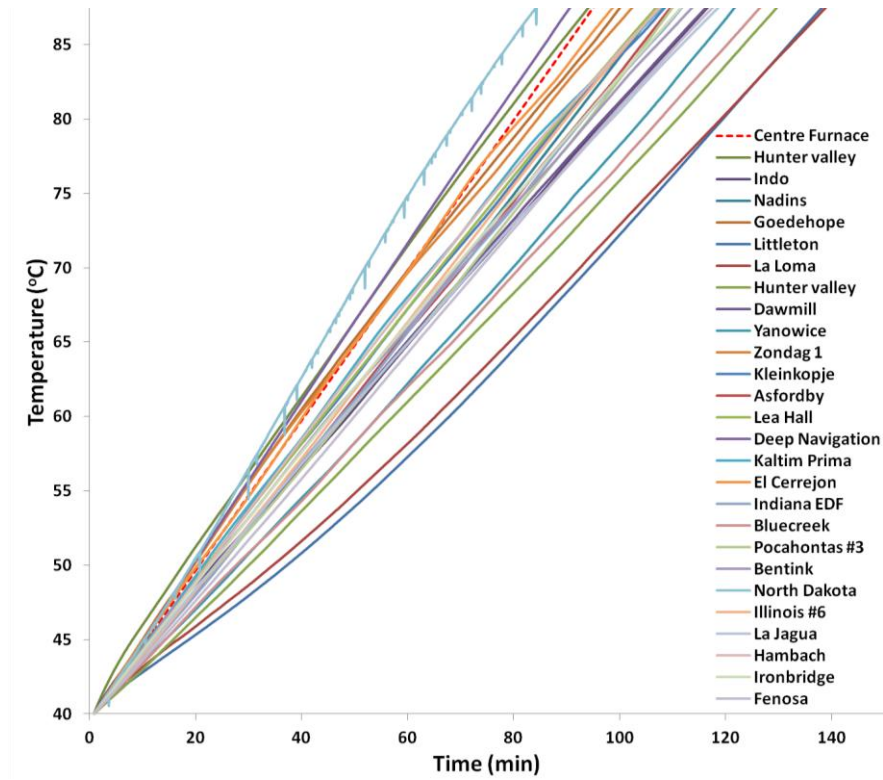
Figure 58: Comparison of the Initial heating rate (IHR) for all samples studied (slope of temperature profile). The red dot curve is the furnace temperature.
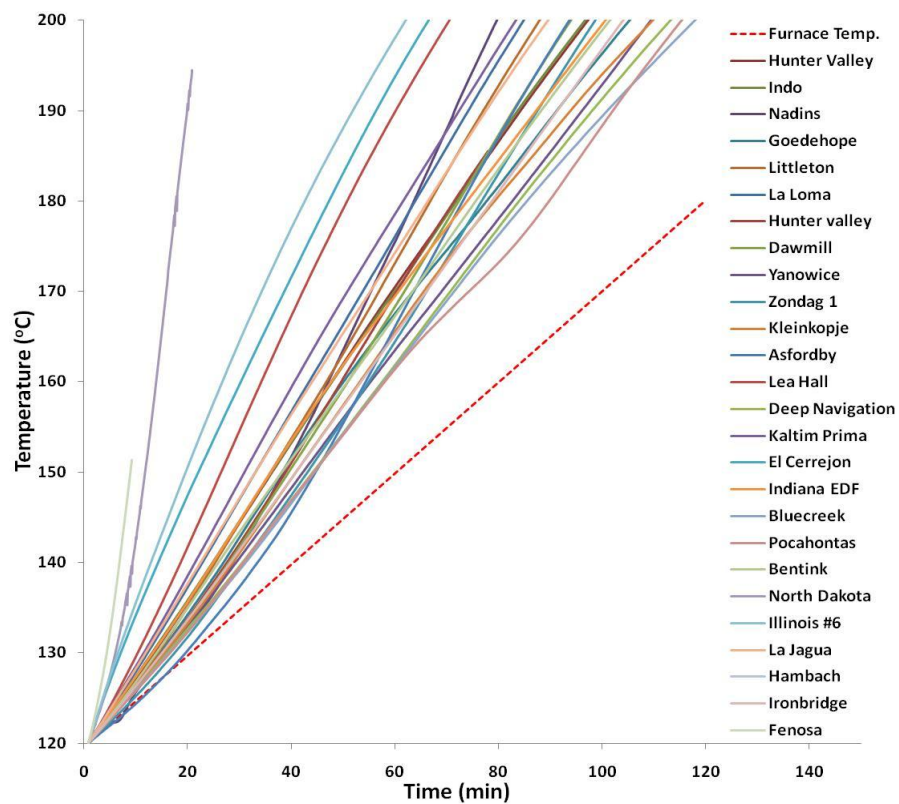
Figure 59: Final heating rate (FHR) for all samples studied.

Table 19: Initial heating rate (IHR) obtained from two central thermocouples

Coal	Thermocouples A, Z=35mm		Thermocouples B, Z=25mm	
	IHR (^{o}C min^{-1})	r^2	IHR (^{o}C min^{-1})	r^2
Indo	0.405	1.000	0.389	1.000
Nadins	0.448	1.000	0.427	1.000
Goedehoop	0.472	0.999	0.481	0.999
Littleton	0.387	0.981	0.382	0.978
La Loma	0.381	0.985	0.368	0.990
Hunter valley	0.377	1.000	0.381	0.998
Dawmill	0.411	1.000	0.399	0.999
Yanowice	0.393	0.999	0.403	0.997
Zondag 1	0.435	0.994	0.427	0.989
Kleinkopje	0.446	0.999	0.434	0.998
Asfordby	0.436	1.000	0.438	1.000
Lea Hall	0.447	1.000	0.437	0.998
Deep Navigation	0.529	1.000	0.544	1.000
Kaltim Prima	0.464	0.999	0.460	0.986
El Cerrejon	0.485	0.999	0.488	0.995
Indiana EDF	0.431	1.000	0.426	1.000
Bluecreek	0.377	1.000	0.380	1.000
Pocahontas	0.432	1.000	0.451	0.999
Bentink	0.425	0.999	0.410	0.999
North Dakota	0.581	0.999	0.588	0.998
Illinois #6	0.450	1.000	0.449	1.000
La Jagua	0.401	0.999	0.380	0.997
Hambach	0.447	0.999	0.443	0.997
Ironbridge	0.426	1.000	0.422	0.999
Fenosa	0.411	1.000	0.415	0.998

A clear dependency of IHR with rank, water, volatile and ash content was not found. The minimum heating rate observed was 0.37^{o}C min^{-1}, which was obtained for a high rank and low water content coal. For all the samples studied, the IHR was calculated considering the range between 40 to 90°C. Above this temperature, in the range between 90 to 120°C, some samples presented a slight inflection in the profile, and some others a large period at constant temperature (100°C), such as Fenosa,

North Dakota and Hambach. For these, the thermal segment was better described by the mass evolution, which was recorded simultaneously (presented in Section 4.3.5). Figure 59 shows the thermal profiles of the FHR zone, considering the temperature range between 120 to 200°C. During this segment, all samples showed heating rates higher than the furnace, with important differences between samples. It confirmed how the system evolution changed before and after the boiling point of water, which is a key temperature for a large scale system. Then, in the same way as the IHR segment, the FHR profiles were approximated by a linear trend. According to these, coals were classified in 5 different groups clearly differentiated by the value of these slopes, from the highest to the lowest FHR. This classification is shown from Figure 60 to Figure 62.

From this classification, Group 1 included the highest heating rate, which was approximately 10 times higher than the furnace heating rate. This group included the three low rank coals with the highest water content. From these, two have a history of spontaneous combustion problems (Fenosa & N. Dakota). The other coal was Hambach, which is considered to be unreactive due to its extreme water content (~37%). As a conclusion, the high water content of these samples has a direct effect on the resulting heating rate observed. This was confirmed by comparing with other samples shown in Table 20.

Group 2 included coals with a FHR approximately 2 to 3 times higher than the furnace heating rate. In this group, Illinois #6 and El Cerrejon were considered to be highly reactive (by intrinsic reactivity tests). The remaining were UK coals with similar properties and were considered to be reactive (by intrinsic reactivity tests), and with vitrinite reflectance values between 0.4 to 0.6%R (explained in Chapter 5).
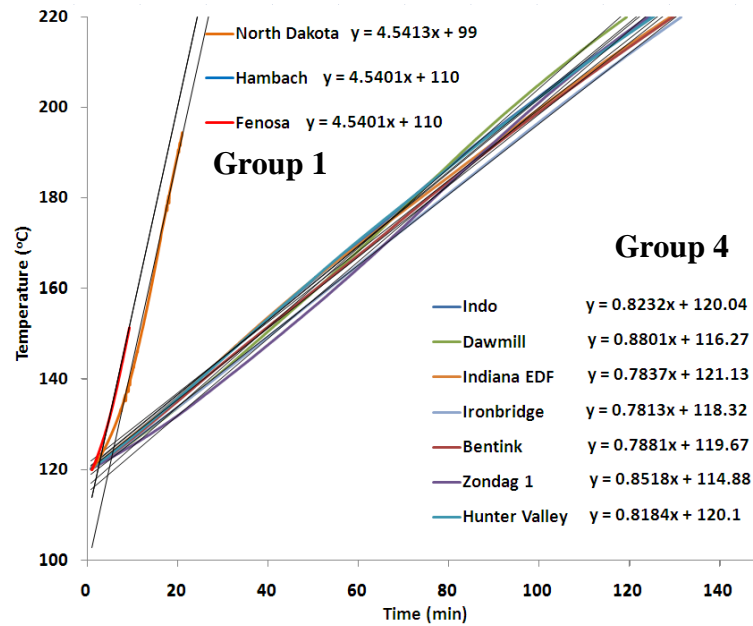
Figure 60: Linear interpolation for two set of coals (Groups 1 and Group 4).
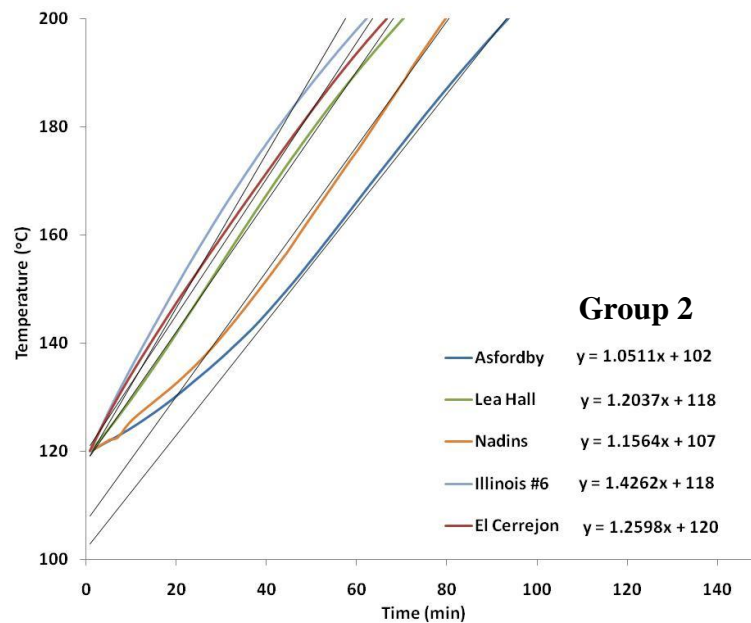
Figure 61: Linear interpolation of coals classified in Group 2.

Group 3 included some carbon rich and low ash content samples, with no information about spontaneous combustion problems. In terms of coal physical properties, this group was similar to Group 2. The difference in the classification was based only on the value of the FHR, which was slightly lower (1.8 to 2 times higher than the furnace heating rate). Finally, the lowest heating rates were included in

155

Groups 4 and 5, which were also characterized by high ash content and low reactivity in terms of peak and burnout temperatures. These coals also had elevated rank values (0.8 to 2.5%R, shown in Chapter 5)
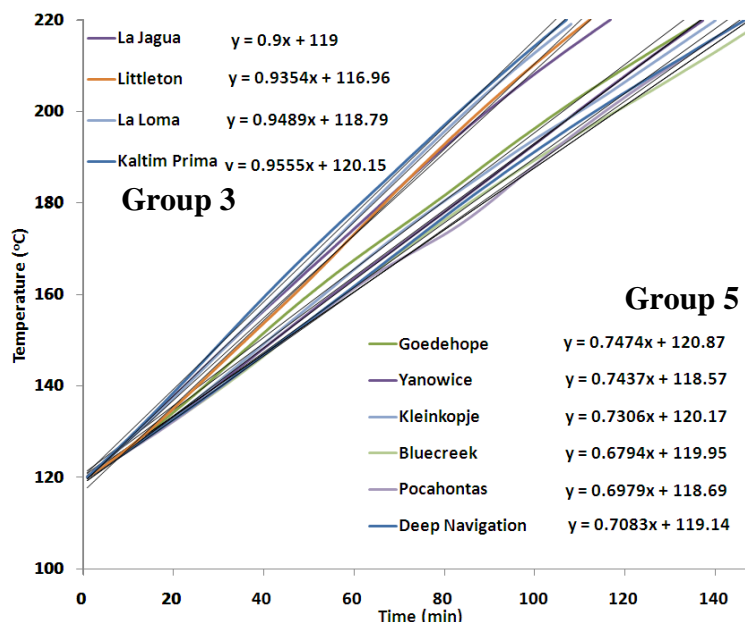
Figure 62: Linear interpolation for two set of coals corresponding to Group 3 and 5.

These groups were simultaneously classified based on their water content and the IHR values, and reported in Table 20. A clear effect of water content was apparent based on the thermal profiles. The difference between the initial and the final heating rate (column *% diff. HR*, Table 20) was directly proportional to this parameter. In addition, water acted as a heat sink at the initial stages of the process. When water was totally released from samples, the temperature in the centre increased sharply. However, from these experiments it was not clear if the temperature variation was produced by changes in thermal conductivity (due to water release), or to an increase in oxidation reaction rate. In the event of an acceleration of the oxidation rate of the sample; the experiment produced an extremely high heating rate compared to the natural rates observed during a thermal runaway. In addition, the furnace ramp used was also comparatively higher than the normal conditions reported for the

phenomenon, concluding that the thermal evolution observed was related to a high temperature combustion reaction (and ignition phenomenon), instead of a self-oxidation phenomenon. For these reasons, it was suggested that these experiments do not conclusively determine coal propensity to spontaneously combust.

Table 20: Coal classification regarding to the final heating rate measured.

	Coal	Water %	IHR (^{o}C min^{-1})	FHR (^{o}C min^{-1})	% Diff. HR
Group 1	Hambach	37.52	0.447	4.540	917
	N. Dakota	22.04	0.581	4.541	681
	Fenosa	10.85	0.411	4.540	1004
Group 2	Illinois #6	3.72	0.450	1.426	217
	El Cerrejon	3.45	0.485	1.260	160
	Lea Hall	5.48	0.447	1.204	170
	Nadins	7.37	0.448	1.156	158
	Asfordby	5.48	0.436	1.051	141
Group 3	Kaltim Prima	3.53	0.464	0.956	106
	La Loma	3.78	0.381	0.949	149
	Littleton	5.03	0.387	0.935	141
	La Jagua	4.32	0.401	0.900	125
Group 4	Dawmill	3.29	0.411	0.880	114
	Zondag 1	3.91	0.435	0.852	96
	Indo	3.83	0.405	0.823	103
	Hunter Valley	2.21	0.377	0.818	117
	Bentink	3.59	0.425	0.788	85
	Indiana EDF	2.84	0.431	0.784	82
	Ironbridge	4.11	0.426	0.781	83
Group 5	Goedehoop	2.33	0.472	0.747	58
	Yanowice	5.05	0.393	0.744	89
	Kleinkopje	3.50	0.446	0.731	64
	Deep Navigation	1.02	0.529	0.708	34
	Pocahontas	0.62	0.432	0.698	62
	Bluecreek	3.50	0.377	0.679	80

Finally, in view of the results obtained from the TGA experiments (low temperature reactivity and oxygen adsorption); a correlation between the high reactive samples, which presented a small or nil oxygen adsorption, with the magnitude of the FHR recorded was found. On the other hand, some of the lowest reactive samples showed the smallest FHR rates. Nevertheless, this correlation was not characteristic of the intermediate samples in both classifications.

4.3.3 Crossing point temperature values

The literature survey showed that the crossing point temperature method (CPT) was the most common technique when estimating coals propensity towards spontaneous combustion. Also, several experimental approaches have been shown to estimate the critical temperature from which the reaction is considered as self-sustaining. However, in most of these cases the terms self-heating and the self-ignition were confused as the same phenomenon. As a result, three different prediction methods were selected for comparison:

i) **The new CPT proposed by Chen** [176]: In this case, the CPT value was obtained when a flat temperature profile was observed within the sample (the temperature in the centre reached the temperature of the local adjacent thermocouples). This was identified in a spatial-transient thermal plot using the information available from all the thermocouples and their respective spatial position. Experimental results for six samples are shown from Figure 63 to Figure 66.

ii) **The classic CPT method:** the CPT value was obtained when the temperature in the centre of the sample reached the temperature in the centre of the furnace. The results of this method are compared in Table 21.

iii) **A modification to the classical CPT test:** this approach measured the crossing temperature when the temperature in the centre of the sample reached the

internal surface temperature of the sample holder. The results for this approach are also shown in Table 21.

From the spatial thermal profiles (Figure 63 to Figure 66) two main characteristics were identified: The first is related to the flat temperature segment (~75-90°C), from which the CPT values were obtained. The period in which this flat segment was established depended on the thermal properties of the coal sample, which was strongly affected by the water and ash content. The second characteristic was the inflection of the temperature profile, which was due to the influence of the water content of the sample. This took place precisely at 100°C, being well-defined for high water content coals (Figure 63, Figure 64 & Figure 65).
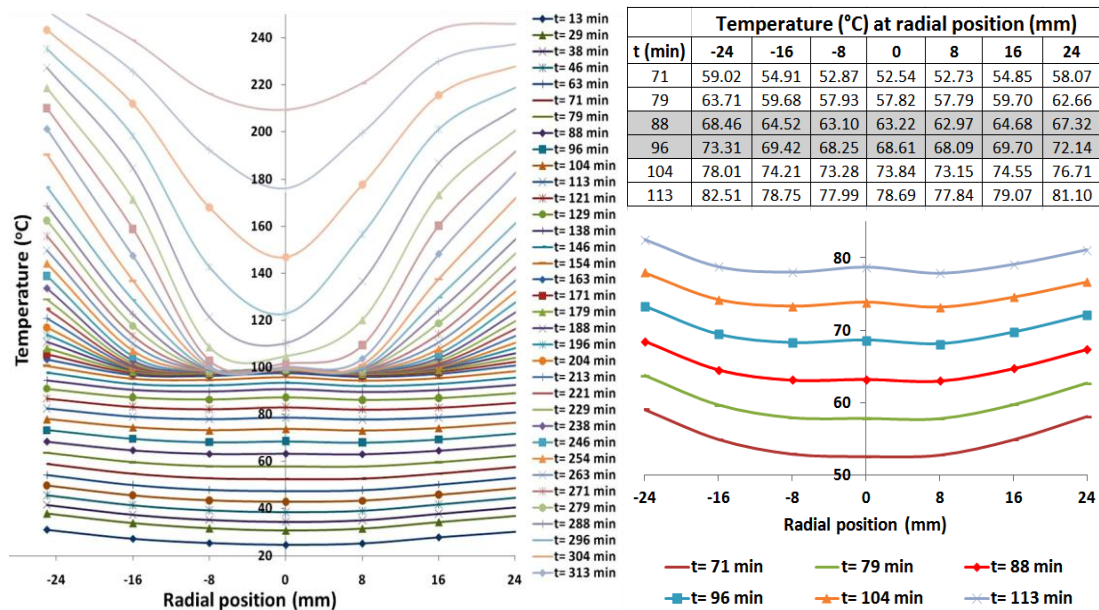
Figure 63: Spatial thermal profile for North Dakota coal (left), and zoom into the region where the flat segment corresponding to the low temperature crossing point was observed (right). The heating rate used was 0.5^{o}C min^{-1} in air.

These thermal profiles also identify a hotspot created in the centre of the sample, which cannot be easily detected when using the graphs shown in Section 4.3.1. For some coals such as North Dakota (Figure 63) and Fenosa (Figure 64), the flat

temperature section occurs twice, before and after the water boiling point. However, for most of the samples it occurs above this temperature (Figure 66). This hotspot could be linked closely to the spontaneous combustion phenomena.

Temperature (°C) at radial position (mm)							
t (min)	-24	-16	-8	0	8	16	24
137	79.82	75.22	74.41	74.74	74.89	75.96	80.53
145	83.34	78.47	77.62	78.06	78.11	79.15	84.00
153	86.82	81.55	80.71	81.22	81.18	82.30	87.54
162	90.32	84.45	83.64	84.26	84.09	85.36	91.05
170	93.58	87.17	86.38	87.17	86.83	88.20	94.45
178	96.85	89.49	88.82	89.57	89.27	90.73	97.73
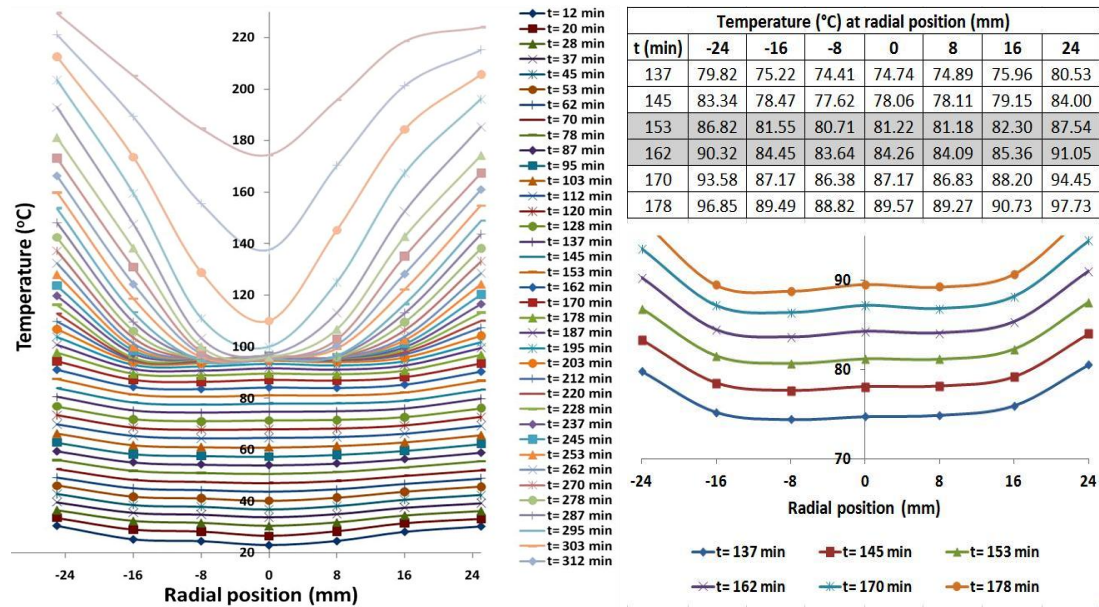
Figure 64: Spatial thermal profile for Fenosa Coal (left), and flat segment corresponding to the CPT (right). The heating rate used was 0.5°C min^{-1} in air.
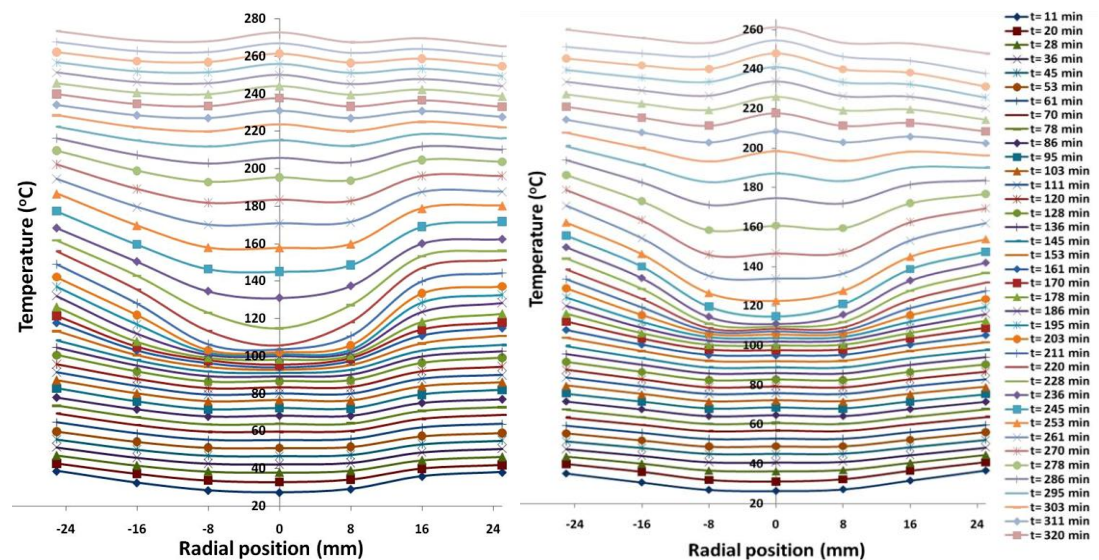
Figure 65: Spatial thermal profile for El Cerrejon coal (high reactive), and Lea hall coal (medium reactive). The heating rate used was 0.5°C min^{-1} in air.
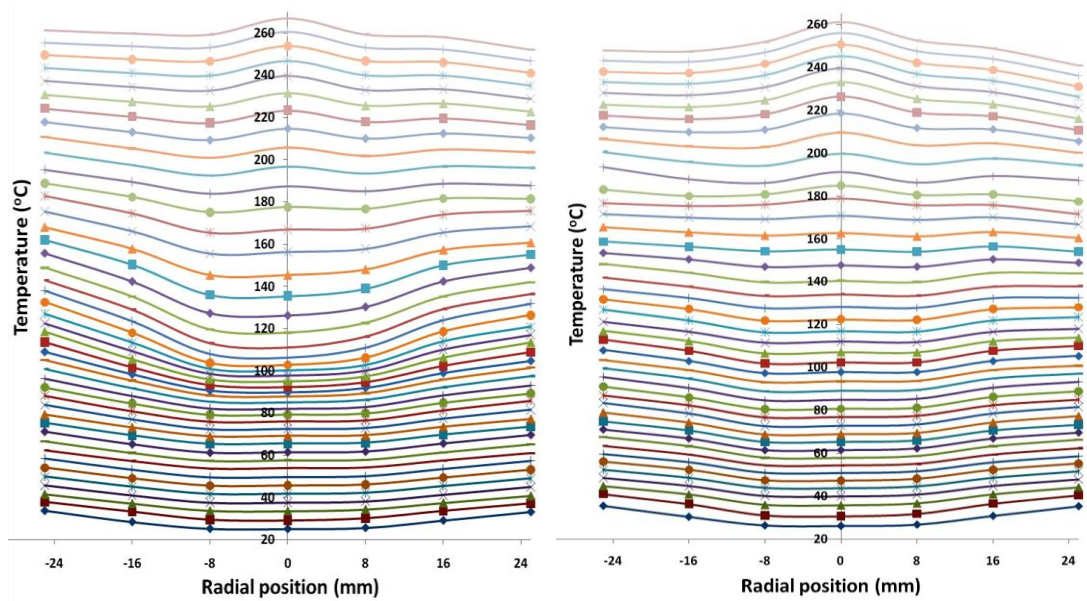
Figure 66: Spatial thermal profiles for Kaltim Prima (left) and Pocahontas#3 (right). The time domain is similar for both coals and analogous to Figure 63.

The spatial thermal profiles expose new information about the water release phenomenon and its influence in a bulk system, which could be more important than the information delivered by the CPT test itself. In this case, if the phenomenon is extrapolated to a larger system, the water boiling point acts as a transitory stop in the process. However, if the reaction at 100°C is already self-sustained, a critical temperature does not seem logical. The intrinsic reaction at this temperature must be evaluated, in order to determine the coal reactivity during water evaporation, and its effect on the whole process. It is confirmed by the information and images available from the spontaneous coal fire described in Chapter 3, which show the release of elevated amounts of steam from the coal stockpile at a constant low temperature.

This finding introduces a doubt about the effectiveness of the crossing point temperature method as a reliable indicator (specifically for the Chen approach), since the flat temperature segment is dependent on the water content, more than the intrinsic reactivity properties of the sample. A clear example of this was found for

Hambach coal (37% water content), which presents two flat segments: the first at low temperature (below 100°C), and the second over 200°C. Despite the low critical temperature prediction, this coal is not reactive at these temperatures even when it was dried, then the test has failed. The second CPT value for Hambach was at high temperature, similar to those found for high water content samples (Fenosa & North Dakota). In this case, if the first crossing value at low temperature was wrong, but the second is right, then the second one does not match the prediction for the high reactive samples because Hambach is nonreactive, meaning that the test failed again.

Table 21: Crossing point temperature values obtained using different approaches (^{o}C)

Coal	Chen CPT approach	Classic CPT approach	Correction classic CPT
Hunter valley	185	166	215
Indo	202	167	220
Nadins	113, 133	160	187
Goedehoop	156	127	162
Littleton	173	191	175
La Loma	171	196	181
Dawmill	158	170	175
Yanowice	132	165	180
Zondag 1	170	146	168
Kleinkopje	172	147	184
Asfordby	144	173	186
Lea Hall	53-89, 160	175	192
Deep Navigation	171	190	178
Kaltim Prima	176	156	182
El Cerrejon	90-98, 176	155	164
Indiana EDF	144	153	176
Bluecreek	155 not clear	173	170
Pocahontas	112	142	152
Bentink	149	154	160
North Dakota	73-98, >200	60-96, >200	250

Table 21, continuation

Coal	Chen CPT approach	Classic CPT approach	Correction classic CPT
Illinois #6	48-105, 176	177	167
La Jagua	167	177	187
Hambach	82-110, >200	>200	~220
Ironbridge	184	166	199
Fenosa	81-96, >200	>200	~210

The classic crossing point temperature approach produces incorrect predictions and it must be considered carefully prior to be applied to coal deposits. In general, the CPT method was developed to assess carbonaceous materials (other than coal), in order to identify the temperature in which a particular thermal runaway starts. For coal research, this method has been partially adapted to assess the propensity towards spontaneous combustion. However, from the results obtained in this research, a series of anomalies produced by coal water associations (present in coal deposits) inhibit the accuracy of the classic CPT test.

As an example, the classic CPT value obtained for Goedehoop coal was roughly $127^{o}C$ (a high rank, water content 2.3%, and low reactive coal). On other hand, Nadins has a classic CPT value near to $160^{o}C$ (low rank, water content 7.37%, and high reactive coal). As can be seen from a differential thermal profile (Figure 67), the Goedehoop temperature remains very close to the furnace temperature, slightly inflecting around $100^{o}C$. However, Nadins temperature also tends to inflect around $100^{o}C$, but it takes longer due to the elevated energy requirements to vaporize the larger quantity of moisture. Then, the coal temperature rises sharply when all free water has been released.
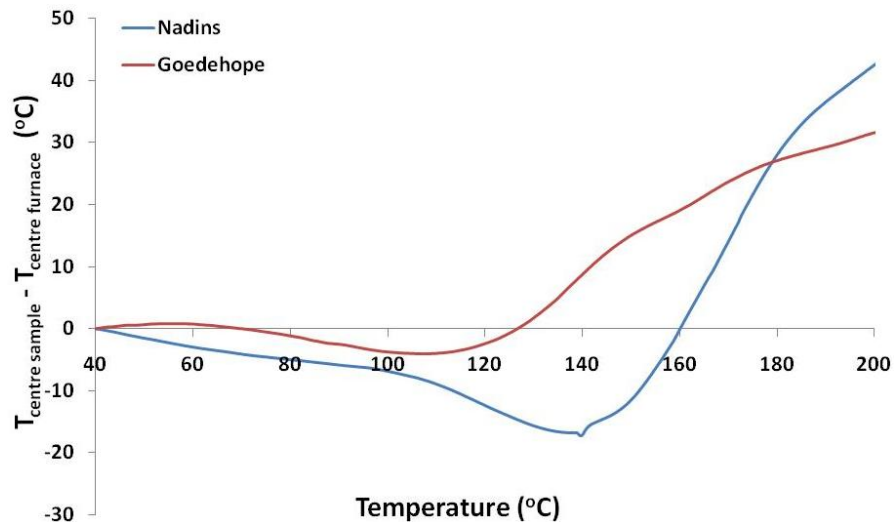
Figure 67: Differential thermal profile for Goedehoop and Nadins coals. The crossing point is reached when the profile become positive. The heating rate used was 0.5^{o}C min^{-1} in air.

This latter effect was not produced by the intrinsic oxidation of the coal itself; this was produced by the heat transfer phenomena taking place, and contradictory to the classic CPT prediction, the ignition of the sample took place at approximately 140°C. In addition, the results obtained using Chen's approach (113-133°C) were lower than the recorded ignition temperature. This supports the idea that Chen's modifications to the CPT method deliver best predictions. However, as it was discussed previously, Chen's CPT approach also has some serious limitations.

Finally, a graphic comparison for all the different CPT values is shown in Figure 68. This figure includes the ignition temperature, which was obtained from the same experiments (discussed in Section 4.3.4). As can be seen, it is not possible to predict the liability of a coal sample just considering the information obtained from this type of test. There are several important factors that are not considered, such as the coal intrinsic reactivity, the critical mass needed to observe the phenomenon, and the influence of the applied external heating rate.
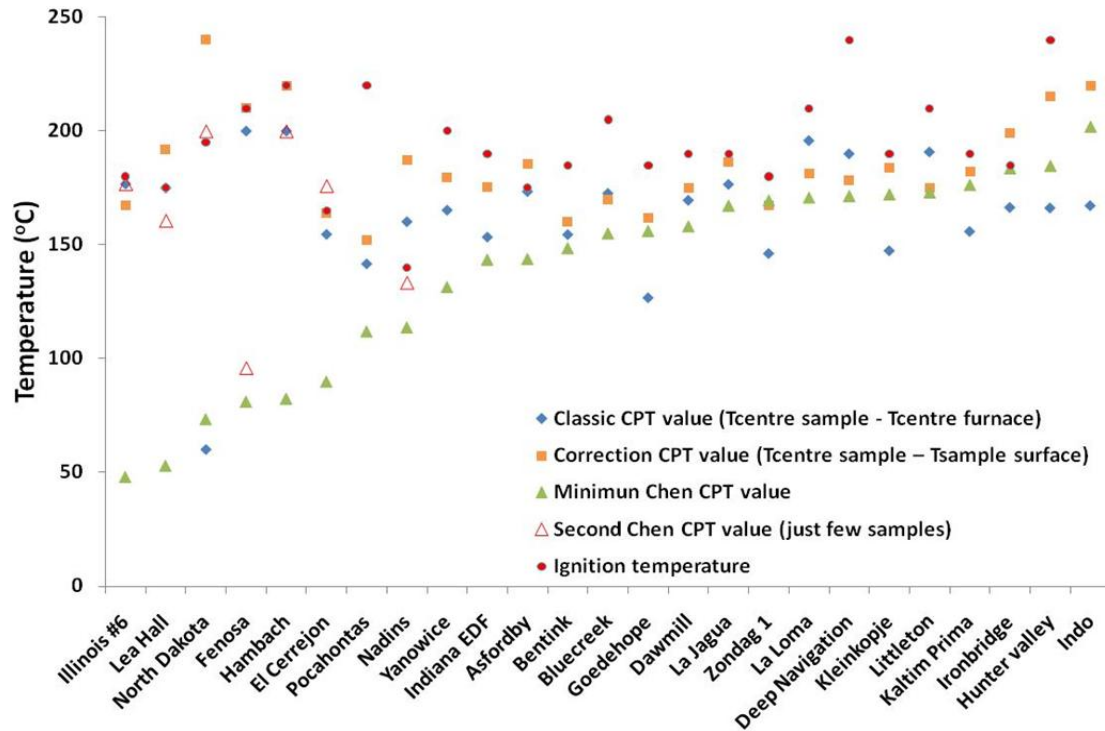
Figure 68: Graphic comparison of the different CPT values. In most of cases, the lowest critical temperature value is obtained using Chen's approach.

4.3.4 Ignition temperature of coals

The ignition temperature was measured for all coal samples studied. It was obtained during the heating experiments, by using a thermocouple located at the top surface of the sample holder. This was the closest experimental procedure to estimate the ignition temperature simultaneously to the development of the thermal profiles. Additionally, the location of the thermocouple at the interface between coal and air allowed the observation of the thermal evolution in one of the frontiers of the system, in which the maximum oxygen-coal contact was produced.

Figure 69 shows a comparison of all the top surface temperature readings recorded. As can be seen in this figure, all the temperature profiles show an initial linear segment below the furnace heating rate. Then, a sudden temperature jump was registered from approximately 160-190°C to 350-400°C (depending of the sample),

due to ignition of the sample. It was confirmed also by the abrupt change in the CO and CO_2 concentration being registered simultaneously in the gas analyzer system.
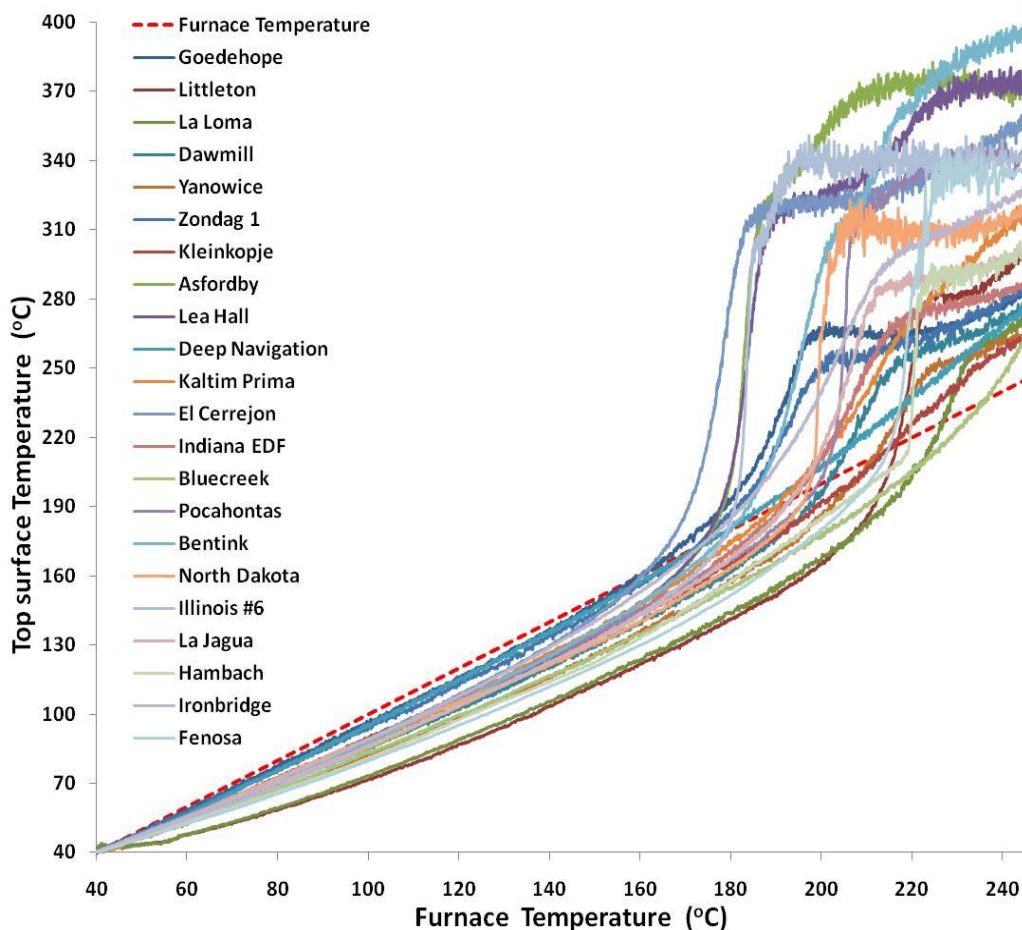
Figure 69: Ignition temperatures recorded for all coal samples studied. The heating rate used was $0.5^{o}C$ min^{-1} in air.

From the thermal profiles, the ignition temperature was estimated for each sample by determining the intersection between the initial heating curve and the temperature curve of the sample after the ignition, as it is shown in Figure 70. The results are shown in Table 22.
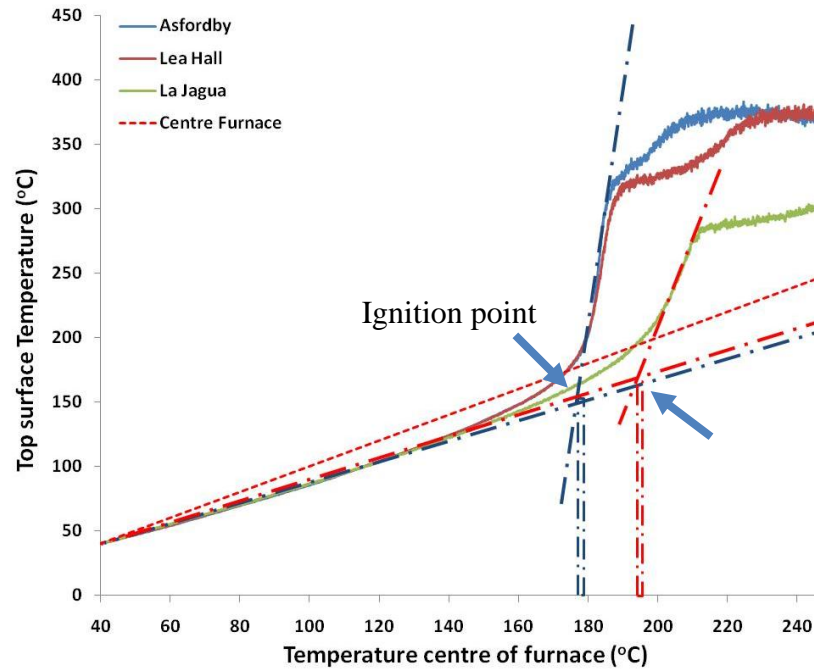
Figure 70: Estimation of the ignition temperature for three coal samples studied. The heating rate used was $0.5^{\circ}C$ min^{-1} in air.

Table 22: Ignition temperatures recorded

Coal	Ignition Temperature ($^{\circ}$C)	Coal	Ignition Temperature ($^{\circ}$C)
Nadins	140	Indiana EDF	190
El Cerrejon	165	La Jagua	190
Asfordby	175	North Dakota	195
Lea Hall	175	Yanowice	200
Zondag 1	180	Pocahontas	205
Illinois #6	180	Littleton	210
Ironbridge	185	La Loma	210
Goedehoop	185	Fenosa	210
Bentinck	185	Blue creek	220
Dawmill	190	Hambach	220
Kleinkopje	190	Hunter valley	>180
Kaltim Prima	190	Deep Navigation	>240

Finally, it was concluded that the ignition temperature does not relate to the crossing point temperature values, as shown in Figure 68. On one side, the ignition of the coal surface interfered with the progress of the transient thermal profiles being recorded,

due to the considerable temperature increase in the surface of the sample holder. However, in most of cases the thermal profiles suffered early inflections due to water release, which subsequently produced crossing points of temperature that took place long before the ignition (Nadins was the only exception). Additionally, the determination of the real value of the ignition temperature for high water content samples requires an intermediate step at constant temperature at 100°C, to remove all water before ramping up beyond 100°C, otherwise this value will be artificially higher.

4.3.5 Mass evolution

The study of the mass evolution of the large coal sample was carried out simultaneously by using the balance attached to the experimental reactor. In this case, mass was recorded during the slow heating (0.5°C min^{-1}) of all the samples. However, a major experimental problem arose: the interference produced in the weight reading due to the use of wired thermocouples, which interconnected the sample holder with the data acquisition system whilst, at the same time, being physically attached to the balance. This unavoidable arrangement introduced substantial errors to the balance readings, allowing only qualitative analysis.

A mass baseline was obtained by running the equipment with a dry sand sample, in order to estimate and reduce the influence of the wires vibration in the sample weight. Then, this baseline was removed from all the sample profiles. However, the effect of an increasing mass loss produced by the water release, introduced larger perturbations in the wires, which increased the error. Despite this problem, clear mass profiles for all the samples were obtained. Figure 71 and Figure 72 show the mass-time profiles obtained. These curves were classified in four groups according to the final mass registered after 350min (equivalent to 200°C in the centre of the

furnace, as can be seen from Table 23). This temperature corresponds to the average ignition temperature for most of the samples. Above this temperature, coal samples tend to lose considerable quantities of material due to the complete combustion.
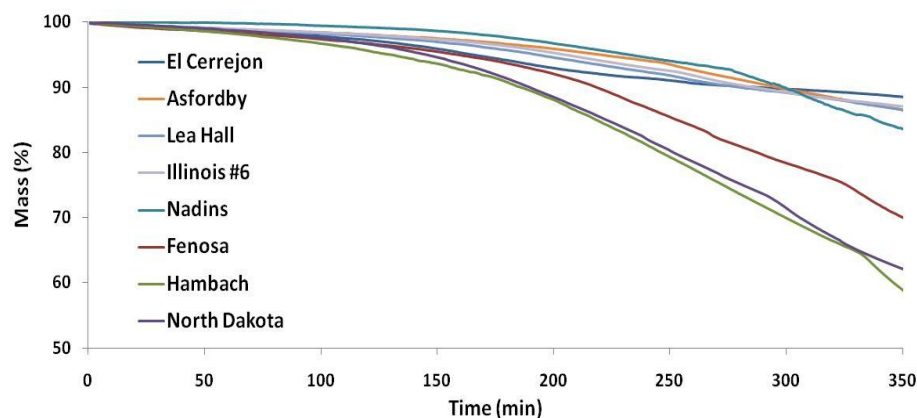

Figure 71: Groups 1 and 2 reaching a weight loss higher than 30% and 10% at the end of the experiment. The heating rate used was 0.5°C min^{-1} in air.
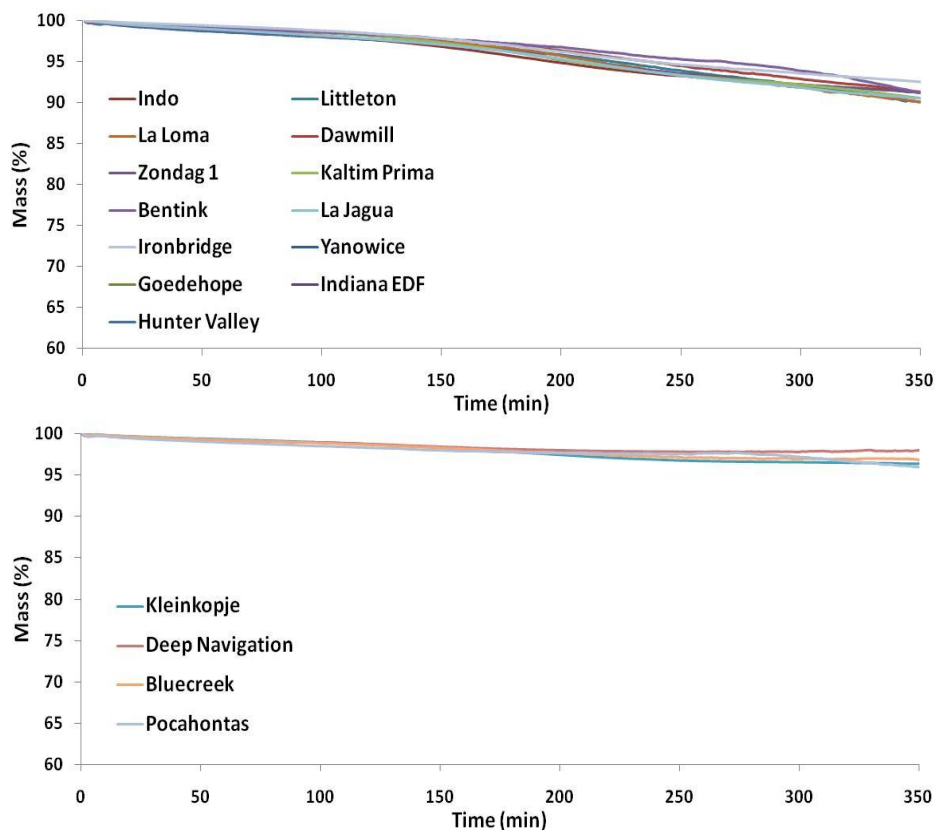
Figure 72: Group 3 (top) and Group 4 (bottom); at the end of the experiment samples reach a weight loss lower than 10% and 5% respectively.

169

As can be seen from the profiles during the first 100min of heating (furnace temperature below 75$^\text{o}$C), there was little change in the sample mass (the maximum change observed was 3% for a high water content coal). Then, when the temperature passed over 100$^\text{o}$C (after 150 min), the mass loss due to the water evaporation was important, particularly for coals of Group 1. These coals immediately followed a different trend, achieving a constant and elevated weight loss rate until the end of the test (Figure 71). In Table 23, there is shown the particular classification and the most relevant time and temperature intervals recorded.

Regarding Group 2, heating above 100$^\text{o}$C produced a change in the weight slope, but was less pronounced than in Group 1. Then, approximately at 300min (175$^\text{o}$C) a second change was observed in the curve, this time produced by the ignition of the sample, which was corroborated independently by the ignition temperature recorded and the readings of CO_2 in the gas analyzer system. All these coals were previously classified as highly reactive towards a complete combustion reaction, by considering the peak and burnout temperature. Before the ignition, the weight loss observed was directly proportional to the water content of the samples, not distinguishing any change due to other chemical reactions. Within this group, El Cerrejon and Nadins coals showed an irregular curve that was explained by the influence of the thermocouple wires during these experiments.

Besides, the larger number of samples is formed in Group 3. This was characterized by a medium weight change, from 5 to 10% in the temperature range below 200$^\text{o}$C. In a similar way than the other groups, these coals also experiment an inflection of the curve approximately at 100$^\text{o}$C, which was a general trend for most of the samples. The specific characteristic of this group was given by the reduction of the weight loss rate approximately at 150$^\text{o}$C. Above this temperature, just some particular coals

showed changes, and in those cases the final weight loss was unaffected by the combustion reaction, as it can be seen from the profiles (Figure 72).

Table 23: Sample classification according to specific temperature intervals

Time (min)		0.0	50	100	150	200	250	300	350
Temperature in centre of furnace (^{o}C)		25	50	75	100	125	150	175	200
Mass		%wt	%wt	%wt	%wt	%wt	%wt	%wt	%wt
Group 1	Hambach	99.9	98.6	96.6	93.6	88.0	79.3	69.9	58.9
	North Dakota	99.9	99.0	97.5	94.6	88.5	80.3	71.5	62.2
	Fenosa	99.7	98.6	97.4	95.4	92.1	85.5	78.4	70.1
Group 2	Nadins	100.0	99.9	99.4	98.6	96.7	94.0	89.9	83.6
	Lea Hall	99.8	99.1	98.2	96.9	94.5	91.8	89.1	86.5
	Asfordby	100.0	99.0	98.3	97.5	95.8	93.5	89.7	86.5
	Illinois #6	99.9	99.1	98.4	97.4	95.3	92.5	89.2	87.0
	El Cerrejon	99.8	98.9	97.8	95.8	92.9	91.0	89.7	88.5
Group 3	Littleton	100.0	98.7	98.0	97.2	95.8	93.9	92.0	90.1
	La Loma	100.0	99.1	98.5	97.5	95.7	93.3	91.9	90.1
	La Jagua	99.9	98.9	98.1	97.0	95.3	93.3	91.8	90.5
	Kaltim Prima	100.0	99.3	98.5	97.3	95.2	93.3	92.2	90.5
	Zondag 1	99.8	98.8	98.0	97.1	95.2	93.5	92.2	91.2
	Bentinck	99.8	99.1	98.5	97.7	96.7	95.3	93.8	91.2
	Indo	100.0	99.0	98.1	96.8	94.9	93.3	92.2	91.3
	Dawmill	99.9	99.1	98.6	97.7	96.3	94.5	92.9	91.3
	Ironbridge	99.9	99.4	98.7	97.7	96.1	94.6	93.5	92.5
	Hunter valley	99.8	99.1	98.5	97.7	96.6	95.4	94.6	93.7
	Indiana EDF	100.0	99.1	98.3	97.4	96.1	95.1	94.7	94.3
	Goedehoop	99.9	98.8	98.1	97.2	96.3	95.7	95.0	94.7
	Yanowice	100.0	99.5	98.9	98.2	97.1	95.9	95.5	94.7
Group 4	Pocahontas	100.0	99.0	98.5	98.0	97.7	97.6	97.2	96.0
	Kleinkopje	100.0	99.5	99.0	98.4	97.5	96.8	96.6	96.4
	Bluecreek	100.0	99.3	98.9	98.3	97.6	97.1	96.9	96.8
	Deep Navigation	100.0	99.3	99.0	98.5	98.1	97.9	97.8	98.1

Finally, coals from Group 4 were characterized by a negligible mass change during the heating. For these, there was no evidence of any chemical reaction during the temperature ramp. It was confirmed by the temperature recorded in the centre of the

sample holder, which showed just a slight inflection around 100°C due to the loss of the minor moisture content present. One particular feature of the results is that all these samples also reported the highest weight increase values due to oxygen adsorption (by using TGA). However, for the large sample experiments, this weight increase was not observed.

The effect of water was evident for all the mass loss profiles obtained. An association between the initial moisture content of the samples and the total weight loss recorded at the end of the experiment is shown in Figure 73 (blue dots).
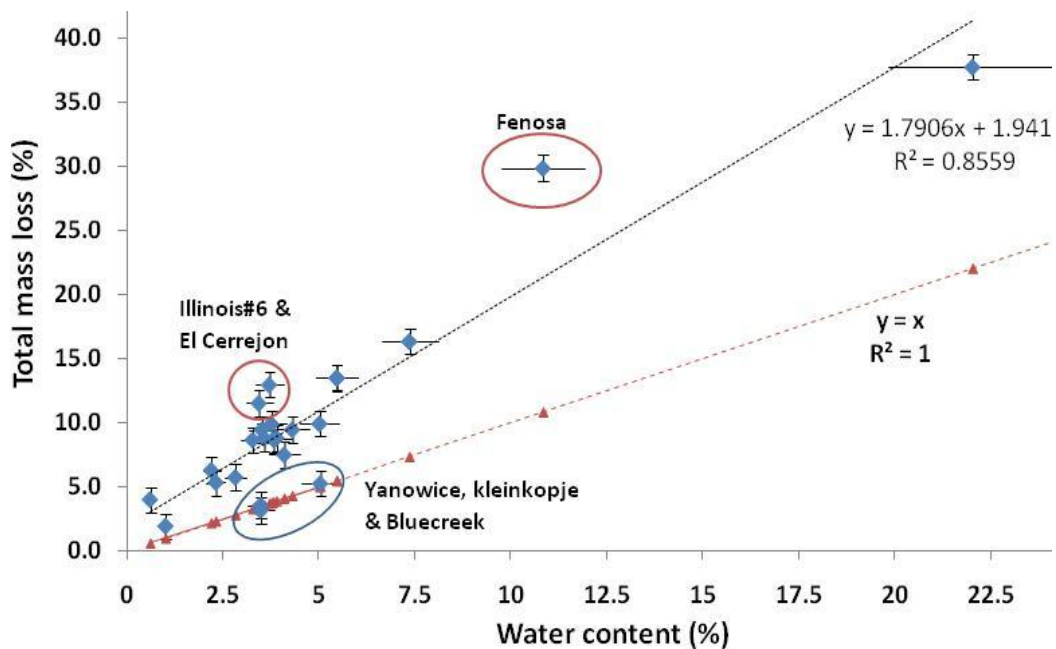
Figure 73: Relationship between initial water content and the total mass loss. Error bars consider 10% of the value, and red dots represent the y=x curve.

This relationship was approximated by a linear trend, obtaining a deficient deviation coefficient (0.86). Compared to the release of free water only (red dots line), the slope of this profile revealed that samples tended to lose 80% more mass than expected. In this figure, 10% error bars were considered, which showed specific samples considerably out of the general trend. Among these, three specific samples

172

showed a perfect match between the water content and the water effectively released after this period (Figure 73, blue circle), which confirms the low reactivity of these coals during the low temperature oxidation.

On the other hand, three samples showed a mass loss considerably higher than the average (Figure 73, red circles). These were Illinois#6, El Cerrejon and Fenosa coals. The first two showed low ignition temperatures (approximately 176°C) that explain why the weight lost was considerably high. The third (Fenosa coal), lost 3 times the amount of the initial water content during the same period of time, and the ignition temperature recorded was higher than 200°C. For this case, there was clearly a parallel reaction taking place simultaneously, which could be related to the spontaneous combustion issue, due to the particular characteristics of this sample visible in all the experiments.

Figure 74 shows the derivative curves calculated from the mass profiles for Groups 1 and 2. These two groups reported the highest mass change during the experiment. As can be seen from this profile, there is a flat mass loss rate in the segment 180-250min, attributable to the water release process. Also among these samples, Fenosa coal does not present a particularly high weight loss rate compared to the other coals as could be expected. The only sample that differed was Nadins coal, which showed an increasing mass loss rate like those seen in Group 1, despite being classified in Group 2. This relates to the low ignition temperature (~140°C) that produced a different slope at the end of the heating.
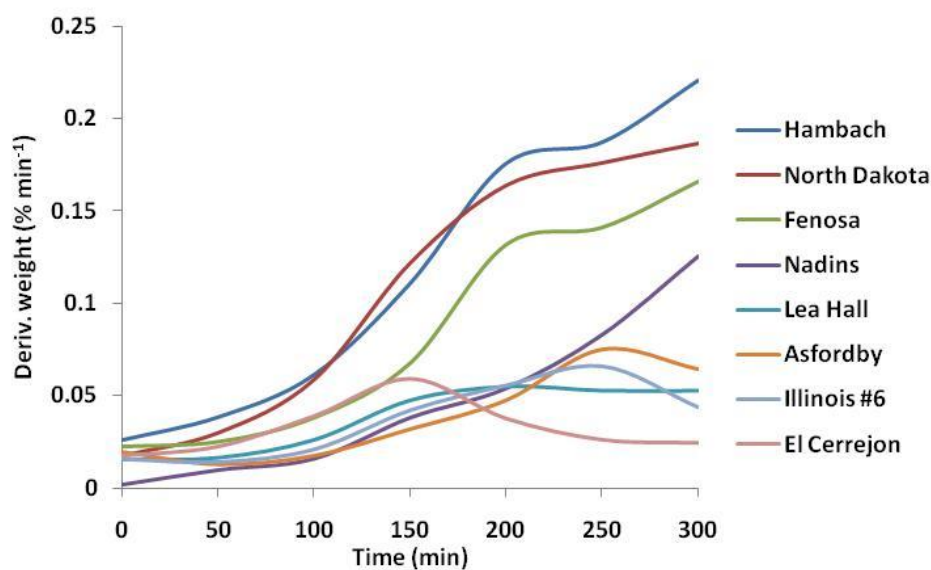
Figure 74: Derivative of weight in time for Groups 1 and 2.

Finally, it was concluded that the weight loss evolution is affected mainly by water release, which was observed during a specific interval dependent on the amount of water involved in each case. Additionally, this phenomenon affected the temperature in the whole system (for a large coal sample the temperature was constant during the water vaporisation), which could mean important technological consequences. Then, the weight loss results agreed with the thermal observations, despite being essentially qualitative. However, this needs to be corroborated since the actual experiments were affected by the lack of sensitivity and accuracy of the balance. Certainly, an examination of the solid residue after the heating is also necessary to complete the observation of the reactions that took place during the heating.

Chapter 5. Microscopy analysis of coals and linked results

5.1 Petrographic analysis of unaltered samples

Petrographic characterization was carried out for all the fresh coal samples. These tests comprised of two different analysis: maceral content (Section 5.1.1), and light reflectance of vitrinite (rank analysis, Section 5.1.2).

5.1.1 Maceral analysis of fresh coals

Maceral characterization was carried out considering the three main maceral components: Vitrinite, Liptinite and Inertinite (results shows in Table 24). In all samples studied, vitrinite was found to be the most abundant maceral (from 50 to 98%), followed by inertinite (from 1 to 51%), and liptinite (from 0 to 17%). Figure 75 outlines the distribution of macerals through the samples.

Maceral composition produced an impact in the reactivity of coals, from which high vitrinite samples were the most reactive (low peak and burnout temperatures). Liptinite rich coals also showed a high reactivity, despite being a less frequent component. Finally, coals rich in fusinite (or inertinite) were found the less reactive, which was produced by the hardest structure of this maceral. The effect of maceral composition on the thermal properties of coal at low temperature is studied in Section 5.4.

Table 24: Maceral analysis of coal samples

Coal	Maceral analysis		
	Vitrinite (%)	Liptinite (%)	Inertinite (%)
Hunter Valley	74.0	2.6	23.4
Indo	84.0	3.0	13.0
Nadins	76.0	10.0	14.0
Goedehoop	66.0	3.0	31.0
Littleton	73.0	9.0	18.0
La Loma	88.5	0.0	11.5

Table 24, continuation

Coal	Maceral analysis		
	Vitrinite (%)	Liptinite (%)	Inertinite (%)
Daw Mill	66.0	13.0	21.0
Yanowice	67.0	10.0	23.0
Zondag 1	48.0	1.0	51.0
Kleinkopje	57.0	1.0	42.0
Asfordby	74.0	13.0	13.0
Lea Hall	76.0	13.0	11.0
Deep Navigation	84.0	1.0	15.0
Cerrejon	91.2	0.4	8.4
Indiana EDF	83.0	2.0	15.0
Blue Creek	90.0	0.0	10.0
Pocahontas	97.5	0.0	2.5
Bentink	78.0	10.0	12.0
North Dakota	93.0	0.0	7.0
Illinois 6	95.0	0.0	5.0
La Jagua	83.0	1.0	16.0
Hambach	82.0	17.0	1.0
Ironbridge	85.0	3.0	12.0
Fenosa	98.0	0.0	2.0
Kaltim Prima	94.8	1.4	3.8
Bulli	78.5	0.0	21.5

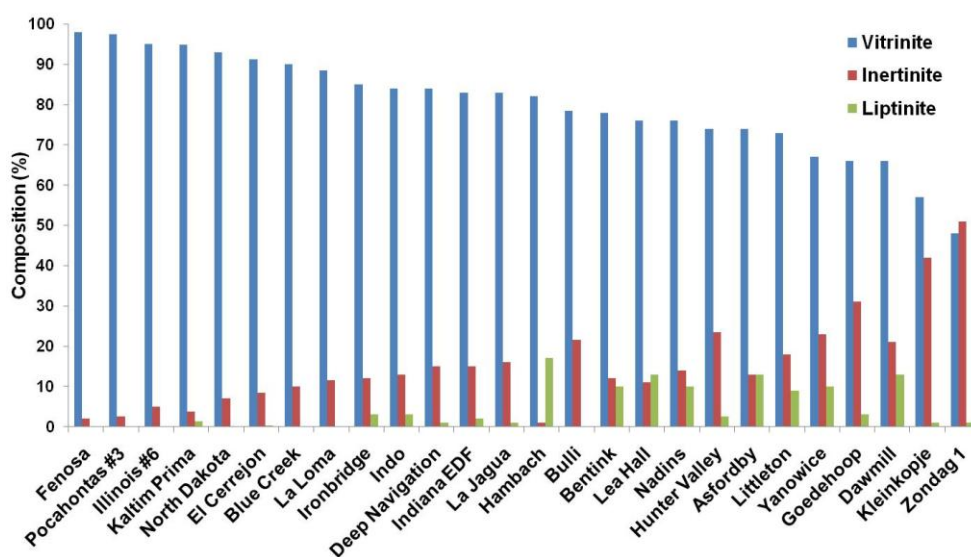Figure 75: Distribution of maceral composition through the samples.

5.1.2 Vitrinite reflectance of coal particles (Rank analysis)

Rank analysis of fresh samples were performed twice: initially, by testing the samples immediately after arrival (Table 25, as received); and after a period of time, in parallel to the main oxidation experiment (Table 25, as used). Despite careful storage, most of samples registered a small change in light reflectance. This was caused by uncontrollable factors such as natural oxidation (air contact with samples) and variations in the environmental moisture. Some samples were stored for several months before the experiments.

Samples studied vary from 0.3 to 1.7%R (percentage of light reflectance); 85% of these were in the range 0.3 to 0.8%R. According to the actual coal classification defined by the ICCP [1,3], samples were classified from lignite (0.3 to 0.4%R) to the limit between the low volatile bituminous coals and semi-anthracite (1.0 to 1.7%R). Consequently, most of the samples studied would be considered to be within the range where spontaneous combustion has been reported. The distribution of rank values across the different samples studied is shown in Figure 76.
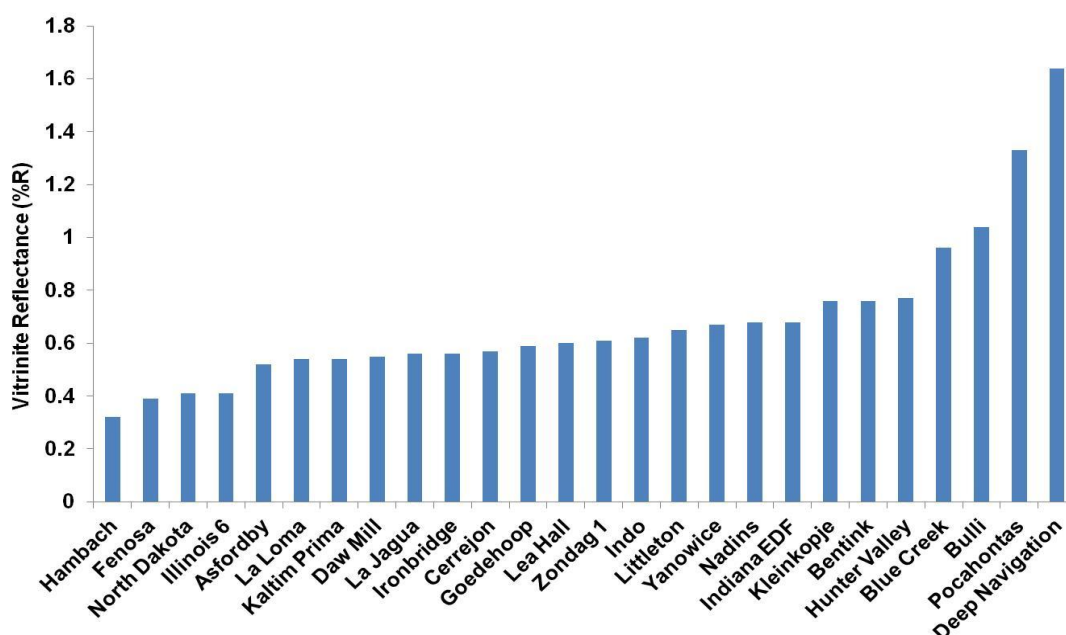
Figure 76: Distribution of light reflectance (%R) across the samples studied.

Table 25: Rank analysis of raw coal samples

Coal	Rank (%R)	
	as used	as received
Hunter Valley	0.77	0.71
Indo	0.62	0.59
Nadins	0.68	0.44
Goedehoop	0.59	0.99
Littleton	0.65	0.72
La Loma	0.54	0.51
Daw Mill	0.55	0.6
Yanowice	0.67	0.76
Zondag 1	0.61	-
Kleinkopje	0.76	-
Asfordby	0.52	0.48
Lea Hall	0.60	0.56
Deep Navigation	1.64	1.98
Cerrejon	0.57	0.54
Indiana EDF	0.68	-
Blue Creek	0.96	-
Pocahontas #3	1.33	1.33
Bentink	0.76	0.71
North Dakota	0.41	0.25
Illinois #6	0.41	0.46
La Jagua	0.56	0.57
Hambach	0.32	0.28
Ironbridge	0.56	-
Fenosa	0.39	0.35
Kaltim Prima	0.54	0.63
Bulli	1.04	-

The vitrinite reflectance was influenced by physical parameters such as water content, volatile and carbon content (Figure 77). Considering the information available from previous research, samples in use followed the general trends expected for industrial coals, representing standard properties.

Figure 77: Influence of physical parameters in the reflectance of coal.

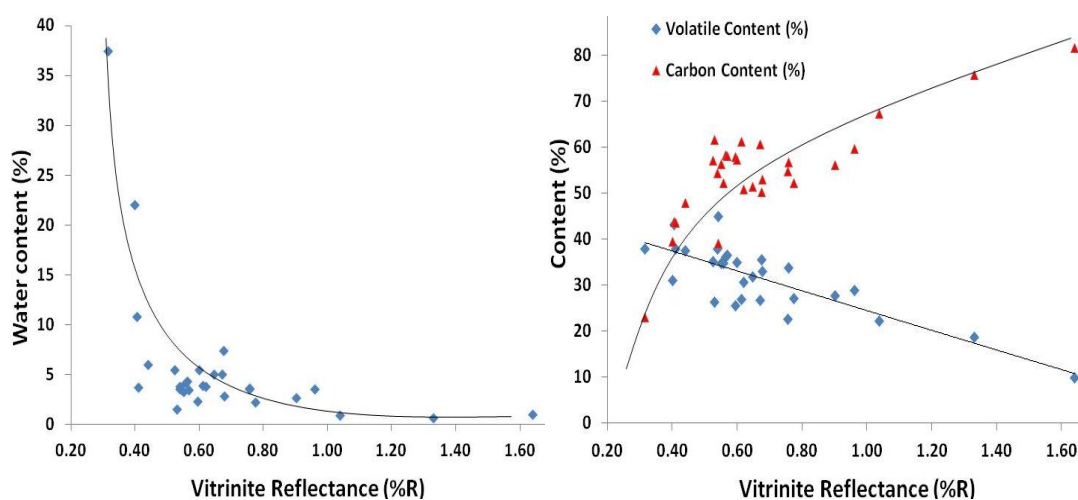For this work, light reflectance was considered an important independent variable that could group a number of physical properties of coals; but also because it was considered to be an indicator of propensity to spontaneous combustion by the early coal industry. Then, a combined assessment including maceral content and light reflectance values could incorporate a more profound meaning for the identification of coals prone to self-heating.

5.2 Characterization of thermally altered coals

Initially, coal samples were thermally treated in the reactor designed following the experimental procedure described in Chapter 3 (by using a heating ramp of 0.5^{o}C min^{-1} in air, from ambient temperature to 250°C). After this, a petrographic characterization was performed to evaluate the impact of heating on the optical properties of samples. These results were subsequently linked to the information of thermal reactivity and propensity available. Particularly, the primary objectives of the petrographic tests were: i) study and classify the different morphotypes created during the sample heating (Section 5.2.1); and ii) study the changes produced in the light reflectance of vitrinite particles due to the low temperature oxidation (Section 5.2.2).

179

5.2.1 Morphologic characterization of altered coal particles

The optical analysis of oxidized coals revealed important changes in the internal structure, shape, alterations in colour and light reflectance of particles. The morphological characteristics of these were classified using several types based on thermal alteration, some of which have not been described previously in literature. Figure 78 shows a mosaic image of a thermally treated coal sample, including some of these alterations produced by the low temperature oxidation.

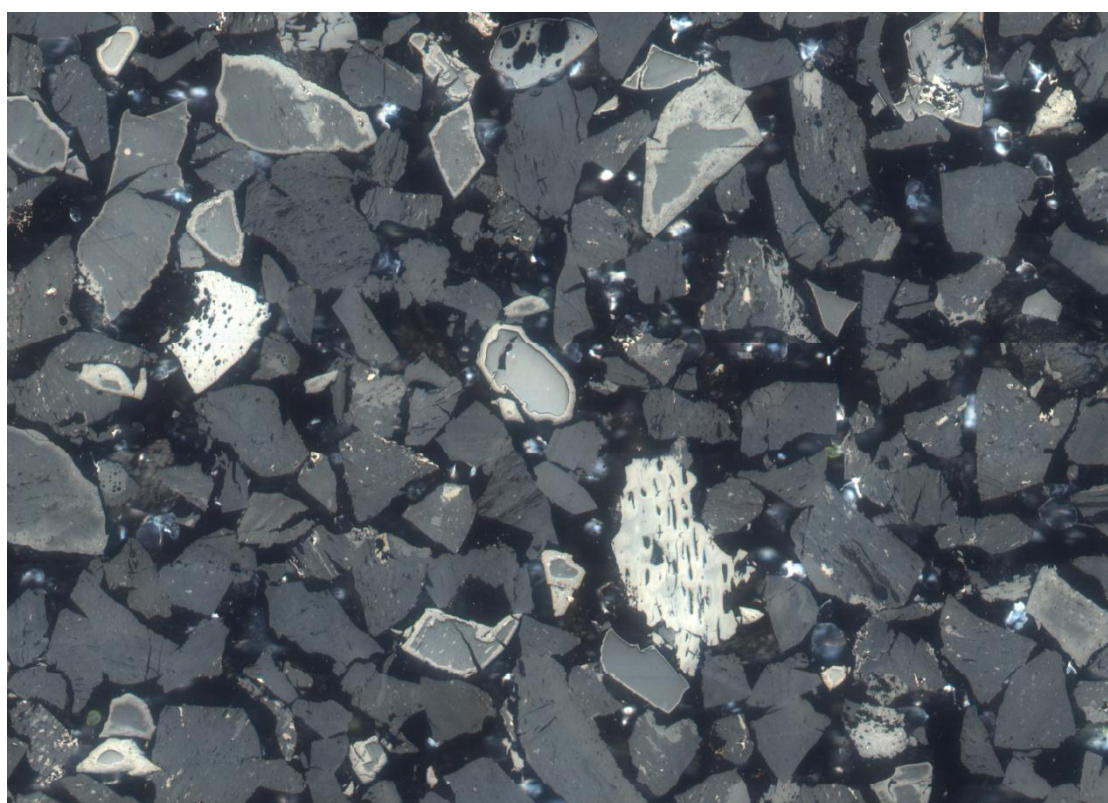Figure 78: Mosaic image of a thermally altered sample containing some of the morphotypes described (El Cerrejon coal).

From a systematic observation of the samples at least six different thermal morphotypes were identified. Subsequently, these particles were classified depending of their apparent origin in primary and secondary alterations (Table 26 shows images of the morphotypes identified).

The first group (primary alterations) included particles with basic transformations produced by the predominant reaction regime developed, representing boundary cases. Definitions of the morphotypes included in the first group are as follows:

A) Homogeneous change of reflectance (Table 26, A): these particles were characterized by an homogeneous change of reflectance across the whole particle, produced by the release of moisture and volatiles from the coal matrix. This change was accompanied by the development of porosity, particularly affecting vitrinite in low rank coals, but also found in specific high rank coal samples. The formation of this morphotype was produced when the oxidation reaction was kinetically controlled during heating, taking place over the whole particle.

B) Oxidation rims (Table 26, B): these particles were characterized by bands or rims in the surface, identified by a distinctive reflectance change in the edges (in cross-section images). These were created by a strong oxidation over the surface when particles were exposed to air at high temperature. In this case, these morphotypes were developed when the oxygen diffusion through the centre of the particles strongly controlled the oxidation reaction, affecting primarily the external surface.

C) Cracks and micro fractures (Table 26, C): this group was characterized by fractures created during the thermal expansion or shrinkage processes that coal particles suffered. These were produced when abrupt temperature changes took place, volatilizing liquid compounds inside cavities producing sudden pressure changes and cracking the particle. In those cases, the fractures produced were perpendicular to the edges, usually at a 90 degree angle of a main fracture, in the surface or inside particles.

The second group (secondary alterations) included a set of particles formed by combined characteristics of the basic morphotypes defined. In this group, three types of particles were identified:

D) Strong reflectance change and cracks (Coke particles) (Table 26, D): these particles were characterized for a substantial reflectance change, which was accompanied for fractures and cracks produced by the volatile release. The formation of these particles can be explained in terms of the combination of the reaction conditions developed for particles A and C, being particularly exacerbated at high temperatures, allowing coal particles to develop a plastic phase, similar than these seen during the coke formation.
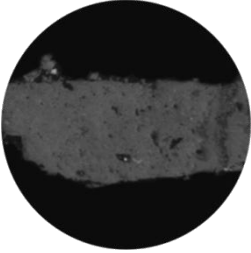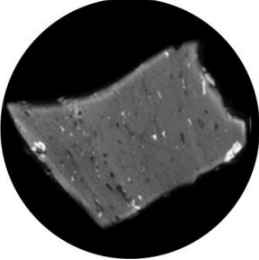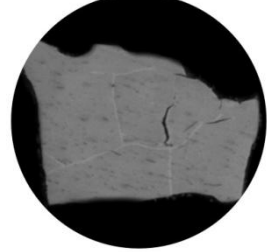
E) Simultaneous reflectance change and oxidation rims (Table 26, E): these particles were characterized for a partial reflectance change across the particle, also accompanied by a strong oxidation in the particle surface forming external rims. The formation of these morphotypes was due to the combined reaction conditions observed for particles A and B.

F) Internal oxidation lines (Table 26, F): these particles were characterized by paler lines across the particle, similar to oxidation rims. These lines follow formed cracks and fissures, and also follow weakness regions of the material from which oxygen diffused. The formation of these particles was explained by similar reaction conditions than these seen for particles B and C.

In parallel to this investigation similar research was carried out simultaneously in collaboration with the Self-oxidation Working Group (SWG) of the International Committee of Organic Petrology (ICCP). In this case, there were identified thermal alterations of coal particles obtained from different natural coal fires. In this study there were identified: natural chars, darker oxidations rims, pyrolitic carbon,

particles with plasticised edges, and isotropic-anisotropic coke particles [240]. However, these were not observed in the samples studied at Nottingham.

Table 26: Micrographs of the main thermal alteration identified

A		Homogeneous change of reflectance (across the whole particle)
B		Paler in colour oxidation rims (in the particle surface)
C		Cracks and Micro fractures (90° to the edge or following a circular curve)
D		Substantial reflectance changes and cracks (Coke)
E		Simultaneous change of reflectance and oxidation rims
F		Internal oxidation lines (similar to pseudo vitrinite)

Considering the morphotype definitions, Figure 79 shows a diagram with the proposed particle classification, including the relationships with the characteristic reaction regimes that promote their formation.
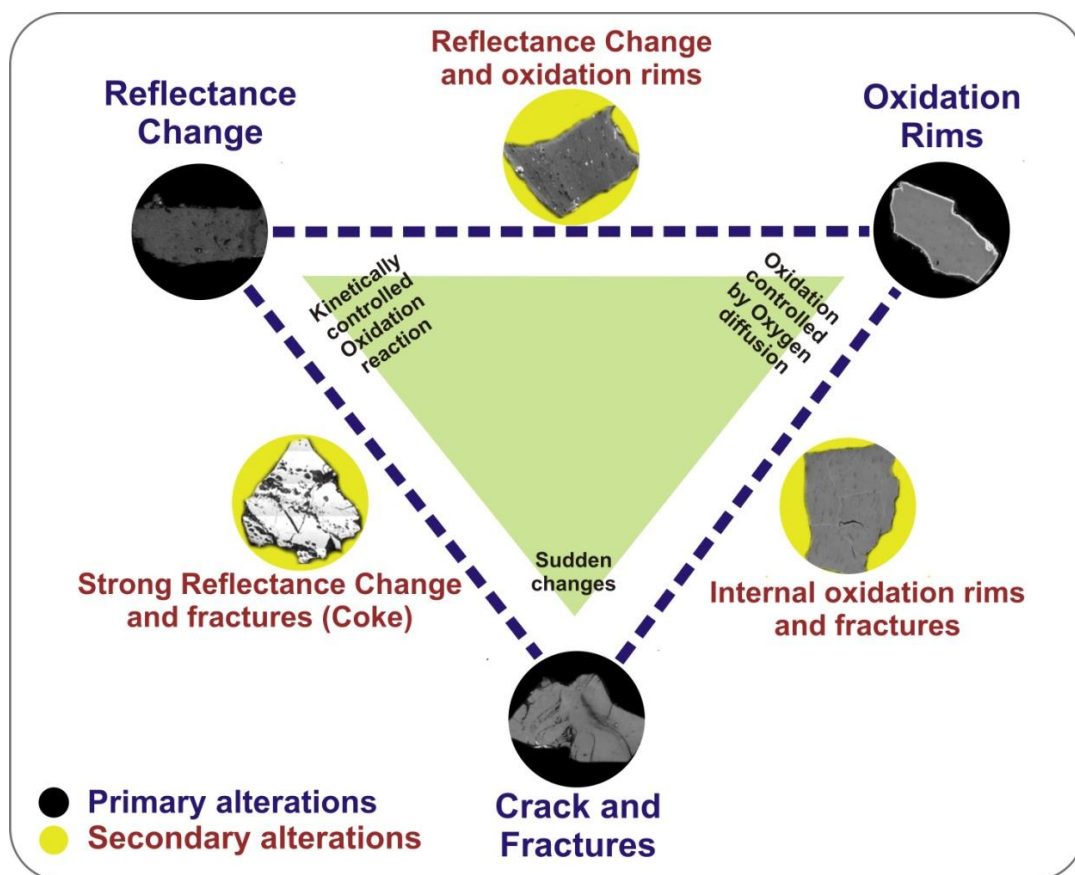
Figure 79: Classification proposed for primary and secondary morphotypes found in thermally altered coals and their respective reaction regimes.

In order to study the dependency of morphotype formation with the reactivity properties of the coal samples, a petrographic test was carried out to quantify the concentration of each morphotype. Coal particles were classified in one of the followings categories: a) unchanged material; b) homogeneous reflectance change; c) oxidation rims; and d) high reflectance particles (the results of this test are shown in Table 27). In these tests, the internal oxidation lines and cracks or micro fractures were not considered, due to their low concentration and the complexity of

identification. Finally, the link between morphotypes and spontaneous combustion is discussed in Section 5.3.

Table 27: Morphologic characterization of oxidized samples

Coal	Altered material (%)	Homogeneous reflectance change (%)	Oxidation rims (%)	High reflectance (%)
Fenosa	99.4	91.4	6.8	1.2
North Dakota	87.4	86.3	1.1	0.0
Hunter Valley	50.7	16.7	34.0	0.0
La Loma	48.7	12.7	29.3	6.7
Nadins	45.3	11.3	24.7	9.3
Indo	40.7	10.0	26.7	4.0
Kaltim Prima	39.3	11.3	27.3	0.7
Asfordby	33.3	11.3	20.0	2.0
Yanowice	33.3	6.0	26.7	0.7
Ironbridge	39.3	6.7	32.7	0.0
EDF	33.3	8.7	22.7	2.0
Cerrejon	31.3	13.3	16.7	1.3
Littleton	31.3	8.7	17.3	5.3
Bentinck	30.0	10.7	17.3	2.0
Blue Creek	28.7	5.3	21.3	2.0
Daw Mill	26.0	3.3	20.7	2.0
La Jagua	24.9	4.0	20.8	0.0
Lea Hall	23.0	7.4	12.2	3.4
Goedehoop	20.0	3.3	16.7	0.0
Illinois 6	18.7	8.1	6.3	4.4
Zondag 1	18.0	3.3	14.0	0.7
Pocahontas	11.0	0.6	8.0	2.5
Kleinkopje	4.0	0.0	4.0	0.0
Deep Navigation	4.0	0.0	4.0	0.0

5.2.2 Changes in light reflectance due to oxidation

The change of reflectance in coal particles through oxidation processes has been widely studied [183,182,114,126]. This was one of the most evident changes that coal samples suffer when heated. At low temperature, these changes are gradually produced, clearly dependant of the period of time for which they are exposed to the temperature variation.

Coal particles were heated from ambient temperature to 250°C (by using the same heating rate previously described), exposed for 460min (7.7hr) to the gradual thermal stress. Under these conditions, significant changes in light reflectance were observed in all the different maceral components. In order to compare these variations with unaltered coal properties, the reflectance of the single maceral vitrinite was measured for all the oxidized coals and compared with the original values. For this, two different methods were used to assess reflectance changes. The first method used classic rank analysis by using a reflectometer attached to the optical microscope (described in Chapter 3, and reported in Section 5.2.2.1). The second used a new approach developed by using image analysis, in which the reflectance changes were simultaneously measured for a large number of particles (Section 5.2.2.2).

5.2.2.1 Manual rank analysis to quantify reflectance changes

Light reflectance of oxidized coal particles was performed following the same procedure described in the British Standard for coal rank analysis [105]. The main advantages of this procedure were: a) It was a standardized technique, widely used by the coal industry; b) It allowed a direct comparison between maximum, minimum and average reflectance; c) no post processing of the data was required. However, this method was time consuming, particularly with the large number of samples involved. Also, it was highly dependent on operator discernment. Table 28 shows the results obtained from this test, including the relative difference compared to the original rank values of each coal (reported in Section 5.1.2).

As expected, the largest changes were found in low rank coals, with variations of up to 45%. In the opposite case, high rank coals showed the smallest change varying from 1 to 3%. These changes were always positive (reflectance of the oxidized samples was higher than the value measured for the original coal samples).

Table 28: Reflectance change of oxidized coal particles

Coal	Reflectance (oxidized particles, %R)	Change (relative to original coal, %R)	% Change
North Dakota	0.59	0.18	45.0
Nadins	0.90	0.23	33.4
Fenosa	0.53	0.13	32.5
Hambach	0.42	0.10	31.9
Daw Mill	0.67	0.12	22.0
Kaltim Prima	0.65	0.11	20.4
La Loma	0.64	0.09	17.4
Asfordby	0.61	0.09	17.1
Indo	0.72	0.10	16.0
Zondag 1	0.71	0.10	15.5
Hunter Valley	0.89	0.11	14.3
Goedehoop	0.67	0.08	12.9
Cerrejon	0.63	0.06	11.2
Ironbridge	0.62	0.06	10.4
Lea Hall	0.66	0.06	10.3
EDF	0.75	0.07	10.1
Illinois 6	0.45	0.04	10.1
Littleton	0.71	0.06	10.0
Bentink	0.82	0.07	8.6
La Jagua	0.61	0.05	8.1
Yanowice	0.73	0.05	8.1
Kleinkopje	0.78	0.03	3.0
Pocahontas	1.36	0.03	2.4
Blue Creek	0.98	0.02	2.3
Deep Navigation	1.68	0.03	2.1

The reflectance of fresh and oxidized coals is shown in Figure 80. This relationship can be adjusted by a linear trend with a satisfactory deviation coefficient (r^2=0.972), which confirmed a linear tendency. In the same figure, the blue line represents the unchanged reflectance scenario. From this, it can be seen that low rank coals reflectance varied considerably more than high rank samples, from which some

particular samples were noticeably out of the trend (North Dakota, Fenosa, Nadins, and Hambach coals).
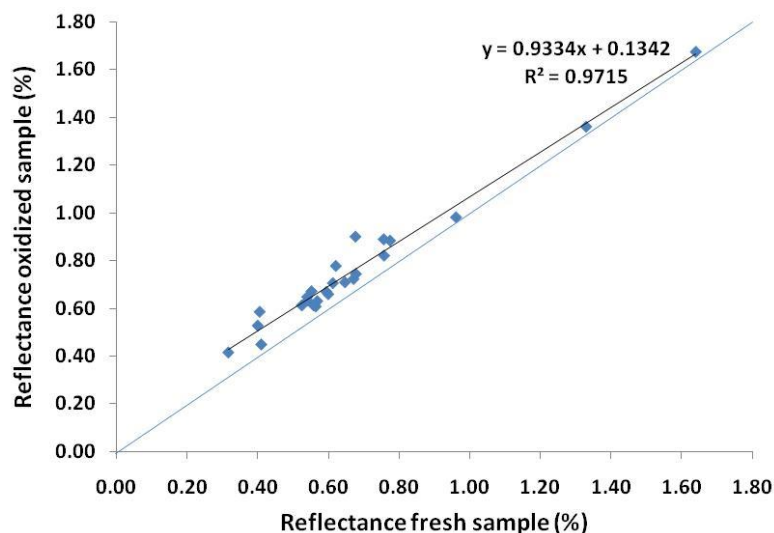
Figure 80: Comparison of reflectance between fresh and oxidized samples.

The particular transformations suffered by low rank coals were studied by using the reflectance histogram. As an example, Figure 81 shows histograms for two representative samples. A horizontal displacement of the reflectance values for the oxidized coals compared to the original sample can be seen. This histogram shape suggests that the average reflectance of oxidized low rank coals is formed by the contribution of changes suffered in all the coal particles. The displacement was more pronounced in these two particular coals, and was characteristic of highly reactive samples.

Conversely, high rank coals showed insignificant changes in the reflectance histogram. Figure 82 shows two profiles for this type of high reflectance coal. For these coals, histograms were slightly displaced, reflecting a decrease in the number of particles with low reflectance, with high reflectance particles keeping their original reflectance values. For this type of coal, a high number of particles with oxidation rims were observed that could also explain the minor shift of these curves.
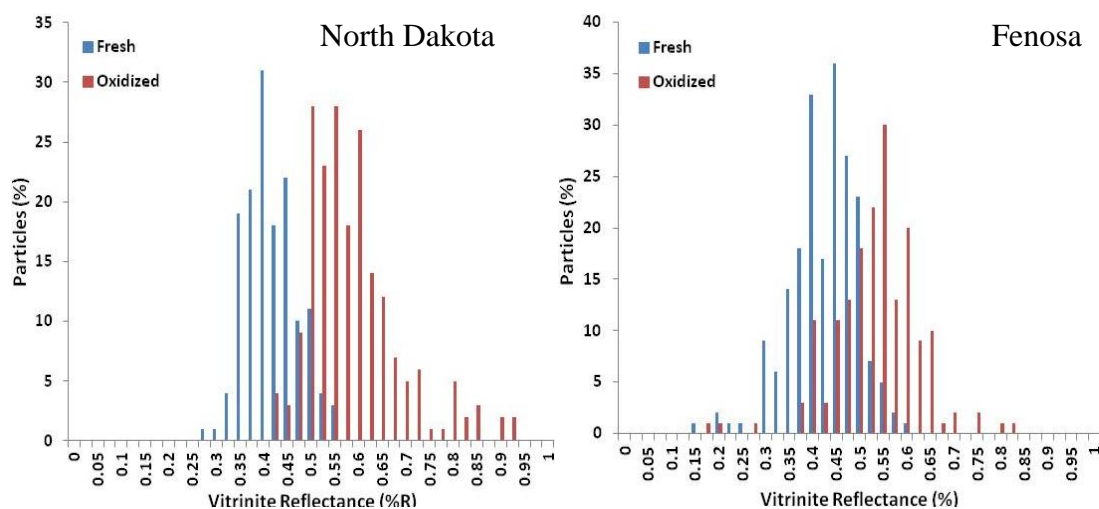
Figure 81: Reflectance histogram of North Dakota and Fenosa, both low rank coals.
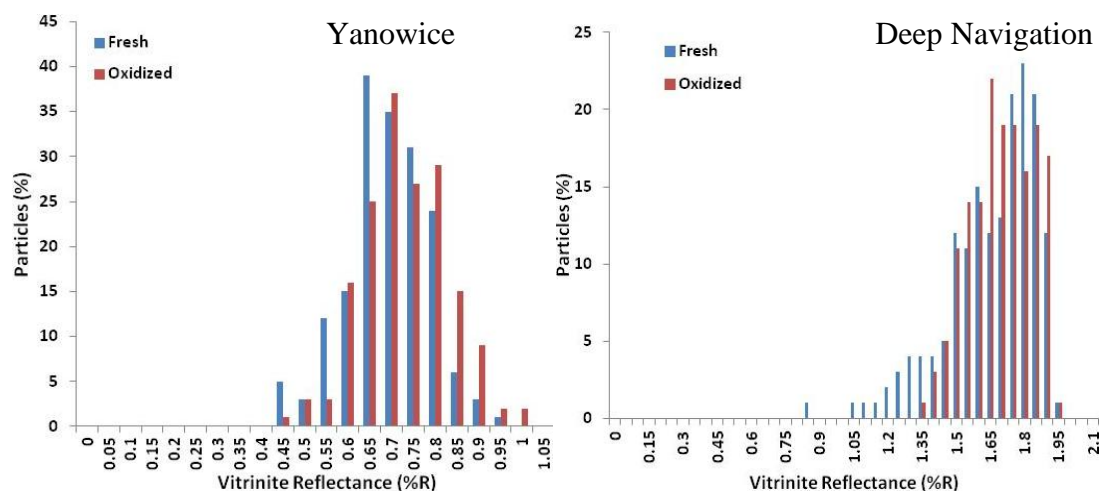
Figure 82: Reflectance histograms of two high rank coals.

In regard to the original physical properties of coal samples, Figure 83 shows that the highest reflectance changes were produced in samples with high moisture and low carbon content. An equivalent pattern occurred in the high rank coals, where the smallest changes occurred in samples with low moisture and high carbon content. These observations suggested that the reflectance change could also be associated with the initial physical properties of the original coal samples.
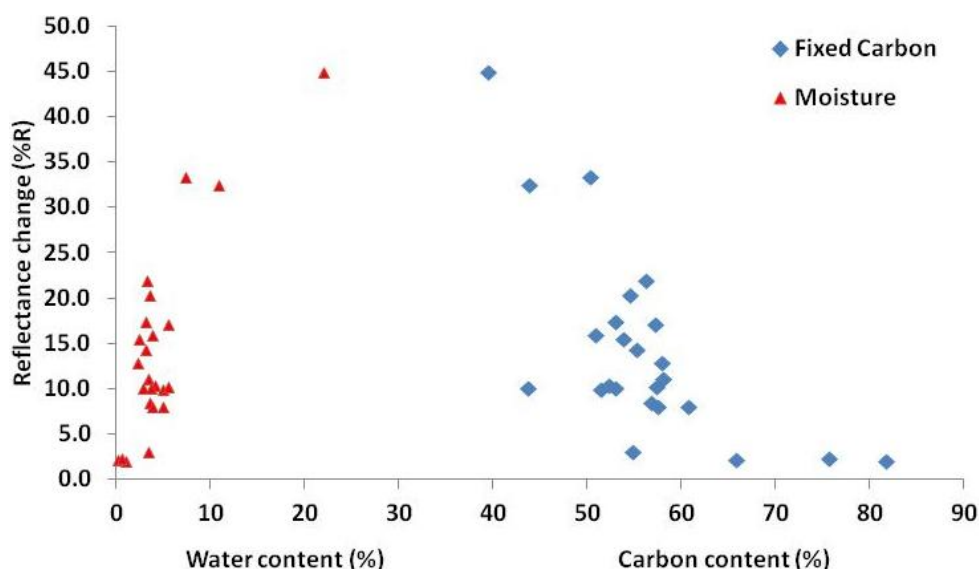
Figure 83: Initial water and carbon content, related to the sample reflectance change.

5.2.2.2 Changes in light reflectance estimated by using image analysis

A second method was performed using image analysis. In this case, colour mosaic images were initially obtained from the petrographic blocks made from fresh and oxidized material. These mosaics images were formed by 15 by 15 single images (225 in total); comprising a total sampling area of $1.2cm^2$, which contained approximately 1000 coal particles in the range of 53 to 75µm. Subsequently, these images were transformed to grey scale level to produce a image histogram; both by using the algorithms developed in Labview (described Chapter 3). These histograms were then used to quantify changes in vitrinite reflectance, which were linked to the spontaneous combustion problem (Section 5.3).

The main advantages of this procedure were: a) It allowed an analysis of a much larger number of particles per sample, minimizing the associated standard deviation; b) this method allowed a fast processing for a large set of samples, once the algorithm was implemented; c) it also avoided the introduction of human errors associated to the identification of the vitrinite maceral; and d) it was flexible to quantify the reflectance changes produced in all maceral components, rather than just

the vitrinite. However, this method also showed some drawbacks. Initially, as it was a new experimental method, the results are difficult to be compared with other independent research. In addition, the implementation of the algorithm was complicated, particularly regarding to the image post processing that required elevated programming resources. The results obtained were also variable and difficult to condense in a single value that represents the general trend of each coal. Finally, there was the possibility of introducing systematic errors during the image post processing, which were impossible to quantify directly.

For each coal, a representative image histogram was obtained after a series of histogram thresholds to remove the background mounting media and the high reflectance particles corresponding to fusinite and semi-fusinite macerals. This procedure was implemented for fresh and oxidized samples. Some images are shown in Figure 84. From this figure, the change in brightness in the vitrinite particles can be clearly differentiated (analogous to the reflectance change).

Subsequently, grey scale histograms were obtained from the images for all the samples. These histograms were a graphical representation of the total number of pixels per each grey level, plotted against the 256 different levels used in this type of image. An example can be seen in Figure 85.

After this, image histograms were standardized to reduce the effects produced by background removal. The standardization proposed was the conversion of the total number of pixels per grey level to percentage (considering the final number of pixels in each histogram); and the transformation of the grey scale levels to reflectance units. The last adaptation was made considering a direct relationship between reflectance and grey scale, deduced from the microscope calibration (procedure described in Chapter 3). An example of these transformations is shown in Figure 85.
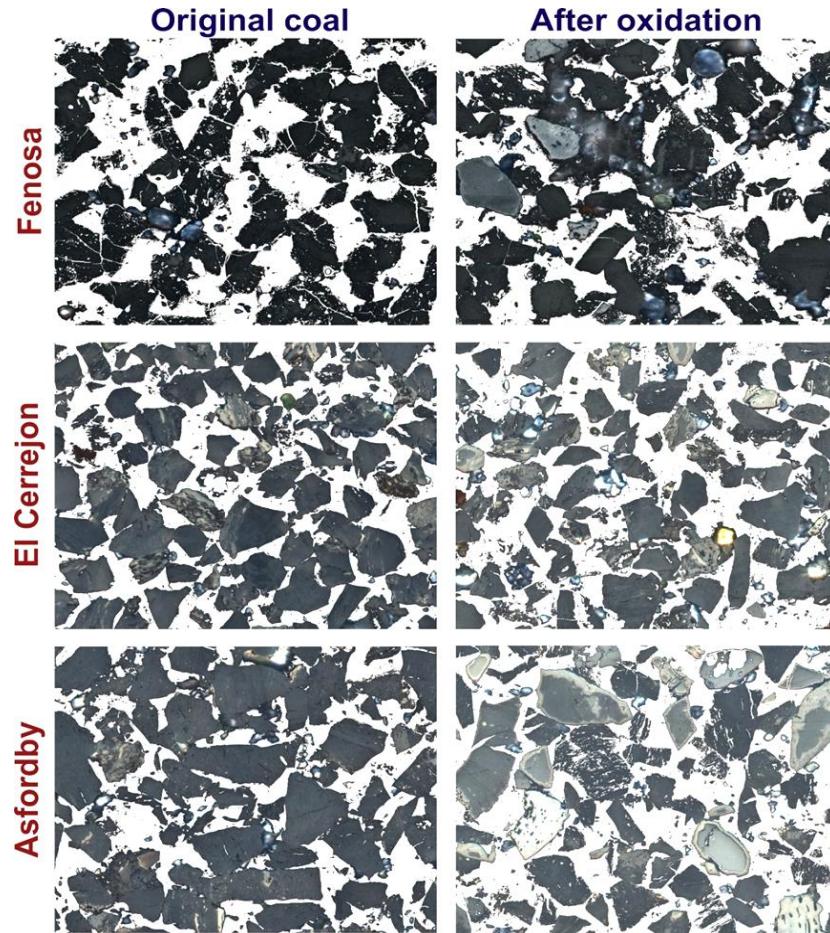
Figure 84: Resulting mosaic images for three representative coal samples.
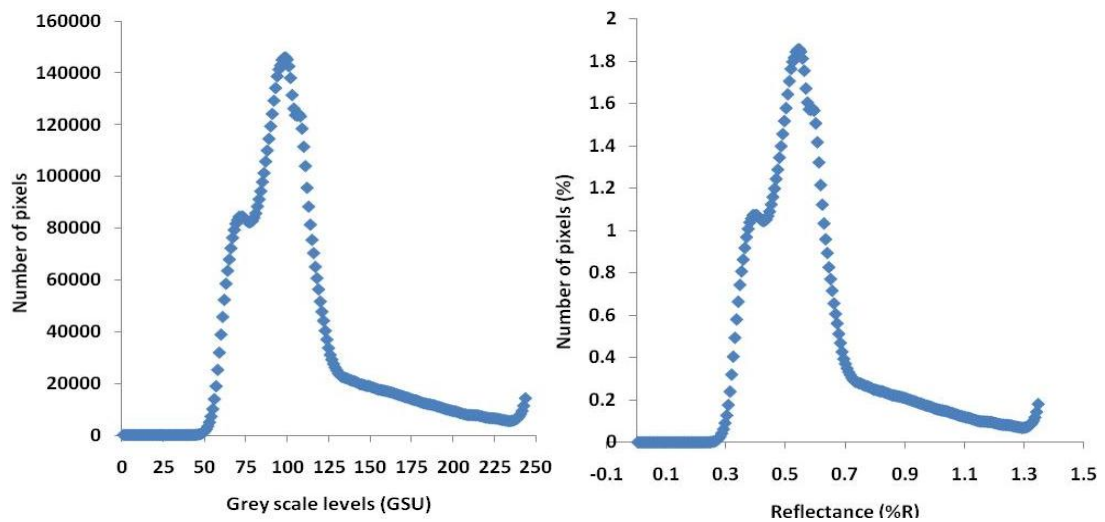
Figure 85: Example of the standardization of number of pixels per image.

Finally, the image histogram of each coal was obtained from an average of the reflectance ($R_{avg}(\%)$) using the equation 14:

$$\text{Equation 14} \qquad R_{avg}(\%) = \sum_{i=0}^{256} \frac{R_i \cdot Pix(\%)_i}{100}$$

In which i represent the number of levels of the histogram (256); R, the correspondent reflectance value; and $Pix(\%)$, the pixel percentage value associated. Then, by using the Equation 14 it was calculated the average reflectance of all the coal samples (original and oxidized material). This information was also used to estimate the reflectance change produced by the thermal treatment (Results shown in Table 29).

Table 29: Average reflectance values obtained from mosaic images

Coal	Avg. Reflectance fresh (%R)	Avg. Reflectance oxidized (%R)	% Change
Fenosa	0.391	0.424	8.4
Illinois 6	0.401	0.435	8.4
North Dakota	0.412	0.447	8.7
Ironbridge	0.478	0.539	12.6
Kaltim Prima	0.495	0.564	14.0
La Jagua	0.497	0.551	11.0
Nadins	0.499	0.732	46.7
Asfordby	0.501	0.585	16.8
Daw Mill	0.508	0.625	23.0
Bentink	0.513	0.586	14.2
Lea Hall	0.525	0.605	15.4
Indo	0.533	0.607	14.0
Cerrejon	0.533	0.624	17.0
La Loma	0.559	0.625	11.7
EDF	0.574	0.637	11.1
Yanowice	0.580	0.620	6.8
Hunter Valley	0.596	0.738	23.8
Littleton	0.616	0.729	18.4
Blue Creek	0.640	0.694	8.4
Deep Navigation	0.675	0.696	3.1
Pocahontas	0.733	0.798	8.9
Zondag 1	0.757	0.806	6.4
Goedehoop	0.823	0.905	10.0
Kleinkopje	0.839	0.847	0.9

The result obtained for 3 representative samples is shown in Figure 86 (same coals used in Figure 84).
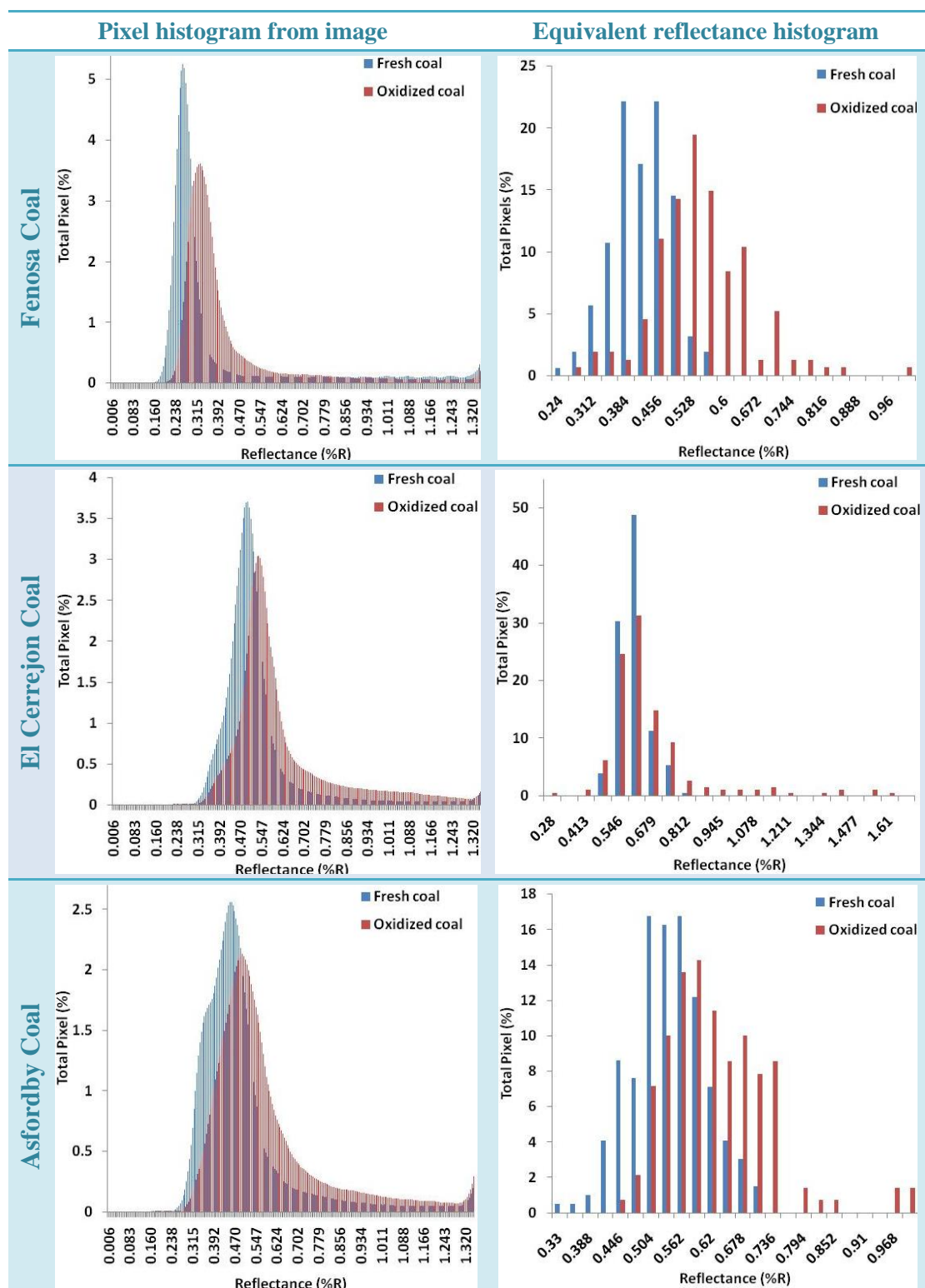
Figure 86: Standardized pixel histograms for 3 representative samples (left), and their equivalent histogram obtained by manual rank analysis (right).

Regarding to the reflectance values obtained by using this approach, results differed considerably from those obtained by manual rank analysis. A graphic comparison (Figure 87) shown that the image analysis (IA) estimates were closer to the manual rank results at low reflectance values. However, for medium and high rank values these differed significantly. These differences can be explained by the calibration of the microscope-camera system, which was performed using a sapphire standard that provides a good approximation for coals with rank values close to 0.6 ± 0.1 %R. For coals with reflectance values significantly higher than this (difference larger than 15%), the estimation showed a huge variation. These results confirmed the difficulties in estimating the average reflectance from images.
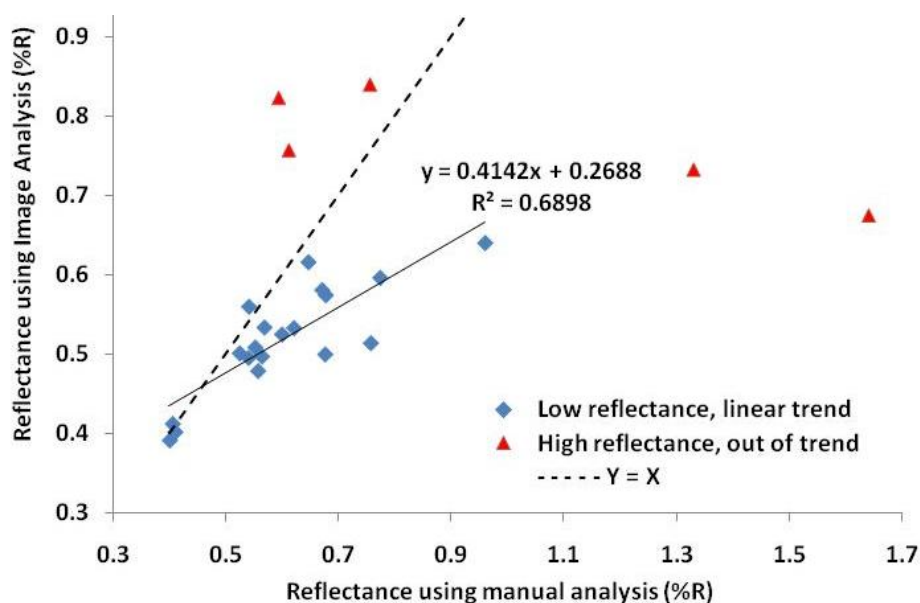
Figure 87: Comparison between reflectance values of fresh samples obtained by manual analysis and image analysis.

Regarding to the differences in reflectance for fresh and oxidized samples by using IA, in Figure 88 is shown a graphic comparison between these two set of results (similar to Figure 80 for manual analysis). From this figure, it can be seen that the estimations follow a linear trend with a deviation coefficient of $r^2=0.8658$. In this

195

case, the difference between fresh and treated samples is small, and the largest differences can be observed for the intermediate samples (column *% change*, Table 29). The discrepancy of these results also affects a possible relationship between this data and the historical information about spontaneous combustion propensity. In this context, no positive association was found. Finally, the differences observed between the manual rank analysis and the automated analysis showed that average reflectance obtained by image analysis was not a simple way to detect and quantify the changes produced by the oxidation.
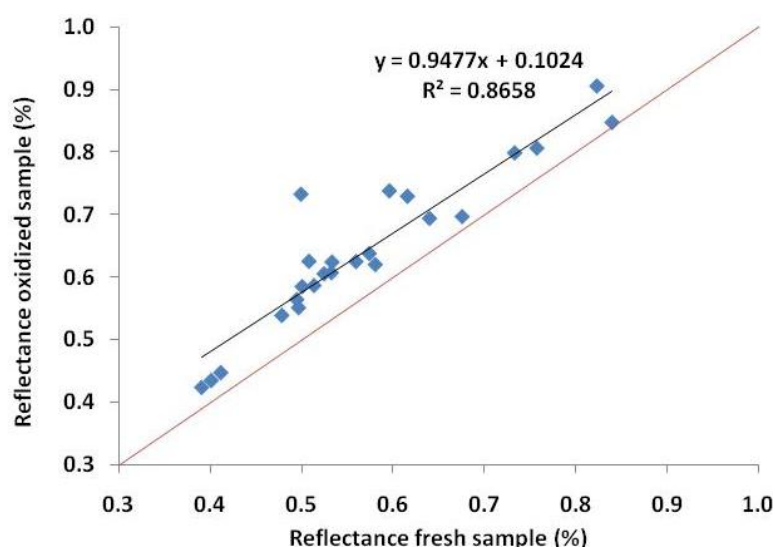
Figure 88: Relationship between reflectance values of fresh and oxidized samples obtained by image analysis.

Despite of these initial results, valuable information was produced from the image histogram. A second alternative was developed to quantify the impact of the reflectance change. This consists of a direct arithmetical comparison of the image histograms for fresh and oxidized samples. As can be seen in Figure 89, this arithmetical difference provides information about where the reflectance change starts and ends, suggesting the magnitude of the material lost or transformed during the heating. Then, from the subtracted curve some key points were identified:

First, two peaks were identified corresponding to the transformed material (positive, left), and the material with new reflectance values (negative, right). As both histograms were previously standardized, the area below these peaks was identical, representing the total percentage of altered material in the sample. Secondly, a single point in which the material started the transformations was identified (e.g. ~0.254 in the figure); and an inflection point in which the curve change from a positive to a negative peak (e.g. ~0.602 in the figure).
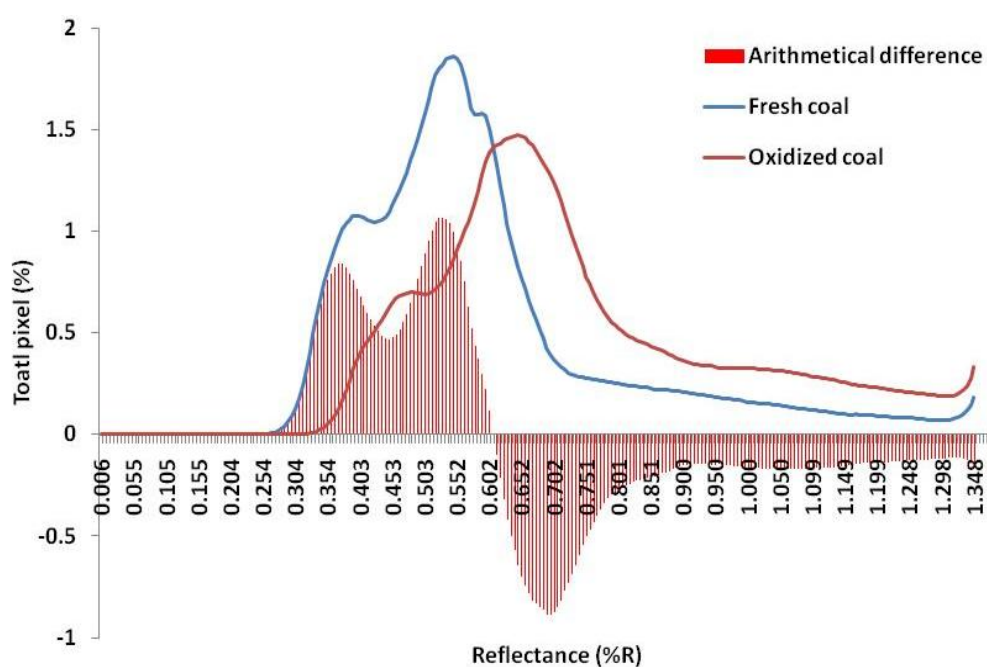
Figure 89: Arithmetical difference of histograms for fresh and oxidized coals.

This information (quantified for all the samples in Table 30) shows a clear link with the statistics about propensity for spontaneous combustion, in which the most reactive samples showed the biggest material transformation. These results were complemented with the information about thermal morphotypes, discussed in Section 5.3.2.

Table 30: Characteristic parameters obtained from histogram subtraction

Coal	Starting (%R)	Inflection (%R)	Peak area (%)
Nadins	0.26	0.54	68.72
Fenosa	0.15	0.30	50.74
North Dakota	0.17	0.32	49.60
Daw Mill	0.23	0.49	40.52
Hunter Valley	0.27	0.61	35.86
El Cerrejon	0.29	0.52	32.61
Lea Hall	0.26	0.52	31.75
Littleton	0.30	0.65	30.95
Ironbridge	0.22	0.50	28.15
Bentink	0.24	0.56	28.06
Kaltim Prima	0.25	0.52	27.24
Indo	0.26	0.54	26.74
La Jagua	0.33	0.48	26.71
Asfordby	0.27	0.50	26.34
Illinois #6	0.18	0.33	24.77
EDF	0.29	0.53	20.48
La Loma	0.26	0.56	19.72
Blue Creek	0.24	0.72	19.65
Goedehoop	0.39	0.69	17.58
Deep Navigation	0.20	0.43	16.20
Yanowice	0.27	0.60	14.04
Pocahontas	0.28	0.80	13.73
Zondag 1	0.36	1.01	12.69

Finally, the amount of material transformed (peak area, Table 30) was also related to the reflectance values (calculated by using IA, and shown in Figure 90). However, as the reflectance data was influenced by the calibration of the image acquisition system, this trend might also differ considerably from the real data. Despite this 'relative' error, it was demonstrated that the image histogram could be used to successfully quantify the impact of the thermal heating in coal samples.
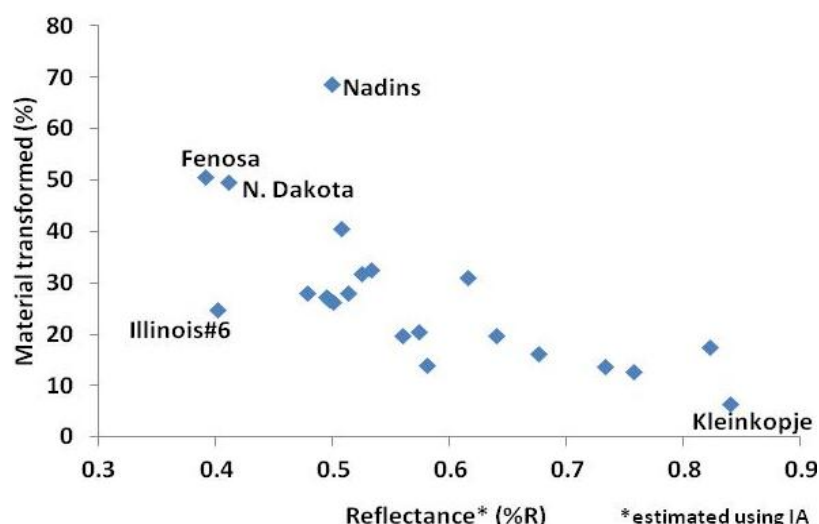
Figure 90: Total material transformed as a function of reflectance.

5.3 Petrographic characteristic of coals prone to spontaneous combustion

In this section, the optical characteristics of coals prone to spontaneous combustion are discussed. These features were established by considering simultaneously the results obtained from the different petrographic tests carried out, and the information about spontaneous combustion of the studied samples. Particularly, it is discussed i) the estimation of the sample propensity based on the reflectance changes and the coal morphology (Section 5.3.1); and ii) the relationship between the different morphotypes created with their respective image histogram (Section 5.3.2).

5.3.1 Reflectance change and coal morphology of prone coals

The light reflectance of coal was considered an important source of information due to its implications with the physical and chemical properties of samples. As previously explained, the variation of this property during oxidation could be related to the spontaneous combustion phenomenon, and experimental results showed that this was an important characteristic developed during the coal heating. This variable could be used to evaluate specific sample characteristics that are difficult to measure using other techniques such as porosity evolution, the identification of the reaction

regimes developed, and the characteristics of the physical transformations in the material.

5.3.1.1 Direct link between the reflectance change and coal propensity

Considering the reflectance change as an independent variable, the first observed association was the direct link between this parameter and the historic statistical data about coal propensity. This initial association is presented in Figure 91. Despite certain discrepancies, an agreement between the historic information and the reflectance variation was observed. There was also a significant difference between the reflectance changes obtained for prone coals compared to the remaining samples, allowing a clear differentiation. Regarding samples in this relationship (e.g. El Cerrejon and Illinois #6 coals), the potential of these samples to absorb oxygen introduce important variations in the reflectance value obtained, which could explain the significant observed differences.

This initial proposed relationship can be strengthened by oxygen adsorption tests in the TGA. The results of this test were directly associated to the chemical mechanism proposed for the spontaneous combustion reaction, and the reflectance change was inversely proportional to this variable (shown in Figure 92). This means that coals with no signal of oxygen adsorption suffered the bigger reflectance changes, and coals with the largest oxygen adsorption showed, at the same time, the lowest reflectance variation. This suggests that the reflectance changes observed at low temperature can be a consequence of the spontaneous combustion reaction.

The mechanism considering the effects in the coal reflectance is given as follows: In the case of prone coals, these samples tend to react fast and homogeneously, creating unstable solid complexes in the carbon matrix produced by the interactions between coal and oxygen. These unstable solids are rapidly desorbed, producing chemical

alterations in the carbon matrix generating a reflectance change. In the case of unreactive or low reactive samples, these coals tend to absorb less oxygen creating more stable components, which are not immediately desorbed (justified by the observed weight increase). These solids remain attached to the coal matrix, introducing just slight changes to the reflectance of particles. Subsequently, it was concluded that the magnitude of these reflectance changes observed was proportional to the total chemical activity suffered by the sample. This supports the initial idea that propensity to spontaneous combustion depends of the prevailing coal-oxygen interactions, which control the whole process (adsorption or desorption).
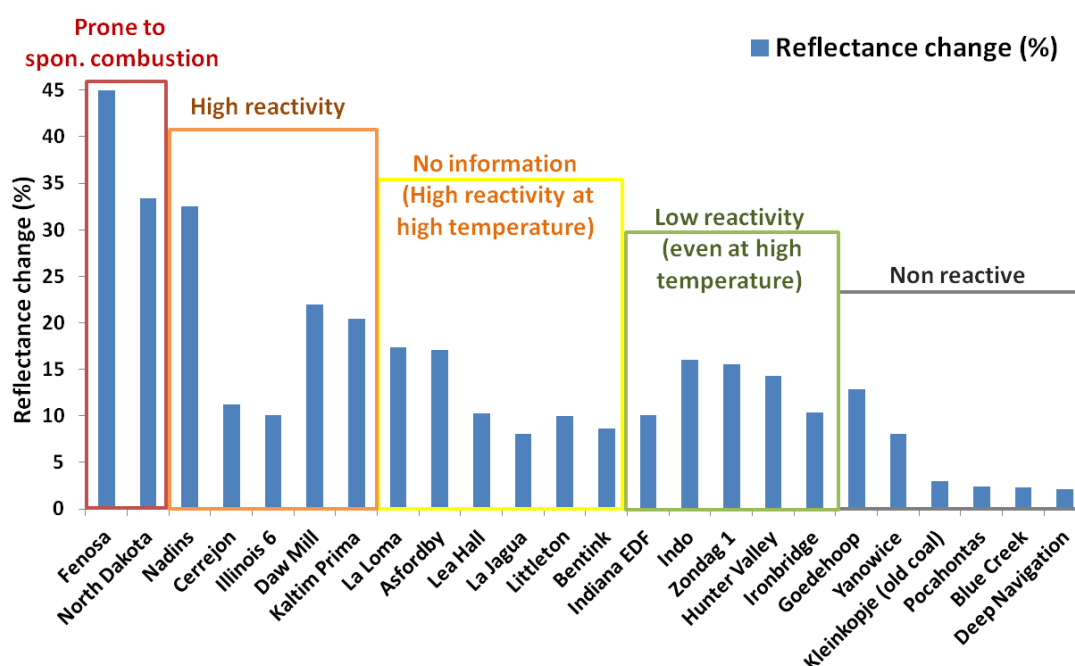
Figure 91: Relationship of reflectance change with the information hold about spontaneous combustion and reactivity of tested coals.

The reflectance change was a particular measurement that only uses vitrinite particles. Therefore, relating these variables (weight increase and reflectance change) with morphology changes in the altered coal would confirm the previous observations.
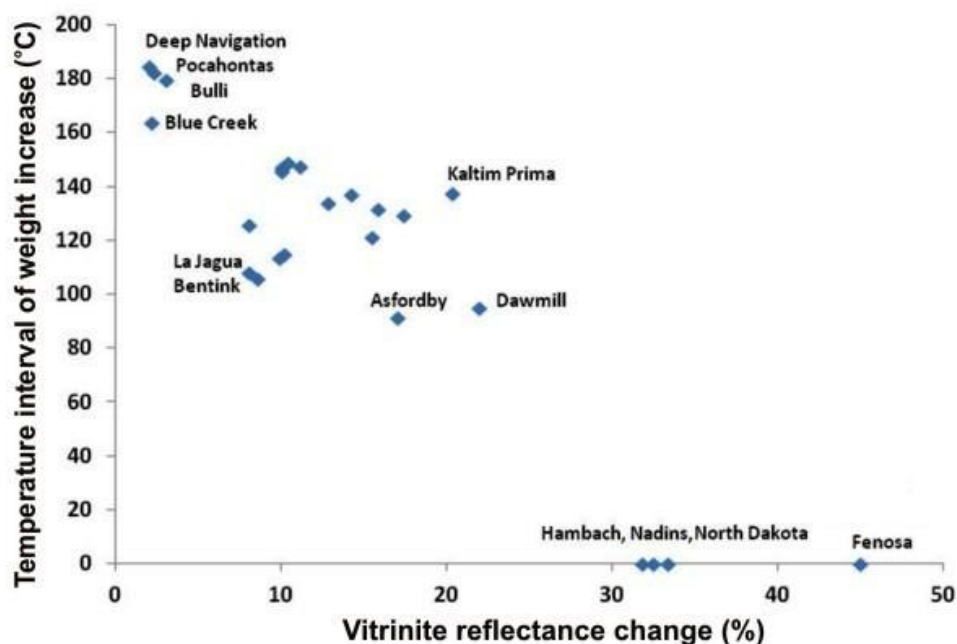
Figure 92: Association between reflectance change and temperature interval in which samples showed a weight increase under TGA (using a heating rate of 3^oC min^{-1}).

5.3.1.2 Reaction regimes developed in altered coal particles

In Section 5.2, each identified morphotype was explained as the result of an specific reaction regime developed, which were dependant of the textural and chemical characteristics of the particles (Figure 79). These initial assumptions were combined with the experimental results from the morphotype quantification (Table 27), confirming three types of interactions (proposed in the initial schematic). The specific details of these interactions are summarized in Figure 93.

From this categorization, a number of samples developed exclusively Type 1 interactions (approximate 95% of tested coals). This means that morphotypes found in these cases comprised all the possible combinations between "homogeneous reflectance change" and "oxidation rims" particles. This interaction was visible in coals from low to medium rank, when samples were heated smoothly at low temperatures (below 250^oC).
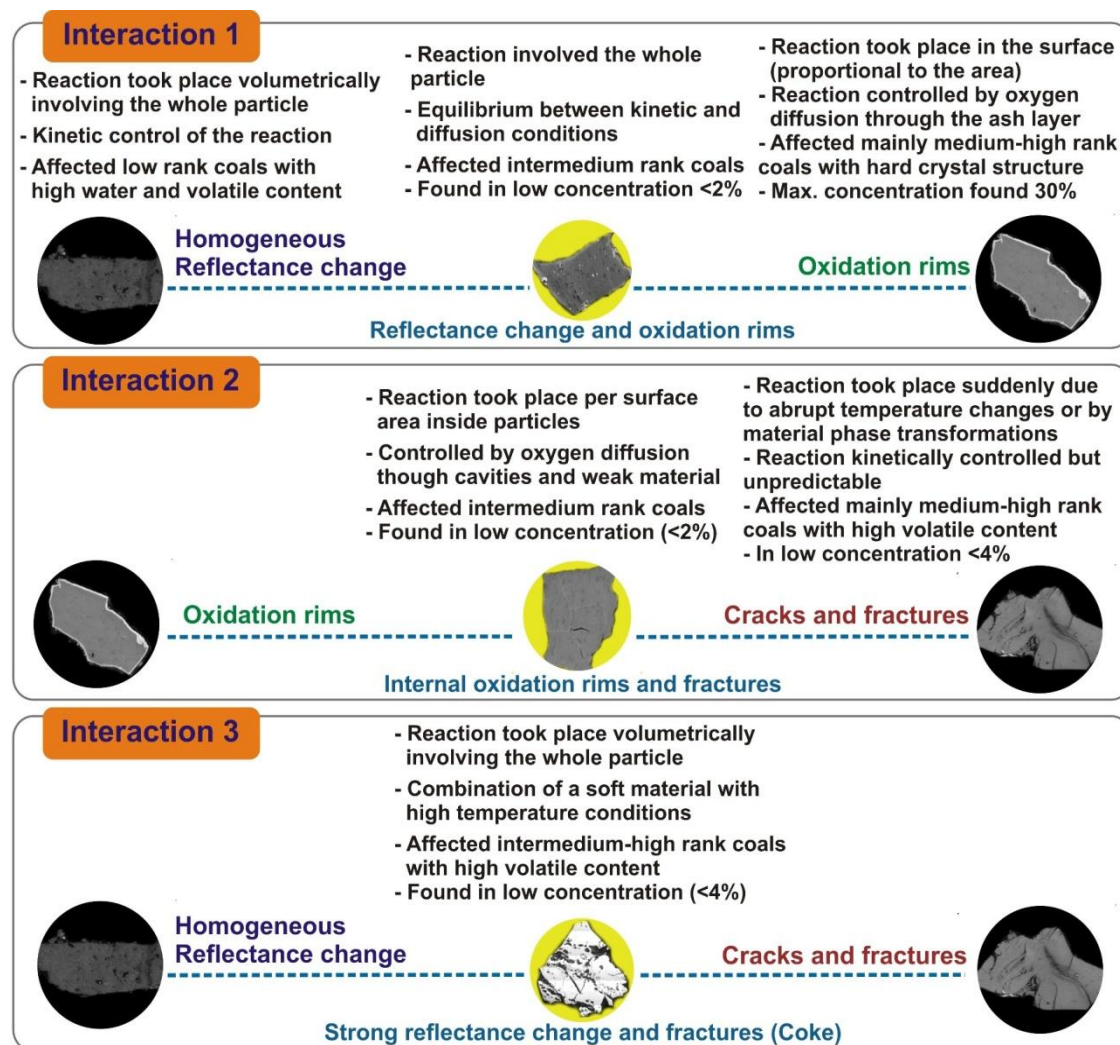
Figure 93: The three types of interactions based on the morphologic features.

In addition, type 2 interactions were only observed in a smaller number of samples. From parallel experiments carried out in a muffle furnace, it was confirmed that these interactions were developed when coal particles were exposed to considerable elevated heating rate environments (e.g. 5 to $20^{o}C$ min^{-1}), independently of their coal rank. Finally, type 3 interactions were observed in a minor number of samples. From parallel experiments in the drop tube furnace, it was confirmed that this interaction is entirely developed when coal particles are exposed to extremely high heating rates (e.g. 50 to $1000^{o}C$ s^{-1}), and was also independent of the coal rank. From all these observations, it was concluded that the different morphotypes are 'clues' about

oxidative conditions and the quantity of each indicates the history of the sample. From the morphologic alterations is possible to identify and quantify the impact of the oxidation reaction from a textural approach.

By considering the number of samples that developed interactions type 1, ψ was defined as the ratio between the "homogeneous reflectance change" and "oxidation rims" particles concentration. This ratio ψ represent the tendency of coals to create one type of morphotype over the other, when subjected to 'gentle' oxidative conditions (low temperatures and low heating rate). From this, samples were organized according to their ψ values and represented as a function of the "reflectance change" results (Figure 94). This figure shows that coals with the largest ψ values also showed the biggest reflectance changes, revealing a remarkable agreement with the previous results.
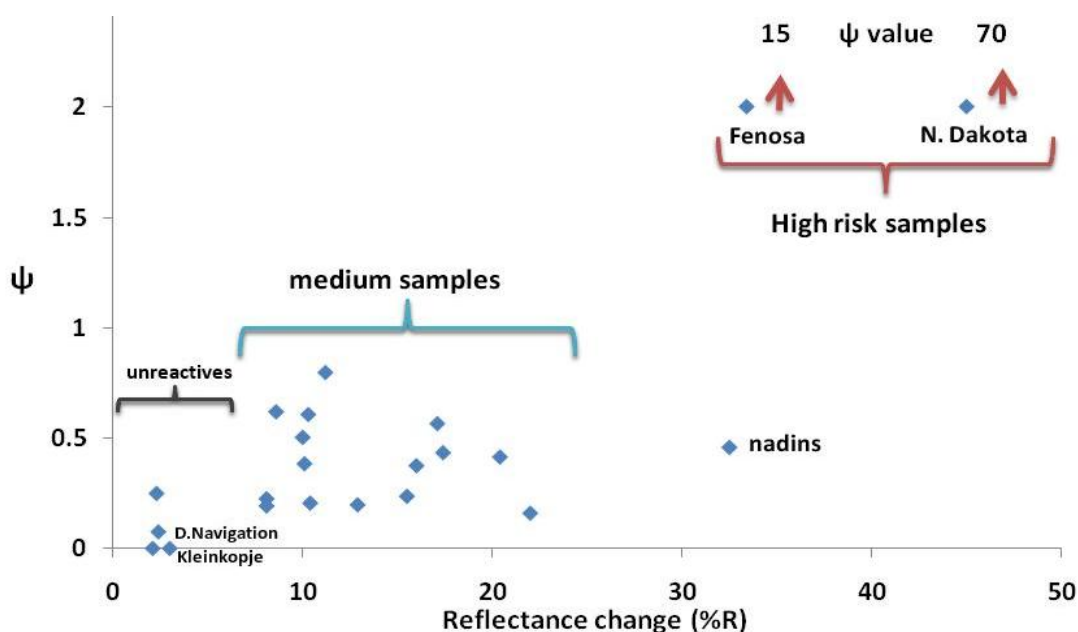
Figure 94: Ratio between "homogeneous reflectance change/oxidation rims" morphotypes as a function of the "reflectance change" test results.

5.3.1.3 Relationship of reflectance change, coal morphology and coal propensity

As discussed previously, the concentration of thermal morphotypes relates to the reactivity of the coal. Estimating the impact of the heating by measuring the reflectance change provides an even more valuable tool for understanding of the problem. Figure 95 shows the combined optical tests allowing a clear identification of the sample propensity.
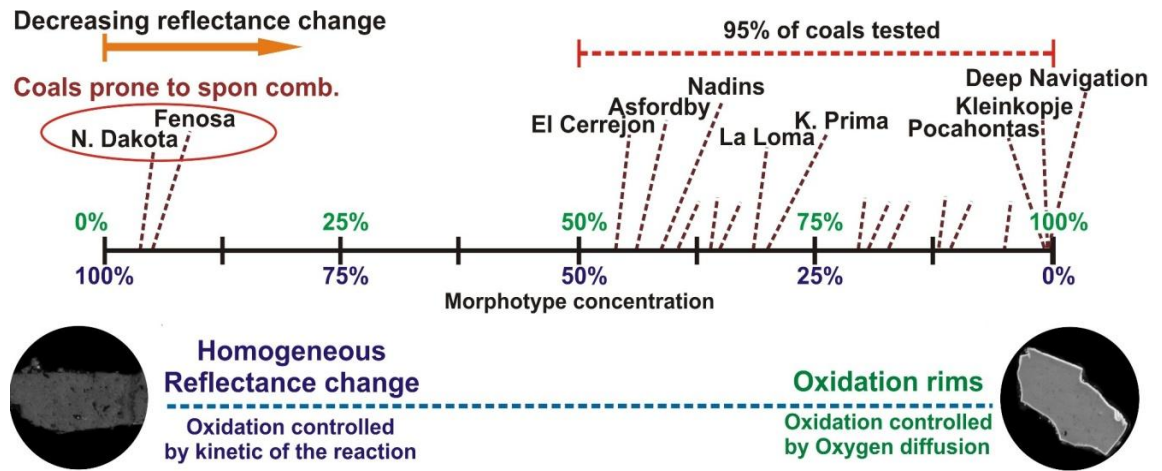
Figure 95: Combination of optical tests applied to the samples under study.

5.3.2 Characteristic image histograms from prone coals

It was shown that reflectance changes and the morphotypes created were both important parameters when identifying reactive samples. Considering these characteristics, the next stage was to develop an automated method to detect these features using image analysis. However, earlier experiments also showed that the reflectance change estimated by this approach produced unsatisfactory results. Consequently, a new method was developed to use the information obtained from the subtraction of the image histograms (shown in Section 5.2.2.2).

Previously, the characteristics of the resulting profiles from the histogram subtraction (Figure 89) were quantified for all the coals under study (results shown in Table 30). From this, the total amount of altered material (area below the peaks)

was compared with the results obtained from the manual petrographic test (Figure 96). The difference between methods was clearly significant, especially for the intermediate coals. This was due to the peak area of the subtracted histograms including all the macerals rather than just the vitrinite.
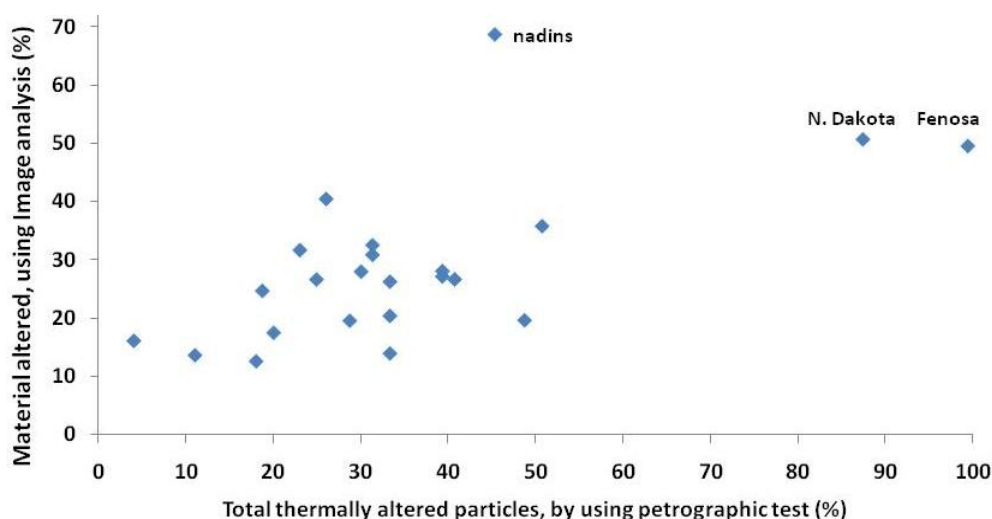
Figure 96: Comparison between the total material altered by using image analysis and the manual petrographic test.

The profiles of the subtracted histograms revealed characteristic features associated with different morphotypes. Figure 97 shows four representative samples. In these profiles, coals with high propensity to spontaneous combustion showed changes in reflectance (<0.3 %R), indicating a considerable proportion of altered material from the total sample (more than 45%). The height and narrow shape also indicated that most of the particles transformed their reflectance (samples with a high number of homogeneous reflectance change particles). For the intermediate coals, this showed a wider and less pronounced peak due to the combination of "homogeneous reflectance change" particles (the height of the peak) and the contribution of the high reflectance material from the oxidation rims created (displaces the inflection point to the right of the graph).
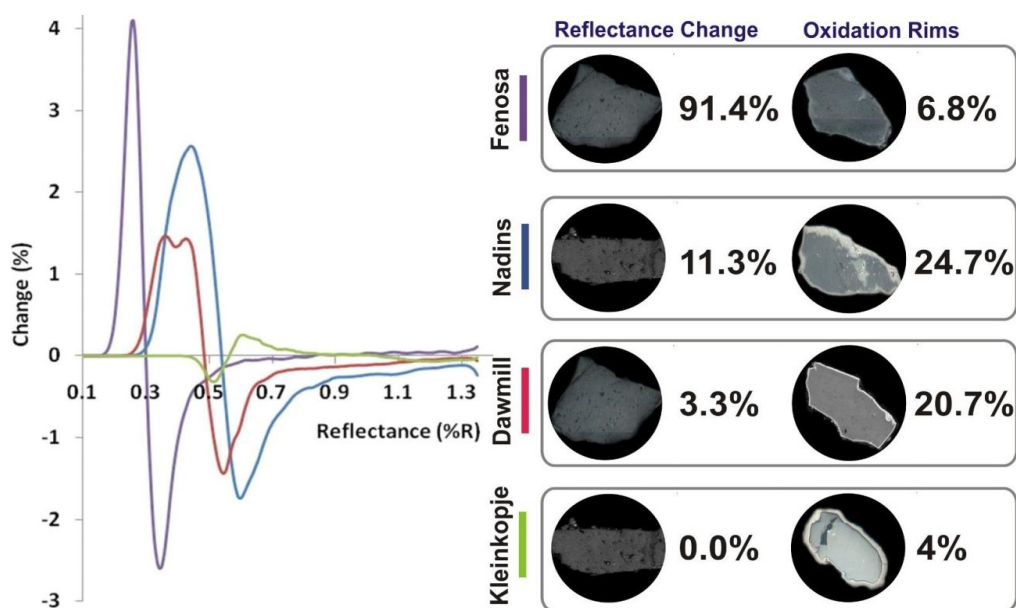
Figure 97: Subtracted histogram curve for four representative samples.

Finally, the unreactive coals tend to show a small peak to the right of the graph, produced by the larger proportion of particles with oxidation rims. The small peak area of these coals corresponds to the small fraction of material that was transformed. This qualitative description was confirmed by the experimental results of all the samples (Figure 98). From these, coals were clearly divided in four groups: a) coals prone to spontaneous combustion and b) high reactive coals (top figure); c) coals medium reactive (middle figure); and d) low reactive coals (bottom figure). Despite the discrepancies between the manual and automated petrographic testing, it was demonstrated that image analysis could be successfully used to quantify the impact of the thermal heating in coal samples. Further technological improvements in the image acquisition system, and enhancements in the image analysis method used, could provide a valuable tool to identify alterations in coals produced by thermal events that can be related to spontaneous combustion.
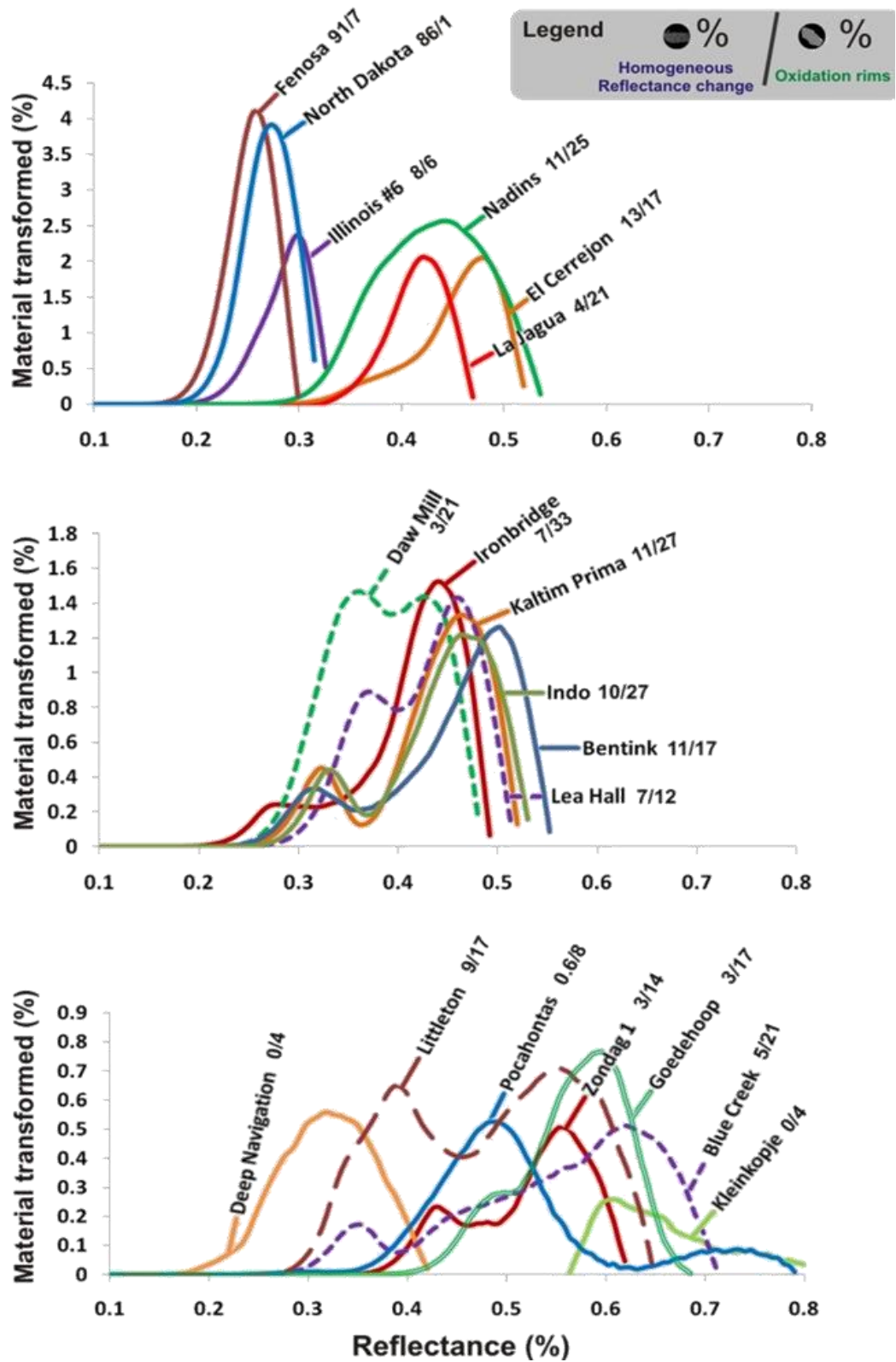
Figure 98: Subtracted histogram profiles (altered material), and the proportion of homogeneous reflectance change and oxidation rims particles present in each sample.

5.4 Relationship between optical properties and thermal reactivity of coals

A comparison of the optical properties and the thermal parameters studied was performed following the scheme shown in Figure 99. These associations allowed an evaluation of all the different tests developed, from which a set of testing procedures to identify coals prone to spontaneous combustion was finally proposed (Chapter 7).
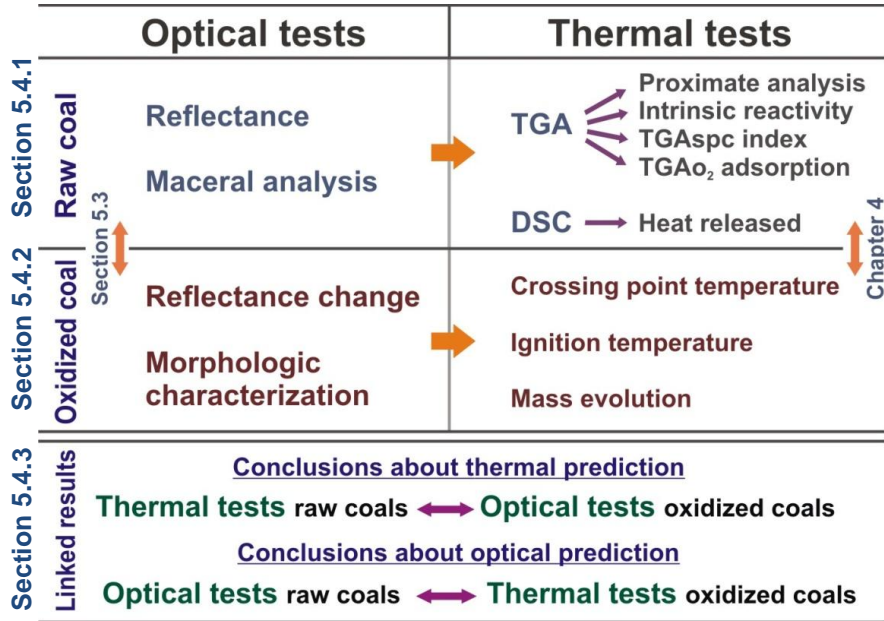
Figure 99: Evaluation scheme for the optical and thermal tests carried out.

5.4.1 Link between optical properties and reactivity of fresh coals

In this section, the results from microscopy and thermal tests of fresh coal samples are compared. The impact of rank and maceral composition on the reactivity at low temperature (TG_{spc} index, Section 5.4.1.1), in the oxygen adsorption (TGO_2 test, Section 5.4.1.2), and in the heat released (DSC, Section 5.4.1.3), was studied.

5.4.1.1 Influence of rank and maceral composition in reactivity at low temperature

For the TG_{spc} index, an inversely proportional relationship with the coal rank was observed (Figure 100). This agreed with the assumption that the reactivity of coals at low temperature is highly dependent on this variable. However, some samples such

as Pocahontas and Hambach coals were out of this trend. Pocahontas is a high rank coal that showed an important weight increase (in TGA) and a high CPT temperature, contradicting the TG_{spc} results. Although the reactivity of this coal seems to be high, it was considerably low compared to the high reactive samples. In the case of the second coal, it was a low rank sample that showed a poor reactivity in air. However, this sample had 37% of free water. For coals with similar rank values, the TG_{spc} index clearly distinguishes their reactivity. It is possible to conclude from this test that the single use of the rank value as an estimator of coal propensity can deliver erroneous predictions.
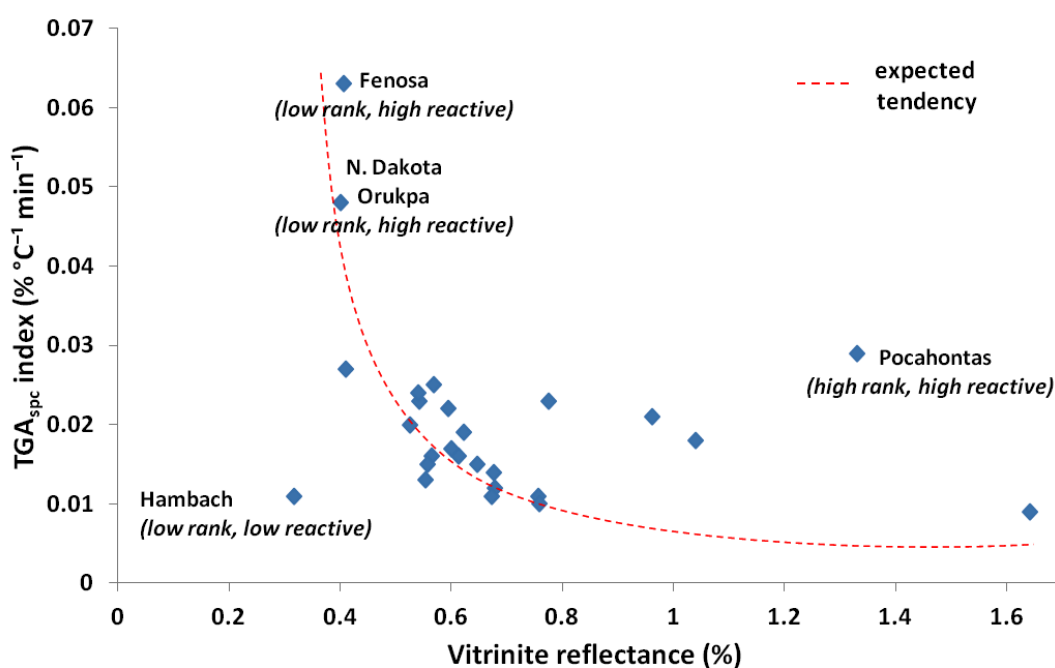
Figure 100: Dependency of TG_{spc} index on coal rank.

An increasing concentration of reactive macerals such as liptinite and vitrinite also increased the overall reactivity of the sample (Figure 101), with regard to the TG_{spc} index. From these results, coals that are prone to spontaneous combustion must have a concentration of vitrinite higher than 90%, and inertinite lower than 10%. These values were identified by using the combined information from all the sample tests.
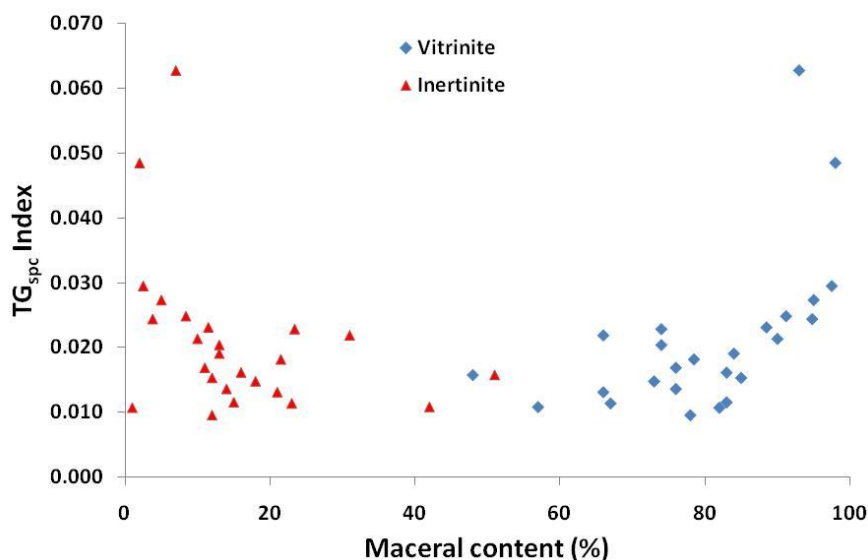
Figure 101: Dependency of TG$_{spc}$ index of maceral composition.

5.4.1.2 Influence of rank and maceral composition in the oxygen adsorption of coals

The adsorption of oxygen at low temperature was a key phenomenon detected in the TGA, which according to the reaction mechanism could be directly linked to the spontaneous combustion. Then, it was expected that low rank coals would tend to capture more oxygen in its porous structure due to the largest surface area offered and availability of active sites. However, low rank coals showed minimum weight increase, and high rank coals the maximum (Figure 102). This was previously explained by suggesting that the TGA profiles revealed only an apparent behaviour, which is conditioned by the stability of any oxygen complex formed (Section 5.3). This means that coals with lowest rank values tend to absorb more oxygen; however, the solids formed in their surface were less stable producing a nil mass increase. Conversely, high rank coals showed the opposite behaviour, producing more stable solids leading to a measurable mass increase in the TGA. The last affirmation was confirmed indirectly by measuring the reflectance change instead to the initial rank value (Section 5.4.2).
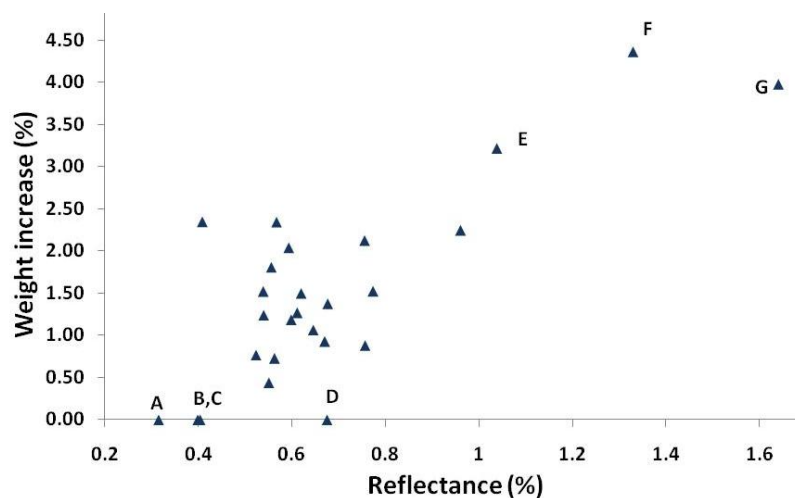
Figure 102: Weight increase of coals in TGA as a function of coal rank. In the figure: Hambach (A); North Dakota & Fenosa (B,C); Nadins (D); Bulli (E); Deep Navigation (F); Pocahontas (G).

The influence of maceral composition on weight increase was also studied. In this case, this effect was difficult to quantify due to the strong influence of coal rank. For this reason, weight increase for 6 coals (with similar rank values) was compared with the concentration of each maceral (Figure 103).
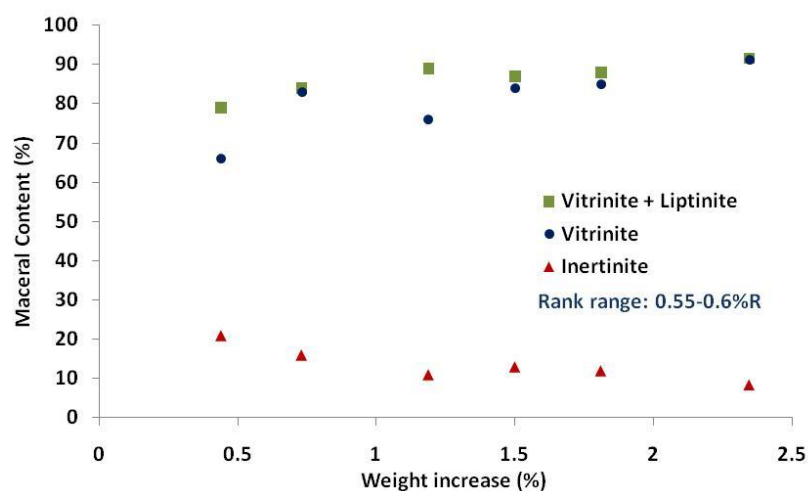
Figure 103: Relationship between weight increase and maceral composition.

This selection included coals with rank values between 0.55 to 0.6% R, confirming that high vitrinite and liptinite content coals tend to absorb more oxygen. On the

212

other hand, coals with increasing inertinite content (unreactive material) showed a reduction of the weight increase. However, these conclusions are questionable due to the small number of samples, and to the stronger influence of variables such as the oxygen adsorption temperature, and physical coal properties (e.g. moisture, porosity) on weight increase.

5.4.1.3 Influence of rank and maceral composition in heat released

In regard to the significance of optical properties in the heat evolution, it was observed that the heat required during the endothermic stages was inversely proportional to the coal rank (Figure 104). It was linked to the water content of coals, which at the same time is related to the coal rank. The heat release at early stages of coal oxidation was higher for low rank coals. Despite the variability of the data, results confirmed that greater heat contribution was observed in coals with nil weight increase (low rank); with the lowest heat release in coals with large weight gains and high rank values. In conclusion, these tendencies support the ideas proposed about the reaction mechanism, relating the heat released with the coal rank, the mass evolution and the coal propensity.
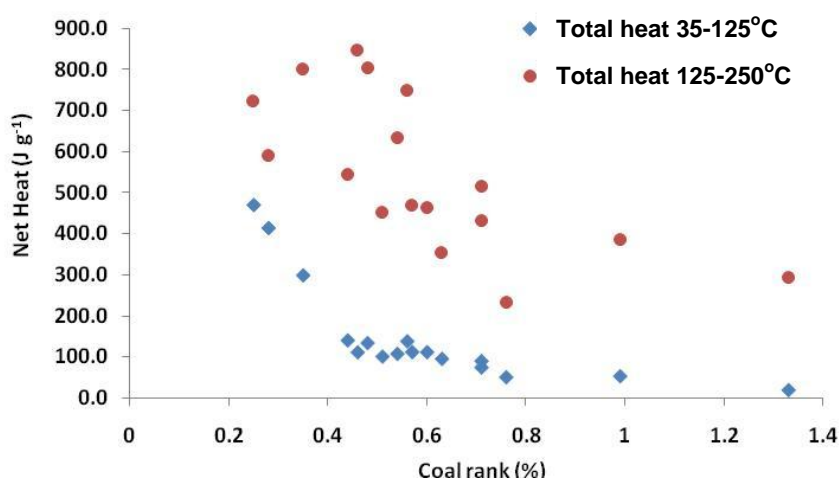
Figure 104: Heat adsorbed (moisture vaporisation, blue) and heat released (early oxidation, red) as a function of coal rank.

Finally, at low temperature it was found a slight association between the heat released and the maceral composition. In this case, from a partial comparison (removing extremely high and low rank coals; Figure 105), it was established that coals richer in vitrinite and liptinite macerals released a higher amount of heat compared to coals richer in inertinite. This is explained in terms of the reactivity of the macerals rather than the contribution to the calorific value of each maceral component. This relationship was not confirmed for extremely low rank coals, since the inertinite content in those samples was negligible. This was also assumed to be invalid for extremely high rank coals (>1.2%R) with a high vitrinite and liptinite content, since in these coals 'reactive' macerals effectively behave as unreactive macerals.
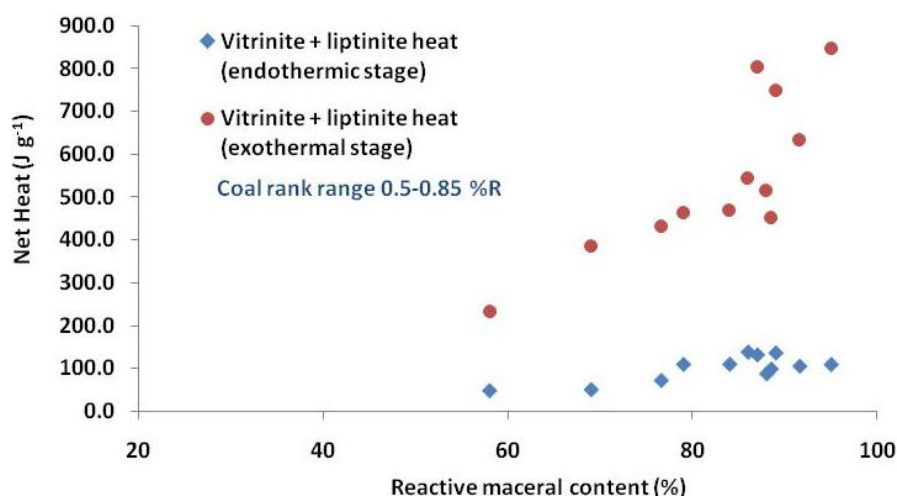
Figure 105: Dependency of heat adsorbed and released with the concentration of reactive maceral components.

In conclusion, optical properties such as coal rank and maceral composition showed a close relationship with the thermal parameters measured directly from raw coal samples (TG$_{spc}$ Index, TGO$_2$ adsorption and heat released). These associations confirmed the preliminary ideas proposed about the dependency of the spontaneous

combustion on to reactive conditions of coals, which also depended strongly on the textural characteristics of particles.

5.4.2 Optical properties of oxidized coals and thermal analysis

This analysis attempted to combine the optical characteristics of the oxidized samples with the thermal evolution of each coal, to determine the impact of the heating applied in the final textural characteristics of samples. In particular, the relationship between the reflectance change and parameters from the thermal analysis such as CPT, FHR and mass evolution (Section 5.4.2.1) was studied; and the link of these variables with the different thermal morphotypes (Section 5.4.2.2).

5.4.2.1 Connection between reflectance change and thermal history

The reflectance change was initially associated with the spontaneous combustion propensity of coals by considering the historical information about spontaneous combustion incidents (Figure 91). Also, the reflectance change was directly linked to the weight increase observed in the TGA, concluding that these transformations were an indication of the reaction process suffered by the coal particles. Then, in order to relate this parameter with the thermal evolution observed during the large sample size experiments, the reflectance change was compared with three representative variables from the thermal analysis: a) the crossing point temperature (CPT, using Chen approach); b) the final heating rate recorded (FHR); and c) the mass loss.

A) Reflectance change and CPT

The crossing point temperature (CPT) was selected as the best estimation of the critical temperature from which the self-heating process starts. Despite this indicator relating to the spontaneous ignition phenomenon, it delivered the lowest temperature estimates. In terms of its relationship with the reflectance change, samples with the lowest CPT showed the largest change in light reflectance (Figure 106). Conversely,

high rank coals appeared to be indifferent to thermal heating until the ignition point, showing elevated CPT values and negligible reflectance alterations. These results were expected since the CPT was an intermediate temperature, indicating the inflection point from an endothermic to an exothermic state (experiments ended at $250^{o}C$). This means that is not clear whether the reflectance change was produced by the elevated temperatures above the CPT rather than the low temperature reactivity of the samples.
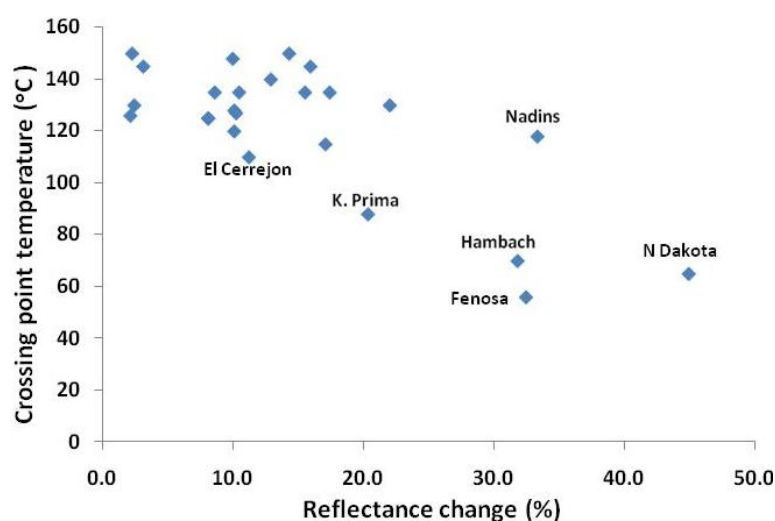
Figure 106: Crossing point temperature as a function of reflectance change.

Additionally, a strong association was observed between the CPT, and the peak and burnout temperatures from the intrinsic reactivity test (TGA). This suggested that the CPT values are linked to the full combustion reaction rather than the low temperature oxidation.

B) Reflectance change and FHR

The internal heating rate measured for each sample was considered as an indicator of the heat evolution of the large system (defined in Section 4.3.2). In the case of the oxidation stage, the final heating rate (FHR) was defined as the internal temperature rise between 120 to $250^{o}C$ (successfully adjusted by a linear trend). Then, the

reflectance change was compared to this variable to determine the impact of the heat evolution on the optical properties. As can be seen from Figure 107, samples with the largest FHR also showed the highest reflectance variation. In addition, an important number of samples showed a direct proportionality between these variables, although high reactive samples did not follow this linear trend. This was the case of low rank coals such as Fenosa, N. Dakota and Hambach, and some reactive samples such as Illinois # 6 and El Cerrejon.
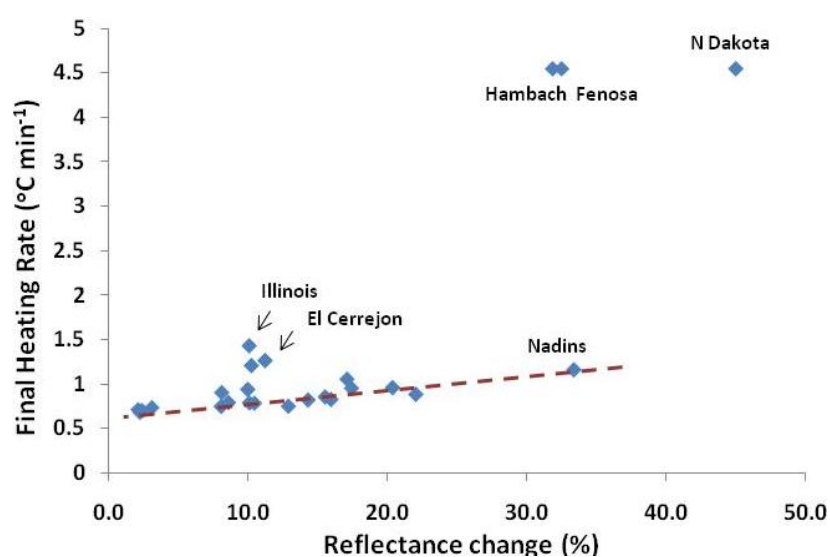
Figure 107: Final heating rate as a function of the reflectance change.

The observed relationship can be explained by the effect of the water content and mass release, since these variables were directly proportional to the FHR. Particularly, the FHR was measured after finishing the water release, when the centre of the sample passed over $120^{o}C$ (FHR definition). The problem is that under these conditions, the temperature in the furnace was different for all the samples. Consequently, the heating rate was higher for coals with higher water content since they were exposed to higher external temperatures at the end of the water vaporisation, increasing the internal temperature sharply. This was supported by a

direct proportionality found between the FHR, the initial water content, and the weight evolution observed for the large system, in all samples. Therefore, despite the fact that this relationship is consistent with the parallel results obtained, it was concluded that the final heating rate is a less reliable indicator of the self-heating process.

C) Reflectance change and mass evolution

The weight evolution was an indicator of the mass transport produced by the physical and chemical reactions that took place in the large size system. In this case, samples that suffered larger mass loss also showed the largest reflectance changes (Figure 108). Although the information obtained from the balance was qualitative rather than quantitative (due to the error introduced by wired thermocouples), this parameter presumed that the water vaporization process was in part responsible for the reflectance change observed. This pattern was similar to the previous variables studied (CPT and FHR), which were also proportional to the initial water content of the samples.
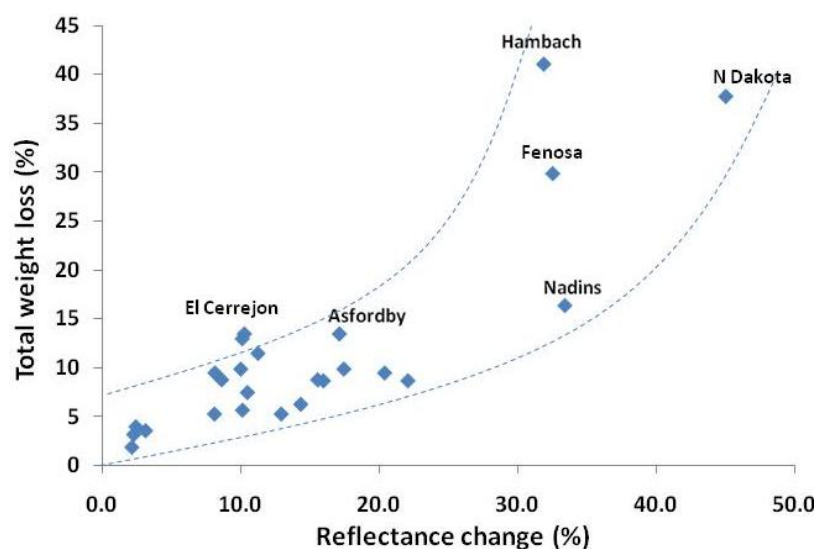
Figure 108: Weight loss as a function of reflectance change

5.4.2.2 Morphology of altered coal particles and thermal parameters

The morphological features of the altered coals were also compared with the information from thermal analysis. As previously shown, the resulting coal morphology was primarily dependant on the thermal conditions in which the samples were exposed (time and heating rate). Subsequently, in order to explain the final particle morphology, these features were compared to the CPT values, the FHR, and the sample mass change. Initially, from the different morphotypes described, those found with the interaction 'Type 1' (Figure 93) were selected due to their closest relationship with the low temperature oxidation. From these, the concentration of "homogeneous reflectance change" particles was compared to the CPT for all coal studied (Figure 109, A). This plot shows that samples with the lowest CPT values produced a larger amount of "homogeneous reflectance change" particles, compared to samples with a higher CPT that tend to generate a larger proportion of "oxidation rims".

When comparing morphotypes with the FHR (Figure 109, B) and the weight loss observed (Figure 109, C), the tendency was not seen. These samples (with the highest FHR) showed a larger proportion of "homogeneous reflectance change" particles, whilst also showing the maximum mass loss. Samples with the lowest FHR developed a larger proportion of "oxidation rims", presenting a negligible mass loss bounded by the initial water content of the sample. All these characteristics indicated that the conditions from which the reaction proceed were closely related to the textural characteristics of particles, which also evolved during the progress of the reaction (e.g. reflectance change, different morphotypes). However, these characteristics were influenced by the thermal conditions imposed, particularly the

heating rates and the final experimental temperature, where it was difficult to determine a clear link between these parameters and the propensity to self-heat.
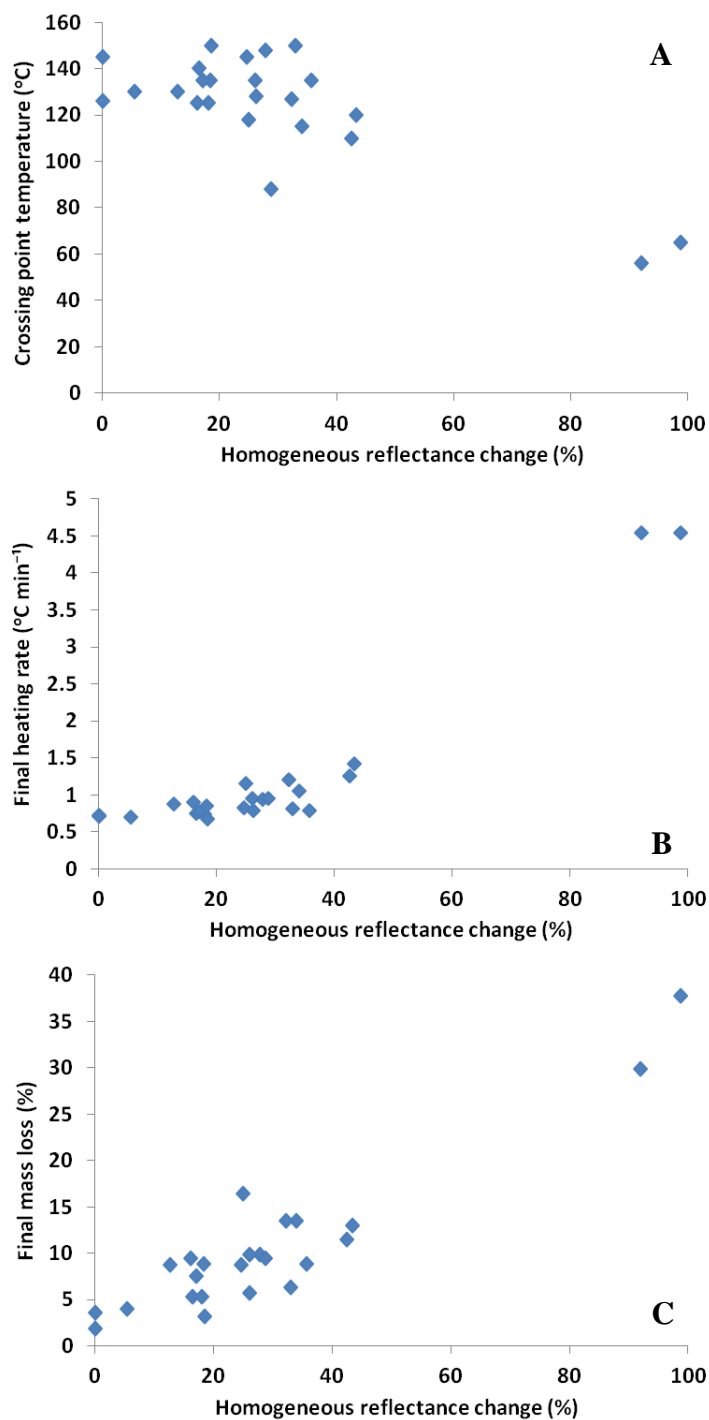
Figure 109: Thermal parameters and morphology of altered coals (in this figure: Homogeneous reflectance change (%) = 1 − oxidation rims (%)).

Finally, considering the complete set of results from the full set of samples, it was concluded that the nature of these experiments and the variables measured do not represent the spontaneous combustion phenomenon. Also, it was confirmed that this type of experiment is inadequate to determine propensity due to the high heating rate used (in this case $0.5^{o}C$ min^{-1}), which favours the development of the direct oxidation reaction of coal to CO_2 and H_2O (full combustion) rather than the slow oxidation reaction that relies in the formation of intermediate solid complexes. Therefore, these results support the initial criticisms about the crossing point temperature test in Chapter 4. In contrast, this accelerated experimental process was useful to uncover important aspects of the morphology of the samples after the reaction. Particularly, it was convenient to establish the way in which the optical properties were transformed during the reaction, and how these transformations depended on the initial textural features of each coal.

5.4.3 Linked results

When considering all the information obtained from the different experimental tests, some key parameters can be identified that are associated with the spontaneous combustion problem. From these, the most relevant quantifiable variables are as follows:

- The initial water content of coal.

- The weight increase at low temperature.

- The coal rank and its degree of change after slight heating.

- The distribution of thermal morphotypes created after slight sample heating.

Some secondary parameters were identified that showed an important influence in the phenomenon, although their impact on the spontaneous combustion was difficult to quantify:

- The heat adsorbed and released during low temperature oxidation.

- The initial reactivity of coals at low temperature.

- The maceral composition and the distribution of reactive and unreactive material in the sample (e.g. ash, inertinite).

Finally, the following parameters do not show any relationship with the spontaneous combustion problem:

- The crossing point temperature of coal.

- The ignition temperature of coal.

- The parameters derived from the intrinsic reactivity test performed in TGA.

This combination of findings provides some support for the conceptual premise that the current thermal tests (used to identify propensity of coals towards the spontaneous combustion) are not accurate. These tests predict a different phenomenon simply because they are based on the measurement of a different set of variables, which relates to the high temperature smouldering reaction instead of low temperature oxidation.

5.4.3.1 Defining reliable tests to identify coals prone to self-heating

In the case of the primary variables associated with thermal and mass changes, thermogravimetric analysis proved to be useful in quantifying the physical characteristics of the original material (proximate analysis used to measure the initial moisture, volatile, carbon and ash content of coals). Also, the thermal methods developed using this technique delivered the most accurate results compared to the information held about coal propensity (the estimation of oxygen adsorption, identified as TGO_2 index; and the low temperature reactivity test, identified as TG_{spc} Index).

In the first case, the TGO_2 test provided an indication about the ability of coals to absorb oxygen. The link between these results and reflectance change was initially discussed in Section 5.3.1.1. From this, a clear connection between the reflectance change and the weight increase was observed during the temperature segment assumed for the spontaneous combustion reaction. These conclusions were then confirmed by studying the link between this test and the proportion of thermal morphotypes created for each coal. As can be seen in Figure 110, the samples that showed the smallest weight increase also presented the larger proportion of thermal morphotypes per sample, which confirmed that these samples had a high susceptibility to react.
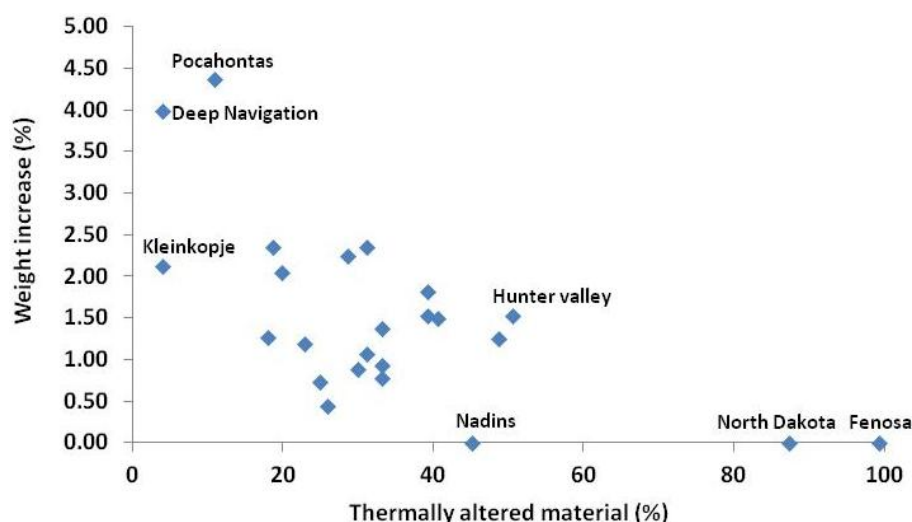
Figure 110: Relationship of initial weight increase with the proportion of thermally altered material.

In the second case, the TG_{spc} index provided a relative estimate of the initial reactivity of samples during heating in air. This test was focused on the reactive conditions developed for temperatures above $150^{o}C$, and it can be interpreted as the initial reactivity of the samples towards the high temperature combustion. The predictions from this test were also linked to the petrographic data by considering the

initial coal rank, the reflectance change and the formation of particular morphotypes in the samples.

In the case of the variables associated with textural and optical characteristics of coals, the microscopy tests allowed an effective quantification of these features. These tests delivered valuable information through the different stages of sample processing, revealing clear links between the optical data and the low temperature oxidation reaction. From the various attempted tests, the direct use of the coal rank and maceral composition of fresh coals was initially considered as a potential source of information to define a simple method of prediction. However, the results were not particularly clear, even after several attempts to combine the information from both techniques. It was possible, however, to corroborate some of the qualitative conclusions mentioned in literature, such as the most reactive coals tending to be low rank, with an elevated content of vitrinite, and a low content of unreactive material (inertinite). Subsequently, the information provided by the petrographic tests of oxidized coals (reflectance change and alterations in coal morphology) showed results clearly associated with the low temperature reaction. These tests were successful as they were able to identify coals prone to spontaneous combustion by assessing the changes produced in the optical properties as a result of slight changes in temperature, which were proportional to the degree of oxidation suffered by those samples.

Finally, the combination of variables was able to link various phenomenon to establish a new set of testing procedures. The single most striking observation that emerged from the data comparison was that connections exist between thermal and optical data, and a reliable test to predict coals prone to self oxidation should consider these two aspects together.

Chapter 6. Potential of biomass and coal-biomass blends to undergo spontaneous combustion

Part A: Biomass

In this section, the results from thermal and microscopy tests applied to biomass particles are reported. Considering that spontaneous combustion of fresh biomass has not been studied before, experimental analysis were focused into identify the general reactivity properties of these materials and the link between reactivity and morphologic properties. In addition, the effect of temperature on the mass loss rate was measured in a temperature range from ambient temperature to $1000^{o}C$, for different particle and mass sample sizes. Subsequently, morphological characterization of these materials was carried out, and related to the thermal results. Particularly, the morphological attributes of char particles were used to classify the fresh material, since raw biomass particles can not be analyzed easily using optical microscopy.

6.1 Thermal characterization of biomass using a small sample size

Fresh biomass materials were divided and sieved to six different ranges of particle size: 53-75, 75-106, 106-212, 212-300, 300-600 and 600-1180μm. For all these fractions, proximate analysis was carried out to standardise the original raw material (Table 31).

Table 31: Proximate analysis for the raw biomass particles as received

Sample	as received			dry, ash free basis		
	moisture (wt.%)	Volatile content (wt.%)	Fixed Carbon (wt.%)	Volatile content (wt.%)	Fixed Carbon (wt.%)	Fuel ratio (volatiles/ carbon)
Miscanthus	5.0	79.8	11.7	87.2	12.8	6.81
DDG	5.2	79.8	10.0	88.9	11.1	8.01
DDGS	4.7	79.7	11.0	87.9	12.1	7.26
Swedish Wood	4.1	78.9	14.7	84.3	15.7	5.37
Corn	6.6	78.8	10.7	88.0	12.0	7.33
Rapeseed	6.3	77.9	10.9	87.8	12.2	7.20
Shorts	8.1	74.9	14.6	83.7	16.3	5.13
Wheat	9.1	74.8	13.5	84.7	15.3	5.54
Sunflower	7.3	70.8	18.0	79.7	20.3	3.93
Olive	2.4	64.9	23.1	73.8	26.2	2.82

DDG: Dried Distillation Grains;

DDGS: Dried Distillation Grains without soluble.

6.1.1 Intrinsic reactivity of fresh biomass

The reactivity of fresh biomass was estimated using the derivative curves of the weight loss profiles obtained when material was heated in air at 10^oC min^{-1}, using a similar procedure as that used for coal, Chapter 4. For all the samples studied, derivative weight loss curves show at least three peaks per sample (Figure 111); the first arises at low temperatures ($\sim 50^o$C), due to moisture loss; the second is between 200 and 500^oC (depending of the sample), which is linked to pyrolysis and volatile release; the last peaks are between 400 and 700^oC and relate to the char combustion stage (dependant on biomass type). All these peaks are formed primarily by the influence of three main reactions linked to the thermal decomposition of hemicelluloses (220-315°C), cellulose (315-400°C) and lignin (in a wide range from 160 to 900°C) [241]. Clearly these burnout ranges cover the same combustion range as the 10 biomass samples and their individual profiles. The reason for this is almost certainly as a result of the varying proportions of each component in each biomass,

along with small amounts of other materials, such as starch. The values for these peaks are given in Table 32.
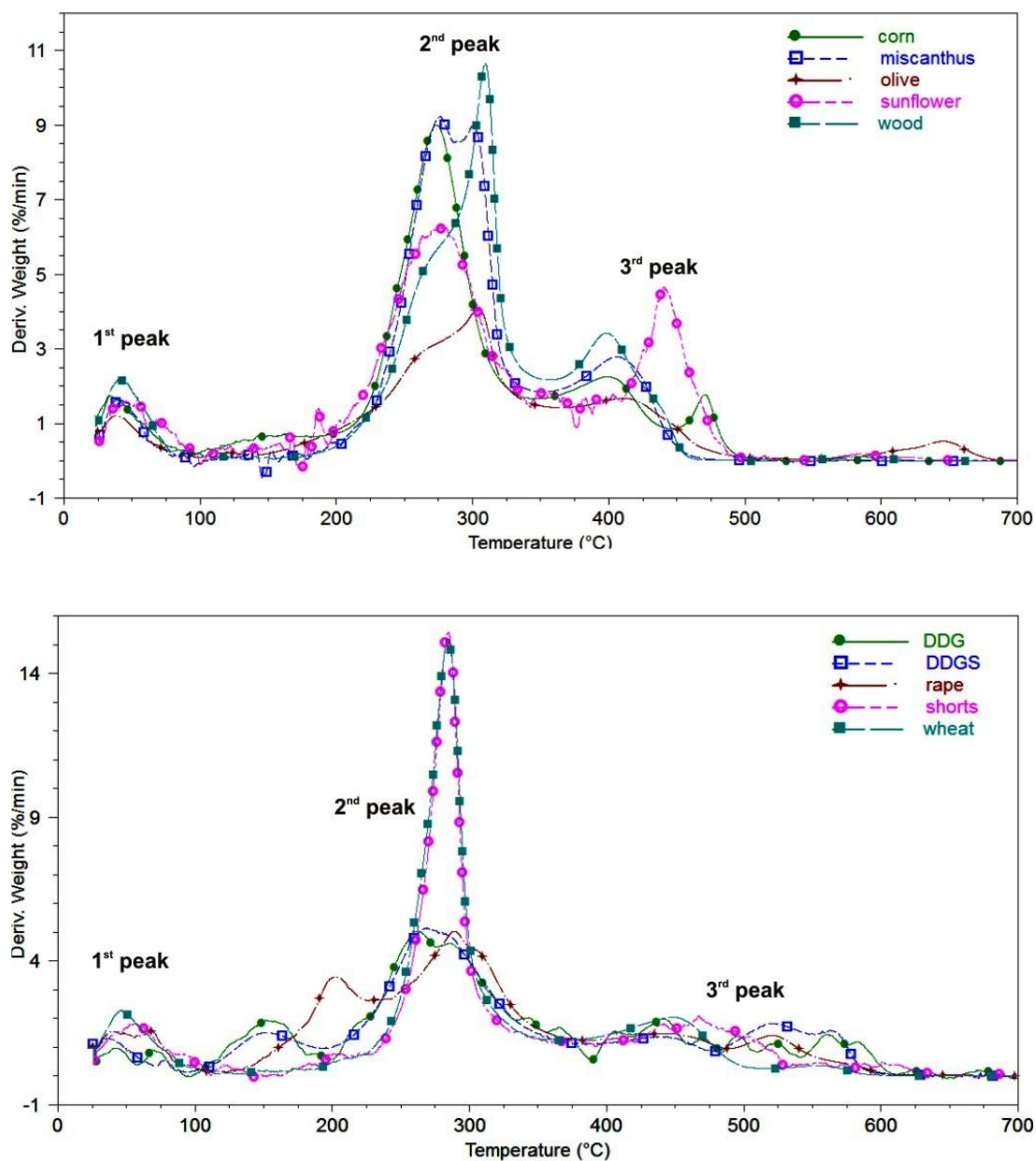
Figure 111: Derivative thermogravimetric profiles for 10 biomass samples (fraction size 53-75 μm).

Table 32: Peak temperatures and their particular mass lose rate for raw biomass particles (fraction size 53-75 µm)

Sample	Moisture 1st peak		Volatile release 2nd peak		Burnout stage 3rd peak		Burnout temper.
	^{o}C	% min^{-1}	^{o}C	% min^{-1}	^{o}C	% min^{-1}	^{o}C
Wheat	44	2.3	284	15.4	448	2	558
Shorts	49	1.4	299	14.3	470	1.8	609
Sunflower	63	1.3	289	11.8	433	6.2	530
Swedish Wood	43	2.2	309	10.7	398	3.4	447
Miscanthus	41	1.5	321	10.5	421	2.7	449
Corn	46	0.9	291	8.9	482	2.9	480
Rapeseed	75	0.8	318	5.4	547	1.7	586
DDGS	38	1.3	270	5.1	521	1.8	579
Olive	37	1.2	304	4.1	411	1.7	658
DDG	49	0.6	288	4.1	562	2.1	694

There are several potential approaches to 'grouping' the biomass types based on peak values e.g. volatile release rates appear to show two behaviours; those that rapidly emit large amount of volatiles including corn, miscanthus, Swedish wood, sunflower, shorts, wheat; and those that release volatiles at a slower rate including DDG, DDGS, rapeseed, olive. From Table 32, these groupings show weight loss values of >9 wt. % min^{-1} for volatile release. The second group show values of 5 wt. % min^{-1} or less. Additionally, the first group evidence clear and sharp Gaussian peaks for the pyrolysis and combustion stages. The second group show multiple overlapping peaks for both the pyrolysis and combustion stages continuing at relatively high temperatures (~700°C). A second way to group the biomass materials from the reactivity data would be from the Burnout Temperature (BT). In this case three main 'groupings' could be formed; biomass with a BT less than 500°C - Swedish wood, miscanthus, corn; less than approximately 610°C - sunflower, wheat, DDGS, rapeseed, shorts; and those >650°C - Olive and DDG. It is possible to make a

distinction by inferring that the more reactive groupings present a higher concentration of hemicelluloses and a lower content of lignin than the groups with lower volatile release rates and higher BT values. These characteristics are significant since they will have an impact on the performance of char particles formed after the pyrolysis step [242,243].

6.1.2 Intrinsic reactivity of biomass char particles

Char particles can be defined as the carbonaceous skeleton forming the main structure of biomass particles, free of volatiles and moisture. These particles can be produced after 'distillation' of the volatile components, from which the remaining structure depends on the thermal and fluid dynamic conditions applied during the process. In this case, char particles were produced at 1000°C in anoxic conditions and without the influence of a gas flow. These allowed a production of carbon skeletons similar in size and shape to the original raw biomass material, which were characterized in terms of reactivity and morphologic features.

As with the raw biomass materials, the intrinsic reactivity test can also be used to compare char burnout profiles for each biomass type. Table 33 shows all the data for peak and burnout temperatures. Sunflower and Corn, Miscanthus and Swedish wood all produce relatively Gaussian like plots with low initial temperatures (~300°C) and peak temperatures (~400-450°C). The final temperatures are also relatively low (~450-500°C) as shown in Figure 112 and all have a mass loss rate >10 wt. % min^{-1}. From Table 33 particle size appears to have a more significant affect on some biomass types. For sunflower, particle size has some influence on the position of the peak temperature and final temperature and has a higher weight loss rate value than the others. Corn, however, does not show any particle size effects on the reactivity profiles.

In the second group, have significantly higher PT and BT values but also show a broadening of the derivative profile (Figure 113) with peak temperatures of (500-600°C) which includes wheat, shorts and olive. Maximum mass loss rates are 5-10 wt. % min^{-1}. The third group (Figure 114) shows Rapeseed, DDG and DDGS. All three give non-Gaussian profiles with merged peaks and slopes. With these samples, the profiles finish at an unusual high temperature of >800°C. The maximum weight loss is consistently lower than the other two 'groups' at 3-6 wt. % min^{-1}.

Table 33: Peak temperatures (PT, ^{o}C) and burnout temperatures (BT, ^{o}C) for the char from each biomass size fraction (μm)

Sample	53–75		75–106		106–212		212–300		300–600		1180–600	
	PT	BT	PT	BT	PT	BT	PT	BT	PT	BT	PT	BT
Sunflower	372	441	373	451	385	448	408	460	406	465	392	429
Swedish wood	430	601	437	459	442	468	444	477	457	487	461	490
Miscanthus	500	509	506	520	502	527	503	524	471	514	488	518
Corn	420	459	438	577	430	536	424	484	420	497	419	469
Olive	488	638	488	636	508	617	473	677	463	622	422	688
Wheat	528	652	545	671	546	694	529	615	530	595	530	708
Shorts	574	687	570	713	554	661	535	731	528	666	537	775
Rapeseed	503	690	510	727	519	718	453	656	441	659	437	657
DDGS	483	691	429	782	447	819	452	813	458	800	518	824
DDG	496	776	531	899	548	900	482	900	544	900	549	900
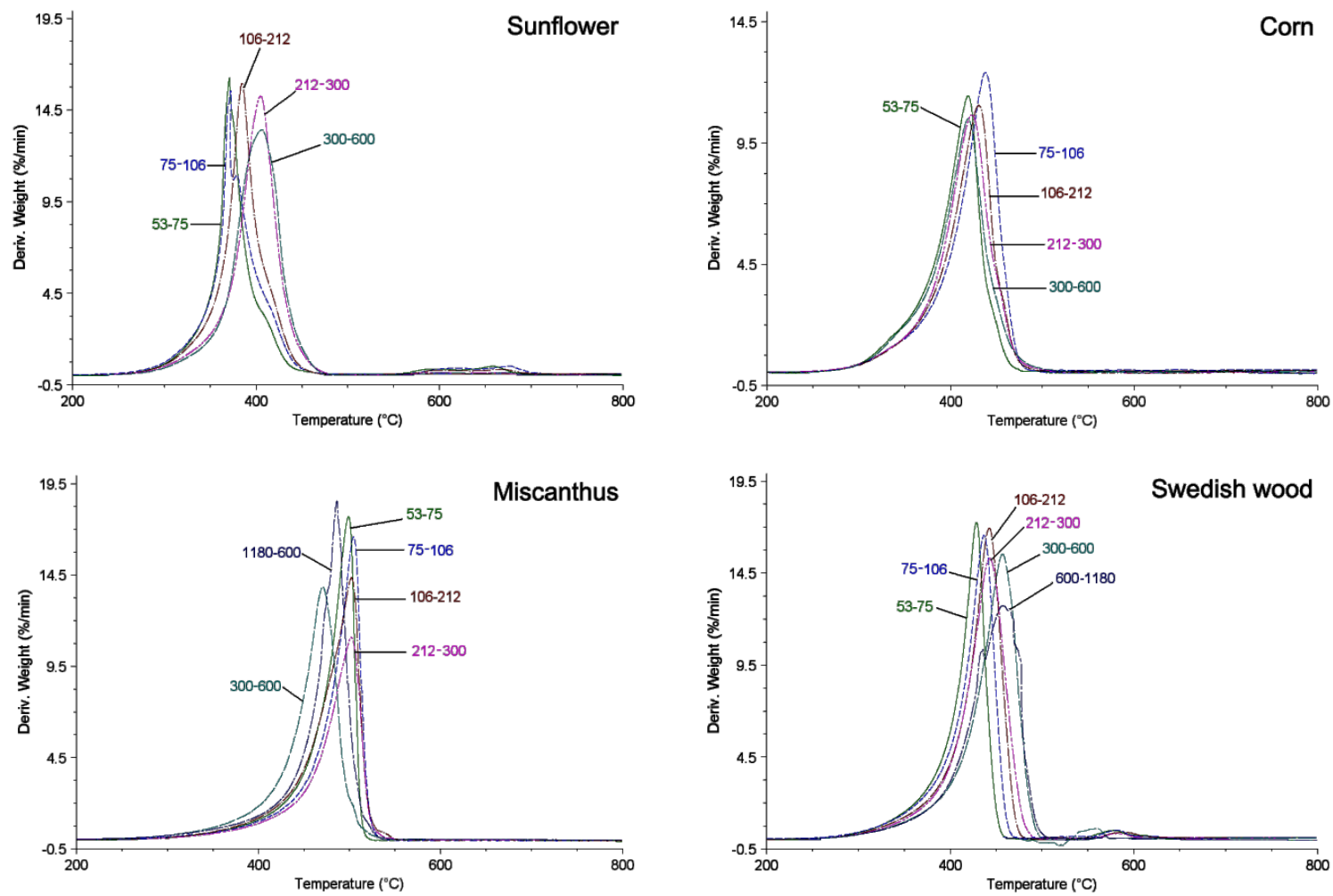
Figure 112: Gaussian shaped derivative weight loss curves for chars from sunflower, corn, miscanthus and Swedish wood in the different particle sizes.
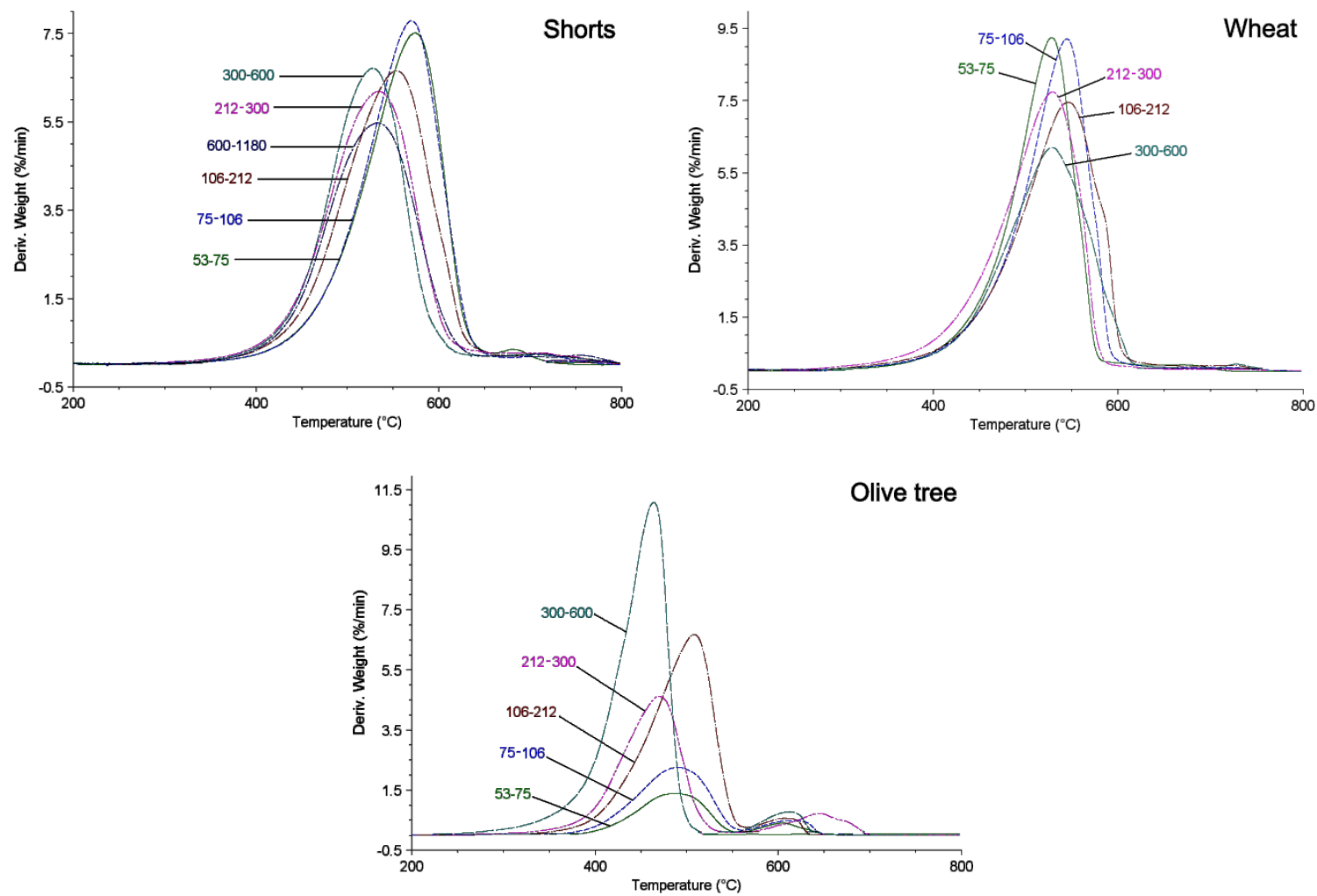
Figure 113: Thermogravimetric derivative curves for wheat, shorts and olive char for different particle sizes.
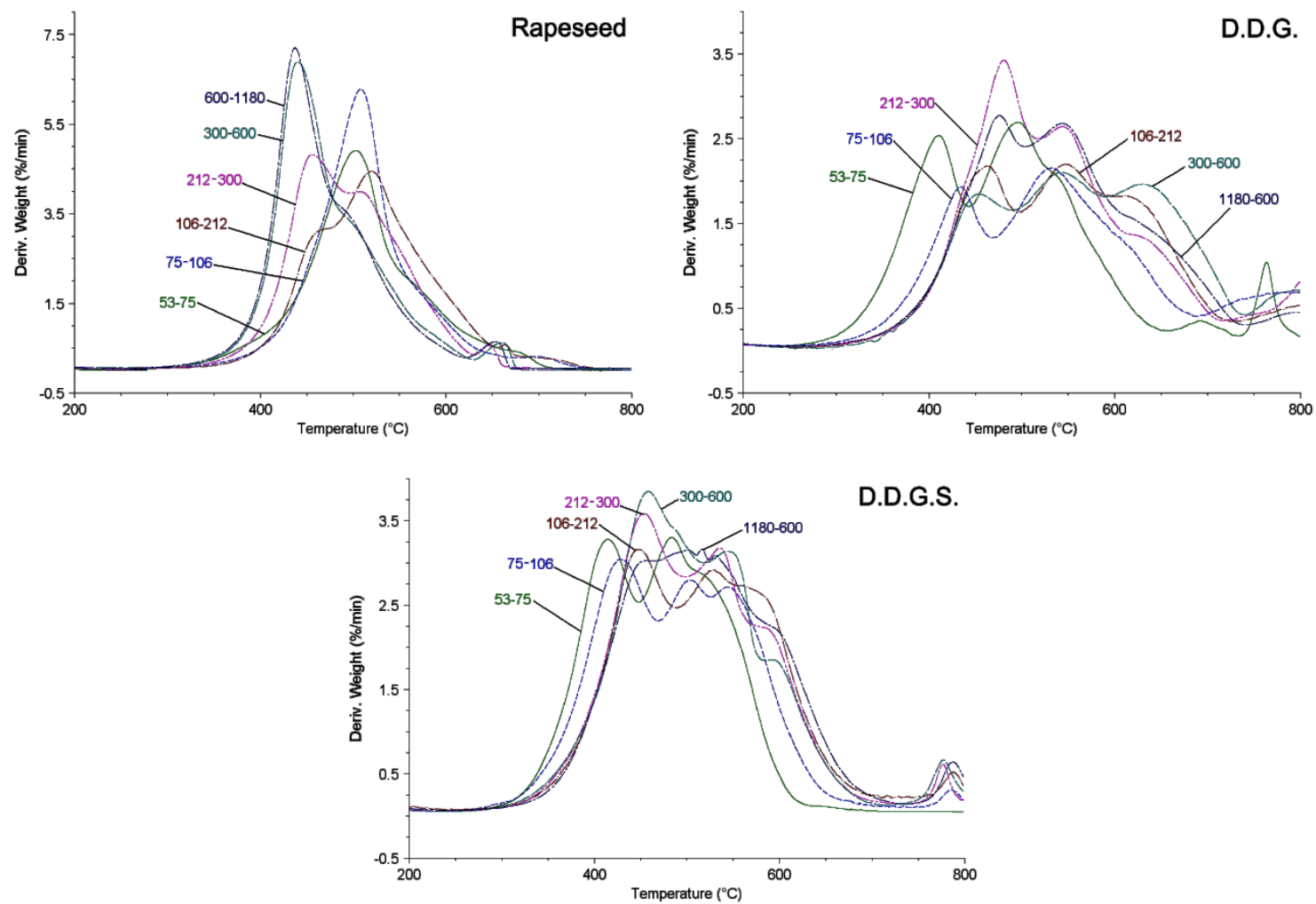
Figure 114: Thermogravimetric derivative curves for Rapeseed, DDG and DDGS residues char for different particle sizes.

There is a poor correlation between the peak temperature and burnout temperature (R^2 correlation values are all less than 0.5). Figure 115 is a plot of peak temperature and burnout temperature against specific biomass type.
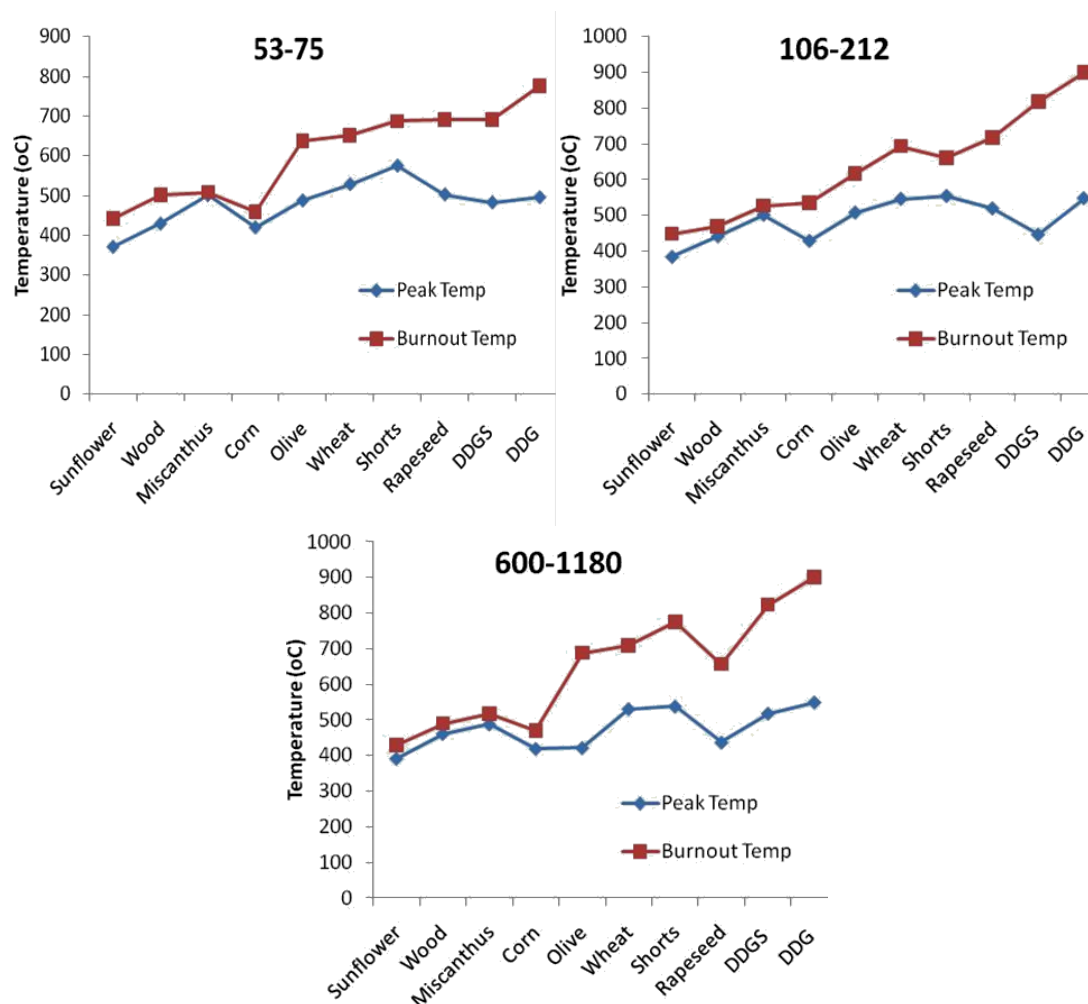
Figure 115: Comparison of peak temperature and burnout temperature for biomass char, at three different sizes of particle. In both cases, the reactive groups are clearly identified in the burnout temperature profiles.

Peak temperatures do not appear to give a trend which is probably indicative of the nature of the position of the maximum burnout rate - i.e. at relatively low temperatures where the hemicelluloses and cellulose structures preferentially burnout. Since all these biomass materials contain such structures, all the peak temperatures are all approximately 400-500°C. However, it is possible to define groups using the

criteria of increasing burnout temperature value. This is dictated by the proportion of the less reactive fractions (cellulose and lignin) in the biomass. Higher levels of lignin tend to generate higher peak temperatures and slower burnout rates.

6.2 Thermal reactivity of biomass in a large sample size

The thermal evolution of a large size biomass sample was studied using the thermal reactor developed, in which six biomass types were exposed to a slow heating rate in air (0.5^oC min^{-1}), recording the thermal evolution and the weight loss.

6.2.1 Transient temperature profiles during a constant heating

Thermal profiles were obtained for two different particle sizes (106-212µm - 500-1180µm). In a similar way to that used to analyze coal particles, the temperature readings of the central thermocouple of the reactor were used to compare between samples (Figure 116). For both particle sizes the thermal profiles showed a similar evolution, although differences were seen in the time period in which the final temperature was reached (ignition). From these, three thermal stages were identified: an initial linear region from room temperature to approximately 95^oC; followed by an inflection of the curve from ~95^oC to ~$110\ ^oC$; finishing with a second linear region from ~$110\ ^oC$ to the ignition point. Particularly, the thermal evolution is shown in detail for two samples (Figure 117). In the first case, rapeseed showed the lowest heating rate among all the samples compared to the imposed furnace heating rate. This sample revealed a kind of thermal buffer produced by the elevated water content, which was gradually released during the experiment (Figure 117, A). In the second case, corn showed a higher thermal conductivity and a less pronounced effect of the water content over the resulting profiles, allowing a faster temperature evolution and an early ignition compared to rapeseed (Figure 117, B).
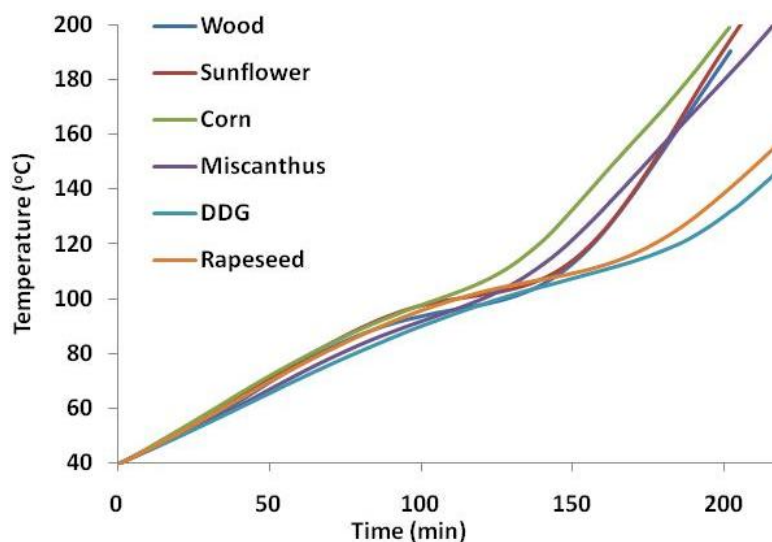
Figure 116: Thermal profiles for six biomass samples (500-1180µm). The heating rate used was $0.5^{o}C$ min^{-1} in air.

In general, the influence of particle size across the set of samples studied was less pronounced than those observed in coal samples. The linear segments observed and the time periods of the profiles were proportional to the water content and the packing density of the samples into the sample holder. Also, the space-temperature profiles used to identify the crossing point temperature were similar than those obtained for high water content coals (Figure 117, A). For biomass, the crossing point was almost undetectable, coinciding in most of cases with the ignition point. In Table 34, the ignition temperatures and the packing density for both particle sizes used are shown, which confirmed the similarities observed in all the biomass profiles.

Table 34: Ignition temperature and packing density for two particle sizes

Biomass	Ignition temperature (^{o}C)		Packing density g/100ml	
	106-212µm	500-1180µm	106-212µm	500-1180µm
Miscanthus	180	175	43.5	40
Rapeseed	180	160	85	80
DDG	185	185	90	77
Corn	180	155	40	40
Sunflower	170	155	70	63
Wood	190	150	53	53
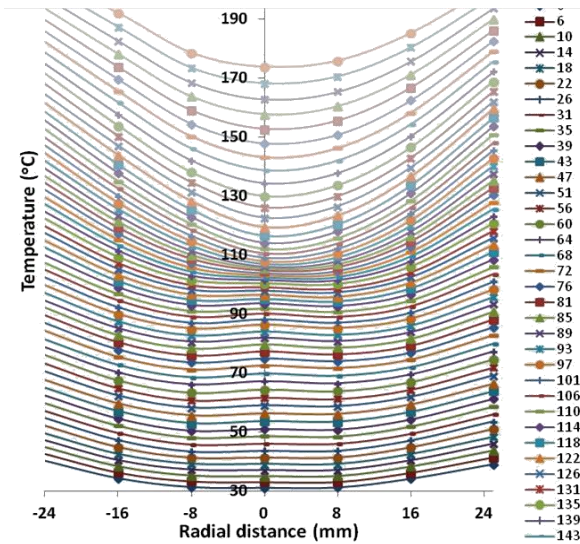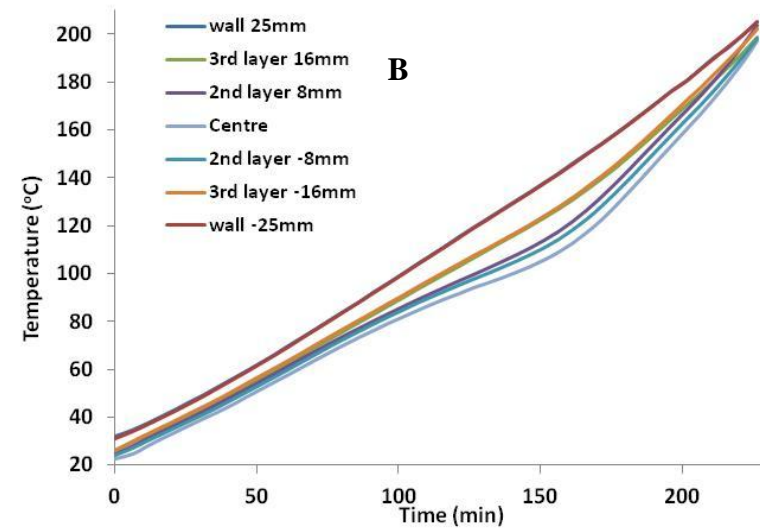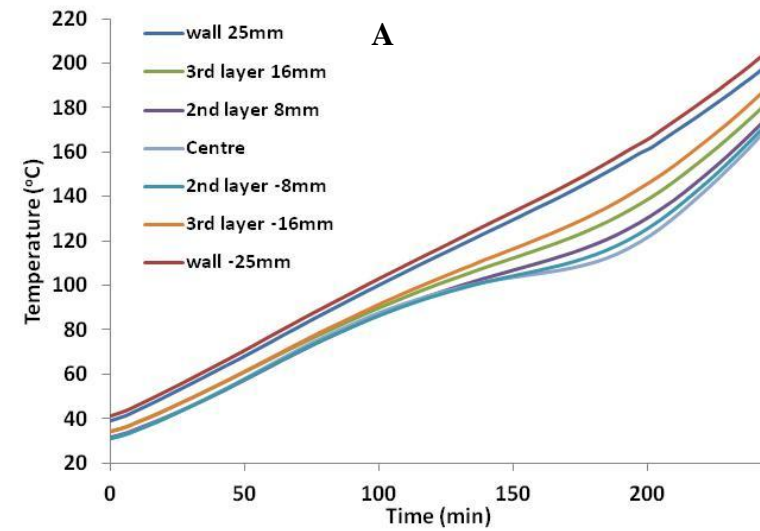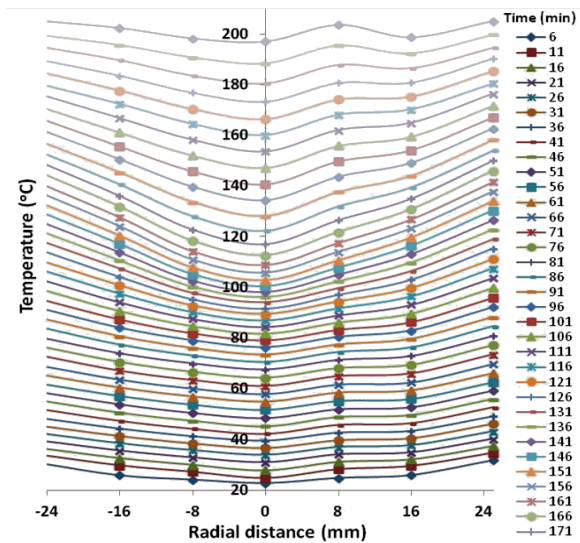
Figure 117: Thermal profiles in time and space for two biomass samples: rapeseed (A) and corn (B). The heating rate was $0.5^{o}C$ min^{-1}.   237

The thermal profiles, miscanthus, rapeseed and DDG were indifferent to particle size reduction, showing similar profiles in time and temperature. However, when the particle size was reduced from 500-1180µm to 106-212µm for wood, sunflower and corn, these thermal profiles took longer periods to reach the same temperature level. As the packing density and the water content were kept almost constant for these experiments, the difference was explained in terms of the intrinsic reactivity of the material (obtained by TGA), in which the first set of samples (miscanthus, rapeseed and DDG) were considerably less reactive than the second set.

This also can be explained in terms of the morphology of the particles (explained in Section 6.3), in which the first group showed high-dense carbon structures with apparent high sphericity, compared to the second group of samples which showed light and highly-porous structures with a high aspect ratio (elongated sticks). These textural attributes influenced the packing of the material and the air circulation inside the sample holder, contributing to enhance (in the case of the second group) the heat and mass transfer through the centre of the sample, accelerating the evolution of the thermal profiles, and subsequently influencing the rate of the oxidation reaction.

About the differences in the ignition temperatures for the two particle sizes studied (Table 34), larger particle sizes were easier to be heated up and burned compared to the smallest particle sizes, which tend to accumulate a large amount of heat before reach the ignition point. These conditions were only possible to be produced and observed during the large sample size experiments, which were undoubtedly influenced by the restricted heat and mass transfer conditions produced in a large system.

6.2.2 Mass evolution under a constant heating

In parallel to the temperature acquisition, weight profiles were obtained for both particle sizes. These revealed interesting characteristics of the process such as the impact of the water release, the initial devolatilisation, and ignition in the sample mass. As can be seen from Figure 118 and Figure 119, all profiles showed at least three stages: first, a slight weight loss produced by the initial release of water. During this stage, samples lost 80% approximately of the free moisture content; secondly, an intermediate stage characterized by the release of the remaining water and initial volatile release; finally, the third stage was characterized for a vigorous volatile release followed by sample ignition.

Regarding the influence of particle size on the mass profiles, these showed the same shape and characteristics stages, although the total mass loss registered for the smallest particle sizes was always lower. The last observation can be explained due to the mass transfer restrictions produced by the compact packing of these particles, which influenced the mass loss rate in the same way as the establishment of the thermal profiles. An explicative diagram of these differences is shown in Figure 119.
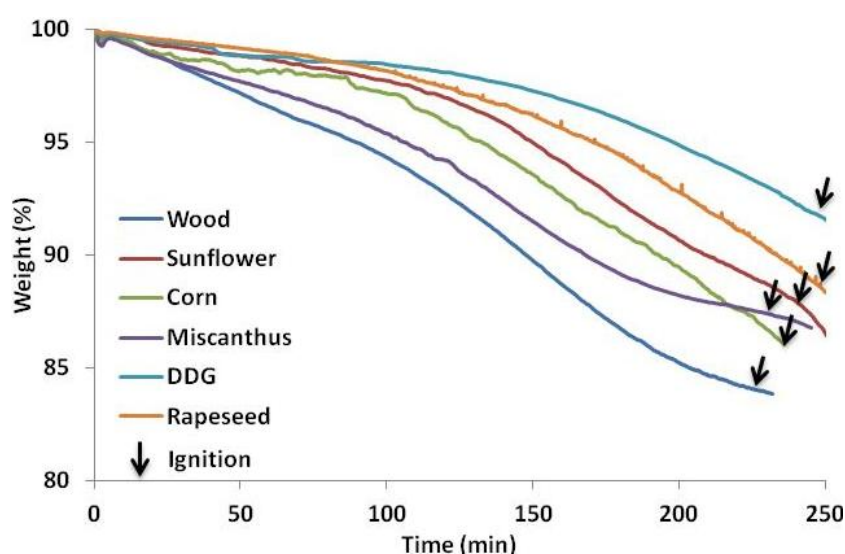
Figure 118: Weight loss profiles for biomass particles (fraction 500-1180µm)
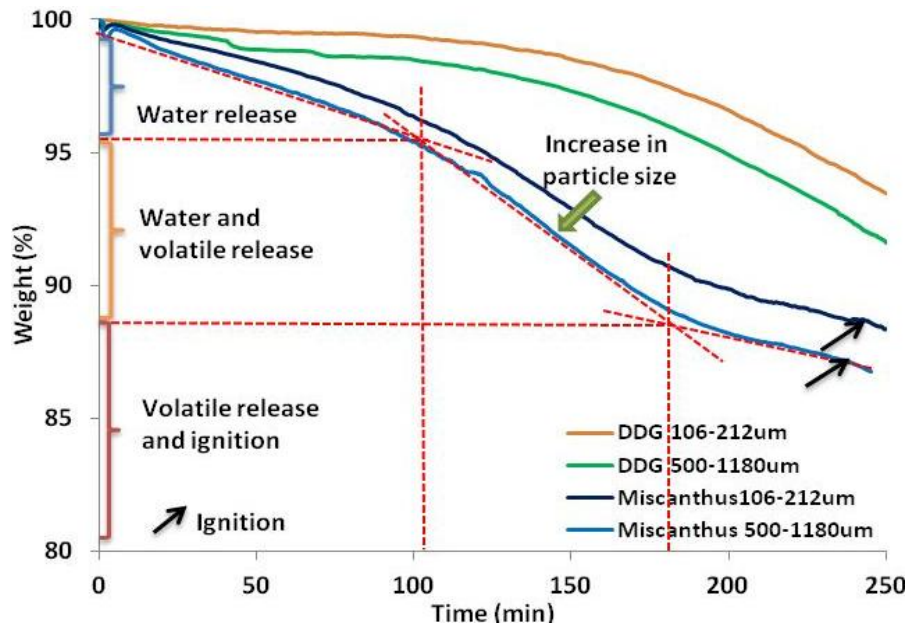
Figure 119: Characteristics observed from the weight loss profiles and the influence of particle size. The heating rate used was $0.5^{o}C$ min^{-1} in air.

Finally, the different stages identified from the mass profiles were similar to those described for the central temperature of the sample holder, coinciding in the time period in which both types of profile changed.

6.3 Optical characterization of biomass

The textural characterization of biomass has been historically performed by using optical microscopy, specifically transmission light techniques due to the transparent nature of plant tissues. This technique requires specialized instruments to produce thin biomass slices that are transparent to a light beam, which can be observed under the microscope after a tinting procedure. This sample preparation is time consuming, restricting the study to a limited number of plant components. These disadvantages made difficult the use of this technique to characterize and quantify a large number of particles.

Alternative to this method is the use of reflective light microscope, which is commonly used to characterize opaque materials such as rocks and minerals (coal

particles), after minimum sample preparation. However, the low light reflectivity of biomass is an impediment to apply this technique directly. Then, a new alternative explored was the characterization of biomass char instead of raw biomass material. Char particles produced under controlled conditions preserve most of the original material structure, and its high light reflectivity allows a clear observation of a large number of particles simultaneously.

6.3.1 Morphology of fresh biomass derived from char particles

Char morphology was studied using polished blocks and oil immersion microscopy. This approach is particularly valuable when seeking to quantify characteristics since they are cross section images, which are useful for determining area, length, diameter, and macro porous calculation. Various systems exist for the classification of coal chars [244] and these classes tend to relate to the original petrographic components in coal. At present, a definitive system for describing chars from biomass has not been established and more work is needed to find the key characteristics that describe these intermediate char structures. Char structures from coal can be classified in terms of level of porosity, wall thickness, and internal structure creating eight different categories for coal char. Figure 120 and Figure 121 (A–J) shows examples of the biomass chars in three different size fractions.

Biomass chars appear to have new morphological features that are unlike those seen in coal char. It is clear that some chars maintain their original fibrous structure such as sunflower, Swedish wood, miscanthus and corn (Figure 120, B–E). Olive char appears to be a combination of this macro fibrous structure along with internal cell structuring with a thicker wall (Figure 120, A). Wheat and shorts have a similar morphology (Figure 121, I and J) with long porous structures with thick walls. As particle size decreases, they appear to melt (and agglomerate) after passing through a

plastic phase. In both cases, the process of volatile release produces a highly porous char structure.
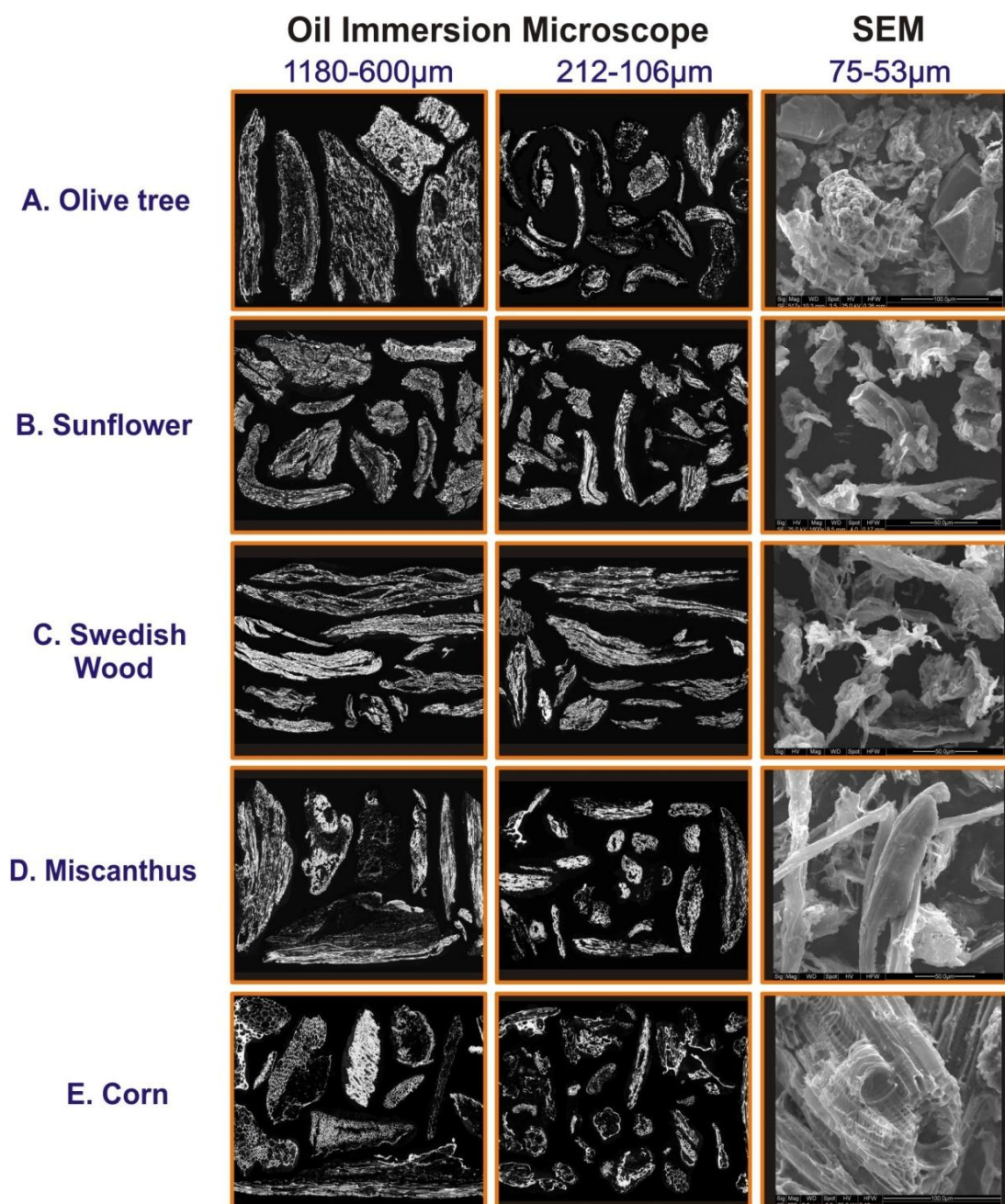
Figure 120: Cross-sections and surface micrographs of biomass char particles.
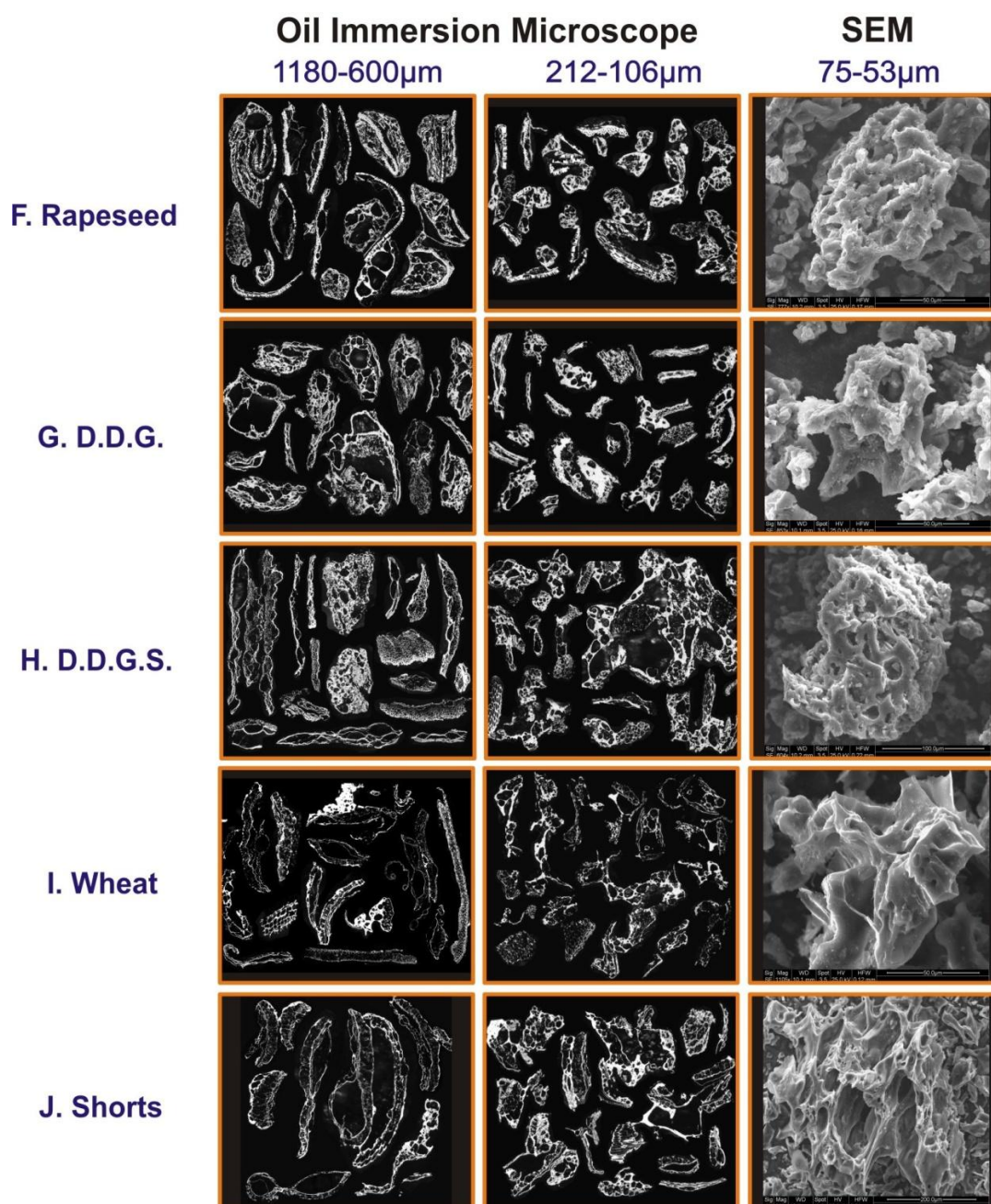
Figure 121: Cross-sections and surface micrographs of biomass char particles (remaining five samples in three particle sizes).

Rapeseed, DDG and DDGS residues all show thicker walled chars with evidence of some solids (Figure 121, F-H) with thick walled chars producing some big open pores, probably formed during volatile release, with a large number of smaller secondary pores.

6.3.2 Biomass char classification system

The coal char classification system has also been simplified to three types – Thin (TenuiSpheres and TenuiNetworks), Thick (CrassiSpheres and Crassi Networks and Mixed Porous) and Solids (Mixed Dense, Fusinoid and Solid) in order to compare different samples more easily. It is apparent that biomass creates new morphologies that are not described fully by the coal char method e.g. the presence of cellular pores that are similar to the original structures in the biomass – where Fusinoid would be the closest to this description, but this originates from the term Fusinite which is an 'inert' sub maceral from the Inertinite class. However, the same basic criterion can be used to summarise these types i.e. Thick, Thin and Solid.

Table 35 shows all the data for the different sizes of each biomass char. There are changes to each group as particle size changes e.g. the proportion of solids appears to drop with the largest size fractions (e.g. wheat 12–0%). The quantity of thicker walled chars does not follow a universal trend – four biomass samples (DDG, DDGS, miscanthus and rapeseed) all show minimal changes with particle size whilst a further four (corn, shorts, wood and wheat) have less thick walled chars in the larger sizes. Only two biomass types (olive and sunflower) show increasing amounts of thick walled char with increasing particle size. There appear to be trends, as with intrinsic reactivity. Figure 122 is a plot of the average data for the three different char types against biomass type. Miscanthus, olive and corn all produce the thinnest chars and DDG, DDGS and rapeseed all produce the thickest. Wheat, sunflower, wood and shorts represent an intermediate region with an elevated level of solids.

Table 35: The char morphology results (thin, thick and solid chars) for each biomass and particle size (μm)

Thin walled	53–75	106–75	212–106	300–212	600–300	1180–600
Corn	45.6	51.2	69.6	76.8	73.6	70.4
DDG	4.0	6.4	12.0	12.0	17.6	17.0
DDGS	7.2	10.4	9.6	10.4	13.6	6.4
Miscanthus	86.4	69.6	60.8	64.8	65.6	65.6
Olive	88.8	64.8	63.0	55.2	48.0	64.8
Rapeseed	0.0	0.0	10.4	20.8	10.4	5.6
Shorts	0.0	4.0	15.2	36.0	40.8	42.0
Sunflower	54.4	58.4	30.4	20.8	18.4	36.0
Swedish wood	16.8	20.0	19.2	59.2	27.2	26.4
Wheat	5.6	15.2	24.8	58.4	60.8	77.6
Thick walled	53–75	106–75	212–106	300–212	600–300	1180–600
Corn	54.4	48.8	29.6	22.4	24.8	29.6
DDG	71.2	74.4	84.0	83.2	80.8	83.0
DDGS	92.8	85.6	89.6	88.8	84.8	93.6
Miscanthus	13.6	30.4	38.4	35.2	34.4	34.4
Olive	8.8	31.2	34.6	44.8	52.0	35.2
Rapeseed	99.2	89.6	87.2	79.2	88.0	94.4
Shorts	99.2	92	67.2	64.0	57.2	57.6
Sunflower	30.4	28.8	64.8	77.6	81.6	64.0
Swedish wood	78.4	76.0	69.6	40.0	66.4	63.2
Wheat	81.6	79.2	68.0	35.2	34.4	22.4
Solids	53–75	106–75	212–106	300–212	600–300	1180–600
Sunflower	15.2	12.8	4.8	1.6	0.0	0.0
Miscanthus	0.0	0.0	0.8	0.0	0.0	0.0
Corn	0.0	0.0	0.8	0.8	1.6	0.0
Olive	2.4	4.0	2.4	0.0	0.0	0.0
Wheat	12.8	5.6	7.2	6.4	4.8	0.0
Rapeseed	0.8	10.4	2.4	0.0	1.6	0.0
DDG	24.8	19.2	4.0	4.8	1.6	0.0
DDGS	0.0	4.0	0.8	0.8	1.6	0.0
Shorts	0.8	4.0	17.6	0.0	2.0	0.4
Swedish wood	4.8	4.0	11.2	0.8	6.4	10.4
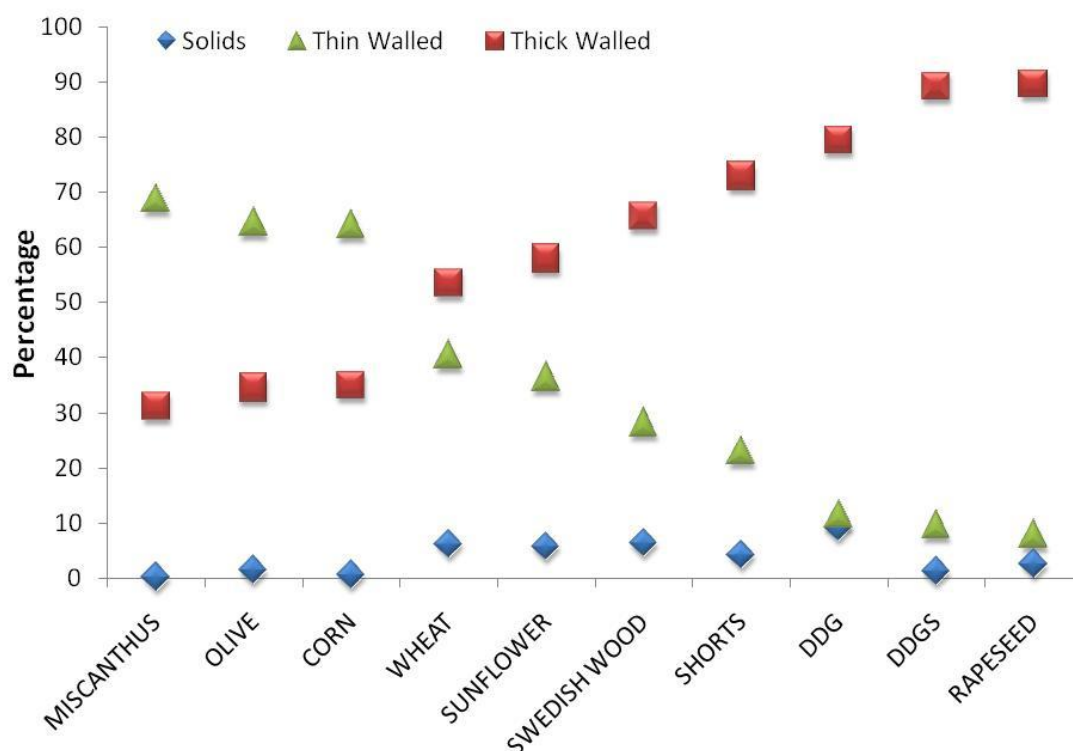
Figure 122: Three basic groupings (average of the size fractions) across the biomass types based on the percentage of thin walled chars.

6.4 Combining char reactivity and particle morphology

General trends are apparent when considering the behaviour of the raw biomass, morphology and reactivity (thermal analysis) i.e. the degree of char deformation and the intrinsic reactivity of the char material is linked to the devolatilisation rate of the raw biomass and the size of the temperature window required to completely burn the biomass. Without pre-measuring the internal structure of the raw biomass samples it is difficult to compare char morphology with intrinsic reactivity and other characteristics such as devolatilisation rates.

When comparing intrinsic reactivity from the chars with char morphology, trends do exist in the data. DDG, DDGS and rapeseed give the lowest reactivity in both chars and raw biomass, and the thickest walled chars. Miscanthus, corn and sunflower all give reactive chars with thinner walls than the other biomass samples. The

intermediate biomass samples would include wheat, olive, swedish wood and shorts. These biomass samples are not the most reactive or the most open, but fall somewhere between the two other groups. Table 36 shows the rankings of the chars based on an average of the measured characteristics.

Table 36: The ranking of the intrinsic reactivity and char morphology data

	Intrinsic reactivity		Char morphology		Combined ranking
	BT	BT & PT	Thin walled	Thick walled	
1	Sunflower	Miscanthus	Miscanthus	Miscanthus	Miscanthus
2	Miscanthus	Swedish wood	Corn	Olive	Corn
3	Swedish wood	Sunflower	Olive	Corn	Sunflower
4	Corn	Corn	Wheat	Wheat	Swedish wood
5	Olive	Wheat	Sunflower	Sunflower	Olive
6	Wheat	Shorts	Swedish wood	Swedish wood	Wheat
7	Shorts	Olive	Shorts	Shorts	Shorts
8	Rapeseed	Rapeseed	DDG	DDG	Rapeseed
9	DDGS	DDGS	DDGS	DDGS	DDG
10	DDG	DDG	Rapeseed	Rapeseed	DDGS

Finally, these results were also linked to the thermal and mass evolution observed for the large size samples. In this case, it was clear that the specific physical and intrinsic reactivity properties influenced the mass and thermal evolution of the large sample, but also the morphological characteristics of particles. Conclusively, the mass and energy transfer restrictions of the whole system depend on the morphological features, which in some cases favoured heat accumulation limiting the mass transfer (in the case of DDG, rapeseed); or favouring the air circulation and heat dissipation (in the case of corn, wood and sunflower).

Part B: Coal-biomass blends

For coal and biomass blends, synergetic interactions during pyrolysis and combustion processing have been reported in literature (discussed in Chapter 3). At low temperature, both materials can suffer aerial oxidation; nevertheless, information about mutual interactions that exacerbate this process when these materials are blended was not found. The spontaneous heating of coal strongly depends of specific variables such as the reactivity of the sample, the air-coal contact due to porosity and compaction of the piles, and the presence of moisture. High moisture content and the impact of particle morphology in the packing were characteristics of biomass materials. These combined characteristics present a significant possibility that biomass could contribute to the spontaneous combustion of coal.

6.5 Physical and reactivity properties of coal-biomass blends

Several coal samples ranging in the middle of the reactivity scales were selected and blended with the highest and lowest reactive biomass. This was done in order to study the physical and reactivity properties of coal-biomass blends and how these differ from their original single constituents. In the case of coals, seven samples were used, from which Dawmill and Asfordby were chosen to study the impact of the blending proportions and the influence of the biomass type in the thermal profiles. The remaining five samples were used to study the influence of the coal type in the blend, by keeping constant the biomass used. For all these blends, two types of biomass were selected: A) wood, to show low ignition temperature, high reactivity, and a large proportion of 'stick' structures; and B) rapeseed, a high ignition temperature, low reactivity, and a large proportion of sphere-shaped particles.

6.5.1 Proximate analysis of coal-biomass blends

Proximate analysis was carried out to characterize the initial physical properties of blends (Table 37 and Table 38).

Table 37: Proximate analysis of coal-biomass blends

	Wood			Rapeseed		
Dawmill	5%	10%	15%	5%	10%	15%
Moisture (%)	5.7	5.5	5.7	5.3	5.4	5.4
Volatiles (%)	35.4	38.4	41.5	36.9	38.4	40.2
Carbon (%)	53.1	51.5	48.1	52.5	51.0	48.9
Ash (%)	5.8	4.7	4.7	5.3	5.3	5.4
Asfordby	5%	10%	15%	5%	10%	15%
Moisture (%)	6.3	6.3	5.9	3.8	5.8	6.8
Volatiles (%)	34.6	37.0	38.3	36.8	36.9	40.8
Carbon (%)	47.2	45.7	45.0	49.0	45.6	42.6
Ash (%)	11.9	11.0	10.8	10.5	11.7	9.9

Table 38: Proximate analysis of coal 90% - biomass 10% blends

	Coals						
Biomass	L. Hall	La Jagua	H. Valley	El Cerrejon	K. Prima	Dawmill	Asfordby
Wood	10%	10%	10%	10%	10%	10%	10%
Moisture (%)	6.9	4.6	2.4	3.5	3.1	5.5	6.3
Volatiles (%)	38.0	40.7	32.5	40.9	42.8	38.4	37.0
Carbon (%)	52.1	51.9	48.5	53.8	48.7	51.5	45.7
Ash (%)	3.0	2.8	16.6	1.8	5.5	4.7	11.0
Rapeseed	10%	10%	10%	10%	10%	10%	10%
Moisture (%)	4.0	2.9	2.6	3.7	3.5	5.4	5.8
Volatiles (%)	38.7	39.9	32.4	40.8	42.6	38.4	36.9
Carbon (%)	53.1	54.5	48.2	53.4	47.5	51.0	45.6
Ash (%)	4.3	2.7	16.9	2.1	6.4	5.3	11.7

As can be seen from Table 37, the amount of moisture and volatiles in the final blend is mainly produced by the direct contribution of biomass according to the proportion used. The opposite effect was observed for the fixed carbon content that was primarily due to the presence of coal, which is reduced when the amount of biomass

in the blend increased. Finally, the total ash content in the blend depends directly on the original composition of the single constituents; for instance, in wood-coal blends the final ash decreases due to the low ash contribution of wood (<2%), although for rapeseed-coal blends the final ash content receive a higher contribution from rapeseed (~6%) .

6.5.2 Intrinsic reactivity of coal-biomass blends

Intrinsic reactivity tests were performed for all the coal-biomass blends (Table 39 and Table 40). From the TGA derivative plots, at least three peaks were identified: 1st, an initial peak at $100^{o}C$ produced by the moisture release of both materials simultaneously; a 2nd peak at $250\text{-}300^{o}C$ produced mainly by the liberation of volatiles from the biomass (the intensity of this peak was proportional to the concentration of biomass in the blend); and 3rd, a final peak above $\sim400^{o}C$ corresponding to the carbon burnout. The intensity of the final peak was mainly dependent of the coal concentration in the blend, although it also included the contribution of the biomass char combustion. Figure 123 illustrates intrinsic reactivity profiles for two blends at different blending proportions.

As it can be seen from these plots, the shape of the profiles and the resulting thermal reactivity depended directly of the main components derived from the single materials (moisture, volatile and carbon concentration). However, an important observation was that the positions of the 2nd and 3rd peaks are shifted to lower temperature values compared to the original materials. The same phenomenon was observed for all the blends studied, concluding that the addition of biomass in a concentration as low as 5% could significantly increase the reactivity of the coal by displacing the main burnout peak in an average of $\sim50^{o}C$. The total displacement of this peak was mainly a function of the type of coal and biomass used; and in a much

lower degree, the fraction of biomass present in the blend. For example in the case of wood-Dawmill (Figure 123, B), the displacement of the main burnout peak of the blends was ~80°C compared to the original coal. The same value was observed in all the blending proportions considered, which can be attributed to the high reactivity of this particular biomass.
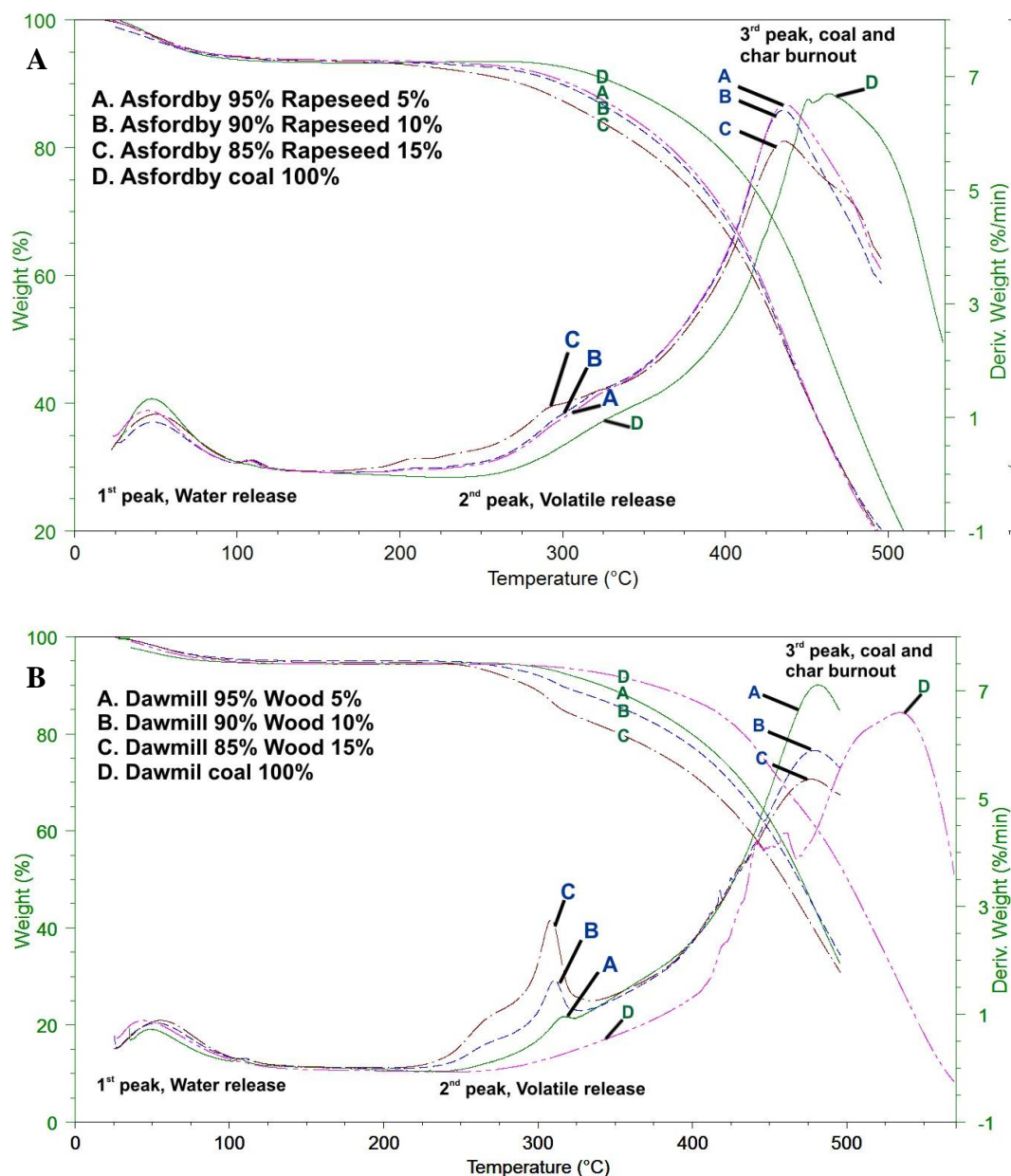
Figure 123: Illustrative intrinsic reactivity profiles for two coal-biomass blends. The heating rate used was 10°C min^{-1} in air.

Table 39: Intrinsic reactivity tests for coal-biomass blends

	Wood			Rapeseed		
Dawmill	5%	10%	15%	5%	10%	15%
2st Peak Temperature (^{o}C)	316	310	308	312	310	307
Deriv. Weight (% min^{-1})	0.95	1.62	2.88	1.67	2.16	2.63
3rd Peak Temperature (^{o}C)	481	478	477	437	437	433
Deriv. Weight (% min^{-1})	7.10	5.89	5.36	6.58	6.39	6.23
Asfordby	5%	10%	15%	5%	10%	15%
2st Peak Temperature (^{o}C)	297	300	300	319	318	292
Deriv. Weight (% min^{-1})	0.51	0.63	0.76	1.41	1.44	1.20
3rd Peak Temperature (^{o}C)	479	483	482	438	436	434
Deriv. Weight (% min^{-1})	6.48	6.85	6.51	6.54	6.44	5.92

Table 40: Intrinsic reactivity tests for coal 90% - biomass 10% blends

	L. Hall	La Jagua	H. Valley	El Cerrejon	K. Prima	Dawmill	Asfordby
Wood	10%	10%	10%	10%	10%	10%	10%
2st Peak Temperature (^{o}C)	305	306	308	301	299	310	300
Deriv. Weight (% min^{-1})	2.15	1.90	1.79	2.27	1.34	1.62	0.637
3rd Peak Temperature (^{o}C)	456	482	469	469	464	478	483
Deriv. Weight (% min^{-1})	7.04	6.31	5.50	6.47	3.21	5.89	6.85
Rapeseed	10%	10%	10%	10%	10%	10%	10%
2st Peak Temperature (^{o}C)	305	303	300	297	314	310	318
Deriv. Weight (% min^{-1})	1.01	1.09	0.76	1.02	1.52	2.16	1.44
3rd Peak Temperature (^{o}C)	455	476	468	476	473	437	436
Deriv. Weight (% min^{-1})	6.82	6.54	5.87	7.12	5.83	6.39	6.44

6.6 Thermal characteristics of coal-biomass blends in a large sample

Thermal experiments using a large sample size were also performed for coal-biomass blends. The experimental procedure was similar than that used for the testing of the single constituents, obtaining mass and temperature profiles when the material was constantly heated in air (0.5^{o}C min^{-1}). The main objective of these tests

was study the thermal behaviour of blends at low temperature. However, the research was focused particularly on the profiles close to the ignition temperature considering:

- The influence of the biomass type, using the same coal;

- The influence of the type of coal blended, using the same biomass;

- The impact of an increasing proportion of biomass in the blend.

6.6.1 Transient temperature profiles during a constant heating

The thermal profiles of coal-biomass blends showed similar characteristics than those obtained for the single components. As it can be seen in Figure 124, blend profiles maintain the original shape, although the temperature values were always in a middle region between the biomass and the pure coal.
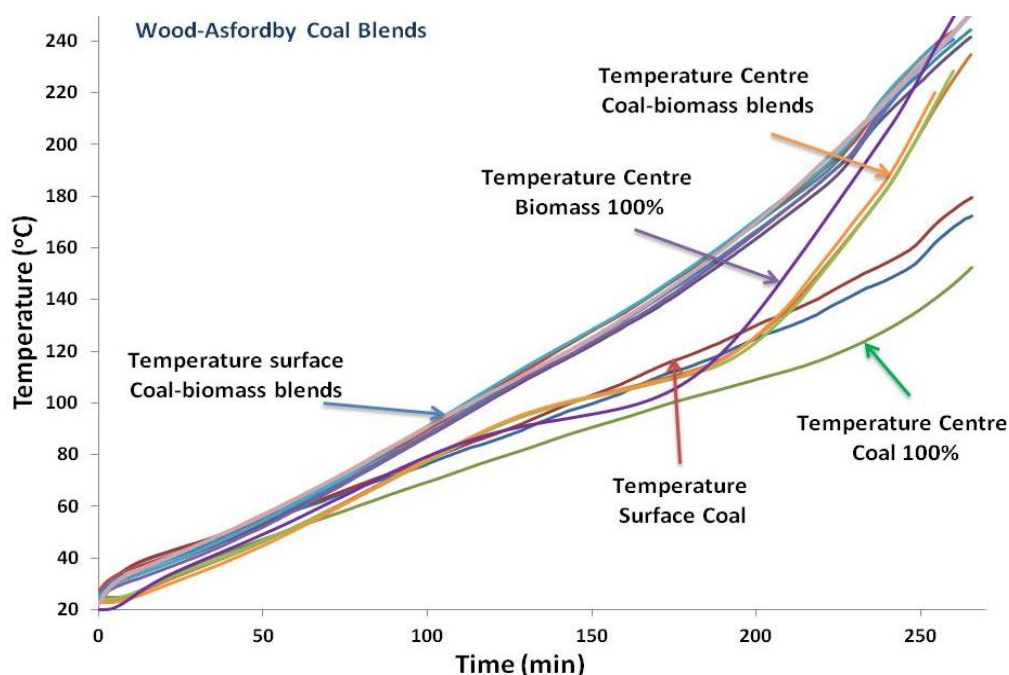
Figure 124: Thermal profiles in time for Asfordby coal, wood, and their different blends (95-5%; 90-10%; 85-15%). The heating rate used is 0.5^{o}C min^{-1} in air.

This behaviour was repeated in all the different coal and biomass blends studied, particularly concluding:

1. The temperature in the single biomass evolved faster than the blends. It was due to a high thermal conductivity in the bulk system, probably caused for the high porosity of these samples, allowing a greater air circulation and mass transfer. Also, it was produced by a poor heat capacity of the biomass that reduce the heat being stored, which combined with the high thermal conductivity increased the temperature of the sample in a rate closer to the furnace heating rate.

2. Coal samples constantly showed the lowest heating rate under the same furnace heating conditions. This was produced essentially by a low thermal conductivity in the bulk system and an elevated heat capacity of the coal, which together produced an increase of the sample temperature at a much lower rate than observed for biomass and its blends.

From these results, the thermal profiles of coal-biomass blends were totally predictable by considering the particular characteristics of the single components. However, the thermocouple placed at the surface of the sample holder showed a significant relevant phenomenon that was totally unpredictable: the ignition temperatures of the blends were always lower than with the initial single constituents. This phenomenon was clearly linked with the reduction of the peak temperatures initially observed in the TGA intrinsic reactivity test. For subsequent analysis, the focus was placed particularly on these temperatures rather than the full thermal profile.

6.6.1.1 Impact of the blending ratio in the temperature profiles

In general, it was evident that an increasing concentration of biomass in the blend displaced the temperatures towards the profile of the single material. However, considering the particular temperature readings obtained at the surface of the sample, the ignition temperature was shifted to lower values independently of the blending

proportions used (Figure 125). The magnitude of the shifting observed depended in part on the coal sample used, but also on the biomass type. The same conclusion was obtained previously from the intrinsic reactivity tests, in which the peak temperatures of the blends remained constant, independent of the blending proportion used, although shifted to lower values compared to those measured for the pure coals.
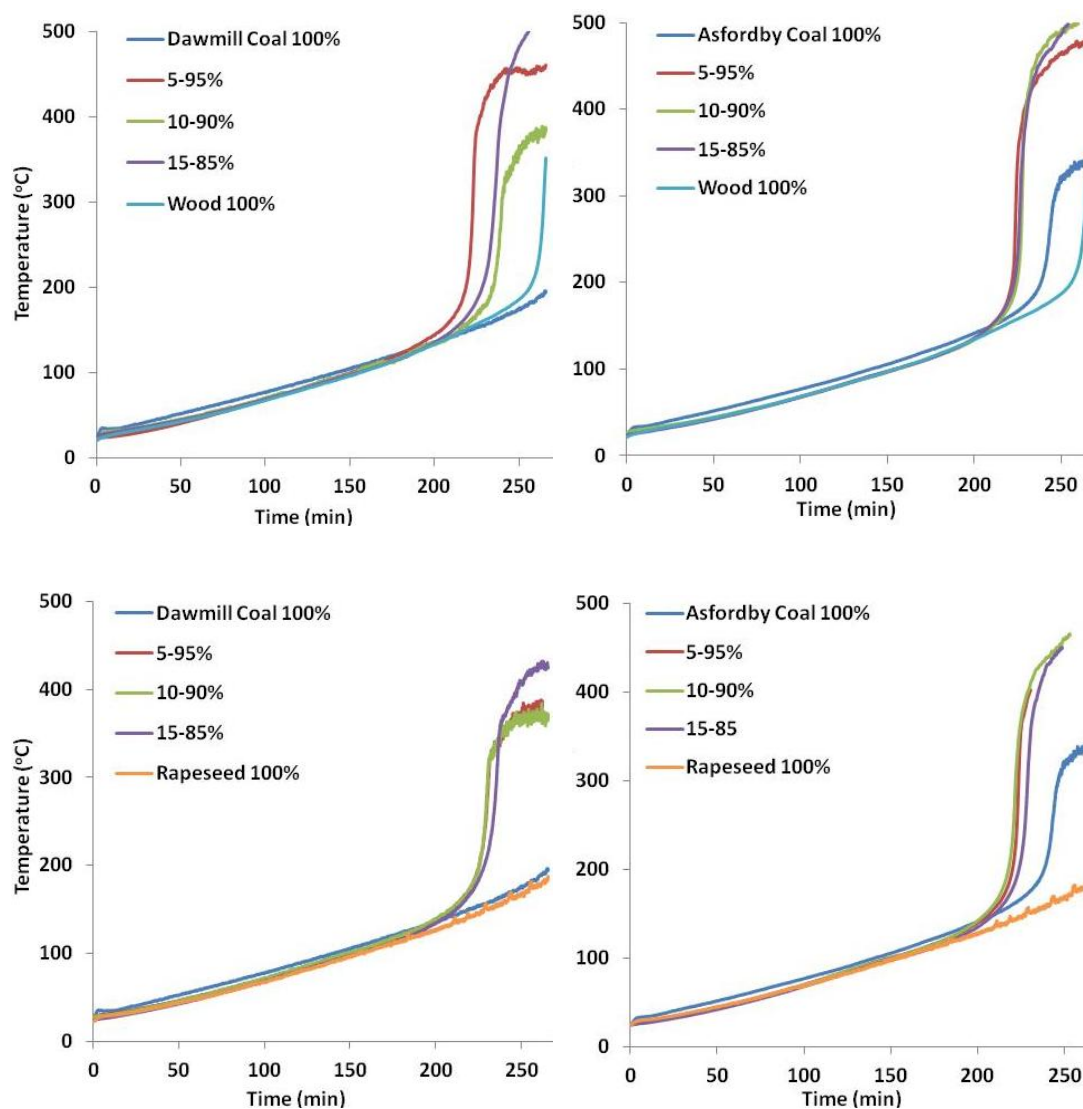
Figure 125: Temperature recorded in the surface of the sample holder for two coals and biomass samples at different blending proportions. The furnace heating rate used was $0.5^{\circ}C$ min^{-1} in air.

6.6.1.2 Influence of biomass type in the ignition temperature of blends

A single coal was blended with three different biomasses 90-10% (target feed ratio in the UK), to evaluate the influence of the biomass type. As it can be seen from Figure 126, the ignition temperature was again lower for all the blends. The impact of the biomass type in these profiles was not clear, since corn and wood blends showed similar characteristics than rapeseed; despite the fact that the behaviour of the single materials differed greatly.
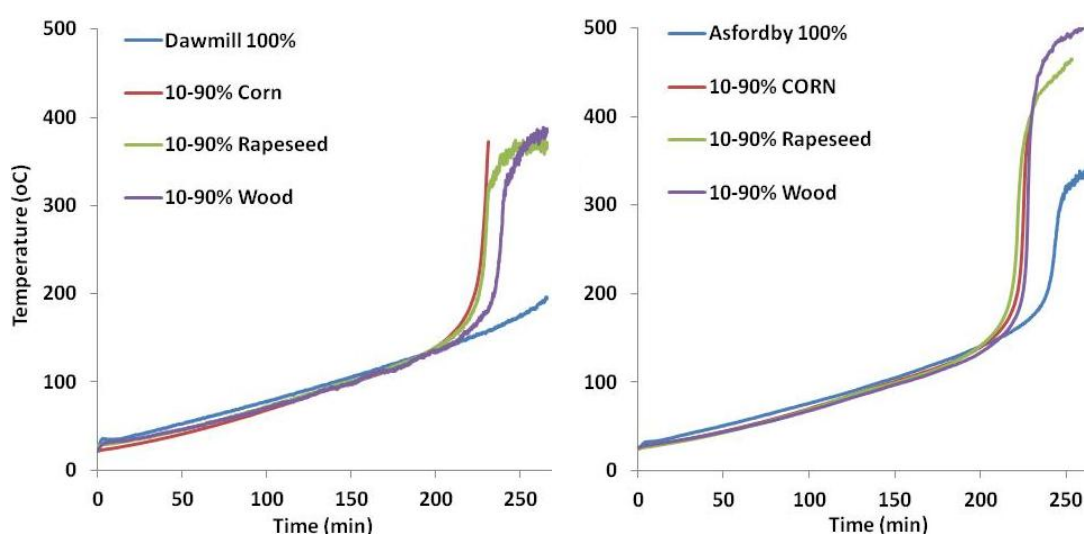
Figure 126: Temperature recorded in the surface of the sample holder for three different biomasses blended at 10-90% with two coal samples. The furnace heating rate used was 0.5^{o}C min^{-1} in air.

An identical shift was observed during the intrinsic reactivity tests (Figure 127). In these tests, the magnitude of the mass loss and the peak temperature of the coal burnout peak were reduced, independently of the biomass type employed in the blend. This confirmed the observations made during the large sample experiments, assuming also that the shift on the ignition temperatures could be predicted from the intrinsic reactivity test. Surprisingly, the same behaviour was found in thermogravimetric profiles obtained during the study of pyrolysis and combustion of

coal-biomass blends reported in literature [245,246]. In those cases, samples were subject to similar heating rates in air, although the shift of the peak temperature in the coal burnout stage has not been discussed.
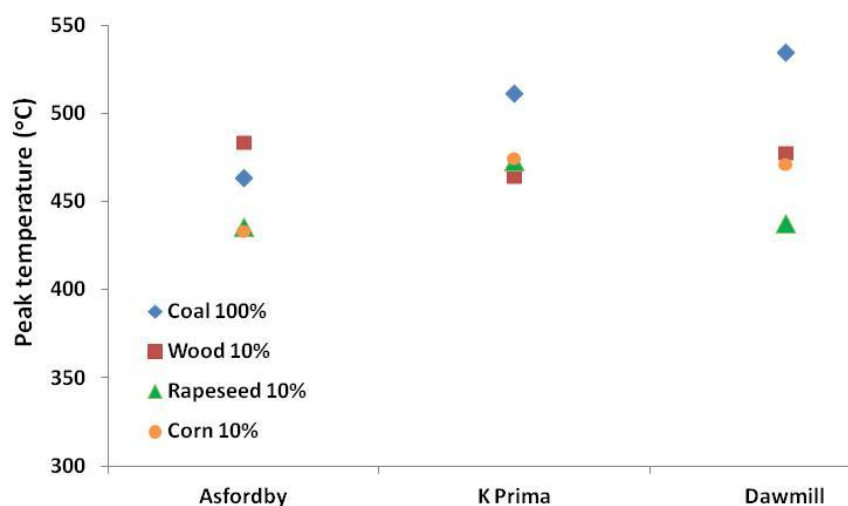
Figure 127: Effect of biomass type in the peak temperature of coals.

6.6.1.3 The influence of coal type on the temperature profiles

In order to study the effect of the coal type, samples of different petrographic characteristics were blended with two types of biomass (using a 90-10% blending ratio). In this case, the ignition temperatures of the blended coals were compared with the values obtained for the original samples (Table 41).

Table 41: Ignition temperatures estimated for coal-biomass blends

Coal	Ignition temperatures estimated from reactor (^{o}C)		
	Wood 10-90%	Rapeseed 10-90%	Coal 100%
El Cerrejon	130	132	165
Asfordby	136	133	175
Lea Hall	136	135	175
H. Valley	133	130	180
La Jagua	133	132	190
K. Prima	140	140	190
Dawmill	145	137	190

257

Initially, these results infer a slight correlation between the ignition temperature and coal rank. This agreed with the trend observed for the original coal samples, in which reactivity increases with a decrease of rank. However, this trend is not conclusive because of the narrow difference in the rank of the samples studied. Additionally, ignition temperature increases with an increase in the unreactive maceral content (i.e. Fusinite); although an exception to this was Hunter Valley coal, which contained a large amount of fusinite and semi-fusinite (and a high amount of ash), but showed a relative low ignition point. Finally, in Figure 128 the ignition values were compared to the peak temperatures obtained from the intrinsic tests. These results confirmed the reduction of the ignition temperature in all the blends, as well as the negligible impact of the biomass type.
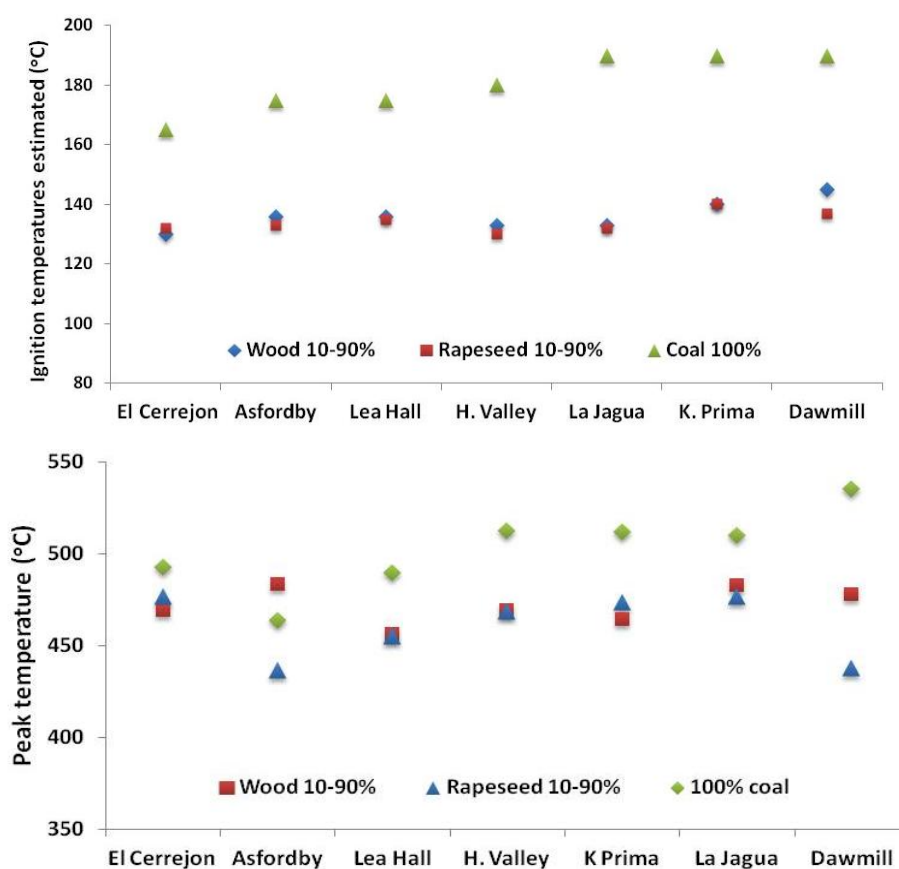
Figure 128: Comparison of ignition temperatures tendencies (top figure) and the results from the intrinsic reactivity tests (peak temperatures, bottom).

The evidence provided by the thermal profiles and the intrinsic reactivity tests must be carefully considered due to the high variability of the data, which was mainly produced by uncontrolled factors such as the different packing density of samples inside the sample holder during both tests (coal ≠ biomass ≠ blends). The thermal tests created one of the most relevant assumptions regarding to the safety of coal-biomass blends: the reactivity of coal at low temperature increases when the material is blended with biomass. Finally, the ignition temperature values obtained must be considered to be a gross estimation of this process, since these measurements did not follow any standard testing procedure. These were experimental observations derived from the large sample size test, which was originally developed to observe only the internal temperature profiles.

6.6.2 Mass loss during a constant heating

For coal-biomass blends, the continuous measure of the sample mass provided an additional and independent source of information. This confirmed the observations described from the temperature profiles, revealing important trends for the study of the ignition of blends.

6.6.2.1 Impact of the blending ratio in the mass profiles

The impact of the blending ratio on mass loss profiles was studied. Figure 129 shows four different weight loss curves for two coal-biomass blends in three different blending ratios. These show an inflection produced by the sample ignition (red arrows), in which the rate of the mass loss changes sharply. Also, these profiles show clear differences between the single components (coals & biomass) and their blends. Several conclusions can be derived from mass profiles regarding the impact of the blending ratio on the weight loss: Firstly, the proportions used in the blends were almost irrelevant on the shape and volatilization rate, producing just a slight shift in

the curve relative to the different blending ratios used. Second, the displacement of the ignition point can be identified in all the profiles (change on the slope of the curve, red arrows Figure 129). It was concluded that as long as the coal pile is contaminated with any type of biomass in a fraction above 5% (as this experiments suggested), the ignition of the blend would be lower than the ignition of the separated components.
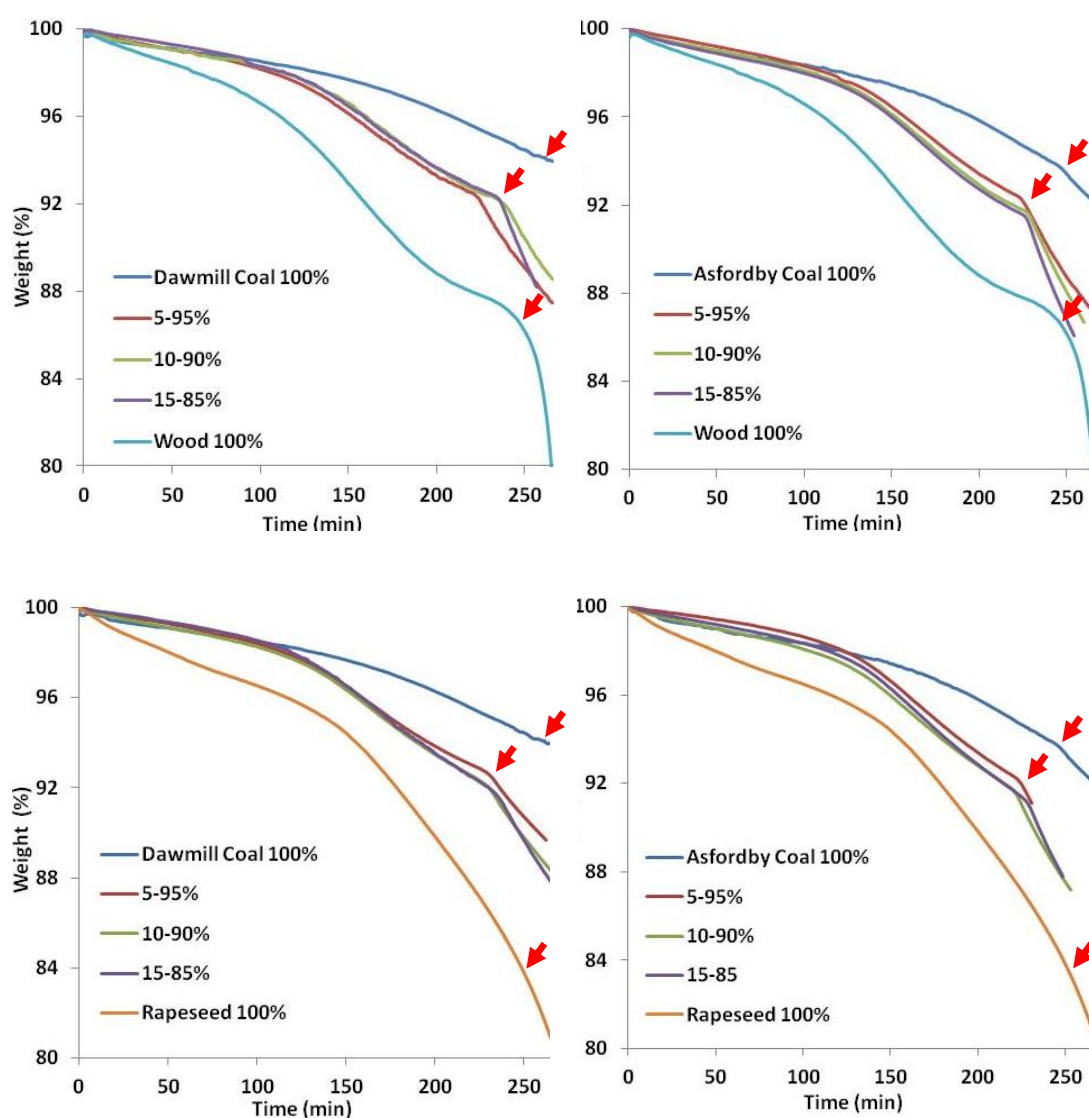
Figure 129: Weight loss profiles of coal-biomass at different blending ratios. The furnace heating rate used was 0.5^{o}C min^{-1} in air.

6.6.2.2 The influence of the biomass type in the mass profiles

The influence of biomass type was studied using a single blending ratio of 10% with three biomass types. Results suggested that the most reactive biomass (corn and wood) presented similar characteristics than the less reactive (rapeseed), although the reactivity of the pure materials differed considerably. These results are similar to those described during the temperature analysis (Figure 130).
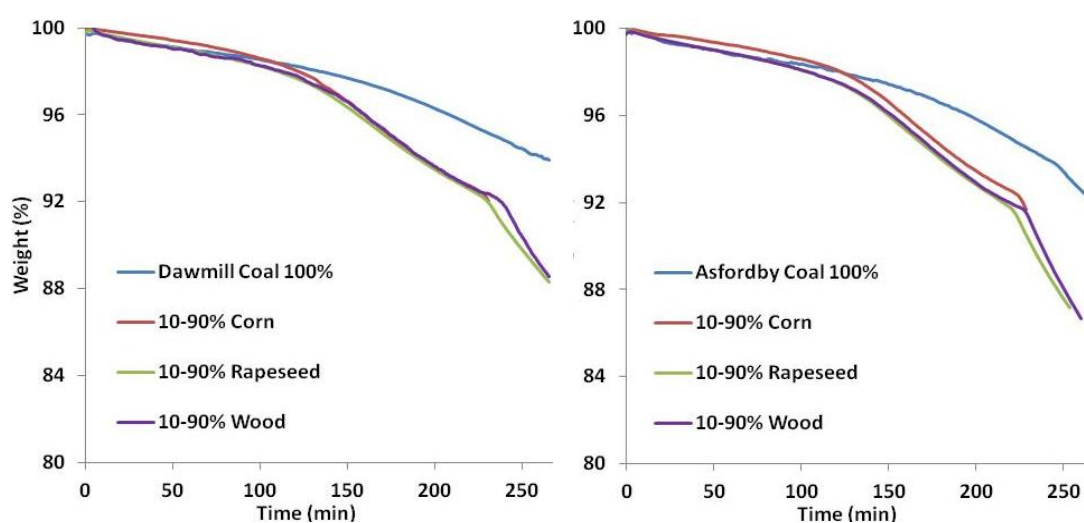
Figure 130: Weight loss profiles of two coals blended with three biomass types. The furnace heating rate used was 0.5^{o}C min^{-1} in air.

A large number of studies comparing the blending characteristics of several different types of biomass with a large number of coals can be found in literature. Several authors concluded that the lack of synergetic effects during the different stages of the coal-biomass blends combustion [225], although most considered high heating rates (due to the technological applications derived such as energy production and gasification) [246,247]. Conversely, low heating rates studies reported similar results (commonly employing TGA and DSC in a range of heating rates between 5 to 50°C min^{-1}). In all these cases, authors have not attempted to extrapolate these results to a larger system (e.g. comparing trends with a large sample size reactor or a big

261

deposit). Considering this information, the experimental results obtained during this work were totally different and difficult to compare with previous results.

6.6.2.3 The influence of the coal type blended in the mass profiles

The influence of the coal type was also observed in mass loss profiles. As Figure 131 and Figure 132 illustrate, below $100^{o}C$ (<140 min) the weight loss maintained a constant rate during water release, which can be explained by the combined moisture contribution of both materials. Above $100^{o}C$, the particular characteristics of each coal begin to be seen, increasing the volatilization rate finally leading to the ignition. At this stage, differences in ignition temperatures can be observed (lines A,B,C), as well as the final conversion reached, which cannot be estimated from the temperature profiles directly.
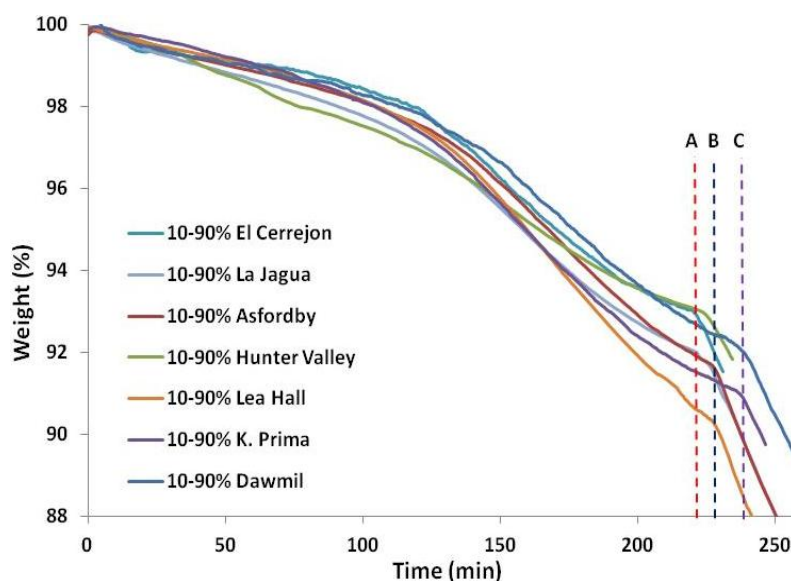
Figure 131: Mass loss of wood blended with coal samples at 10-90% ratio. The furnace heating rate used was $0.5^{o}C$ min^{-1} in air.

In particular, these results differed with the observation made during the temperature analysis, suggesting that biomass type does not influence the resulting temperature profiles (originally suggested in Sections 6.6.1.2 and 6.6.2.2). This difference can be

explained as a function of the types of profiles, since the evolution of the temperature did not necessarily represent the same behaviour as the weight loss curves. Ultimately, considering all the information from the temperature and mass analysis, it was concluded that the influence of the coal type was much more profound than the effects produced by the different kinds of biomass.
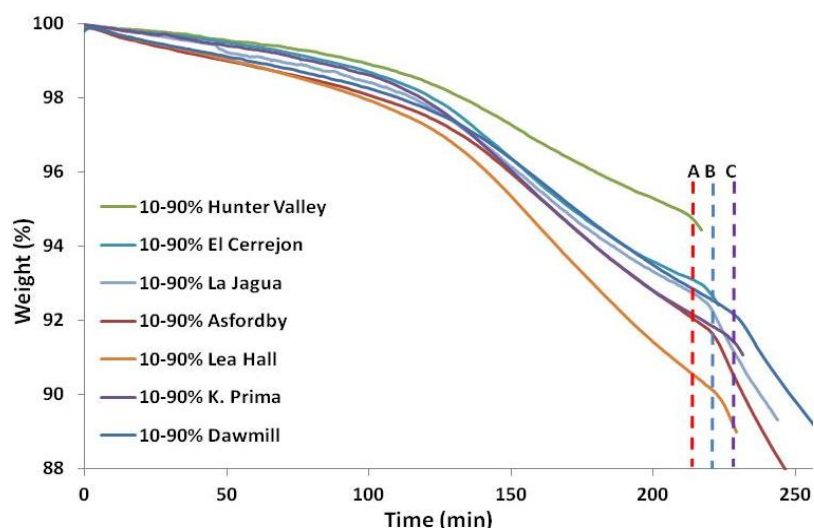
Figure 132: Mass loss profiles of rapeseed blended with coals at 10-90% ratio. The furnace heating rate used was 0.5^{o}C min^{-1} in air.

6.7 Spontaneous combustion of biomass and coal-biomass blends

For biomass, it is still not clear whether these materials can undergo spontaneous combustion in the same way as with coals. For these materials, no significant air-biomass interactions at low temperature were found. Additionally, the influence of biological activity on the self-heating processes was totally ignored during this study, although this needs to be considered in further studies. Raw biomass can be grouped in terms of characteristics reactivity profiles. Particle size did not have a significant impact on this classification. The rate of release of volatiles varied depending on the starting biomass material. The biomass materials that have the widest intrinsic reactivity profiles also produce the least reactive chars with the thickest walls and

solids content. Future work could include an investigation into the interaction between lignin, hemicellulose and cellulose components to link the reactivity of the raw material with the char material.

Besides, when coal was blended with biomass, the characteristic mass increase produced by the oxygen adsorption in coals at low temperatures was not observed. As the magnitude of this weight increase was interpreted as a sign of stability of the solid complex formed in the coal surface, the influence of biomass in this interaction is almost certain. However, it is not clear whether the blending produced an inhibition of the oxygen adsorption, or if it reduced the stability of the complex formed, characterized by a nil weight gain due to an increase of the desorption rate and thermal cracking. If the later mechanism is true, blending coal with biomass could amplify the potential to suffer a spontaneous combustion, and further work should investigate this more thoroughly. Finally, the lower ignition temperatures recorded for blends were also relevant, which was not described in literature before and requires additional study.

Chapter 7. Testing procedures developed to estimate spontaneous combustion potential

In this chapter, a set of functional experimental procedures are proposed for spontaneous combustion detection. These were based on the conclusions obtained during experiments, considering the direct evidence of the self-oxidation reaction observed in coals, and the thermal irregularities found for biomass and coal-biomass blends that could lead to a spontaneous fire. In general, methods are initially described step by step, followed by the results of additional experiments (using a new set of samples with a well-known liability to spontaneous combustion), finishing with a discussion about the consistency of each method. The final aim of these tests was to provide industries and researchers with alternative tools for spontaneous combustion assessment.

7.1 Validation of the experimental procedures proposed

7.1.1 Coal samples used for validation tests

A set of 13 samples were provided by the Federal Institute of Material Research of Berlin (BAM) to be used as a reference material to evaluate the prediction of the methods developed. These samples were collected from active natural fires and coal deposits, and tested in a large scale facility available at BAM. Results of these tests were added to the historic information available (for those samples) in order to establish clearly the propensity towards self-oxidation (Table 42). Then, samples were sent to Nottingham in a random order and without any identification to be classified according to the actual methods proposed. After three months of testing, results were sent back to Berlin, to be compared with the original database.

Table 42: Characteristic of coal samples provided by BAM

	Name	Origin	Type of coal	Characteristics
1	Sample 1	China Wuda region	Bituminous coal	Safe, low reactive
2	Sample 2	China Wuda region	Bituminous coal	From an active coal fire in China
3	Sample 3	China Wuda region	Bituminous coal	Reactive coal
4	Sample 4	China Wuda region	Bituminous coal	Reactive coal
5	Sample 5	China Wuda region	Bituminous coal	Reactive coal
6	Sample 6	China Rugigou region	High rank coal	medium reactive
7	Sample 7	China Rugigou region	Bituminous coal	From an active coal fire in China
8	Sample 8	China Gulaben region	High rank coal	Safe, low reactive
9	Sample 9	Norway, Svalbard 2685	Bituminous coal	medium reactive
10	Sample 10	China Rugigou region	High rank coal	Safe, low reactive
11	Sample 11	Norway, Svalbard 2564	Bituminous coal	medium reactive
12	Sample 12	Norway, Svalbard 2560	Bituminous coal	medium reactive
13	Sample 13	Norway, Svalbard 2553	Bituminous coal	medium reactive

7.1.2 Physical properties of BAM coals

Proximate analysis was carried out to characterize the samples immediately after arrival (Table 43). This test indicated some particular physical characteristics of samples such as the elevated water content of samples 2, 3, 4, 6 and 7, and the high ash content found in samples 1, 5, 9, 10, 11, 12 and 13.

Table 43: Proximate analysis for coal samples used as a reference

Coal	As received				Dry, ash free basis		
	Moisture (wt.%)	Volatiles (wt.%)	Fixed Carbon (wt.%)	Ash (wt.%)	Volatiles (wt.%)	Fixed Carbon (wt.%)	Carbon/ Volatiles ratio
Sample 1	1.0	21.2	38.2	39.6	21.4	38.6	40.0
Sample 2	7.4	26.3	61.2	5.1	28.3	66.1	5.6
Sample 3	9.1	27.4	60.3	3.3	30.1	66.3	3.7
Sample 4	8.4	27.2	61.4	2.8	29.8	67.2	3.1
Sample 5	4.2	28.5	41.2	26.1	29.8	43.0	27.2
Sample 6	8.7	26.4	59.8	5.1	28.9	65.4	5.6
Sample 7	7.2	25.2	59.9	7.7	27.1	64.6	8.3
Sample 8	0.8	6.7	90.3	2.1	6.7	91.1	2.1
Sample 9	0.9	35.2	43.1	20.7	35.6	43.6	20.9
Sample 10	1.6	6.1	49.9	42.5	6.2	50.7	43.2
Sample 11	0.9	31.9	48.1	19.0	32.3	48.6	19.2
Sample 12	1.2	27.7	31.2	39.9	28.04	31.6	40.4
Sample 13	0.9	38.7	43.5	16.8	39.1	43.9	17.0

7.1.3 Validation of biomass and coal-biomass blends tests

Information on biomass and coal-biomass blends that are susceptible to self-heating and spontaneous combustion is scarce. The direct action of the aerial oxidation over these materials was negligible compared to that seen in coals. Therefore, identifying biomass and coal-biomass blends samples that are prone to spontaneous combustion (to be used as a reference) was not possible. For that reason, the proposed tests for biomass and coal-biomass blends assessment were supported just in the information available from the previous experimental trials.

7.2 Thermogravimetric tests to identify coals prone to self-oxidation

Thermogravimetric analysis reveals characteristics about coals intrinsic reactivity, and also it allows the measurement of oxygen adsorption at low temperatures. Then, two tests were proposed using this technique:

7.2.1 Reactivity at low temperature using TGA

This test was based on the results showed in Chapter 4, Section 4.2.1. In this case, the reactivity at low temperature is calculated from a set of different heating ramps applied to a freshly pulverized coal sample. The experimental procedure, data analysis, and results are explained as follows:

7.2.1.1 Sample preparation and experimental procedure

First, the coal sample must be freshly mined. If the age of the coal is unknown, the largest particles must be selected and ground since these particles are less affected by the oxygen oxidation and will deliver the highest possible reactivity. Secondly, coal must be pulverized in a particle size below 106μm. The time between the milling and the TGA test must be as short as possible, and it is recommended to be less than 24hrs. For a single coal test, at least 120mg of sample (enough to run 6 heating ramps) is required. Finally, five single heating ramps are executed in the TGA: 3, 5, 7, 10 and 20°C min^{-1}, from ambient temperature to 600°C. These runs are executed under air atmosphere, and the gas flow must be selected depending on the equipment availability. Regarding to the last parameter, the highest possible air flow should be used without cooling the sample, whilst allowing stable balance reading.

7.2.1.2 Data analysis

The raw data delivered by the TGA is a sample weight profile (%) in time. These are continuous profiles, from which the time derivative must be calculated for each heating rate applied. This derivative is a secondary continuous profile (weight loss rate vs time) from which the linear segment located between the water release stage (approximately above 100°C), and the main devolatilisation peak (below 400°C) must be identified. This segment is interpolated by a linear trend, from which the slope is calculated. Appling the same procedure for the five different heating runs

produces five slopes; each related to a specific heating rate. Then, these slopes are plotted against their respective heating rates to achieve a second order representation. Finally, a linear correlation can be obtained from the second order graph, in which the slope is defined as the TG_{spc} index (a summary diagram is shown in Figure 133). In this test, high reactive coals show higher values of the TG_{spc} index. As it is a relative test, the reactivity of a well known prone sample is used as a reference.
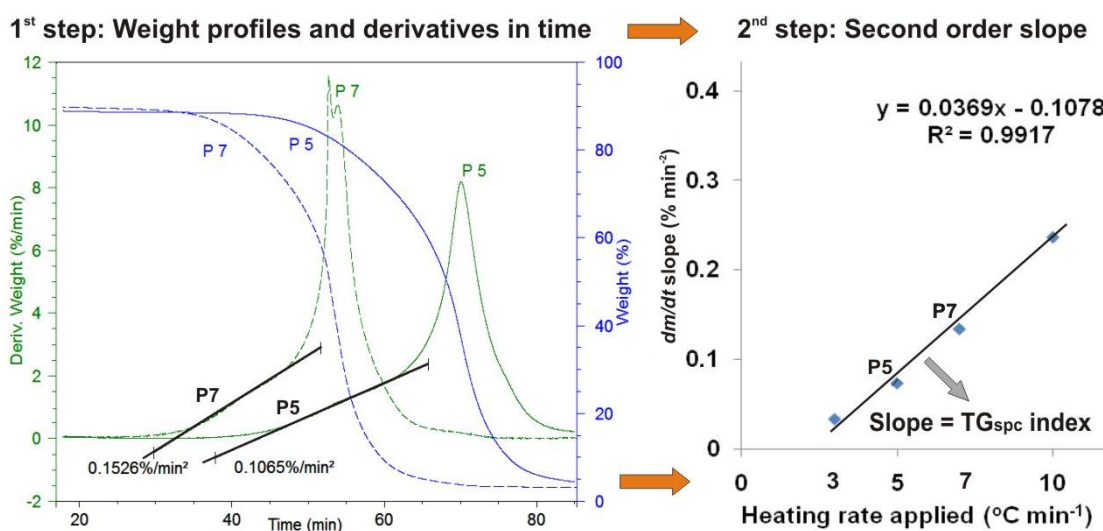
Figure 133: Data analysis to obtain the TG_{spc} index (TG_{spc}=0.0369 wt % $^{o}C^{-1}$ min^{-1}).

7.2.1.3 Experimental analysis using reference samples

BAM samples were tested accordingly to the experimental procedure described and results are shown in Figure 134 and Table 44 (using Fenosa coal as the referencing sample). As can be seen, sample 7 was far more reactive than the other samples (four times), even compared to Fenosa coal. This sample was successfully identified by the TG_{spc} test, since this was obtained from a natural coal fire (Table 42). In addition, samples 3, 4 and 2 were at the top of the reactivity scale of the remaining samples, agreeing with the reactivity data from Table 42. Finally, samples 6, 8 and 10 showed a reduced reactivity that agreed with the information provided by BAM, which had catalogued these samples as safe and low reactive.
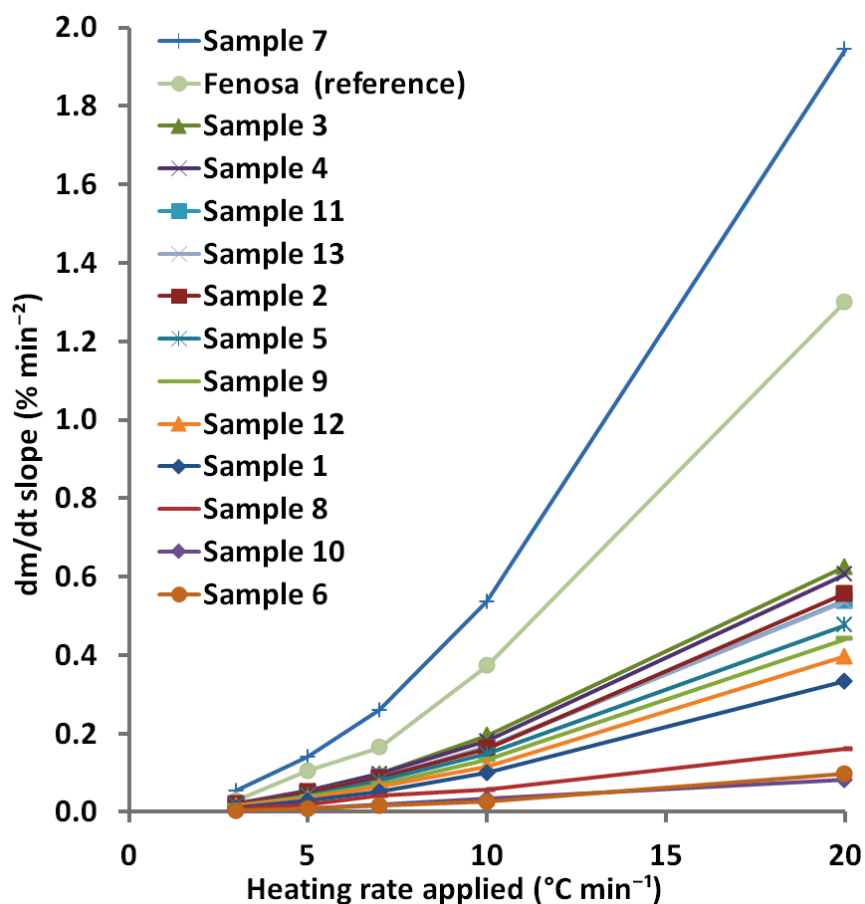
Figure 134: Second order curves obtained for reference coals.

Table 44: TG$_{spc}$ index for coal reference samples in decreasing order

Coal	TG$_{spc}$ (wt % $^{o}C^{-1}$ min^{-1})	Dev. Coef.
Sample 7	0.1153	0.97
Fenosa (Reference)	0.0773	0.97
Sample 3	0.0368	0.98
Sample 4	0.0355	0.98
Sample 2	0.0325	0.98
Sample 11	0.0315	0.98
Sample 13	0.0313	0.98
Sample 5	0.0279	0.98
Sample 9	0.0258	0.98
Sample 12	0.0232	0.98
Sample 1	0.0196	0.98
Sample 8	0.0091	0.99
Sample 6	0.0057	0.97
Sample 10	0.0046	1.00

7.2.2 Low temperature oxygen adsorption using TGA

This test was based on the results showed in Chapter 4, Section 4.2.1. In this case, the maximum oxygen adsorption at low temperature is quantified during a slow heating ramp in air. The experimental procedure, data analysis, and results are explained as follows:

7.2.2.1 Sample preparation and experimental procedure

In the same way as described in the previous test, the coal sample must be freshly mined. Then, the larger particles must be selected and pulverized to a particle size below 106μm. The milling method selected must be as low impact as possible, in order to avoid overheating the sample and losing some of the original water content. Also, the time between the milling and the TGA test must be minimized, and it is recommended to be less than 24hrs. For a single coal test, 40mg of sample are required (enough to run 2 heating ramps). The sample must be spread in the TGA crucible covering all the area available and without any type of compression to secure the maximum coal-air contact. Finally, a single heating ramp in air is executed in the TGA at $3^{o}C$ min^{-1}, from room temperature to $500^{o}C$. As the test time is short, it is recommended that this procedure is carried out in duplicate. The gas flow used rate should be maximized whilst avoiding cooling or interference with the balance reading.

7.2.2.2 Data analysis

In this case, the raw data delivered by the TGA is a sample weight profile (%) in temperature. From this profile, the key values can be obtained directly: a) the initial temperature (the stage at which starts an increase in sample weight); b) peak temperature (where increased weight of the sample reach a maximum); c) the maximum oxygen absorption (% of weight increase reached at the peak temperature).

From this information, coals must be classified by the maximum weight increase and temperature range observed (the temperature range is defined as the difference between peak and starting temperature). Then, coals with a nil weight increase and initial water content below 30% are classified as highly reactive; coals with a nil weight increase and initial water content above 30% are classified as unreactive; coals with a maximum weight increase below 1% and a temperature range under 150°C are classified as medium reactive; and coals with a maximum weight increase higher than 1% and a temperature range bigger than 150°C are classified as unreactive. In Figure 135, profiles of a high reactive and an unreactive coal sample are shown, indicating the key values obtained from this test.
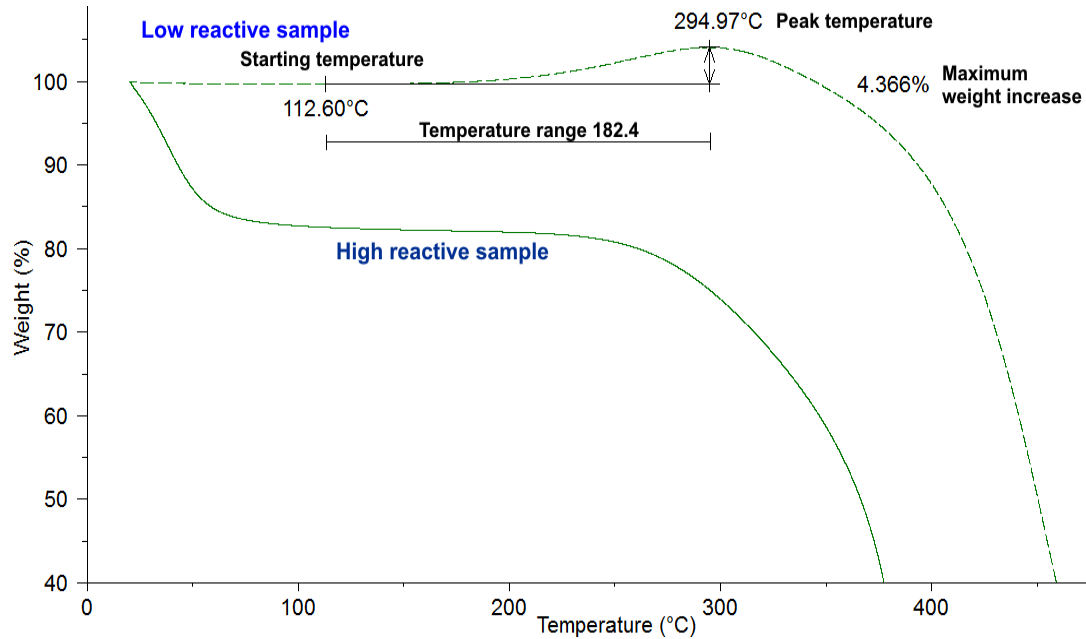
Figure 135: Examples of coal oxygen adsorption profiles obtained from TGA.

7.2.2.3 Experimental analysis using reference samples

BAM samples were subjected to the experimental procedure described, and their results are shown in Figure 136 and Table 45.
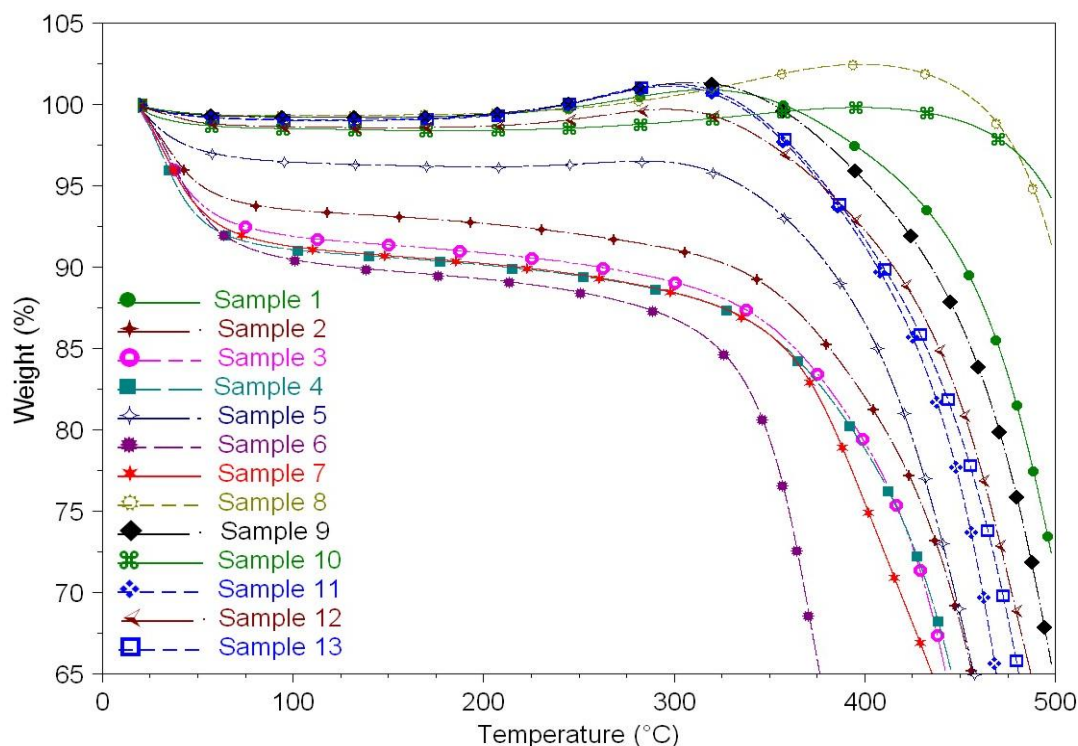
Figure 136: TGA profiles for BAM samples (heating ramp of $3^{\circ}C$ min^{-1} in air).

From Figure 136, samples that showed a weight increase can be clearly identified. In particular, TGA profiles were numerically analyzed to obtain the key parameters shown in Table 45, alongside with the coal classification estimated from these results. From this test, samples 2,3,4,6 and 7 were classified as "highly reactive", which agreed with the original information provided in Table 42. Conversely, samples 8 and 10 showed the widest temperature range that means the less reactive samples of the whole set, which totally corresponded to the information hold for these samples. Conclusively, the results obtained from this particular test have delivered accurate predictions about the ability of these coals to adsorb oxygen; and more importantly, to identify the type of interaction that oxygen molecules and coals suffered (formation of stable or unstable solid complexes in the coal surface).

Table 45: Coal classification regarding to weight increase

Coal	Weight increase (%)	Starting temperature (^{o}C)	Peak temperature (^{o}C)	Temperature range (^{o}C)	Coal Classification
Fenosa	0.000	-	-	-	Highly reactive
Sample 4	0.000	-	-	-	Highly reactive
Sample 2	0.000	-	-	-	Highly reactive
Sample 3	0.000	-	-	-	Highly reactive
Sample 7	0.000	-	-	-	Highly reactive
Sample 6	0.000	-	-	-	Highly reactive
Sample 5	0.377	193	275	81	Medium reactive
Sample 12	1.354	136	285	148	Unreactive
Sample 10	1.549	169	384	214	Unreactive
Sample 1	1.840	130	305	174	Unreactive
Sample 9	2.443	115	301	185	Unreactive
Sample 11	2.444	108	289	181	Unreactive
Sample 13	2.542	111	288	176	Unreactive
Sample 8	3.431	111	384	272	Unreactive

7.3 Thermo-petrographic tests to identify coals prone to self-oxidation

Microscopic features of coal also reveal characteristics associated to its reactivity. Particularly, the characterization of induced thermal changes of coals revealed the way in which particles interact with oxygen, identifying the most probable reaction regimes suffered, which were related to the self heating phenomena. Consequently, two tests are proposed using petrographic characterization of thermally altered particles.

7.3.1 Thermo-petrographic test based on coal vitrinite reflectance change

This test was based in the change of vitrinite reflectance after a slow thermal oxidation of the sample. This test was developed considering the results showed in Chapter 5, Section 5.2.2. The experimental procedure, data analysis, and experimental validation are explained as follows:

7.3.1.1 Sample preparation and experimental procedure

Figure 137 shows a general description of this test. First, the vitrinite reflectance of the original material must be obtained following the procedure described in the British standard [105]. In this case, petrographic blocks are prepared for fresh and oxidized samples using the same particle size, ideally with a size fraction of 212-106µm. This particle size fraction is big enough to avoid effects produced by particle edges in the measurements, and at the same time, it is small enough to include a large number of particles per petrographic block (~1000 particles for cm^2).
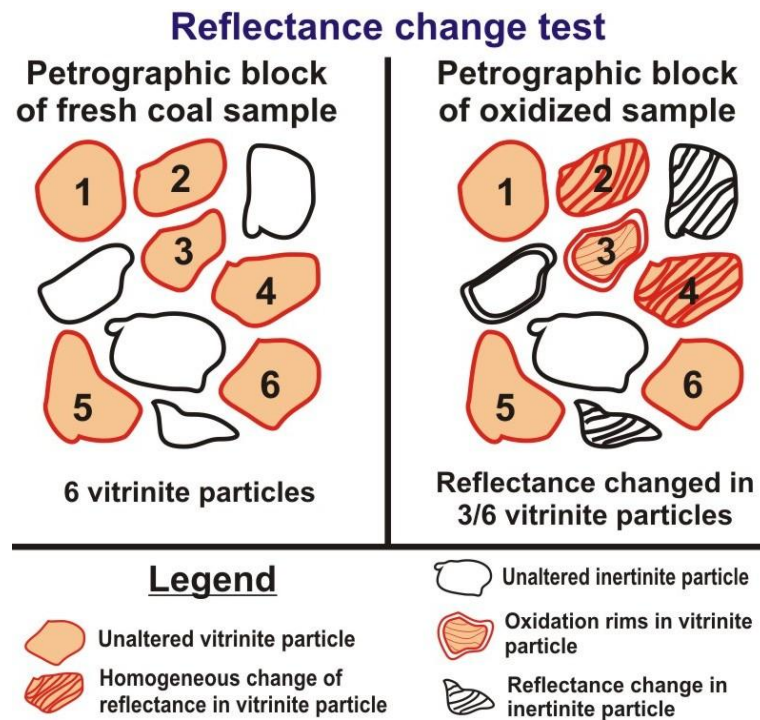
Figure 137: Descriptive figure of the reflectance change test proposed.

Second, the oxidized material is produced by constantly heating a well packed coal sample (100g) from room temperature to 250°C in air, using the target particle size. In this case, the heating rate applied must be as slow as possible to allow the air diffusion through the sample during the heating. A recommended heating rate is 0.5^{o}C min^{-1}, which is the highest heating rate that can produce oxidized material in

less than 8 hours. In any case, the selected heating rate must be the same for all samples. After this, the vitrinite reflectance of the altered material must be estimated following the same procedure as for the fresh coal sample. Finally, the results from both analyses are compared.

7.3.1.2 Data analysis

The vitrinite reflectance is usually expressed as a percentage of light reflected from the material (%R). Then, the reflectance of fresh and oxidized coals can be arithmetically compared:

$$\text{Equation 15} \qquad \%R \text{ change} = \frac{\%R_{\text{Fresh coal}} - \%R_{\text{Oxidized coal}}}{\%R_{\text{Fresh coal}}} * 100\%$$

From this information, coals are classified depending on the maximum reflectance change observed: coals with a percentage of reflectance change higher than 15% are classified as "extremely reactive"; samples with a reflectance change between 10 to 15% are classified as "reactive"; coals with a reflectance change between 5 to 10% are classified as "low reactive", and finally, coals with a reflectance below 5% are classified as "unreactive". In addition, it is recommended that coals with a percentage of reflectance change higher than 10% must be subject to additional experimental tests to confirm the coal classification. Particularly, the original rank value must be considered along with the ash and unreactive maceral content, and the maximum mass increase observed during a slow heating ramp in air by using the TGA.

7.3.1.3 Experimental analysis using reference samples

Results of the reflectance change test for BAM samples are shown in Table 46. From this test, samples 2,3,4 and 7 were classified as "highly reactive", the same result obtained from the second TGA tests, which also agreed with the original information

provided in Table 42. Samples 6 and 12 were slightly less reactive and located at the middle of the table, although these results were also agreed with the second TGA test and with the original information provided. The remaining samples were classified as unreactive, particularly samples 8 and 11 that showed a negative reflectance change (reflectance of vitrinite decreased). In this particular case, from the proximate tests was observed that sample 11 had a high ash (19%) and a low water content (<1%). In the other case, sample 8 had an elevated coal rank (2.45%R) and elevated carbon content (92%). Considering these characteristics, the classification of both samples as "unreactive" was confirmed.

Table 46: Reflectance variation in BAM samples after a slow heating

Sample name	Coal reflectance		Change (%R)	Change (%)	Coal Classification
	Fresh (%R)	Oxidized (%R)			
Fenosa	0.42	0.54	0.12	28.6	Highly reactive
Sample 3	0.96	1.20	0.24	25.0	Highly reactive
Sample 4	0.88	1.06	0.18	20.5	Highly reactive
Sample 2	0.95	1.14	0.18	18.9	Highly reactive
Sample 7	0.98	1.14	0.16	16.3	Highly reactive
Sample 12	0.69	0.77	0.08	11.6	Reactive
Sample 6	1.79	1.98	0.18	10.1	Reactive
Sample 9	0.89	0.94	0.05	5.6	Less Reactive
Sample 13	0.84	0.88	0.04	4.8	Unreactive
Sample 5	0.69	0.72	0.03	4.3	Unreactive
Sample 10	2.57	2.66	0.09	3.5	Unreactive
Sample 1	1.04	1.05	0.01	1.0	Unreactive
Sample 8	2.45	2.34	-0.11	-4.5	Unreactive
Sample 11	0.72	0.66	-0.06	-8.3	Unreactive

7.3.2 Thermo-petrographic test based on morphologic classification of coal particles

This test relies on the quantification of the morphological features created during a slow heating of coals, which were examined in Chapter 5, Section 5.2.1. Since the formation of the different particle morphotypes depends on several factors (e.g. temperature, exposure time, heating rate applied and initial degree of coal oxidation), this is a qualitative method that can provide confirmation for some of the previous tests described. As a result, this test should not be used as a primary indicator of coal propensity.

7.3.2.1 Sample preparation and experimental procedure

Thermally altered coal particles are produced by heating a well packed coal sample (100g) from room temperature to 250°C in air, by using a particle size fraction of 212-106μm and a heating rate of 0.5^{o}C min^{-1} (similar experimental method than this described in Section 7.3.1.1). Petrographic blocks are prepared using the oxidized material, in order to quantify the different thermal morphotypes formed. Figure 138 shows a general description of the petrographic test applied. As can be seen, the identification is restricted to two different morphotypes: a) particles with homogeneous change of reflectance; and b) particles with oxidation rims. Different thermal alterations are considered as "unclassified altered material", and the material remaining unchanged is classified as "unaltered material". In all cases, particles are classified independently of the maceral group that they belong.
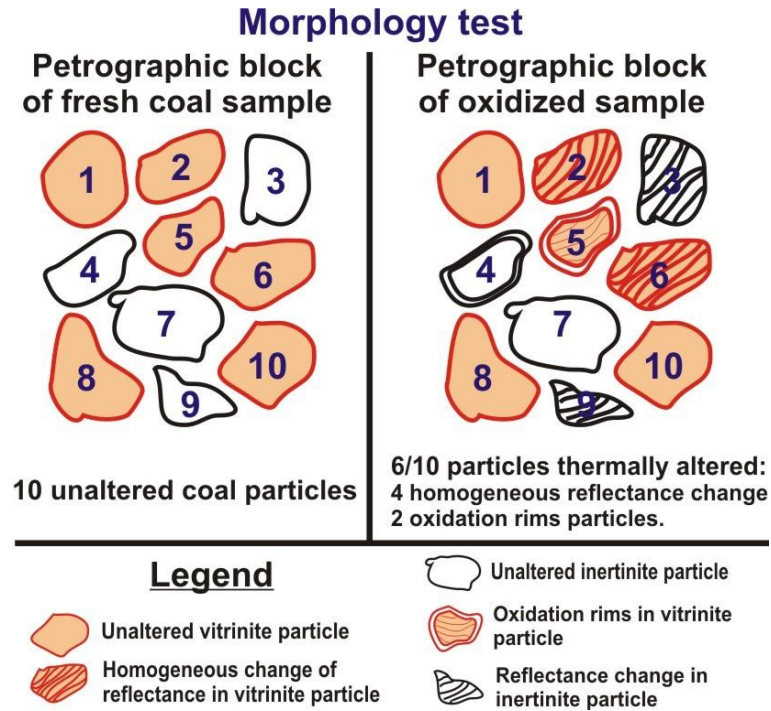
Figure 138: Descriptive figure of the morphology classification test for thermally altered coal particles.

7.3.2.2 Data analysis

Three indices are calculated using the results from the petrographic characterization (summarized in Table 47), indicating the degree of reactivity and the tendency to develop a specific reaction regime in each coal:

A) % altered material: the total fraction of the material thermally altered, which is defined as:

$$\text{Equation 16} \quad \% \text{ Altered material} = \frac{\text{Total particles counted -Unaltered particles}}{\text{Total particles counted}} * 100\%$$

The experimental conclusions suggested that a coal sample with a fraction of altered material higher than 50% must be considered as "high reactive". Coal samples with a fraction of altered material between 25% and 50% can be classified as "medium reactive", although these coals must be subject to additional tests. Samples with a fraction of altered material lower than 25% can be classified as "unreactive".

279

B) % of each morphotype: the corresponding percentage of homogeneous reflectance change and oxidation rims particles in each coal are both considered as indices. In the first case, coals prone to spontaneous combustion tend to develop a large number of homogeneous reflectance change particles (>50%). Additionally, the rate of the oxidation of coals that develop a large number of oxidation rims particles (>50%) tend to be controlled by oxygen diffusion, showing globally a lower reaction rate than the first morphotype. Then, the fractions of these morphotypes are employed to calculate the ψ ratio of each coal.

C) Ψ ratio: this index is defined as the ratio between the homogeneous reflectance change and oxidation rims particles of each coal (ψ):

$$\text{Equation 17} \qquad \psi = \frac{\text{Total homogeneous reflectance change particles counted}}{\text{Total oxidation rims particles counted}} * 100\%$$

This index provided an indication about the tendency of each coal to develop a particular reaction regime over its opposite possible behaviour at low temperature. As the experimental conclusions suggested, a coal sample with a ψ value higher than 1.5 must be considered as "high reactive"; this is because the thermal oxidation of this type of coals tends to be controlled by the kinetic of the reaction. Coal samples with a ψ value from 1.0 to 0.25 can be classified as "medium reactive". In this case, the rate of oxidation tends to be controlled by both the kinetic of the reaction and the oxygen diffusion through the particle. Finally, samples with a ψ value lower than 0.25 can be classified as "unreactive".

For this particular test, the scale of the ψ value was obtained using a particle size fraction of 212-106μm. For different particle sizes, the classification based in the ψ value must be confirmed, since the particle size also has influence on the rate of the reaction, as it was explained in Chapter 3.

Table 47: Summary of indices obtained from petrographic characterization

Coal Classification	Altered material (%)	Morphotype concentration		Ψ ratio
		Homogeneous reflectance change (%)	Oxidation rims (%)	
Highly reactive	> 50%	> 50%	-	> 1.5
Medium reactive	25 – 50%	-	-	0.25 - 1.5
Unreactive	< 25%	-	> 50%	< 0.25

7.3.2.3 Experimental analysis using reference samples

Unfortunately, the validation of this test by using the samples provided for BAM was not possible due to the low amounts of available material. As a result, the consistency of this test only relies on the information already discussed in Chapter 5.

7.4 Tests to identify self-oxidation of biomass and coal-biomass blends

Information about aerial oxidation of biomass and coal-biomass blends is limited, making it difficult to establish whether self-heating would be likely with these types of materials. There are just a few reports were self-heating reactions were shown by biomass, although it still is not clear whether these were caused by aerial oxidation or by microbial breathing (discussed in Chapter 3). Additionally, scientific papers describing the reactivity of these materials at medium and elevated temperatures (above 200°C) were also limited. Subsequently, considering this data and the experimental results currently reported, the focus was maintained on potential testing procedures which could quantify the reactivity of those materials in air, at temperatures closed to their ignition.

The last option was selected since the most realistic alternative to biomass use would be through blending with coal. In this case, the safety issues derived from synergic interactions could be significant. In this context, experimental results suggested the use of TGA as a tool to evaluate biomass reactivity in air; and the study of the

ignition temperature in a large sample size could provide a suitable indicator for coal-biomass blends.

7.4.1 Thermogravimetric tests to estimate biomass reactivity

The TGA intrinsic reactivity test used for biomass characterization was one of the best alternatives to quantify the reactivity of these materials. Experimental results suggested that the peak temperatures obtained were directly proportional to the ignition temperatures; however, due to the limited number of samples employed, additional experiments would be needed to corroborate this information. A summary of this test is given as follows:

7.4.1.1 Experimental procedure

First, the biomass material must be crushed and sieved to a particle size below 100μm. The use of larger particle sizes influenced the rate of the oxidation, although the peak temperatures remained constant. Second, samples are placed in the TGA crucible (sample weight must be selected according to the instrument range) and exposed to a heating rate of $10^{o}C$ min^{-1} in air, from room temperature to $900^{o}C$. Previous results suggested that the use of lower heating rates influence the peak temperatures recorded. Additionally, a suitable air flow would be 100ml min^{-1} (depending of the instrument range). Lower air flows allow the condensation of volatiles in the sample surface, increasing the magnitude of the peak temperatures obtained.

7.4.1.2 Data analysis

Commonly, TGA instruments provide a mass curve as a function of time or temperature. From this raw data, the first step is to calculate the derivative curve of mass in temperature (similar than this shown in Figure 139). Secondly, the derivative curve identifies the different peaks corresponding to the water release (1st),

volatilization stage (2nd) and char combustion (3rd). Finally, samples are classified according to the peak temperature values obtained for the 2nd and 3rd peaks, in which the lowest values correspond to the highest reactive samples.
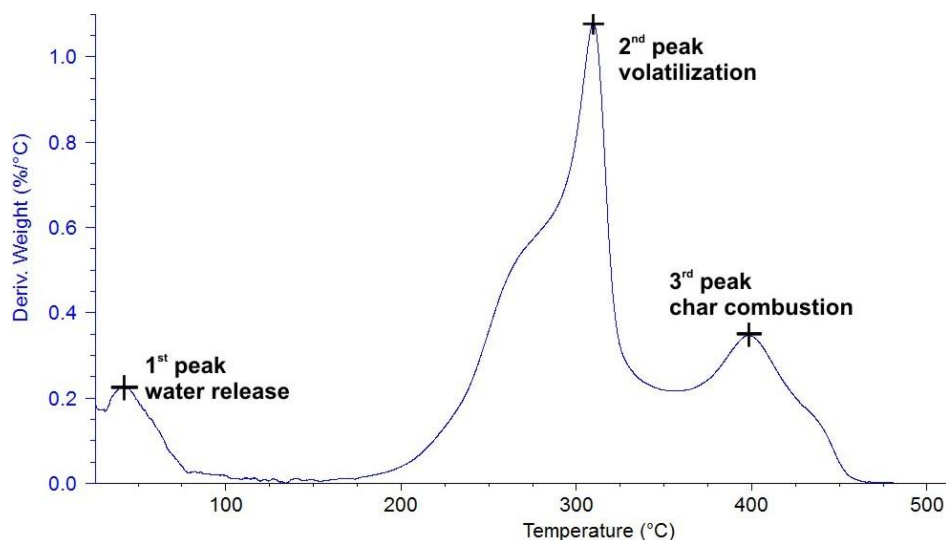
Figure 139: Illustrative DTGA curve for a biomass material.

The advantage of this test is that it provides an analytic tool to compare between different biomass types, which is also useful as a reference for different coals and coal-biomass blends.

7.4.2 Furnace test to estimate ignition shift in coal-biomass blends

For coal-biomass blends, experimental results indicated a shift on ignition temperature compared to the values obtained for raw coals. Considering this, the standard test tries to quantify the magnitude of this shift, based on a similar experimental procedure than this described in Chapter 6. However, the repeatability of this test needs to be confirmed, since the mass and energy transfer conditions of these systems drastically influence the results. A summary of this test is given as follows:

7.4.2.1 Experimental procedure

First, a fresh coal-biomass blend is prepared using a proportion of 90-10% of a recently grinded coal (pulverized in a particle size below 106µm), and the crushed biomass sample (particle size fraction below 212µm). Ideally, this blend must be as fresh as possible, with blending carried out in situ. Then, the initial feed materials and the blends are tested in a furnace with similar characteristics than those explained in Chapter 3. Adaptations of this design are possible with equivalent experimental conditions during the testing of different samples, to allow a relative comparison.

Secondly, samples must be placed in a metallic sample holder of ~100ml of capacity, with the option to locate a thermocouple between the air and the material interface. The packed density of the material in the sample holder must be maximized with a reasonable value between 90-110g per 100ml. Finally, each material is constantly heated from room temperature to $250\pm50^{o}C$ (~$20^{o}C$ above ignition) in air, under a slow heating rate (suggested values in the range $1\pm0.5^{o}C$ min^{-1}). As it is a comparative test, the selected conditions applied must be the same for all the samples studied.

7.4.2.2 Data analysis

The temperature in the sample surface is obtained as a function of time or furnace temperature. From these, the estimation of the shift in the ignition temperature could be obtained directly (as shown in Figure 140, left). However, a more precise result can be achieved from the derivative of the sample temperature curve as a function of furnace temperature. In this case, the ignition temperature is located in a narrowed region (Figure 140, right).
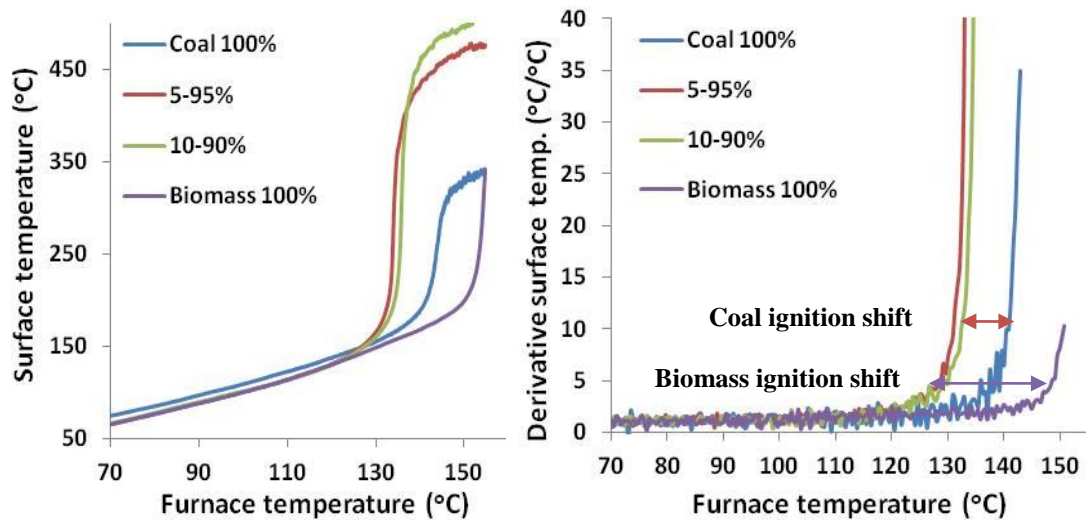
Figure 140: Illustrative profile of the temperature in the surface of the sample as a function of the furnace temperature (left), and the derivative of the sample temperature as function of temperature (right).

As experimental results suggested, the shift of the ignition temperature observed for a large mass system depends of the biomass type, and also the coal type employed in the blend. Finally, the aim of this test is to obtain an estimate of the shift in the ignition temperature, which may not represent the values that would be observed in a much larger system (e.g. a coal or biomass stockpile), but can be used as a reference for how the system behave.

Chapter 8. Conclusions and recommendations for further work

In this final chapter, a review of the objectives achieved and a summary of the most important findings is presented, discussing also the main limitations of this research, including some recommendations for further work.

8.1 General conclusions

The primary focus of this investigation was to identify and evaluate the use of alternative variables to predict the phenomenon of spontaneous combustion of coals, establishing a new set of experimental methods to predict this reaction. Additionally, the work was also focused on whether the actual methods available to predict the self-heating of coals could be extended to biomass and coal-biomass blends, with a particular interest in searching potential synergetic effects during the aerial oxidation of those combined materials.

In general, the initial objectives and required methodologies were all successfully completed. From this study the evidence suggests that there are indeed a number of alternative variables from which the phenomenon of spontaneous combustion of coals can be identified and predicted. Consequently, some of these variables were used to define a set of new testing procedures. These procedures were effectively validated by using a standard set of samples with a well known propensity to self-heating. In the case of biomass, the thermal and optical characterization of these materials concluded that the mechanism of the aerial oxidation of this material is completely different to those experienced during coal oxidation, which means that the current methods used for coal assessment provide inconsistent and unreliable results when applied to biomass. Finally, a particular synergistic interaction was

found that affected the ignition temperature of coal-biomass blends, with a lower ignition for all the blends studied compared to their single components. From this result, it was concluded that spontaneous combustion increases when coal and biomass are combined. A general summary with the precise findings that answered those questions is given as follow:

8.1.1 Spontaneous combustion of coal

The research on spontaneous combustion of coal was initially focussed on identifying alternative variables associated with this phenomenon. Experimental results revealed that several parameters such as sample weight, the mass loss rate, the change of vitrinite reflectance, the proportion of thermal morphotypes and the heat release during the oxidation could all be used as indicators of this reaction. In general, this conclusion was achieved by using two main approaches: thermal analysis and optical microscopy. From the first approach (Chapter 4), the following conclusions were established:

- The thermogravimetric analysis of coal is a valuable tool for assessing the coal properties at low temperatures. Particularly the mass increase detected using this tool between 100 to 250°C, produced by the oxygen adsorption in the coal surface, when samples were slowly heated under an air atmosphere. The explanation of this observation agrees directly with the reaction mechanism of the coal self-oxidation described in literature, which relates mass increase to the formation of oxygenated carbon-solid complexes on the coal surface.

- Subsequently, the stability of these solid complexes can be determined by the magnitude of the mass gained during sample heating. Highly reactive coals that are prone to spontaneous combustion tend to produce unstable solids complexes, which are thermally decomposed at low temperatures, releasing heat and

showing a nil mass increase. Low reactive coals produce highly stable solid complexes that break up at much higher temperatures, reacting more slowly producing a visible mass increase. Consequently, the observation of this phenomenon by using thermogravimetric analysis provided a new approach for identifying coals prone to self-oxidation.

- Thermogravimetric analysis was also useful in determining how the reactivity of coals vary with temperature. In this case, mass loss was associated with the heating rate applied to calculate a second order parameter, which indicates the tendency of coals to react under a gradient of temperature. Due to the nature of these results, this parameter was calculated for a slightly higher temperature range, closer to the ignition temperature. This was confirmed after observing its linear relationship with the crossing point temperature. This procedure was also presented to identify coals prone to self-oxidation.

- Differential scanning calorimeter experiments showed that the heat released during the oxidation stage was proportional to the endothermic heat adsorbed during moisture vaporization. This heat depended directly on the original water content of coals, suggesting that water strongly influenced the oxidation phenomenon, although the mechanism is still not entirely clear.

- The water content of coals also influences the thermal profiles obtained during large sample size experiments. For all the samples studied, this parameter controlled the evolution of temperature and the specific periods during the different reaction stages. Particularly, all the samples with a water content higher than 5% showed a crossing point temperature exactly at 100°C. The subsequent isothermal period that accompanied the crossing point temperature

was directly proportional to this parameter. Three conclusions were made from these results:

1. Water acted as heat sink, although it does not imply a slowdown in the rate of the oxidation reaction.

2. These results invalidated the crossing point temperature method since this predicted that the reaction should be self-sustained after the crossing, which was not seen.

3. For a large system, the water boiling point seems to be a huge barrier for temperature increase, suggesting that the spontaneous combustion could be developed around this point rather than higher temperatures.

- From the experimental results, it was also concluded that the critical temperatures predicted by the crossing point temperature test were related to the ignition phenomenon, which were different from the origin of the self-heating. These conclusions are sustained, in part, by considering the original basis of this test, which comes from an adaptation of a thermal test developed to predict the self-heating of substances such as milk that react in air under completely different circumstances. Consequently, this explained why these results disagree with the information obtained from the oxygen adsorption and the heat release experiments. This also indicate that the application of the crossing point temperature test to predict the spontaneous combustion of coals is inadequate (it suggested well-known prone samples to be 'low reactive').

- Finally, the parallel measurement of the sample mass during the large sample size experiments was useful to quantify the impact of the heating from a different perspective. From this approach, it was concluded that the sample weight was directly linked to the reaction stages, identified by the temperature

profiles. Also, the mass evolution observed for the large sample size system was related to the thermogravimetric characterization of each sample, validating the consistency of both experiments.

In parallel to the thermal analysis, a second approach employed to study the self-heating of coal was through optical microscopy. This technique was applied to identify textural and morphological characteristics produced by the oxidation reaction in coals. According to the results presented in Chapter 5, the most significant conclusions obtained are summarized as follows:

- Coal rank and maceral content of fresh samples provided valuable information about textural characteristics of samples, from which the oxidation reaction depends. However, it was concluded that these parameters alone provided just partial information about the potential of samples to undergo self-oxidation.

- The petrographic analysis of coal particles subjected to a controlled heating revealed a number of thermal alterations. These corresponded to alterations in vitrinite reflectance as well as changes in coal morphology. From this characterization, six different thermal morphotypes were identified and classified as primary or secondary alterations. In those cases, primary alterations were defined as basic morphological changes produced by a single reaction regime acting over the particle. Secondary alterations were defined as those produced by a combination of basic transformations i.e. different reaction regimes acting simultaneously.

- Subsequently, from the morphological classification it was concluded that the type of thermal alterations depended of the reaction regimes developed during the reaction. Particularly, two basic morphotypes represented extreme possible scenarios: particles with homogeneous reflectance change, produced by a kinetic

control of the oxidation (altering the nature of the whole particle); and particles with oxidation rims, produced when the reaction was controlled by the oxygen diffusion (altering the particle just around its surface). Then, it was concluded that the analysis of thermally altered particles could be used for identifying reactive characteristics of coals.

- The variation of the vitrinite reflectance produced by controlled heating was also considered to be an important characteristic associated with low temperature oxidation. Considering that vitrinite is the major reactive maceral component, the change in this property can be interpreted quantitatively as the degree of oxidation suffered by coals. This was corroborated by the experimental results obtained from oxygen adsorption in TGA, in which samples with nil mass increase showed the largest reflectance change, and coals with the highest mass increase showed an insignificant reflectance variation. This confirmed that the samples with the lowest 'apparent' mass increase were strongly transformed. Therefore, it was inferred that the change in reflectance can also be explained as a function of the reaction mechanisms of the self-oxidation that are currently accepted in the literature.

- From the previous information it was concluded that the magnitude of the reflectance change, and the data obtained from the morphological characterization of thermally altered coal particles could be used as potential indicators to determine coal propensity towards spontaneous combustion.

- The use of image analysis to quantify thermal alterations of coals is also a feasible alternative. Despite the fact that experimental results using these methods disagree with those obtained directly from manual microscopy analysis, these results were consistent with the predicted tendencies. Then, improvements

to the technique e.g. calibration to the microscope & camera, and improvements to the image analysis algorithms, could allow its use to evaluate properties of large amounts of samples, removing the subjectivity that is inherent in manual analysis.

- One of the most direct uses of image analysis for coal assessment was the arithmetical comparison of image histograms of fresh and oxidized samples. In this case, experiments showed a smaller variation to manual analysis.

Finally, the combination of thermal and microscopy analysis revealed important associations, which were useful in establishing a final set of experimental procedures:

- It confirmed the link between coal rank and reactivity at low temperatures, although this tendency could also contain exceptions. For fresh samples, experimental results showed that low rank coals offered the highest thermal reactivity in air. Conversely, high rank coals corresponded to the less reactive samples. However, a number of coals contradicted this trend concluding that the use of coal rank not always provides a reliable indication of propensity to spontaneous combustion.

- In a similar way, oxidized samples revealed that alterations of the optical properties were proportional to the changes in coal reactivity. Particularly, the changes in the vitrinite reflectance produced by the oxidation were proportional to the temperature range in which the sample mass increase took place (measured using TGA). Consequently, the magnitude of the textural changes produced by the oxidation could be used to predict changes in coal reactivity, thus creating a completely different approach.

- Finally, the most important conclusion was the need for the combined use of different techniques, as a key to develop reliable methods to predict spontaneous

combustion of coal. Since this phenomenon is a mixture of several and complicated reaction stages produced by textural, physical and chemical conditions, its identification needs to consider several parameters simultaneously, making it difficult to predict based on one single test.

8.1.2 Low temperature reactivity of biomass

The original question about the feasibility of applying the same testing procedures to identify spontaneous combustion of coal, in biomass materials pointed to several different issues. First, could biomass suffer self-heating and spontaneous combustion? If this is the case, does this progress in the same way that in coals? How it could be detected or predicted?. According to the information available in literature and the experimental results, the self-heating of biomass is a real possibility. However, the mechanism of self-heating is completely different to that seen in coals, suggesting biological activity rather than the self-heating produced by the aerial oxidation of the sample. Then, the use of the same testing procedures applied for coals is inadequate. Alternatively, several experiments carried out during this study have contributed to increase the scarce information about the reactivity properties of biomass. One particular finding was the link between char morphology and thermal reactivity. A summary containing the main conclusions derived from the biomass study is given as follows:

- From basic thermogravimetric tests applied to biomass, it was observed that the reactivity of these materials was totally different to that shown by coals. In this case, the low temperature oxidation stages are controlled entirely by water and volatile content, which is found in elevated proportions (>60%). In parallel to this, the rate of the reaction also depended on the main chemical components found in samples such as cellulose, hemicelluloses and lignin, on which the

characteristic temperatures depends (i.e. initial devolatilisation, peak and burnout temperatures).

- Understanding biomass reactivity was achieved by considering the contribution of the char particles, which was determined by studying the remaining material after a controlled pyrolysis process. Char particles, considered as an important intermediary during the combustion process, were responsible for the highest calorific fraction during the material oxidation. From the optical examination of this material, the morphology of the original biomass particles was estimated, as well its impact on the reactivity of the fresh material.

- The characteristics of the char particles were used to develop a basic char classification system, analogous to that already established for coal particles. This characterization is a major contribution since it is convenient not only for describing morphological features, but also because it is useful for understanding several different processes that involve biomass such as gasification, direct combustion and biomass co-firing.

- The combination of particle morphology and reactivity revealed a clear link between these parameters. Morphology features of char particles such as the degree of deformation, internal particle structure and wall thickness corresponded directly with intrinsic reactivity parameters obtained. Then, it was concluded that reactivity properties of fresh biomass particles could be estimated by using the information of char structures produced under specific controlled conditions.

- This information was also extended to a larger sample size system. In this case, the reactive characteristics observed by using the experimental reactor, were directly related to the intrinsic material properties measured using TGA. The

thermal and mass evolution of the large system showed a dependency on particle morphology and in the original physical properties of samples, and evolving accordingly to the intrinsic information obtained from the reactivity tests. Additionally, the ignition temperatures estimated from the large sample tests were directly associated to the peak temperatures obtained from TGA.

- The different approaches created a better idea about the potential of biomass to undergo spontaneous combustion. No observations were made to suggest that biomass interacts directly with air, in a similar way than this observed for coals to produce a self-heating. Also, the thermal test using a large sample size failed to predict reasonable crossing point temperatures, showing a single cross exactly at the same time that the sample ignites. This information (added to the results from the TGA tests), led to the conclusion that the application of the testing procedures, originally developed to assess coal tendency towards spontaneous combustion, produced incongruent results when applied to biomass. For this reason, particular tests for estimating biomass propensity to self-heating need to be developed, including the potential effects produced by biological activity in these materials.

8.1.3 Reactivity of coal-biomass blends at low temperature

The main concern related to the coal and biomass blending was the presence of synergistic interactions that could reduce or increase the probability of suffering spontaneous fire. Then, according to the results shown in Chapter 6, the main findings related are summarized as follows:

- The study of coal-biomass blends using thermogravimetric analysis can provide fast and accurate data about the thermal behaviour of blends. Firstly, proximate analysis easily identified how physical properties change across the different

blending proportions (e.g. moisture, volatiles and carbon). Second, the intrinsic reactivity test provided important information about how the different components of the blend react, in a single or combined way. Then, TGA analysis was a reliable and effective experimental method when studying coal-biomass interactions at low temperature.

- Particularly, TGA profiles of coal-biomass blends behave as a partial combination of the profiles obtained for single original components. From these, it was clearly identified a joint contribution during the water release stage; also it was observed during the volatilization stage, although with a major influence of the biomass volatiles. Finally, the burnout stage was mainly dependent on the coal proportion in the blend. A single anomaly was observed from these profiles, which was the shift of the peak temperature during the burnout stage to a lower value (compared to the pure coal).

- The information obtained from TGA was corroborated during the large sample size experiments, in which temperature and mass profiles revealed similar stages than those observed using a small sample. However, the extrapolation of the TGA profiles to the large system is not straightforward since the large system also included effects produced by the restricted conditions imposed to the mass and energy transport (e.g. a constant temperature across the sample during the water vaporization).

- For coal-biomass blends, the thermal profiles obtained from the large sample size tests failed to reveal crossing point temperatures, concluding that the application of this test is also inadequate for these materials. However, during the same experiments the temperature readings obtained on the surface of the sample holder revealed a shift of the ignition temperature of blends. This shift

displaces the ignition point to lower values, compared with the ignition temperature of the single components.

- This temperature shift was explained due to the influence of the biomass volatile release, which produced an early ignition of the coal in the blend. Considering a pure biomass sample, the ignition temperature is higher because the volatiles are found in a much larger proportion than the burnable carbon fraction, showing an elevated ignition temperature. However, the proportion of biomass in the blend is much lower, but enough to facilitate the ignition of the coal fraction. Consequently, an unprecedented synergetic effect was found, affecting the ignition of the coal-biomass blends when these are blended in a large volume.

- The early ignition of the combined materials was also observed from the sample mass profiles during the large sample size experiments. In this case, the ignition of the sample can be identified from the slope change of the weight loss curve.

- Additionally, the sample mass profiles revealed similar stages to those identified from the temperature profiles. Subsequently, an important characteristic of the large sample size experiments was the independence between the temperature and mass data recorded, since both were obtained simultaneously without any type of interconnection in the instrument. This feature allowed the observation of the same phenomenon, although studied by using a different set of variables.

- Considering the combined results from the TGA and the large sample size reactor, additional work is needed to evaluate the potential of coal-biomass blends to undergo spontaneous combustion. From both experimental approaches, signs of the aerial oxidation in biomass and coal biomass blends at low temperature, similar than those found for single coals, were not observed. However, the characteristic weight increase due to the oxygen adsorption in

single coals was different (no weight increase seen), suggesting that biomass could interfere in this process. Particularly, it was not clear if biomass inhibits the oxygen adsorption in coals or if this reduces the stability of the solid complex formed. The last alternative needs to be considered in further studies, since this indicate that blending coal with biomass could increase the potential of suffer an spontaneous combustion in a stockpile, compared to the separate storage of the single constituents.

8.1.4 Predictive methods to estimate the potential of coal, biomass and coal-biomass blends to suffer spontaneous combustion

Finally, one of the main goals of this study was developing a new set of experimental procedures to identify coals prone to spontaneous combustion. A list with the different tests and their particular characteristics is shown in Table 48.

Table 48: Summary of tests developed.

Test name	Instrument used	Property measured	Test aim
TG_{spc} Index for coals	TGA	Mass change	Measure how mass changes due to a temperature gradient applied.
TGO_2 adsorption for coals	TGA	Mass change	Calculate the maximum mass increase produced by oxygen adsorption at low temperatures
Thermo-petrographic test of vitrinite reflectance change	Furnace and optical microscope	Vitrinite reflectance	Obtain an estimation of the reflectance change in vitrinite particles produced by a controlled heating.
Morphotype identification in oxidized coals	Furnace and optical microscope	Particle morphology	Calculate the proportion of thermal morphotypes produced after a controlled heating.
Intrinsic reactivity test for biomass	TGA	Mass change	Obtain characteristic temperatures for different oxidation stages
Shift of ignition temperature in coal-biomass blends	Furnace	Ignition temperature	Calculated the shift of the ignition temperature relative to the single components of the blend.

These tests were presented in Chapter 7, including three tests based on thermal analysis by using TGA, and two based on optical microscopy of thermally altered coal samples. Particularly, for biomass and coal-biomass blends, two tests were suggested considering the information acquired during the experimental work, although these need to be validated by further experiments.

8.2 Limitations and recommendations for further work

Although extensive research has been carried out on spontaneous combustion, no single study exists which adequately covers all the different aspects of this reaction. For this particular investigation, the main restrictions were associated to the number, type and conditions of the samples used, which directly affected the results obtained. Also, the access to equipment for the experimental work and the limited amount of time has restricted the extent of this study. A list of these limitations and some recommendations for further work is summarized as follows:

- The main limitation faced in this study was the restricted number of samples that are already known to be prone to spontaneous combustion. An extensive search was carried out contacting mining companies and research groups across the world; however, just a few samples were obtained. This can be justified by the scarce number of accidents involving spontaneous combustion well documented, but also because mining industries refuse to make this information public due to the economic interests behind coal extraction, especially if samples could be labelled as unsafe.

- The use of additional samples would be ideal to validate the general trends, establishing clear patterns statistically representatives of coal behaviour at low temperature. This problem was solved in part by the academic collaboration involving research centres from China, Germany and U.S.A., which cooperated

with specific samples, although the use of a large number of samples is an aspect that needs to be considered in further work.

- Regarding experimental experience, this type of study deals with several uncontrolled factors. One of the most important is the sample age, which has an incalculable influence on the analysis. After the mining stage, the considerable pressure change suffered by coals produces the highest variation in its physical and chemical characteristics. These changes progress gradually, finishing with the total lost all the reactive potential of coals at ambient temperatures. Ideally, freshly mined coal must be used in all the experiments; however, this has practical problems related to obtaining fresh samples. This can be solved in part by using big lump rocks crushed just before the experiments, which are less affected by the ageing. However, this procedure could also bias the results, representing the characteristics of a particular rock rather than the behaviour of the whole seam.

- Alongside the ageing problem, coal samples also suffer natural oxidation produced by contact with oxygen in the atmosphere, which is the main reason of spontaneous combustion. This reaction can be slowed down by freezing the sample. This minimizes the adsorption of air and also preserves the moisture and volatile content of the sample. Then, before the experiment it must be unfrozen and crushed just before testing. This method resulted in the highest values for reactivity, and for this reason it is highly recommended as a procedure.

- The sensitivity of the instruments is another important issue that must be considered. As the reaction of self-oxidation is slow, the change in the measured variables is almost unperceivable and the range in which these vary is close to the instruments sensitivity. Then, special attention must be placed on clearly

differentiating between the conditions of the self-heating phenomenon from the self-ignition events. Additionally, it is important to avoid the use of heating rates higher than 5°C min^{-1} during the experiments to obtain intrinsic properties, since values above this increase chance of developing the full combustion reaction. For large sample size experiments, heating rates higher than 1°C min^{-1} make no sense.

- Finally, the application of any of the experimental methods described to identify coals samples prone to spontaneous combustion must be contrasted with an alternative test. As previously stated, the phenomenon of self-heating depends of several different factors that cannot be covered by a single test. Particularly, the tests developed in this thesis still need experimental verification from an independent research group in order to be fully validated.

8.3 Original contribution of this thesis

The journal papers publications related to this work and the presentations offered in international conferences are outlined as follows:

8.3.1 Journal Papers

- C. Avila, C. Pang, T. Wu and E. Lester. Morphology and reactivity characteristics of char biomass particles. Bioresource Technology 102, 8 (2011) 5237–5243.

- H. Kumar, E. Lester, S. Kingman, R. Bourne, C. Avila , A. Jones, J. Robinson, P. Halleck and J. Mathews. Inducing fractures and increasing cleat apertures in a bituminous coal under isotropic stress via application of microwave energy. International Journal of Coal Geology 88 (2011) 75-82.

8.3.2 Conference papers

- C. Avila & E. Lester: Characterization of biomass chars using petrographic methods. International Conference on Coal and Organic Petrology ICCP-TSOP 2008. Oviedo, Spain.

- C. Avila & E. Lester: Spontaneous combustion of coal. 7th European Conference on Coal Research and its Applications, Coal Research Forum UK 2008, Cardiff, Wales.

- C. Avila & E. Lester: The link between reactivity and morphology for biomass particles. Efficient and Environmentally Friendly Energy Generation from Biomass Meeting, Organized by RCUK China-Kent University, Sept. 2008, Hangzhou, China.

- C. Avila & E. Lester: A novel method to identify propensity to spontaneous combustion in coals using thermogravimetric analysis. International Conference of Coal, Science and Technology 2009, Cape Town, South Africa.

- Vilas, C. Avila & E. Lester: Biomass pre-treatment by microwaves to improve grindability, International Conference of Coal, Science and Technology 2009, Cape Town, South Africa.

- Avila & E. Lester: Characterization of biomass chars using microscopy and thermogravimetric analysis. International Conference of Coal, Science and Technology 2009, Cape Town, South Africa.

- Pang, C. Avila & E. Lester: Ash Sintering Strength and Pellet making. International Conference of Coal, Science and Technology 2009, Cape Town, South Africa.

- Avila & E. Lester: Study of coal oxidation at low temperature using thermogravimetric analysis. Fourth International Clean Coal Conference 2009, Dresden, Germany.

- Avila & E. Lester: Thermal study of coal oxidation at low temperature. Second International Conference in Coal Fire Research 2010, Berlin, Germany.

- Avila & E. Lester: Thermal study of coal oxidation at low temperature. Second International Conference in Coal Fire Research 2010, Berlin, Germany.

- M. Misz-Kennan, J. Kus, D. Flores, C. Avila, K. Christanis, J. Hower, S. Kalaitzidis, J. O'Keefe, M. Marques, S. Pusz, J. Ribeiro, I. Suárez-Ruiz, I. Sýkorová, N. Wagner and D. Životić. Self-heating of Coal and Coal Wastes Working Group: a new approach to classify altered and newly formed particles as result of self-heating and self-combustion processes. Second International Conference in Coal Fire Research 2010, Berlin, Germany.

- Avila & E. Lester: A new thermo-petrographic method to identify coals prone to spontaneous combustion. 8th European Conference on Coal Research and its Applications, Coal Research Forum UK 2010, Leeds, England.

- Avila & E. Lester: Study of coal oxidation at low temperatures. Fifth International Clean Coal Conference 2011, Zaragoza, Spain.

- C. Avila & E. Lester: Thermo-petrographic methods to identify coals prone to spontaneous combustion. International Conference of Coal, Science and Technology 2011, Oviedo, Spain.

References

1   Crelling, J. and Russel, D. *Principles and applications of coal petrology*. Indiana University at Bloomington, United States, 1980.

2   Van Krevelen., D. *Coal*. Elsevier scientific publishing, New York, 1961.

3   Suarez-Ruiz, I. and Crelling, J. *Applied coal petrology, the role of petrology in coal utilization*. Oxford, 2007.

4   Thery, I, Gril, J., Vernet, J., Meignen, L., and Maury, J. First use of coal. *Nature*, 373 (1995), 480-481.

5   Thery, I., Gril, J., Vernet, J., Meignen, L., and Maury, J. Coal used for Fuel at two prehistoric sites in Southern France: Les Canalettes (Mousterian) and Les Usclades (Mesolithic). *Journal of Archeological Science*, 23 (1995), 509-512.

6   Peters, C., Church, M., and Mitchell, C. Investigation of fire ash residues using mineral magnetism. *Archaelogical Prospection*, 8, 4 (2001), 227-237.

7   Renfrew, C and Bahn, P. *Archaeology: theory, methods and practices*. Thames and Hudson, London, 1991.

8   Evelyn, J. *FUMIFUNGIUM: For the Inconvenience of the Aer and Smoake of London Dissipated*. London, 1661.

9   Gernet, J. *A history of Chinese civilization*. Cambridge University Press, Cambridge, 1982.

10 Stockwel, F. *Westerns in China*. McFarland and Company Inc. Publishers, Jefferson, North Carolina, 2003.

11 Freese, B. *Coal, a human history*. William Henemann, London, 2003.

12 Hirschberg, S., Burgherr, P., Spiekerman, G., Cazzoli, E., Vitazek, J., and

Cheng, L. *Comparative assessment of severe accidents in the Chinese energy sector*. Paul Scherrer Institut, Switzerland, 2003, available at www.psi.ch.

13 U.S. ENERGY INFORMATION ADMINISTRATION, (EIA). International energy outlook 2010. *www.eia.doe.gov* (latest access 1st November, 2011).

14 WORLD COAL INSTITUTE. Coal, delivering sustainable development. *Report 2007, Available at www.worldcoal.org* (Latest access 08th November, 2011).

15 CONGRESS OF THE UNITED STATES. *The Direct Use of Coal. Prospects and problems of production and combustion*. Office of Technology Assessment, Washington, 1979.

16 Cassedy, E. and Grossman, P. *Introduction to energy: resources, technology and society*. Cambridge University Press, Cambridge, 1998.

17 EUROPEAN PARLIAMENT. *Council Directive 91/383/EEC of 25 June 1991 supplementing the measures to encourage improvements in the safety and health at work of workers with a fixed- duration employment relationship or a temporary employment relationship*. European Parliament, Brussels, 1991.

18 Gaffney, J. and Marley, N. The impacts of combustion emissions on air quality and climate - From coal to biofuels and beyond. *Atmospheric Environment*, 43 (2009), 23-36.

19 Leeder, M. and Perez, M. *Physical processes in earth and environmental sciences*. Blackwell, United Kingdom, 2006.

20 INTERGOVERNMENTAL PANEL ON CLIMATE CHANGE IPCC. *Observed climate variations and change. Contribution in support of section 7 of the 1990 IPCC Scientific Assessment*. available at www.ipcc.ch, Latest acces, 1st December 2011.

21 INTERNATIONAL RESEARCH FOR SUSTAINABLE CONTROL AND MANAGEMENT, UNESCO. *Proceedings of the International Conference "Spontaneous coal seam fires: mitigating a global disaster"*. Tsinghua University Press and Springer Verlag, Beijing, 2005.

22 Stracher, G. and Taylor, T. Coal fires burning out of control around the world: thermodynamic recipe for environmental catastrophe. *International Journal of Coal Geology*, 59 (2004), 7-17.

23 SINO-GERMAN COAL FIRE RESEARCH. Innovative technologies for exploration, extinction and monitoring of coal fires in northern china. *Available at www.coalfire.caf.dlr.de* (Latest access 08th November, 2011.).

24 UNITED STATES BUREAU OF MINES. Study and Control of Fires in Abandoned Mines and Waste Banks. Compilation of actions. In Stracher, G., ed., *Available at Coal and Peat Fires, a Global Perspective, Chapter 16*. Elsevier, United Kingdom, 2011.

25 Banerjee, S. *Prevention and combating mine fires*. Balkema, Rotterdam, 2000.

26 Sinha, A. and Singh, V. Spontaneous coal seam fires: A global phenomenon. (Beijing Proceedings of the International Conference "Spontaneous coal seam fires: mitigating a global disaster" 2005), Tsinghua University Press and Springer Verlag.

27 Parr, S. and Wheeler, W. The deterioration of coal. *Journal of American Chemical Society*, 30 (1908), 1027-1033.

28 Parr, S. and Kressman, F. The spontaneous combustion of coal. *The Journal of Industrial and Engineering Chemistry* (1911), 152-158.

29 Wang, H., Dlugogorski, B., and Kennedy, E. Coal oxidation at low

temperatures: oxygen consumption, oxidation products, reaction mechanism and kinetic modelling. *Progress in Energy and Combustion Science*, 29 (2003), 487-513.

30 Frank-Kamenetskii, D. Conditions for the applicability of the Bodenstein method in chemical kinetics. *Zurnal Fizicheskoy Himii*, 14 (1940), 695-700 (Available at T. Turanyi and J. Toth. Comments to an article of Frank-Kamenetskii on The quasi-steady-state approximation. Acta Chimica Hungarica–Models in Chemistry 129 (1992) 903-911. Appendix).

31 Frandsen, W. Ignition probability of organic soils. *Canadian Journal of Forest Research*, 27 (1997), 1471-1477.

32 Ohlemiller, T. Smoldering combustion. In Beyler, C. et al., eds., *SFPE Handbook of Fire Protection Engineering*. National Fire Protection Association, 2002.

33 Barth, U., Grashorn, B., and Bandelow, F. Sustainable control of coal fires through systematic decision processes and cyclic management. In *Proceedings of the International Conference "Spontaneous coal seam fires: mitigating a global disaster"*. Tsinghua University Press and Springer Verlag, Beijing, 2005.

34 Haiyan, G. Spontaneous coal seam fires: The Chinese perspective. In *Proceedings of the International Conference "Spontaneous coal seam fires: mitigating a global disaster"*. Tsinghua University Press and Springer Verlag, Beijing, 2005.

35 Bekker, C. Spontaneous combustion at a South African open cast colliery. In *Proceedings of the second international conference on coal fire research*. Berlin, 2010.

36 Quintero, J., Rios, C., and Stracher, G. Clinker at El Cerrejón coal mine, Colombia: characteristics and potential uses. In Stracher, G. et al., eds., *Coal and Peat Fires: A Global Perspective, Volume 2: Photographs and Multimedia Tours*. Elsevier, Amsterdam, 2011.

37 Walters, A. Joseph Conrad and the Spontaneous Combustion of Coal Part I. *International Journal of Coal Preparation and Utilization*, 17 (1996), 147-165.

38 Incendio en la medusa de carbon en puerto de A Coruna. *La Voz de Galicia* (November 15 2007).

39 Cai, Z. and Wei, J. Coalfield fire fighting in Xinjiang: successes and challenges. In *Proceedings of the second international conference on coal fire research*. Berlin, 2010.

40 Xue, S., Guo, H., and Xie, J. Spontaneous heating f coal in Australian coal mines. In *Proceedings of the second international conference on coal fire research*. Berlin, 2010.

41 Gielisch, H. and Kayser, J. Coal fire scenarios - Experiences from fieldwork in India. In *Proceedings of the second international conference on coal fire research*. Berlin, 2010.

42 Pone, J., Hein, K., Stracher, G. et al. The spontaneous combustion of coal and its by-products in the Witbank and Sasolburg coalfields of South Africa. *Journal of Coal Geology*, 72 (2007), 124–140.

43 Stracher, G. et al., eds. *Coal and peat fires: A global perspective: Volume 1: Coal - Geology and Combustion*. Elsevier Science, Amsterdam, 2010.

44 Prakash, A. Coal fire research: heading from remote sensing to remote measurement. In *Proceedings of the second international conference on coal fire*

research. Berlin, 2010.

45   Liu, X. and Wu, J. Estimating CO2 emissions from underground coal fires at regional scale. In *Proceedings of the second international conference on coal fire research*. Berlin, 2010.

46   Finkelman, R. Potential human health impacts from coal fire emissions. In *Proceedings of the second international conference on coal fire research*. Berlin, 2010.

47   Stracher, G. *Geology of coal fires: case studies from around the world*. The Geological Society of America, Boulder, Colorado, 2007.

48   U.S. DEPARTMENT OF ENERGY. *Energy efficiency and renewable energy*. U.S. Department of Energy, 2009, available at http://www1.eere.energy.gov/biomass.

49   Pérez, S., Renedo, C., Ortiz, A., and Mañana, M. Energy potential of waste from 10 forest species in the North of Spain (Cantabria). *Bioresource Technology*, 36 (1991), 215-221.

50   Hoffmann, G., Schingnitz, D., Schnapke, A., and Bilitewski, B. Reduction of CO2-emissions by using biomass in combustion and digestion plants. *Waste Management*, 30 (2010), 893-901.

51   Baxter, L. Biomass-coal co-combustion: opportunity for affordable renewable energy. *Fuel*, 84 (2005), 1295-1302.

52   EUROPEAN ENVIRONMENTAL AGENCY. *EEA Technical report No 10/2008: Maximising the environmental benefits of Europe's bioenergy potential*. European Environmental Agency, Brussels, 2008.

53   THE HOUSE OF COMMONS. *Briefing for the House of Commons, energy and*

climate change committee. The Electricity Generating Landscape in Great Britain. The National Audit Office, the House of Commons UK, 2010.

54 Benetto, E., Popovici, E., Rousseaux, P., and Blondin, J. Life cycle assessment of fossil CO2 emissions reduction scenarios in coal-biomass based electricity production. *Energy Conversion and Management*, 45 (2004), 3053-3074.

55 EUROPEAN BIOMASS INDUSTRY ASSOCIATION, EUBIA. *Typical characteristics of biomass fuels*. European Biomass Industry Association, EUBIA, 2010, available at http://www.eubia.org.

56 Saidur, R., Abdelaziz, E., Demirbas, A., Hossain, M., and Mekhilef, S. A review on biomass as a fuel for boilers. *Renewable and Sustainable Energy Reviews*, 15 (2011), 2262-2289.

57 Li, X., Koseki, H., and Momota, M. Evaluation of danger from fermentation-induced spontaneous ignition of wood chips. *Journal of Hazardous Materials*, 135 (2006), 15-20.

58 Rynk, R. Fires at composting facilities: causes and conditions. *BioCycle Magazine*, 41 (2000), 54-58.

59 Sturaro, A., Rella, R., Parvoli, G., Ferrara, D., and Dorett, L. Chemical evidence and risks associated with soybean and rapeseed meal fermentation. *Chemosphere*, 52 (2003), 1259-1262.

60 Sami, M., Annamalai, K., and Wooldridge, M. Co-firing of coal and biomass fuel blends. *Progress in Energy and Combustion Science*, 27 (2001), 171–214.

61 Parr, S. and Hilgard, E. Oxidation of sulphur as a factor in coal storage. *Industrial and Engineering Chemistry* (1925), 117.

62 Lee, S. and Parr, S. The oxidation of pyrites as a factor in the spontaneous

combustion of coal. *The Journal of Industrial and Engineering Chemistry*, 18 (1926), 1299-1304.

63 Parr, S. and Milner, R. The oxidation of coal at storage temperatures. *Industrial and Engineering Chemistry* (1925), 115-117.

64 Parr, S. Low-temperature carbonization of coal. *Industrial and Engineering Chemistry*, 21 (1929), 164-168.

65 Byrne, J. and Davis, J. Loss of heating value of bituminous coal on exposure to air. *Industrial and Engineering Chemistry*, 16 (1924), 775-778.

66 Davis, J. and Byrne, J. Spontaneous combustion of coal. Characteristics shown by and adiabatic calorimeter. *Industrial and Engineering Chemistry* (1925), 125.

67 Davis, J. and Byrne, J. Influence of Moisture on the Spontaneous Heating of Coal. *Industrial and Engineering Chemistry* (1926), 233-236.

68 Bhattacharyya, K. The role of desorption of moisture from coal in its spontaneous heating. *Symposium on Combustion* , 15 (1975), 127-136.

69 Misra, B. and Singh, B. Susceptibility to spontaneous combustion of Indian coals and lignites: an organic petrographic autopsy. *International Journal of Coal Geology*, 25 (1994), 265-286.

70 Chen, X. On basket heating methods for obtaining exothermic reactivity of solid materials: The extent and impact of the departure of the crossing-point temperature from the oven temperature. *Trans IChemE*, 77 (1999), 187-192.

71 Fuchs, W. Action of bacteria on coal. *Brennstoffchemie*, 8 (1927), 20.

72 Potter, M. Bacteria as agents in the oxidation of amorphous carbon. *Proceedings of the Royal Society of Britain*, 80 (1908), 239.

73 Singh, R. and Demirbilek, S. Statistical appraisal of intrinsic factors affecting

spontaneous combustion of coal. *Mining Science and Technology*, 4 (1987), 155-165.

74 Fierro, V., Miranda, J., Romero, C., Andrés, J., Arriaga, A., Schmal, D., and Visser, G. Prevention of spontaneous combustion in coal stockpiles: Experimental results in coal storage yard. *Fuel Processing Technology*, 59 (1999), 23-34.

75 Carpenter, D. and Giddings, D. The initial stages of oxidation of coal with molecular oxygen I - effect of time temperature + coal rank on rate of oxygen consumption. *Fuel*, 43 (1964), 247-266.

76 Nugroho, Y., McIntosh, A., and Gibbs, B. On the prediction of thermal runaway of coal piles of differing dimension by using a correlation between heat release and activation energy. *Symposium on Combustion*, 28 (2000), 2321-2327.

77 Jimenez, A., Iglesias, M., Laggoun-Defarge, F., and Suarez-Ruiz, I. Effect of the increase in temperature on the evolution of the physical and chemical structure of vitrinite. *Journal of Analytical and Applied Pyrolysis*, 50 (1999), 117–148.

78 Carpenter, D. and Sergeant, C. The initial stages of the oxidation of coal with molecular oxygen IV-The accessibility of the internal surface to oxygen. *Fuel*, 45 (1966), 429-446.

79 Bhattacharyya, K. The role of sorption of water vapour in the spontaneous heating of coal. *Fuel* , 50 (1971), 367-380.

80 Krajciova, M., Jelemensky, L., Kisa, M., and Markos, J. Model predictions on self-heating and prevention of stockpiled coals. *Journal of Loss Prevention in the Process Industries*, 17 (2004), 205–216.

81 Hull, A., Lanthier, J., and Agarwal, P. The role of the diffusion of oxygen in the

ignition of a coal stockpile in confined storage. *Fuel*, 76 (1997), 975-983.

82 Marinov, V. Self-ignition and mechanisms of interaction of coal with oxygen at low temperatures. 3. Changes in the composition of coal heated in air at 60°C. *Fuel*, 56 (1977), 165-170.

83 Van der Plaats, G., Soons, H., and Chermin, H. Low-temperature oxidation of coal. *Thermochimica Acta*, 82 (1984), 131-136.

84 Medek, J. and Weishauptova, Z. Effect of coal interaction with oxygen on its ignition temperature. *Energy & Fuels*, 13 (1999), 77-81.

85 Bhattacharyya, K. The role of desorption of moisture from coal in its spontaneous heating. *Fuel*, 51 (1972), 214-220.

86 Qi, X., Wang, D., Zhong, X., Gu, J., and Xu, T. Characteristics of oxygen consumption of coal at programmed temperatures. *Mining Science and Technology*, 20 (2010), 372–377.

87 Chen, X. The effect of drying heat and moisture content on the maximum temperature rise during spontaneous heating of a moist coal pile. *International Journal of Coal Preparation and Utilization*, 14 (1994), 223-236.

88 Bhat, S. and Agarwal, P. The effect of moisture condensation on the spontaneous combustibility of coal. *Fuel*, 75 (1996), 1523-1532.

89 Clemens, A. and Matheson, T. The role of moisture in the self-heating of low-rank coals. *Fuel* , 75 (1996), 891-895.

90 Mahajan, O. and Walker, P. Water adsorption on coals. *Fuel*, 50 (1971), 308-317.

91 Herman, R., Simmons, G., Cole, D., Kuzmicz, V., and Klier, K. Catalytic action of minerals in the low temperature oxidation of coal. *Fuel*, 63 (1984), 673-678.

92 Sujanti, W. and Zhang, D. A laboratory study of spontaneous combustion of coal: the influence of inorganic matter and reactor size. *Fuel*, 78 (1999), 549–556.

93 Sujanti, W. and Zhang, D. The effect of inherent and added inorganic matter on low-temperature oxidation reaction of coal. *Fuel Processing Technology*, 74 (2001), 145–160.

94 Beamish, B. and Arisoy, A. Effect of mineral matter on coal self-heating rate. *Fuel*, 87 (2008), 125-130.

95 Mathews, J., Hatcher, P., and Scaroni, A. Particle size dependence of coal volatile matter: is there a non-maceral-related effect? *Fuel* , 76 (1997), 359-362.

96 Akgün, F. and Arisoy, A. Effect of particle size on the spontaneous heating of a coal stockpile. *Combustion and Flame*, 99 (1994), 137-146.

97 Carpenter, D. and Sergeant, C. The initial stages of the oxidation of coal with molecular oxygen III-effect of particle size on rate of oxygen consumption. *Fuel*, 45 (1966), 311-327.

98 Kucuk, A., Kadıoglu, Y., and Gulaboglu, M. A study of spontaneous combustion characteristics of a Turkish lignite: particle size, moisture of coal, humidity of air. *Combustion and Flame*, 133 (2003), 255–261.

99 Wang, H., Dlugogorski, B., and Kennedy, E. Theoretical analysis of reaction regimes in low-temperature oxidation of coal. *Fuel*, 78 (1999), 1073-1081.

100 Wang, H., Dlugogorski, B., and Kennedy, E. Analysis of the mechanism of the low-temperature oxidation of coal. *Combustion and Flame*, 134 (2003), 107-117.

101 Jones, J. and Vais, M. Factors influencing the spontaneous heating of low-rank

coals. *Journal of Hazardous Materials*, 26 (1991), 203-212.

102 McMahon, P., Snook, I., Moss, S., and Johnston, P. Influence of fractal pores on the oxidation behaviour of brown coal. *Energy & Fuels*, 13 (1999), 965-968.

103 Kuili, J., Jian, X., and Duohu, H. The use of automated coal petrography in determining maceral group composition and the reflectance of vitrinite. *International journal of coal geology*, 9 (1988), 385-395.

104 Lester, E., Allen, M., Cloke, M., and Miles, N. An automated image analysis system for major maceral group of analysis in coals. *Fuel*, 73 (1994), 1729-1734.

105 BRITISH STANDARDS INSTITUTE. *[BS 6127-5:1995] Petrographic analysis of bituminous coal and anthracite — Part 5: Method of determining microscopically the reflectance of vitrinite*. British Standards Institute, London, 1995.

106 Fredericks, P., Warbrooke, P., and Wilson, M. Chemical changes during natural oxidation of a high volatile bituminous coal. *Organic Geochemistry*, 5 (1983), 89-97.

107 BRITISH STANDARDS INSTITUTE. *[BS 1016-104:1991] Methods for Analysis and testing of coal and coke. Proximate analysis of coal*. British Standards Institute, London, 1995.

108 Marinov, V. Self-ignition and mechanisms of interaction of coal with oxygen at low temperatures. 2. Changes in weight and thermal effects on gradual heating of coal in air in the range 20–300°C. *Fuel*, 56 (1977), 158-164.

109 Avila, C. Study of spontaneous combustion of coals by means of Thernogravimetric analysis. (Berlin 2010), Proceedings of the Second

International Conference on Coal Fire Research.

110 Havenga, W. Rapid gas analyses for the investigation of spontaneous combustion using capillary gas chromatography. *Talanta*, 40 (1993), 213-219.

111 Pisupati, S., Scaroni, A., and Hatcher, P. Devolatilization behaviour of naturally weathered and laboratory oxidized bituminous coals. *Fuel*, 72 (1993), 165-173.

112 Jakab, E., Hoesterey, B., Windig, W., Hill, G., and Meuzelaar, H. Effects of low temperature air oxidation (weathering) reactions on the pyrolysis mass spectra of US coals. *Fuel*, 67 (1988), 73-79.

113 Mathews, W. and Bustin, R. Changes associated with natural in situ weathering of a coking coal from south-eastern British Columbia. *Fuel*, 63 (1984), 548-550.

114 Iglesias, M., De la Puente, G., Fuente, E., and Pis, J. Compositional and structural changes during aerial oxidation of coal and their relations with technological properties. *Vibrational Spectroscopy*, 17 (1998), 41-52.

115 Marchioni, D. The detection of weathering in coal by petrographic, rheologic and chemical methods. *International Journal of Coal Geology*, 2 (1983), 231-259.

116 Carras, J. and Young, B. Self-heating of coal and related materials: Models, application and test methods. *Progress in Energy and Combustion Science*, 20 (1994), 1-15.

117 Fierro, V., Miranda, J., Romero, C., Andrés, J., Arriaga, A., and Schmal, D. Model predictions and experimental results on self-heating prevention of stockpiled coals. *Fuel*, 80 (2001), 125.

118 Akgün, F. and Essenhigh, R. Self-ignition characteristics of coal stockpiles: theoretical prediction from a two-dimensional unsteady-state model. *Fuel*, 80

(2001), 409.

119 Moghtaderi, B., Dlugogorski, B., and Kennedy, E. Effects of wind flow on self-heating characteristics of coal stockpiles. *Trans IChemE*, 78 (2000), 445-453.

120 Porter, C. and Ralston, O. A study of the oxidation of coal. *Technical Paper 66, U.S. Bureau of Mines* (1914).

121 Schmidt, L., Elder, J., and Davis, J. Oxidation properties of coal at storage temperatures. Effect on carbonizing properties. *Industrial and Engineering Chemistry* (1936), 1346-1353.

122 Carpenter, D. and Giddings, D. The initial stages of the oxidation of coal with molecular oxygen II - order of reaction. *Fuel*, 43 (1964), 375-383.

123 Schmidt, L. and Elder, J. Atmospheric oxidation of coal at moderate temperatures. Rates of the oxidation reaction for representative coking coals. *Industrial and Engineering Chemistry*, 32 (1945), 249-256.

124 Marinov, V. Self-ignition and mechanisms of interaction of coal with oxygen at low temperatures. 1. Changes in the composition of coal heated at constant rate to 250°C in air. *Fuel*, 56 (1977), 153-157.

125 Kaji, R., Hishinum, Y., and Nakamur, Y. Low temperature oxidation of coals: Effects of pore structure and coal composition. *Fuel*, 1985 (64), 297-302.

126 Pisupati, S. and Scaroni, A. Natural weathering and laboratory oxidation of bituminous coals: Organic and inorganic structural changes. *Fuel*, 72 (1993), 531-542.

127 Gethner, J. Optical spectroscopy of coal. *American Chemical Society*, 43 (1980), 413-419.

128 Gethner, J. Thermal and oxidation chemistry of coal at low temperatures. *Fuel*,

64 (1985), 1443-1446.

129 Gethner, J. FT-IR Studies of the low-temperature-induced chemical changes in Rawhide coal. *Applied Spectroscopy*, 39 (1985), 753-889.

130 Gethner, J. Coal oxidation and thermal chemistry. *ACS Division of Fuel Chemistry*, 31 (1986), 103-110.

131 Gethner, J. Kinetic study of the oxidation of Illinois No. 6 coal at low temperatures. Evidence for simultaneous reactions. *Fuel*, 66 (1987), 1091-1096.

132 Gethner, J. The mechanism of the low temperature oxidation of coal by O2: observation and separation of simultaneous reactions using in situ FT-IR difference spectroscopy. *Applied Spectroscopy*, 41 (1987), 50-63.

133 Wang, H., Dlugogorski, B., and Kennedy, E. Kinetic modelling of low-temperature oxidation of coal. *Combustion and Flame*, 131 (2002), 452-469.

134 Wang, H., Dlugogorski, B., and Kennedy, E. Examination of CO2, CO and H2O formation during low-temperature oxidation of a bituminous coal. *Energy & Fuels*, 16 (2002), 586-592.

135 Shi, T., Wang, X., Deng, J., and Wen, Z. The mechanism at the initial stage of the room-temperature oxidation of coal. *Combustion and Flame*, 140 (2005), 332–345.

136 Petit, J. and Boettner, J. Evidence of hydrogen peroxide formation in the early stages of coal oxidation. In H. Charcosset, B. Nickel-Pepin-Donat, B. Nickel-Pepin-Donat, ed., *Advanced Methodologies in Coal Characterization (Coal Science & Technology)*. Elsevier, Amsterdam, 1990.

137 Allardice, D. and Evans, D. The-brown coal/water system: Part 2. Water sorption isotherms on bed-moist Yallourn brown coal. *Fuel*, 50 (1971), 236-253.

138 McCutcheon, A. and Wilson, M. Low-temperature oxidation of bituminous coal and the influence of moisture. *Energy & fuels*, 17 (2003), 923-933.

139 Vance, W., Chen, X., and Scott, S. The rate of temperature rise of a subbituminous coal during spontaneous combustion in an adiabatic device: The effect of moisture content and drying. *Combustion and Flame*, 106 (1996), 261-270.

140 Beamish, B. and Hamilton, G. Effect of moisture content on the R70 self-heating rate of Callide coal. *International Journal of Coal Geology*, 64 (2005), 133-138.

141 Guln, J., Curtis, C., and Sahawneh, B. Laboratory study of the self-heating tendency of coals and their pyrolysis chars. *Industrial and Engineering Chemistry Process Design and Development*, 25 (1986), 543-546.

142 Nordon, P., Young, B., and Bainbridge, N. The rate of oxidation of char and coal in relation to their tendency to self-heat. *Fuel*, 58 (1979), 443-449.

143 Graham, J. Pyrites as a Cause of Spontaneous Combustion in Coal Mines. *Transaction of the Institution of Mining Engineers*, 67 (1923), 100.

144 Wiese, R. and Fyfe, W. Occurrences of iron sulphides in Ohio coals. *International Journal of Coal Geology*, 6 (1986), 251-276.

145 Chandra, D. and Prasad, Y. Effect of coalification on spontaneous combustion of coals. *International Journal of Coal Geology*, 16 (1990), 225-229.

146 Nelson, M. and Chen, X. Survey of experimental work on the self-heating and spontaneous combustion of coal. In Stracher, Glen, ed., *Geology of coal fires: Cases studies from around the world. Reviews in Engineering Geology XVIII.* The Geological Society of America, Boulder, Colorado, 2007.

147 Banerjee, S. and Chakravarty, R. Use of D.T.A. in the study of spontaneous combustion of coal. *Journal of Mines, Metals and Fuels* (1967), 1-5.

148 Gouws, M. and Wade, L. The self-heating liability of coal: Predictions based on simple indices. *Mining Science and Technology*, 9 (1989), 75-80.

149 Gouws, M. and Wade, L. The self-heating liability of coal: Predictions based on composite indices. *Mining Science and Technology*, 9 (1989), 81-85.

150 Pis, J., De la Puente, G., Fuente, E., Morán, A., and Rubiera, F. A study of the self-heating of fresh and oxidized coals by differential thermal analysis. *Thermochimica Acta*, 279 (1996), 93.

151 William, W. *Thermal methods of analysis*. Wiley Interscience, New York, 1986.

152 Garcia, P., Hall, P., and Mondragon, F. The use of differential scanning calorimetry to identify coals susceptible to spontaneous combustion. *Thermochimica Acta*, 336 (1999), 41-46.

153 Sahu, B., Panigrahi, D., and Mishra, N. Assesment of spontaneous heating susceptibility of coals seams by differential scanning calorimetry. *Journal of Mines, Metals & Fuels*, July-August (2004), 117-121.

154 Mohalik, N., Panigrahi, D., Singh, V., and Singh, R. Assessment of spontaneous heating of coal by Differential Scanning Calorimetric technique - an overview. *2009 Coal Operators Conference* (2009), 303-310.

155 Mohalik, N., Panigrahi, D., and Singh, V. Application of thermal analysis techniques to assess proneness of coal to spontaneous heating - An overview. *Journal of Thermal Analysis and Calorimetry*, 98 (2009), 507-519.

156 Nishimoto, T., Morita, M., and Yajima, H. Spontaneous Combustion of Coal (III). Isothermal Method. *Fire science and technology*, 6 (1986), 1-6.

157 Kidena, K., Murakami, M., Murata, S., and Nomura, M. Low-temperature oxidation of coal − Suggestion of evaluation method of active methylene sites. *Energy & Fuels*, 17 (2003), 1043-1047.

158 Nishimoto, T., Hosoya, M., Kodama, J., and Morita, M. Spontaneous combustion of coal (II). Studying the effects of oxygen concentration in the method of Thermogravimetric Analysis. *Fire Science and Technology*, 5 (1985), 123-128.

159 Ren, T., Edwards, J., and Clarke, D. Adiabatic oxidation study on the propensity of pulverised coals to spontaneous combustion. *Fuel*, 78 (1999), 1611-1620.

160 Beamish, B., Barakat, M., and George, J. Adiabatic testing procedures for determining the self-heating propensity of coal and sample ageing effects. *Thermochimica Acta*, 362 (2000), 79-87.

161 Beamish, B., Barakat, M., and George, J. Spontaneous-combustion propensity of New Zealand coals under adiabatic conditions. *International Journal of coal Geology*, 45 (2001), 217-224.

162 Shonhardt, J. Calorimeter design and the assessment of self heating in coal. *The Coal Journal* (1984), 79-85.

163 Gouws, M., Gibbon, G., Wade, L., and Phillips, H. An adiabatic apparatus to establish the spontaneous combustion propensity of coal. *Mining Science and Technology*, 13 (1991), 417-422.

164 Beamish, B. Comparison of the R70 self-heating rate of New Zealand and Australian coals to Suggate rank parameter. *International Journal of Coal Geology*, 64 (2005), 139-144.

165 Nordon, P., Bainbridge, N., Szemes, F., and Myers, C. A low temperature

reaction calorimeter of the Calvet type for the measurement of the heat of coal oxidation. *Journal of physics E: scientific instrumentation*, 18 (338-341 1985).

166 Humphreys, D., Rowlands, D., and Cudmore, J. Spontaneous combustion of some Queensland coals. (1981), Proceedings of the Ignitions, Explosions and Fires in Coal Mines Symposium.

167 Jones, J. and Raj, S. The propensity to self-heating of solar-dried coal slurry. *Fuel*, 68 (1989), 648-650.

168 Gray, B., Griffiths, J., and Hasko, S. Spontaneous ignition hazards in stockpiles of cellulosic materials: criteria for safe storage. *Journal of Chemical Technology & Biotechnology*, 34 (453-463 1984).

169 Jones, J. Calculation of the Frank–Kamenetskii critical parameter for a cubic reactant shape from experimental results on bituminous coals. *Fuel*, 78 (89–91 1999).

170 Jones, J. Recent developments and improvements in test methods for propensity towards spontaneous heating. *Fire and Materials*, 23 (1999), 239–243.

171 Lohrer, C., Krause, U., and Steinbach, J. Self-ignition under combustible bulk materials under various ambient conditions. *Trans IChemE, Part B, Process safety and environmental protection*, 83 (2005), 145-150.

172 Parr, S. and Coons, C. Carbon dioxide as an index of the critical oxidation temperature for coal in storage. *Industrial and Engineering Chemistry*, 17 (1925), 118-120.

173 Nandy, D., Banerjee, S., and Chakravorty, R. Application of crossing point temperature for determining the spontaneous heating characteristics of coals. *Journal of Mines, Metals and Fuels*, 2 (1972), 41.

174 Feng, K., Chakravo, R., and Cochrane, T. Spontaneous combustion-coal mining hazard. *Canadian Institute of Mining Bulletin*, 66 (1973), 75-84.

175 Mahadevan, V. and Ramiu, M. Fire risk rating of coal mines due to spontaneous heating. *Journal of Mines, Metals and Fuels* (1985), 357-362.

176 Chen, X. and Chong, L. Several important issues related to the crossing-point temperature (CPT) method for measuring self-ignition kinetics of combustible solids. *Trans IChemE*, 76 (1998), 90-93.

177 Nugroho, Y., Mcintosh, A., and Gibbs, B. Using the crossing point method to assess the self-heating behaviour of Indonesian coals. *Twenty-Seventh Symposium on Combustion, The Combustion Institute* (1998), 2981-2989.

178 Beamish, B. and Hughes, R. Comparison of laboratory bulk coal spontaneous combustion testing and site experience - A case of study from Spring Creek mine. (Australia 2009), Underground Coal Operator Conference.

179 QI, X., Wang, D., Zhong, X., and Xu, Y. Oxygen consumption of coal at low temperatures. *Procedia Earth and Planetary Science*, 1 (2009), 366–370.

180 Qi, X., Wang, D., Zhong, X., Gu, J., and Xu, T. Characteristics of oxygen consumption of coal at programmed temperatures. *Mining Science and Technology*, 20 (2010), 372–377.

181 BRITISH STANDARDS INSTITUTE. *[BS ISO 7404-3:2009] Methods for the petrographic analysis of coals. Method of determining maceral group composition*. British Standards Institute, London, 2009.

182 Calemma, V., Del Piero, G., Rausa, R., and Girardi, E. Changes in optical properties of coals during air oxidation at moderate Temperature. *Fuel*, 74 (1995), 383-388.

183 Bend, S. and Koslosld, D. A petrographic examination of coal oxidation. *International Journal of Coal Geology*, 24 (1993), 233-243.

184 Lester, E., Watts, D., and Cloke, M. A novel automated image analysis method for maceral analysis. *Fuel*, 81 (2002), 2209-2217.

185 Cliff, D., Davis, R., Bennet, T., Galvin, G., and Clarksosn, F. Large scale laboratory testing of the spontaneous combustibility of Australian coals. *Queensland Mining Industry Health and Safety Conference Proceedings* (1998), 175-179.

186 Stott, J., Harris, B., and Hansen, P. A 'full-scale' laboratory test for the spontaneous heating of coal. *Fuel*, 66 (1987), 1012-1013.

187 Hornsby, C. and Makower, A. Early detection of open fires and spontaneous combustion in mines. *Revue Institut Hygiene des Mines*, 38 (1983), 147-53.

188 Sima-Ella, E., Yuan, G., and Mays, T. A simple kinetic analysis to determine the intrinsic reactivity of coal chars. Fuel 84 (2005). *Fuel*, 84 (2005), 1920-1925.

189 Vamvuka, D., Kastanaki, E., and Lasithiotakis, M. Devolatilization and combustion kinetics of low-rank coal blends from dynamic measurements. *Industrial and Engineering Chemistry Research*, 42 (2003), 4732–4740.

190 Kizgut, S. and Yilmaz, S. Characterization and non-isothermal decomposition kinetics of some Turkish bituminous coals by thermal analysis. *Fuel Processing Technology*, 85 (2004), 103-111.

191 Serageldin, M. and Pan, W. Coal analysis using thermogravimetry. *Thermochimica Acta*, 76 (1984), 145-160.

192 Elder, J. Proximate analysis by automated thermogravimetry. *Fuel*, 62 (1983), 580-584.

193 Norton, G. A review of the derivative thermogravimetric technique (burning profile) for fuel combustion studies. *Thermochimica Acta*, 214 (1993), 171-182.

194 Morgan, P., Robertson, S., and Unsworth, J. Combustion studies by thermogravimetric analysis: 1. Coal oxidation. *Fuel*, 65 (1986), 1546-1551.

195 Cumming, J. and McLaughlin, J. The thermogravimetric behaviour of coal. *Thermochimica Acta*, 57 (1982), 253-272.

196 Mayoral, M., Izquierdo, M., Andrés, J., and Rubio, B. Different approaches to proximate analysis by thermogravimetry analysis. *Thermochimica Acta*, 370 (2001), 91-97.

197 TA INSTRUMENTS. *High resolution thermogravimetric analysis - A new technique for obtaining superior analytical results*. Report TA-023B, available at http://www.tainstruments.co.jp. Latest access March 2010.

198 Earnest, C. *Compositional analysis by thermogravimetry*. American society for testing and materials, Baltimore, 1988.

199 Wang, H. Kinetic analysis of dehydration of a bituminous coal using the TGA technique. *Energy & Fuels*, 21 (2007), 3070-3075.

200 Russ, J. *The Image Processing Handbook*. CRC press, New York, 1999.

201 Crelling, J. Automated petrographic characterization of coal lithotypes. *International journal of coal geology*, 1 (1982), 347-359.

202 Riepe, W. and Steller, M. Characterization of coal and coal blends by automatic image analysis. Use of the Leitz texture analysis system. *Fuel*, 63 (1984), 313-317.

203 Davis, A., Kuehn, K., Maylotte, D., and Peters, R. Mapping of polished coal surfaces by automated reflectance microscopy. *Journal of microscopy*, 132

(1983), 297-302.

204 Cloke, M., Lester, E., Allen, M., and Miles, N. Automated maceral analysis using fluorescence microscopy and image analysis. *Fuel*, 74 (1995), 659-670.

205 Agus, M., Bonifazi, G., and Massacci, P. Image texture analysis based procedure to characterize and recognise coal macerals. *Minerals engineering*, 7 (1994), 1124-1147.

206 Lester, E., Cloke, M., and Allen, M. Char characterization using image analysis techniques. *Energy & Fuels*, 10 (1996), 696-703.

207 BRITISH STANDARDS INSTITUTE. *[BS ISO 13322-1:2004] Static image analysis methods*. British standards Institute , London, 2004.

208 Field, L., Sternhell, S., and Kalman, J. *Organic structures from spectra*. Wiley, London, 2002.

209 Geng, W., Nakajima, T., Takanashi, H., and Ohki, A. Analysis of carboxyl group in coal and coal aromaticity by Fourier transform infrared (FT-IR) spectrometry. *Fuel*, 88 (2009), 139–144.

210 Ibarra, J. and Miranda, J. Detection of weathering in stockpiled coals by Fourier transform infrared spectroscopy. *Vibrational Spectroscopy*, 10 (1996), 311-318.

211 Machnikowska, H., Krzton, A., and Machnikowski, J. The characterization of coal macerals by diffuse reflectance infrared spectroscopy. *Fuel*, 81 (2002), 245-252.

212 Cloke, M., Gilfillan, A., and Lester, E. The characterization of coals and density separated coal fractions using FTIR and manual and automated petrographic analysis. *Fuel*, 76 (1997), 1289-1296.

213 Guo, Y. and Marc Bustin, R. Micro-FTIR spectroscopy of liptinite macerals in

coal. *International Journal of Coal Geology*, 36 (1998), 259–275.

214 Solomon, P. and Carangelo, R. FT-i.r. analysis of coal: 2. Aliphatic and aromatic hydrogen concentration. *Fuel*, 67 (1988), 949-959.

215 Deming, W., Xiaoxing, Z., Junjie, G., and Xuyao, Q. Changes in active functional groups during low-temperature oxidation of coal. *Mining Science and Technology*, 20 (2010), 35-40.

216 Buggeln, R. and Rynk, R. Self-heating in yard trimmings: Conditions leading to spontaneous combustion. *Compost Science & Utilization*, 10 (2002), 162-182.

217 Armstrong, J. *Spontaneous combustion of forest fuels: a review*. Canadian Forestry Service., 1973.

218 Jones, J. and Puignou, A. On the thermal ignition of wood waste. *Trans IChemE*, 76 (1998), 205-210.

219 Shimizu, Y., Wakakura, M., and Arai, M. Heat accumulations and fire accidents of waste piles. *Journal of Loss Prevention in the Process Industries* , 22 (2009), 86–90.

220 Van Blijderveen, M., Gucho, E., Bramer, E., and Brem, G. Spontaneous ignition of wood, char and RDF in a lab scale packed bed. *Fuel* , 89 (2010), 2393–2404.

221 Kayser, E. and Boyers, C. *Spontaneous combustible solids - A literature study*. Naval surface weapons center, Maryland, 1975.

222 Yuan Kun, L. *Microbial biotechnology: principles and applications*. World Scientific Publishing Co., Singapore, 2006.

223 Avila, C., Pang, C., Wu, T., and Lester, E. Morphology and reactivity characteristics of char biomass particles. *Bioresource Technology* , 102 (2011), 5237–5243.

224 Al-Mansour, F. and Zuwala, J. An evaluation of biomass co-firing in Europe. *Biomass and Bioenergy*, 34 (2010), 620-629.

225 Kazagic, A. and Smajevic, I. Synergy effects of co-firing wooden biomass with Bosnian coal. *Energy* , 34 (2009), 699–707.

226 Konings, T. *Increasing co-firing of biomass in Dutch coal-fired power plants*. Kema Power Generation & Sustainables, 2010. available at www.iea-coal.co.uk.

227 Cloke, M., Wu, T., Barranco, R., and Lester, E. Char characterization and its application for a coal burnout model. *Fuel*, 82 (2003), 1989–2000.

228 Álvarez, D., Borrego, A., and Menéndez, R. Unbiased methods for the morphological descriptions of char structures. *Fuel* , 1241–1248 (1997), 76.

229 Biagini, E., Fantei, A., and Tognotti, L. Effect of the heating rate on the devolatilization of biomass residues. *Thermochemica Acta*, 472 (2008), 55–63.

230 Biagini, E., Simone, M., and Tognotti, L. Characterization of high heating rate chars of biomass fuels. *Proceedings of the Combustion Institute*, 32 (2009), 2043–2050.

231 Cetin, E., Moghtaderi, B., Gupta, R., and Wall, T. Influence of pyrolysis conditions on the structure and gasification reactivity of biomass chars. *Fuel*, 83 (2004), 2139–2150.

232 Guerrero, M., Ruiz, M., Millera, A., Alzueta, M., and Bilbao, R. Characterization of biomass chars formed under different devolatilization conditions: differences between rice husk and eucalyptus. *Energy & Fuels* , 22 (2008), 1275–1284.

233 Xie, X., Goodell, B., Zhang, D., Nagle, D., Qian, Y., Peterson, M., and Jellison, J. Characterization of carbons derived from cellulose and lignin and their

oxidative behaviour. *bioresource Technology*, 100 (2008), 1797–1802.

234 Borrego, A., Garavaglia, L., and Kalkreuth, W. Characteristics of high heating rate biomass chars prepared under N2 and CO2 atmospheres. *International Journal of Coal Geology*, 77 (2009), 409-415.

235 Campbell, P., Mitchell, R., and Ma, L. Characterization of coal char and biomass char reactivities to oxygen. *Proceedings of the Combust. Institute*, 20 (2002), 519–526.

236 Biagini, E., Narducci, P., and Tognotti, L. Size and structural characterization of lignin-cellulosic fuels after the rapid devolatilization. *Fuel*, 87 (2008), 177–186.

237 BRITISH STANDARDS INSTITUTE. *[BS 1016-110:1996] Methods for analysis and testing of coal and coke. Size analysis of coke.* British Standards Institute, London, 1996.

238 THE BRITISH COAL UTILIZATION RESEARCH ASSOCIATION LIMITED, (BCURA). *The BCURA Coal Sample Bank, Users Handbook.* BCURA, 2002.

239 Qi, X., Wang, D., Milke, J., and Zhong, X. Crossing point temperature of coal. *Mining Science and Technology (China)* (2011), 1-6.

240 Misz-Kennan, M., Kus, J., Flores, D. et al. Self-heating of coal and coal wastes working group: a new approach to classify altered and newly formed particles as result of self-heating and self-combustion processes. In *Second International Conference on Coal Fire Research* (Berlin 2010).

241 Yang, H., Yan, R., Chen, H., Lee, D., and Zheng, C. Characteristics of hemicellulose,cellulose and lignin pyrolysis. *Fuel*, 68 (2007), 1781–1788.

242 Dangzhen, L., Minghou, X., Xiaowei, L., Zhonghua, Z., Zhiyuan, L., and Hong,

Y. Effect of cellulose, lignin, alkali and alkaline earth metallic species on biomass pyrolysis and gasification. *Fuel Processing Technology*, 91 (2010), 903–909.

243 Gani, A. and Naruse, I. Effect of cellulose and lignin content on pyrolysis and combustion characteristics for several types of biomass. *Renewable Energy*, 32, 649–661 (2007).

244 Kwiecinska, B. and Petersen, H. Graphite, semi-graphite, natural coke, and natural char classification-ICCP system. *International Journal of Coal Geology*, 57–2 (2004), 99–116.

245 Kubacki, M., Ross, A., Jones, J., and Williams, A. Small-scale co-utilisation of coal and biomass. *Fuel*, (Article in press) (2011).

246 Wang, C., Wang, F.: Yang, Q., and Liang, R. Thermogravimetric studies of the behavior of wheat straw with added coal during combustion. *Biomass and Bioenergy*, 33 (2009), 50-56.

247 Meesri, C. and Moghtaderi, B. Lack of synergetic effects in the pyrolytic characteristics of woody biomass/coal blends under low and high heating rate regimes. *Biomass and Bioenergy*, 23 (2002), 55 – 66.

248 Kadioiglu, Y. and Varamaz, M. The effect of moisture content and air-drying on spontaneous combustion characteristics of two Turkish lignites. *Fuel*, 82 (2003), 1685-1693.

Appendix 1. Software used for data acquisition and analysis

Data acquisition and data analysis algorithms were developed in Labview 2009 (version 9.0) from National Instruments. Labview scripts were characterized for two areas of work: front panel and back panel. The front panel was the normal screen of work, which provides the interface between the user and the scientific instrument to execute a specific predefined task. The work space (or back panel) is a piece of code that contains the task to be executed. This back panel is hidden from the ordinary user, but modified by the software developer. In addition, the back panel of Labview is a graphic code with a set of tasks by default and included in the program ready to be used. These tasks appear with an icon structure, which can be joined by wires and executed sequentially in a "single" loop or in a "while" loop.

A) Data acquisition software

In general, all the data acquisition algorithms used a "while" loop, which start once the initial conditions for each device were set, and stopped by the user once completed. The simple cycle is implemented in a major code, from which the loop described is programmed to be executed 4 times independently (in parallel); one for each of these elements: a) Mass balance; b) Gas analyzer; c) Thermocouple reader 1; and d) Thermocouple reader 2. The graphic interface developed for each loop is presented in Figure 141.
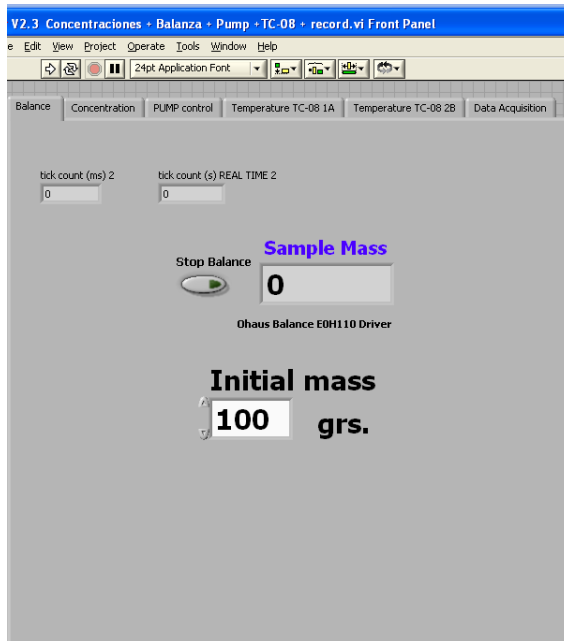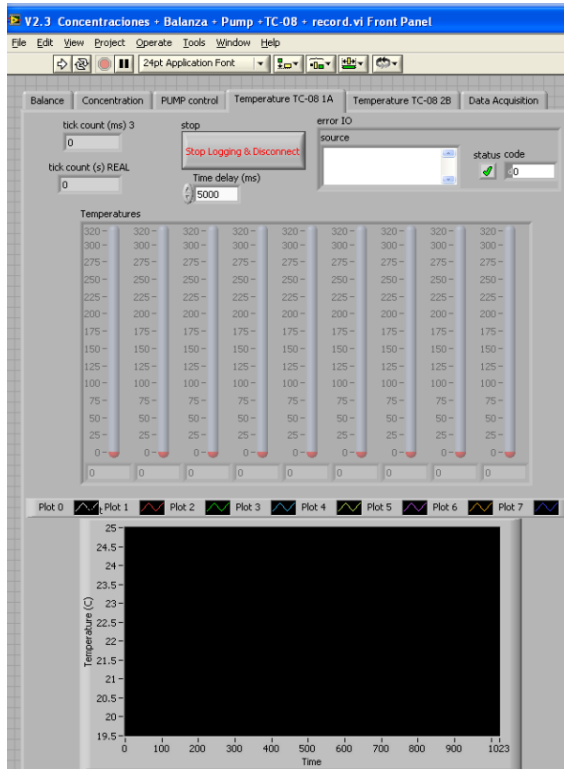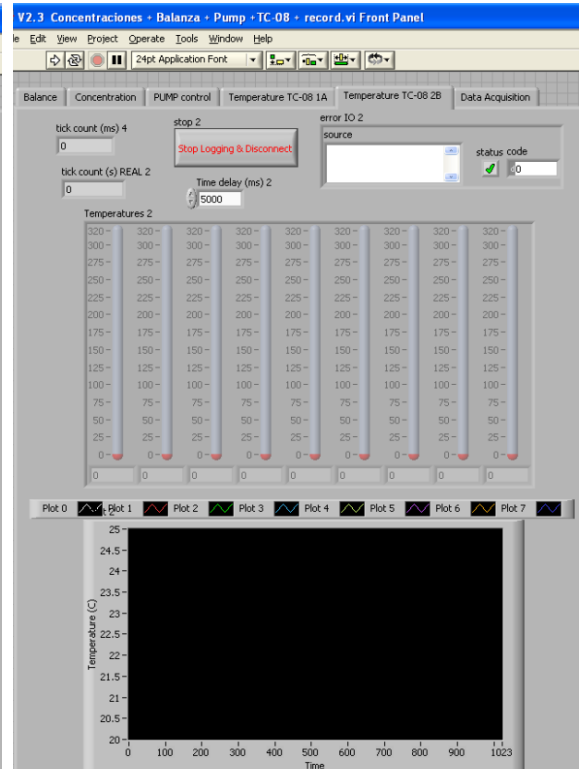
a) Front panel of the balance
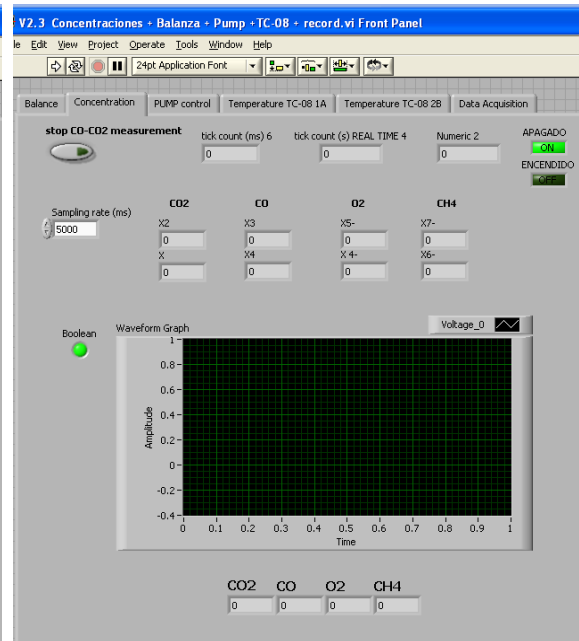
b) Front panel of the Gas Analyzer

c) Front panel of the thermocouples 1

d) Front panel of the thermocouples 2

Figure 141: Front panel of the main application developed for data acquisition.

B) Image analysis software to detect morphologic changes in oxidized coals

An algorithm was partially developed to quantify the thermal alterations produced in treated coal samples (Figure 142). The initial inputs of this program were images

obtained from an oxidized sample; and the morphologic information obtained for the same raw coal using the second algorithm (morphologic characterization of particles, Section 3.6.3). Initially, the image is standardized at grey scale and cleaned by a Fourier transform filter. After this, it was transformed using a binary mode to apply a threshold in the histogram, removing all high reflectance material (not including the rims produced by thermal alterations). In parallel, the same operation is applied to the oxidized samples. Then, the average percentage of altered material per particle was obtained, and compared to the initial sample to calculate the impact of the thermal oxidation.
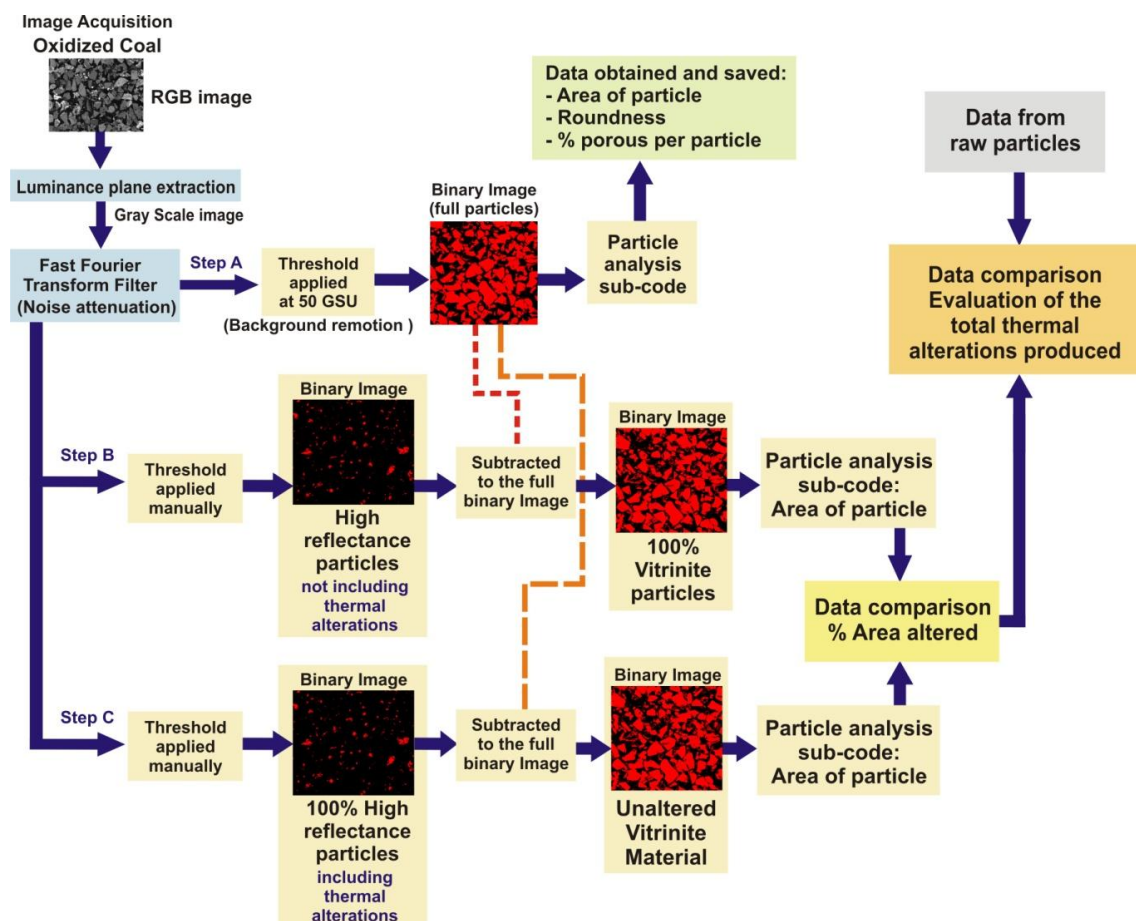

Figure 142: Algorithm used to evaluate the impact of oxidation in coal samples.

Appendix 2. Repeatability of TG_{spc} and TGO_2 tests

The sensitivity of the TGA instrument employed is ±0.1ºC (given by the TGA manufacturer). However, due to the instrument ageing, a conservative sensitivity was experimentally estimated in ±0.5ºC.

The variability of the TG_{spc} was studied using four high reactive samples, subjected to a repeatability tests (Figure 143) that consisted in four different runs using the same sample under the similar experimental conditions. From these, the main differences in the index calculation were estimated in around 14 to 24% for slow heating rates (3,5,7 and 10ºC min^{-1}, Table 49). For high heating rates (20,30,40 and 50ºC min^{-1}), the difference in the index values obtained was up to 35%.

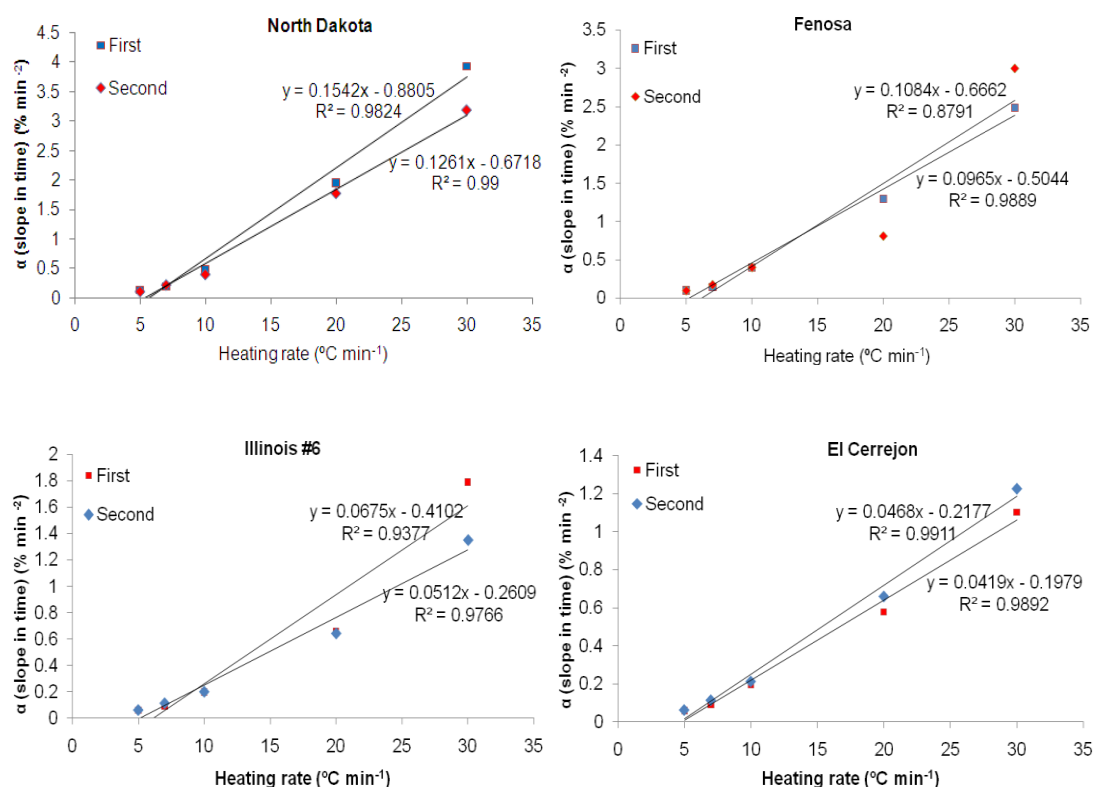Figure 143: Repetition of TG_{spc} calculation for four samples, using 5,7,10,20 and 30ºC min^{-1} heating rates.

The main contribution of error observed come from the inherent inaccuracies of the TGA instrument used, rather than human interpretation, as Figure 144 shows. However, results obtained from this test were also high sensitive to the initial condition of the sample such as weathering degree of the raw material, particle size used, and the time of contact with air prior to execute the experiment. The interpretation of the curves does not have major influence in the differences found.

Table 49: Relative deviation for three experiments carried out for main coals.

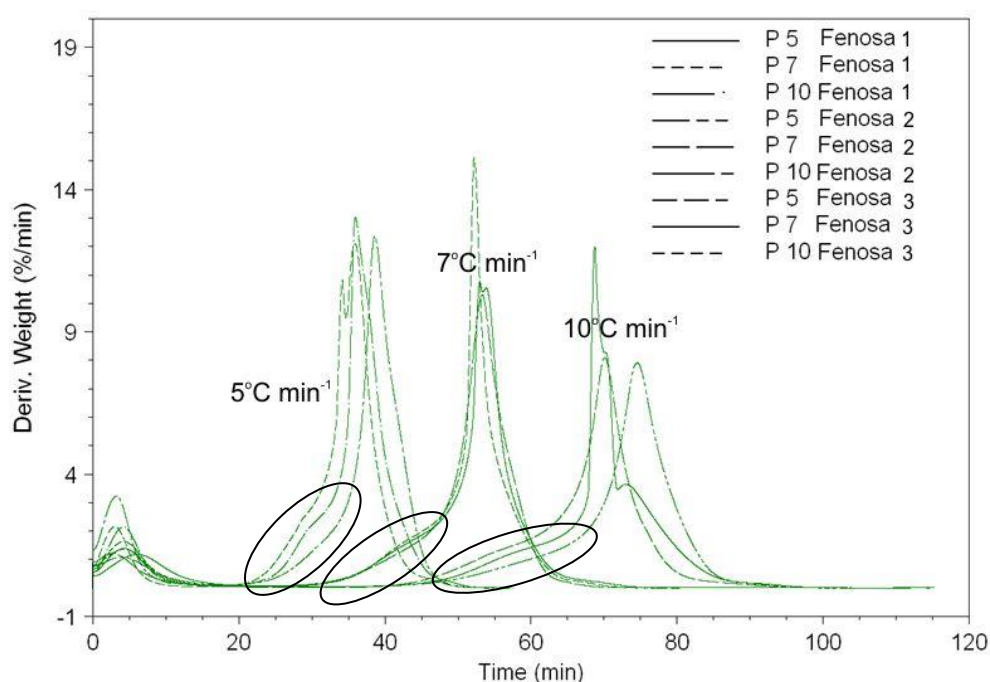| Coal	TG_{spc} values (wt % $^oC^{-1}$ min^{-1})				R^2
	Test 1	Test 2	Test 3	Max. difference	
North Dakota	0.1501	0.1542	0.1261	18%	89.4
Fenosa	0.0920	0.1084	0.0965	15%	91.4
Illinois #6	0.0568	0.0675	0.0512	24%	85.8
El Cerrejon	0.0402	0.0468	0.0419	14%	92.0

Figure 144: Different derivative TGA profiles for Fenosa coal at different heating rates (5,7 and 10°C min^{-1}). The differences in the slopes calculated are related to the intrinsic error of the TGA instrument (shown in a circle).

Appendix 3. Repeatability of the furnace tests

The variability of the furnace test for studying large size samples depended entirely on the heating ramp applied. In this case, the repeatability was estimated from four single tests (Figure 145) that consisted in running an empty crucible four different times under similar experimental conditions. These experiments were carried out twice at the beginning of the coal tests; once at the beginning of the biomass experiments; and once at the beginning of the coal-biomass tests. From these, the maximum differences in the heating rate were estimated overall in around ±10% for the heating rate applied (0.5°C min^{-1}). This was obtained considering the first trials. By using this information, the furnace controller was recalibrated and the variability of the heating ramp was reduced to a maximum of ±5% (as can be seen from the figure, curves 17/08 and 20/08 show more noise and an initial jump in the temperature, which were both later corrected). However in this case, the heating ramp was slightly higher than the heating ramp targeted (0.55°C min^{-1}).
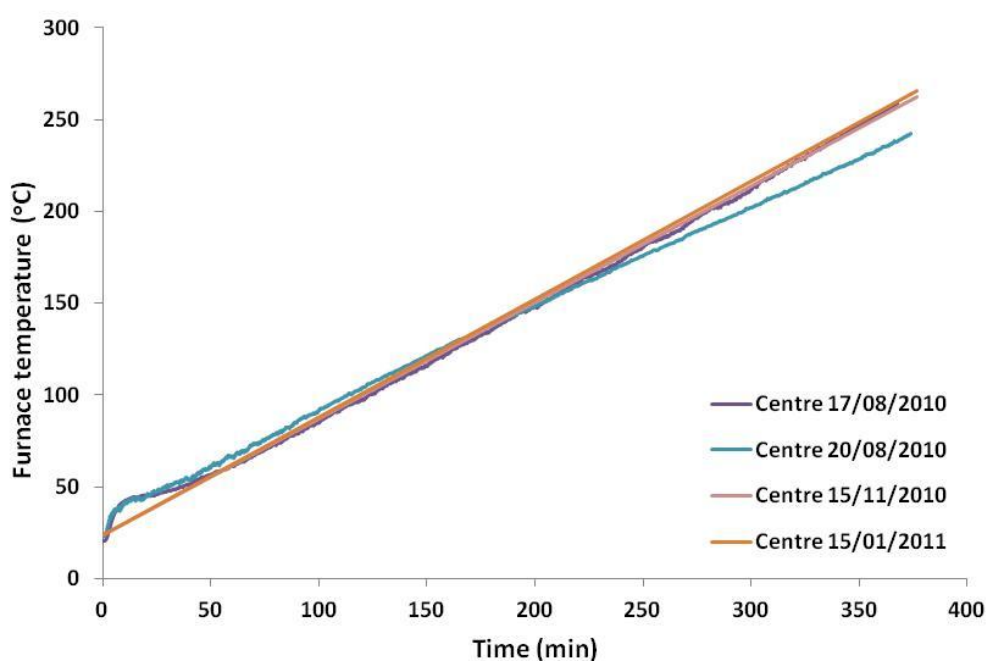

Figure 145: Comparison of the four different runs using an empty crucible.